Localization and Free Positioning with a Cooperative Multiple Coil Transmitter for Wireless Power Transfer

Von der Fakultät für Ingenieurwissenschaften,
Abteilung Elektrotechnik und Informationstechnik
der Universität Duisburg-Essen

zur Erlangung des akademischen Grades

Doktor der Ingenieurwissenschaften (Dr.-Ing.)

genehmigte Dissertation

von

Wei Chen
aus
Jiangsu, China

Gutachter: Prof. Dr.-Ing. habil. Peter Jung
Gutachter: Prof. Dr. –Ing. Klaus Solbach
Tag der mündlichen Prüfung: 24. November 2017

Acknowledgements

"*Reading is easy*, *thinking is difficult*,

but the lack of one, *it is no use*."

- Benjamin Franklin (January 1706 – April, 1790)

This thesis is carried out in the period of my work as a research scientist in the Department of Communication Technologies, the University of Duisburg-Essen. I would like to acknowledge people who played a role in my work and thesis.

I am very grateful to my supervisor Professor Dr.- Ing. habil. Peter Jung, the chair of the Department of Communication Technologies at the University of Duisburg-Essen, for providing me the opportunity to join the KT group, for his dedicated support and encouragement during my Ph.D. study, for his suggestions and assistance in my thesis accomplishment. I'd like to express my gratitude to Professor Dr.- Ing. Klaus Solbach, the chair of Microwave and RF-Technology Department at the University of Duisburg-Essen, for his suggestions and review for my thesis.

I would like to thank all present and past colleagues in the Department of Communication Technologies: Dr. Guido Bruck, Sven Dudda, Li Luo, Stanislaus Iwelski, Andreas Friedrich, Erfan Hashim Majeed, Ziad Youssef, Lucas Grinewitschus, Xue Liu, Bärbel Clausen, Barbara Frischemeier, Peter van del Wel, Dr. Zijian Bai, Dr. Dong Xu, Dr. Shangbo Wang, Duan Zhao, Dr. Sebastian Rickers, Dr. Alexander Viessmann, Dr. Ernest Scheiber, Dr. Christian Kocks, Dr. Christoph Spiegel, Andreas Waadt, Andrey Skrebstov, Dr. Rani Al-Maharmah, Dr. Mohammed Al-Olofi.

Finally, I want to express my deepest thanks to my family, especially my parents, for their love, their selfless support and encouragement in my general life and entire thesis writing. I am grateful to all of my friends for being with me, for their assistance, comfort and affirmation during my work on the thesis.

Duisburg, December 2017

Wei Chen

Übersicht

Mit fortschreitender Entwicklung der Kommunikationstechnik steigt die Anzahl tragbarer Geräte, die einen wiederholten Ladevorgang über ein Kabel benötigen, kontinuierlich. Drahtlose Energieübertragung (Wireless Power Transfer, WPT) umgeht die damit verbundenen Sicherheitsrisiken sowie die Unbequemlichkeiten und Unansehnlichkeit, die eine große Zahl an Ladekabeln mit sich bringt. Im Rahmen dieser Arbeit ist ein konzeptueller Entwurf für ein optimiertes 100 kHz WPT-System entstanden, welcher einen großen Ladebereich mit der Möglichkeit zur freien Platzierung des zu ladenden Gerätes erlaubt. Das System zeichnet sich durch eine hohe Effizienz und elektromagnetische Verträglichkeit aus.

Ein Dreispulensystem, bestehend aus einer Sendespule und zwei Empfängerspulen in Serienresonanz, wird hinsichtlich Kopplungsfaktor und Gütefaktor optimiert. Die Sendespule wird durch eine 4-Spulen Struktur ersetzt, die eine Feldformung ermöglicht, so dass eine Verstärkung des Feldes im Zentrum der Struktur erreicht wird bei gleichzeitiger Abschwächung an den Rändern. Sendermatrizen aus kooperativen Mehrspulensystemen werden untersucht mit dem Ziel, die Fläche des Ladefeldes zu vergrößern und das externe magnetische Feld zu reduzieren. Ein System aus 16 Spulen wird als das mit dem besten Kosten-Effizienz Verhältnis identifiziert. Der Radius der Senderspulen wird nach einem Kriterium der gewichteten Gesamteffizienz optimiert. Ziel ist eine hohe Effizienz bei gleichzeitig minimalen Emissionen in die Umgebung. Beim Ladevorgang wird in Abhängigkeit von der Position des zu ladenden Geräts die passende 4-Spulen Struktur aktiviert während die übrigen deaktiviert bleiben. Zur Lokalisierung des Empfängers werden die Algorithmen Rastersuche, Gauss-Newton und reflektierte Impedanz für kombinierte Spulen vorgestellt. Zur Untersuchung der Effekte von Ferriten und Aluminium sowie reaktiver resonanter Spulen wurden Simulationen mit COMSOL durchgeführt, mit dem Ziel die Effizienz zu erhöhen und die externen Felder zu reduzieren, so dass die Grenzwerte für die menschliche Exposition unterschritten werden.

Diese Arbeit liefert eine WPT-Lösung für das Laden mobiler und portabler Geräte welche zahlreiche Vorteile bietet. Das vorgeschlagene 100 kHz 16-Spulen Matrixsystem, bestehend aus individuell aktivierbaren 4-Spulen Teilstrukturen, ermöglicht eine freie Platzierung auf dem Ladebereich, mehr als 65 % Übertragungseffizient im Abstand von 10 cm sowie deutlich geringere Elektromagnetische Feld Emissionen als in den Richtlinien gefordert.

Abstract

With the continuous development of communication technology there are more and more portable devices requiring periodic charging with a cable and power socket. Wireless power transfer (WPT) technology provides a promising solution to overcome the inconvenience, potential safety hazard and unsightliness of power supply cables. The result of this thesis is a conceptual design for an optimized 100 kHz WPT system having a large charging pad allowing free placement of the device to be charged. The system has high efficiency and is Electromagnetic Compatibility friendly.

The three-coil system, composed of a single transmitter coil and two coils in the receiver, is operating in series resonance and has been optimized by synthesis of the coupling coefficient and quality factor to provide maximum efficiency and power simultaneously. Unique to the proposed design is that the single transmitter coil is replaced with 4-coil structure which enables field forming to strengthen the field in the center of the 4-coil structure and reduce it at the margins. A transmitter matrix consisting of cooperative multiple coils is proposed to increase the charging pad area and reduce the external magnetic field. A 16 coils system is selected as most cost efficiency. The transmitter coil radius is optimized using the criterion of weighted overall efficiency, which results in high efficiency with minimal emission to the surroundings. During charging, the appropriate 4-coil structure is activated, depending on the device location, with the other coils turned off. Several algorithms are presented that enable localization of the receiver position including: grid search, Gauss-Newton and reflected impedance for combined coils. COMSOL simulation is used to investigate the effects of using ferrite, aluminum loading and a reactive resonant coil to improve system efficiency and reduce external fields below specified human exposure limits.

This thesis provides a WPT solution for charging mobile and portable devices that has many advantages. The proposed 100 kHz 16 coils transmitter matrix WPT system, consisting of individually activated 4-coil sub structures, allows free placement within the charging area, more than 65% transfer efficiency at 10 cm transmission distance and electromagnetic field emission considerably less than required by guidelines.

Table of Contents

Chapter 1

Introduction

1.1 Overview of Wireless Power Transfer

1.1.1 History and Development of Wireless Power Transfer

Wireless power transfer (WPT) systems employ no direct electrical connection between the transmitter (power source) and the receiver (load) [Aug14]. With the continuous development of communication technology, more and more portable devices need periodic charging or replacement of the battery [Bit14]. WPT technology introduces a promising solution to overcome the inconvenience, unsightliness and safety hazard associated with power supply cables [Vae09]. The technology of WPT makes a great contribution to improve quality of life and comfort of life [Sai14,Aza14].

This method is not new and strange to human beings, since this idea of WPT is established with the pioneering work on electromagnetism in the 19th century by physicists, who showed that an alternating current (AC) produces a magnetic field and vice versa [LYO01]. There are two fundamental theories involving magnetic field and inductive coupling that apply to WPT systems: Ampere's and Faraday's laws [LuX15,Vil15]. According to the concept of displacement current in electromagnetic field theory, any time-varying electric field will generate a time varying magnetic field in the nearby space (Ampere's circuit law) [Vil15]. As well as any time-varying magnetic field results in an induced voltage produced in

a circuit enclosing the magnetic fields (Faraday's Law of induction), as shown (1.1) [Sve13]. ε_{in}, ψ, B, S and t are the induced electromotive force (IEF), magnetic flux linkage, magnetic induction intensity, area of receiver coil and time separately. The negative sign means the magnetic flux linkage generated by induced current is in opposition to the magnetic flux linkage from transmitter coil. The AC current generates magnetic field in the transmitter that produces the voltage in the receiver based on two fundamental laws of physics [Sin16]. This is the basic principle for applications, such as a transformer, AC motor and AC generator [Mik06].

$$\varepsilon_{\text{in}} = -\frac{d\psi}{dt} = -\frac{d\left(B \cdot S\right)}{dt} \tag{1.1}$$

Nikola Tesla made a significant, and well ahead of the time, contribution to wireless charging in the late 19th and early 20th century [Goo13]. The concept of resonance inductive coupling was first proposed by Tesla in 1900 [Sah11]. In this case a light was successfully turned on using a resonance circuit containing a symmetrical transmitter and receiver coil, using two ball electrodes on the top as capacitance with the other end connected to ground [Tes00,Sin12,Was00]. One of most famous contributions designed and constructed by Tesla is Wardenclyffe tower (Tesla tower), which was constructed for sending a message across the globe and to transfer electrical energy wirelessly with no more than 5% loss [Pet13]. However, the attempt to use this tower to demonstrate wireless energy distribution was abandoned because of lack of funds [Bom05]. In Tesla's conception of wireless energy transfer, the earth is taken as the inner conductor, while the earth's ionosphere is regarded as the outer conductor [Val02]. The energy is transferred through electromagnetic waves generated by connecting a transmitter between the earth and ionosphere at the resonance frequency of about 8 Hz. However, the attempt at this audacious idea was not completed because of shortage of funds [Tes04,Tes27,Wad16].

In the 1960s, William C. Brown started to develop the power transfer system with microwave technology [Man06,Tom12]. Brown designed a high efficiency antenna with simple structure by using a half wave electric dipole semiconductor diode rectenna to convert 2.45 GHz microwave energy into direct current [Bro96,Tom12]. Using this rectifier technology power transfer to a helicopter was demonstrated using a microwave beam [Bro66]. Between 1969 and 1975 William, of Jet Propulsion Laboratory (JPL), demonstrated a microwave power system that could transfer 30 kilowatts of direct current (DC) power to a receiver at a distance of one mile with 84 % efficiency [Nag09,Bro89].

Following William.C. Brown's successful implementation, the interest in WPT grew rapidly [Red13]. A lot of scientists and engineers devoted themselves into the research and development of this technology in the 1980s. In 1983, the Microwave Ionosphere Nonlinear Interaction Experiment (MINIX) was the world's first demonstration of microwave power transfer (MPT) with the ionosphere at 2.45 GHz in Japan [Kay86,Nag86]. The next major MPT technology achievement was powering an airplane, carried out in Canada, known as the Stationary High Altitude Relay Platform (SHARP) program [Sch88]. Using solar power satellite (SPS) to capture power from the sun and transmit to the earth using electromagnetic energy is another use of long distance wireless energy transfer that has been investigated [Bro81]. The first SPS was proposed by Dr. Peter Glaser in 1968 [Bro96]. In 2001, the Japan Aerospace Exploration Agency (JAXA) developed a transmitter antenna for SPS which worked at frequency of 5.8 GHz and provided 1 GW output power. The US National Aeronautics and Space Administration (NASA) did a lot research into large-scale space solar power (SSP) systems. The basic concept of SSP is same as SPS, which was replaced due to high technological risk and cost. From 1999 to 2000, NASA ran a program of SSP Exploratory Research and Technology (SERT) that was intended for both the space and terrestrial market [MaS02]. The recent Exploration Systems Research and Technology (ESR&T) program for developing technologies for space operations in the Earth's neighborhood includes research and development for High-Efficiency / High Power SSP [URS07]. It is possible for SPS or SSP to beam the solar energy to the earth by microwave or laser technology [Duk14]. A laser powered aircraft was developed by laser was developed by NASA's Marshall Space Flight Center (MSFC) in 2003 [Dry04]. JAXA demonstrated terrestrial laser WPT power transfer over 500 m transmission distance during 2012 and 2013 [Got14].

John Boys and Grant Covic provided a detailed analysis for hardware design and operating principle for inductive power transfer (IPT). This technology has been applied to wireless rail cars and electromagnetic induction wireless charging for electric appliances [Pow16]. In 1994, the concept of IPT was proposed and applied to moving electric vehicles (EVs) on a 200 m track. The pick-up coil received 1.2 kilowatts for a 75 mm transmission distance with lateral misalignment tolerance of 400 mm [Gre94,Ell95]. The inductively coupled power transfer (ICPT) system was developed for vehicle applications to multiple receivers, whose power reached up to 150 kW [Boy00]. Different types of pick-up shapes in the ICPT system were investigated compared and analyzed [Ell06]. The three-phase ICPT system was invented by the University of Auckland, which supplied 40 Amperes per phase to flat pick-ups on the underside of moving

vehicles. This development was used for providing power across the complete width of a roadway [Cov06,Cov07]. Furthermore Prof. Ron S.Y. Hui led a team engaged in WPT research that successfully demonstrated a coreless PCB transformer with multiple secondary outputs [Tan99]. The coreless planar printed-circuit-board transformers have the advantage of low cost and high power density, which transferred 19 W with greater than 90 % efficiency [Tan00]. Ferrite plates and copper sheets were applied to the PCB transformer, which improved the shielding and energy efficiency [Tan02]. Contactless battery charging platform for portable consumer electronic devices was achieved regardless of the receivers' position and orientation. The multilayer planar PCB winding composed of a hexagonal structure was shown to successfully charge mobile devices by simulation and experiment. Electromagnetic compatibility (EMC) was also considered for the charging platform to diminish the electromagnetic field (EMF) emission [Liu07].

In the meantime many unusual and innovative technical proposals emerged in the scientific community and industrial circles for applying WPT to daily life. The Oral-B electronic toothbrush was invented with IPT technology by Braun Company in the early 1990's [Man13]. A type of implanted in vivo telemetry device was invented in Germany that can supervise the state of electronic medical devices implanted inside the human body. The advantage of this device is that, not only does it transfer the power wirelessly, but real time data is exchanged in vitro and vivo as well [Gra99]. The EV1 EVs contactless conductive charging system was developed by American General Motors. The charging paddle is inserted into the car to supply power to charge battery [Man13,Cov10]. The charging process has the advantage of high efficiency, safety and simplicity [Hay98]. An electric bus with IPT technology was developed by Conductix-WAMPFLER in Germany in 1997 [Cov10]. The flat pick-up in the bus has 20 kW total capacity charging power with modified AC inverter power supply. The electric bus has the capability of rapid charging and is computer controlled [Pow10].

WPT technology has developed very rapidly in recent years because of the increasing emergence of electronic devices [Wan12a]. In order to increase the transmission range and efficiency of WPT systems, strong resonant magnetic coupling is the new WPT innovation which was proposed by MIT, led by Prof. Marin Solijacic [Zhu15]. In July of 2007, researchers in MIT published a new method for contactless power transmission. The transmitter coil can transfer energy to the receiver coil at a distance which is several times as large as diameter of the coil. They successfully demonstrated lighting a 60 watt bulb at a distance of 2 meters [Kur07]. The emerging method for contactless power transfer is the use

of magnetic resonant coupling [Can09]. The improvement comes from the fact that two same-frequency resonant objects tend to couple and exchange power efficiently while interacting weakly with other off-resonant objects [Kar06]. For example, if a singer makes the specific treble note at which a wine glass is resonant, the sound can shatter the glass [Ite15]. In order to illustrate the advantage of strong resonant coupling, Figure 1.1 presents the difference of electric field strength between inductive coupling and resonance coupling wireless transfer methods. The receiver obtains power from the source that has the same initial input energy on the basic of Faraday's law of electromagnetic induction. When the source and receiver are in a non-resonant state, the receiver almost has no receiving power, which is expressed with electric field strength in Figure 1.1 (a). When the source and receiver are resonant at the same frequency, the energy is successfully transferred as illustrated in Figure 1.1 (b). The power transfer from source to receiver was simulated with the software of MaxwellFDFD [Shi12]. Then in 2008 the famous wireless charging standard "Qi" was developed by the Wireless Power Consortium (WPC). This standard is mainly used for charging low power mobile devices [Auv15]. The Wireless Electricity (WiTricity) company was founded by Prof. Marin Solijacic based on the concept of near field and strong resonance coupling. Witricity is focusing on the application of WPT for consumer electronic devices, medical, automotive etc. [Aje14].

An On-Line Electric Vehicle (OLEV) has been developed by the Korean Advanced Institute of Science and Technology (KAIST) in South Korean. The air gap between the OLEV bus and charging ground is 17 cm. The bus receives 100 kW and the efficiency reaches up to 85 % [Hly13]. KAIST successfully demonstrated trams and railroad cars at 60 kHz. The transfer efficiency was up to 85 % with air gap 10 cm. The pick-up device could receive up to 180 kW [KAI15]. Also, Bombardier has developed IPT electric buses, trucks, cars and rail trams for the public. In Manheim, Germany, the company Primove developed a charging system that has the advantage of rapid charging, easy installation, high power, high efficiency and safety [Bom13]. They successfully demonstrated a dynamic charging truck system, which charges above 10 meter long charging segments supplied with 200 kW power [Bom16].

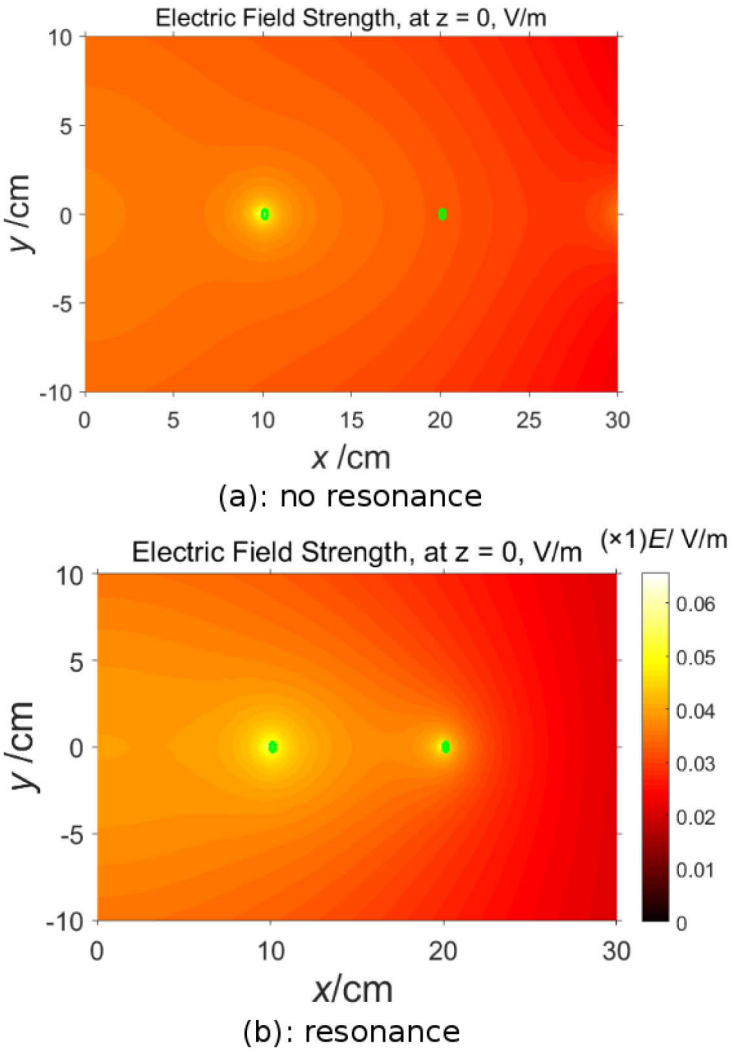

Figure 1.1 Energy transfer between two antennas through non-resonance and resonance (conceptual representation of resources in **[Kar07]**)

1.1.2 Wireless Charging Methods

1.1.2.1 Classification Basis

WPT technology has a long development history of different types of transmission methods and mechanisms. There are three categories according to transmission distance compared with wavelength: near field, middle field and far field. Far field is defined as having a transmission distance longer than two wavelengths. Transmission distance between one and two wavelengths is categorized as middle field. Transmission distance shorter than one wavelength is classified as near field. The recent developments of WPT systems can be

categorized as near field and far field based on different transporting mechanisms and transmission distance [Man14]. Microwave and laser transmission methods are regarded as far field WPT systems. Inductive coupled power transfer and resonant coupled transfer are categorized as near field technology [Vil15]. Generally speaking, the far field transfer approach works at high frequency reaching several GHz, while near field WPT systems can transfer power with high efficiency from several kHz to several MHz [Vil15].

1.1.2.2 Electromagnetic Radiation (RF radiation)

The first WPT method is electromagnetic radiation which is also named far field wireless transfer technology [Man14]. The energy is transferred wirelessly by the electromagnetic wave, which is similar to radio frequency transmitting [Bro84]. Two mainstream approaches of radiation power transfer are MPT and laser power transfer (LPT) [Man14]. They are being investigated for application to SPS which collects solar power and transfers it to ground by microwave or laser beam [Got14]. The sun energy acquired by the solar energy collector is converted into electric power by photovoltaic cell. Then the DC power can be transformed into microwave or laser beam with microwave tube system converter or beam converter. Then the microwave or laser energy is beamed to the ground where it is converted into useful electrical power by a rectenna or photovoltaic respectively [Got14,Maq13].

The received power using the far field approach can reach several kW with a transmission distance of thousands of meters [Tom12]. However this technology has the inverse relation between the transfer efficiency and the transmission directionality. If the transmission is omnidirectional, the transfer efficiency is low due to energy lost to space [Kar07,Tom12,Lee12a]. However, for a transmission mode with one single direction, a complex tracking and pointing system is required to guarantee the point to point power transfer to mobile receiver devices [Sum09,Kar07]. Electromagnetic Radiation is dangerous and painful to humans and animals at high levels of exposure [Shu15]. Therefore it is undesirable for living beings to be in the transmission beam path [Lan05]. What is more, microwave and laser technologies can cause significant heating, which may have a negative influence on the human body and other different kinds of biology [Rao16].

1.1.2.3 Inductively Coupled Power Transfer

Non-radiation inductively coupled power transfer (ICPT) belongs to near field wireless transmission technology. The theoretical foundation of ICPT is based on the law of electromagnetic induction and Ampere's circuital law [Vil15]. An electric transformer, operating under the principle of inductive coupling, is the simplest, most efficient and prevalent form of a WPT systems [Kes13a]. The primary coil of the transformer transfers power to a secondary coil without connection. The transformer can be classified as air core, iron core and ferrite core transformer based on different transmission media [Rob13]. The air core transformer has weak inductive coupling between the primary and secondary coil due to high leakage loss [Pra12]. The iron core transformer provides a controlled path for the magnetic flux and reinforces the magnetic field by adding high permeability material in the magnetic transmission path [Rob13,Ram16]. The advantage of ferrite core transformer technology is the efficiency and the power of transmission can be increased substantially by increased the coupling between the primary and secondary coil and minimizing the leakage loss [Rob13].

Typical ICPT commercial products are electric toothbrush, electric shaver and induction cooker [Zhe15]. However, the transmission efficiency of inductive coupling power transfer decreases inversely with the sixth power of the distance between transmitter and receiver coils due to power lost through radiation [Agb13]. Normally, the transfer distance of ICPT is limited in the range of from several millimeters to several centimeters [Ped99,Aya02,LuR10]. Moreover, the relative location of transmitter and receiver with ICPT technology is fixed because lateral misalignment results in dramatically reduced efficiency [Mou15]. Thus ICPT does not really satisfy the expectation for WPT due to the short range transmission distance and low efficiency [Tah12].

1.1.2.4 Electromagnetism Resonance Coupled Power Transfer

Depending on the transmission medium, near field resonance coupled power transfer is classified as magnetic resonance coupled power transfer (MRCPT) or electric resonance coupled power transfer (ERCPT). However, ERCPT has lower transfer efficiency than MRCPT [Has15]. MRCPT is recommended for higher transfer efficiency and longer distances. Capacitors are used to tune the resonant circuits in both transmitter and receiver sides of MRCPT. [Wei14]. Energy is exchanged between the magnetic field and electric field in the inductor and capacitor respectively [Kes13a]. A resonant inductive coupling system, where

both the transmitter and receiver coils resonate at the same frequency, is an improvement over inductive coupling because the two same frequency resonators have strong magnetic field coupling [Kar06].

As long as the transmitter and receiver are within the non-radiative near field region, wireless power can be transmitted with minimal radiation loss [Zhu15]. This technique can also provide satisfactory efficiency for medium power WPT over middle range distances in terms of the characteristic size of the device [Ley08]. The characteristics of MRCPT are as follows: It can provide power to the receiver in an omnidirectional, non-loss way and penetrate non-magnetic material objects [Kar07,Kur07,Zhu08]. Also it has advantages of high receiving power, higher transfer efficiency and middle range transfer distance [Kes13a]. Furthermore, because the MRCPT technique is non-radiative transfer by the medium of magnetic field, there is very little effect on the ecosystem [Kar07,Pra15]. Therefore it is possible to be a safe and reliable system for human beings, animals and the ambient environment according to international safety guidelines [Kes13a]. MRCPT stands out when considering and comparing the advantages and disadvantages of the above three types of WPT technologies and for that reason is widely used for consumer electronics, medical devices, EVs and so on [Kes13a].

MPT, LPT, IPT and MRCPT approaches have advantages and disadvantages according to their different transmission method, distance and system efficiency [Bar15]. Table 1.1 compares and summarizes different charging methods. Of these techniques, the strongly coupled magnetic resonant transmission method is considered to have the greatest potential and to be the most practical scheme. MRCPT has attracted much attention due to its high efficiency, safety, ease of control and lack of radiation [Kes13a]. There are five application benefits of strongly coupled magnetic resonance WPT systems. First, the system efficiency and the load power are greatly improved by resonant coupling transmission between the transmitter and the receiver [Kes13a,Liu14]. Secondly, the receiver is allowed to have some angular and lateral misalignment, making it more convenient for users to place the mobile devices wherever they want to [Wan12b,Jon13]. Thirdly, the strong magnetic coupling tolerates a receiver size smaller than the transmitter [Can09]. Moreover, the transmitter can provide power wirelessly to multiple receivers simultaneously. For example, one charger source can supply power to a mobile phone, iPad and laptop at the same time [Can09,Zho15a]. Finally, the transmission distance can be enlarged by multiple hops which have a similar function as a router, where the energy is transmitted through the hops to the terminal device [Zho13,Zha15].

Table 1.1 Comparison of advantages and disadvantages among different WPT methods (summary resources in **[Bar15,Mou15,LuX15,Cho11]**)

WPT Technologies	MPT(LPT)	IPT	MRCPT
Transmission Method	Microwave or Laser Beam	Inductive Coupling	Magnetic Resonance
Transfer Distance Class	Kilometers (Long Range)	Millimeters (Short Range)	Centimeters or Meters (Middle Range)
Transfer Efficiency	High	Low	High
Advantages	Energy Conserving	No Radiation	No Radiation
Disadvantages	Radiation, harmful to human beings	Accurate Alignment Requirement	Efficiency Decline due to Lateral and Angle Misalignment
Typical Application	Unmanned Airplane	Toothbrush	Electric Vehicles, Mobile Devices

1.1.3 Inductive Power Standards of WPT

At present the three mainstream WPT technology international standards are Wireless Power Consortium ("Qi" standard), Power Matters Alliance (PMA) and Alliance for Wireless Power (A4WP) [Rao16]. In 2008, WPC standards were established by a group of electronic companies which established the standard of "Qi" with inductive coupling technology [Wir16]. The standard provides for the low power portable devices under 5 W and defines the communication protocol between the transmitter and receiver. The transmission distance is increased from 0 mm to 40 mm for Qi compatible products, such as smart phones, tablets, camera, laptop and other mobile devices [Man13]. PMA is the international and non-profit organization which was founded in 2012. PMA provides specifications and protocols for wireless charging products according to existing international

standards [PMA16]. The purpose of PMA coordinates and unifies different standards so as to realize the global interoperability [PMA16,Kha15]. The A4WP standard adopts the technology of magnetic resonance. It has the advantage of middle range transmission distance and higher transfer power [Kha15]. On June.1 2005, PMA and A4WP made agreement for their merger [PMA16]. Comparison of the main characteristics of the three standards Qi, PMA and A4WP is shown in Table 1.2.

Table 1.2 Comparison of different standards for WPT systems (summary resources in **[Nam15,Zhe15,Kha15]**)

Organizations	WPC(Qi)	PMA	A4WP
Transmission Method	Inductive Coupling	Inductive Coupling	Magnetic Resonance
Power Frequency Band	100 - 205 kHz	277 – 357 kHz	6.78 MHz
Communications Frequency Band	100 - 205 kHz	277 – 357 kHz	2.4 GHz (ISM Band)
Transfer Range	Short Range	Short Range	Middle Range
Typical Transfer Power	5 W	5 W	50 W
Spatial Freedom	Yes	No	Yes

1.2 Electromagnetic compatibility Issues for WPT Systems

1.2.1 Introduction

Electromagnetic compatibility (EMC) is desideratum for WPT systems due to the harmful influence of electromagnetic energy that can occur to electronic devices, or surroundings [Hir08]. Electromagnetic energy radiating from a source could damage organisms and or electronic systems [Ozo15]. The target of EMC is to make sure electric equipment or system can be correctly operated in the

electromagnetic environment [WIK16a]. The avoidance of intolerable electromagnetic disturbance from other electronic devices is the second target of EMC [Irs13].

EMC considerations include two main problems which are emission and susceptibility issues [WIK16a]. The aim of the emission issue is to reduce unintentional electromagnetic energy generation, and even more restrain the unwanted energy from being transferred into the external environment [WIK16a,Sri15]. For the susceptibility issue, the goal is that the electrical and electronic equipment is still operate correctly even in the case of electromagnetic disturbances [WIK16a,Del01]. Therefore, the electrical science of EMC includes electromagnetic interference (EMI) and electromagnetic susceptibility (EMS) [Hir08]. The EMF is produced by voltage and current, which can lead to EMI [Kra95]. Nevertheless EMS is related to the issue of a products' ability to avoid of any interference effects [WIK16a,Del01].

1.2.2 EMC Regulations for WPT Systems

1.2.2.1 Emission and Immunity

In order to make sure that equipment and other electro devices satisfy the operating characteristic of EMC, international agencies and national governments in many countries have developed the various EMC standards, which stipulate limiting values for EMI, EMS and human body exposure safety [Oba14]. The most important EMC standards for WPT systems and human radiation exposure safety regulations that have been drawn up by different countries and international standardizing bodies are shown in Table 1.3.

The International Electrotechnical Commission (IEC) has three organizations that are responsible to draw up EMC standards for WPT. These three organizations are the International Special Committee on Radio Interference (CISPR), Technical Committee 69 (TC69) and, Technical Committee 100 (TC100) [Oba14,Kal14]. The standard developed by TC69 is JPT 61980, which is related to electric vehicles, including industrial trucks, buses and scooters [Tec16]. The TC 100 works on audio, video and multimedia systems and equipment about WPT systems, such as IEC 62827, IEC 63006 and IEC 63095 [Tec12]. CISPR 11 defines limitations for the industrial, scientific and medical (ISM) equipment, as well as CISPR 22 specified the EMC requirement for information technology (IT)

equipment [Yam11]. CISPR 24 works on EMI standards of information technology equipment (ITE) [Oba14,CIS10].

Table 1.3 Standardizing bodies and standards (representation of resources in **[Car15,Kal14]**)

Countries or Organizations	Entity	Sector
IEC	CISPR	Electrical
IEC	TC69/TC100	Electrical
European Community	CENELEC ETSI CEPT/ECC	Electrical Telecoms Telecoms
USA	FCC	Telecoms
IEEE		Telecoms/Electrical/Health
ICNIRP		Health

The European community has three main organizations to develop standards: European Committee for Electrotechnical Standardization (CENELEC), European Telecommunications Standards Institute (ETSI) and European Conference of Postal and Telecommunications Administrations/Electronic Communications Committee (CEPT/ECC) [Kal14]. CENELEC produced EN 55011, EN 55022 and EN 55024, which are a modified version of CISPR 11, CISPR 22 and CISPR 24 respectively [Lea16,Oba14]. What's more, CENELEC body responsible for the work/technical committee (CLC/TC) 69X of CENELEC defined a standard for electric vehicle WPT systems that is similar to the IEC standard [Kal14,CLC16]. The ETSI drafted EN 300 330 for EMC, Radio Spectrum Matters (ERM) and Short Range Devices (SRD). Frequency ranges of radio equipment and inductive loop systems are from 9 kHz to 25 MHz and 9 kHz to 30 MHz separately [ETS15]. Technical Report of ETSI 103 409 specified the high-power WPT systems for EVs with frequency range from 79 kHz to 90 kHz [ETS16]. In the world radio communication conference (WRC-19) agenda item 9.1.6 discussed

the effect of electric vehicle WPT systems on radio communication services and researched on the frequency ranges which have less influence on radio communication services [ECC16].

In the United States, Federal Communications Commission (FCC) formulates EMC issues standards mainly in FCC part 15 and FCC part 18 [Kal14]. FCC part 15 works on radio frequency devices with respect to conducted limits and radiated emission, FCC part 18 is similar to CISPR 11 in the frequency range for ISM equipment [ECF16]. In addition, Society of Automotive Engineers (SAE) J2954 describes testing method, safety, performance, positioning and charging efficiency for WPT systems [Sch10].

1.2.2.2 Human Exposures Safety Standards

WPT systems providers must consider human exposure safety in the near field of the transmitter, because the EMF can affect a nearby human body. The level of allowable human exposure to EMF is frequency dependent [Man14]. The frequency band from 3-30 kHz termed very low frequency (VLF), whose wavelength ranges from 100 m to 10 km. The low frequency (LF) band is from 30 kHz to 300 kHz [Bre14]. The working frequency of the WPT systems proposed in this thesis is 100 kHz and the corresponding wavelength is 3 km.

It is essential to apply safety standards or regulations to WPT systems to protect human health. Two mainstream international guidelines for human exposure safety are International Commission on Non-Ionizing Radiation Protection (ICNIRP) and Institute of Electrical and Electronics Engineers (IEEE) [Kha15]. Both ICNIRP and IEEE guidelines are endorsed by the World Health Organization (WHO) [Kha15]. IEEE formulates standard for safety levels with respect to human exposure to radio frequency electromagnetic fields from 3 kHz to 300 GHz [IEE06]. ICNIRP guidelines are for limiting exposure to time-varying electric and magnetic fields [ICN10]. In IEEE Std. C95.1-2005, the maximum permissible exposure of head and torso is 205 μT for general public and 615 μT for persons in controlled environments at the frequency 100 kHz [IEE06]. While the maximum permissible exposure for the limbs has more terlerence, the magnetic fulx density is 1130 μT for both general public and in occupational environment [IEE06]. The magnetic field strength exposure limitation for whole body is 163 A/m for both general public and controlled environments [IEE06].

The typical human exposure safety ICNIRP standard gives limitations of human magnetic field as the function of operating frequency from 1 Hz to 10 MHz, which is shown in Figure 1.2. ICNIRP guidelines also give the human exposure safety limitation of EMF in the workplace (occupational or controlled environments) and public (uncontrolled environment) [ICN10]. Figure 1.2 shows ICNIRP guidelines for human exposures EMF emission limitation in occupational and public environment: 100 μT for workers and 27 μT for general public from 3 kHz to 10 MHz in the vicinity of other equipment [ICN10]. It is observed to see that ICNIRP guidelines are more rigorous and conservative compared with IEEE standards. In this thesis, the ICNIRP guidelines are applied for human exposure safety limitation standards.

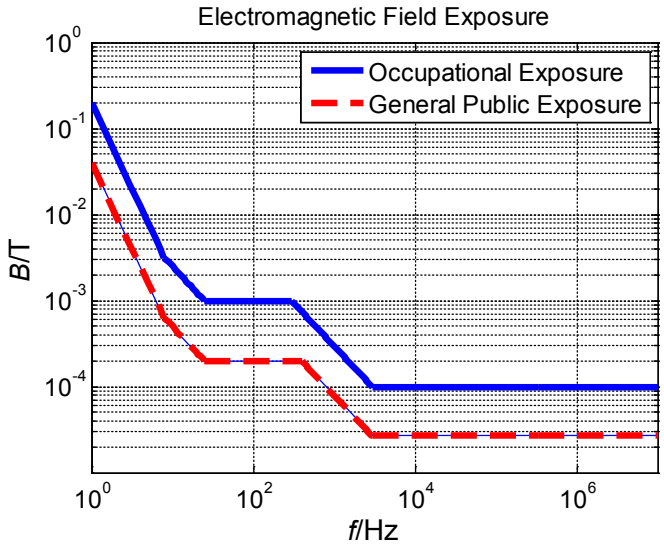

Figure 1.2 Electromagnetic field emission levels published by ICNIRP in 2010 (representation of resources in **[ICN10]**)

1.2.3 EMC Testing

The EMC standards not only provide guidance of the limitations for different applications, but also provide the basis for EMC testing and measurement methods [WuT16]. EMC testing can be divided into EMI and EMS testing [WIK16a]. This thesis just discusses the EMI testing aspects. The EMI testing instruments usually include EMI Test Receiver or EMI analyzer, isotropic field probe, loop antenna and RF cable [Spi15]. EMI testing is intended to confirm that the electronic devices satisfy the magnetic field strength emission limitations in ICNIRP 2010 guidelines. Therefore, an isotropic field probe or loop antenna is

used to measure the EMF emission levels from the WPT system, which is shown in Figure 1.3. This WPT system is also named as the device under test (DUT) [Nar16,Roh01]. An oscilloscope is very useful to capture pulse waveforms in the time domain for pulse emissions [Tek13]. The measurements must be taken in all directions around the DUT to determine the maximum radiated emissions [ITU15]. The measurement setup for magnetic field strength emission of WPT systems is shown in Figure 1.3. The power supply provides the voltage to the WPT system. An insulation panel is placed between the WPT system and a turn table. The maximum magnetic flux density is measured with a loop antenna by rotating the WPT system with a turn table. The distance between loop antenna center and front face of the WPT system is regarded as measurement distance.

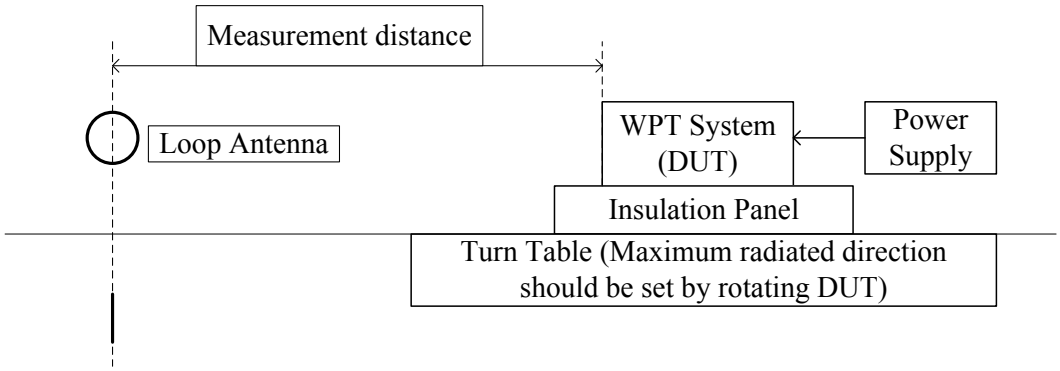

Figure 1.3 EMF emission of WPT systems setup at 100 kHz frequency (representation of resources in **[ITU15]**)

1.2.4 Method for Improving EMC

In order to improve the EMC of electronic products, grounding, shielding and filtering are the three main methods to restrain EMI [Irs13]. In this thesis, the shielding approach is chosen as the most effective technique to reduce the EMF emission generated from WPT systems [Elm96].

The shielding method is the basic and most important solution for reducing electromagnetic emission and protecting electronic systems from electromagnetic disturbance [Ahn13a]. There are two purposes accomplished by using shielding technology for WPT systems. First, it is used to restrict or reduce the radiation of electromagnetic energy generated in the interior region, which are not allowed to propagate in the specified space or exceed certain values in the specified space. Secondarily shielding is used to prevent incoming EMF emission from entering certain zones [Irs13]. The familiar mechanisms of shielding are conductive

shielding, magnetic shielding, active shielding and passive shielding [Kim14]. The shielding structure design could be aimed at the bottom of the transmitter coil and above of the receiver coil [Tan02]. On one hand, the coupling factor between the transmitter and receiver will be strengthened by the shielding and therefore, the efficiency of the WPT system is increased. On the other hand, the leakage magnetic field is suppressed by the shielding structure reducing external emissions [Kim12a].

1.3 State of the Art

This thesis focuses on realizing wireless charging for consumer electronic portable devices, such as tablet, mobile phone, laptop and so on. In Section 1.1.2 the author discusses and analyzes different transfer methods. It is easily concluded that MRCPT has the advantage of high efficiency with tolerance for transfer distances from several centimeters to meters [LuX15]. Therefore, MRCPT technology is the ideal method for wireless charging of consumer electronic devices. However, the WPT systems have challenges with transmission efficiency involving reduction due to radial and axial misalignment and the corresponding inconvenience for precise receiver positioning [Bar15]. What's more, human exposure safety is the essential outside of WPT systems [Bar15]. The author researches the MRCPT method in this thesis and solves existing problems of WPT systems for mobile devices application, such as transfer efficiency, received power level, longer transfer distance, convenience for consumers and safety issues. Scientists have already done a lot of research and made contribution to different aspects about WPT systems summarized in Table 1.4, which are related to the work this thesis focuses on.

Table 1.4 State of the art summarization

System Model	Objective	Method
Topologies	robustness WPT transmission efficiency	four-coil WPT systems [Ram11]
	maximum both PTE and PDL	three-coil WPT systems [Kia11]

System Model	Objective	Method
Impedance matching	minimize the reflection	L-matching network [Beh13] or π-matching network [Wat12] is used in WPT systems
	increase transfer efficiency	adjust coupling factors [Che10]
Multiple hops	increase transfer distance, improve transfer efficiency	*n* nonadjacent resonators between transmitter and receiver [Lee12b]
Multiple receivers	good performance of overall efficiency	transmitter located between two receivers [Kur10]
Multiple transmitters	improve efficiency	receiver located between two transmitters [Lee13]
	localization	impedance amplitude variation [Son09],
	free positioning	selected excitation of coil array according to receiver position [Zho11]
Additional components to WTP systems	EMC friendly, minimize EMF noise	active resonant loop coil [Ahn11]
		passive resonant loop coil [Kim13b]
		conductive shielding (aluminum or copper) [Tan16]
	minimize EMF noise and improve WPT efficiency	magnetic shielding (ferrite) [Kim12b]

Topology of two-coil, three-coil and four-coil WPT systems comparison and analysis: The efficiency of the two-coil WPT systems is sensitive to transmission distance variations. A four-coil WPT system has been proposed to reduce or eliminate this disadvantage of two-coil WPT systems. [Kum09,Kur07]. The four-coil WPT systems consist of transmitter primary coil and secondary coil, receiver primary coil and secondary coil separately. The two-coil WPT systems have only primary and secondary coils [Ram11]. The prototype four-coil system has robustness for WPT transmission efficiency versus distance, which can achieve more than two times than transmission efficiency of a two-coil WPT system having the same coils size and transmission distance [Ram11,LiX12]. The primary coil and the secondary coil quality factor (Q) has a very strong effect on the transmission efficiency. In the four-coil WPT system, the transmission efficiency has little sensitivity to the quality factor of the primary coil of transmitter and secondary coil of receiver [Ram11]. What's more, four-coil WPT system can be designed to achieve better impedance matching [Che11,Par11,Duo11,Che10]. More details will be given in the section on "impedance matching for WPT systems".

In [Kia11], the authors point out power transfer efficiency (PTE) and power delivered to the load (PDL) are the two most important parameters for WPT systems. The maximum PTE and PDL cannot be achieved simultaneously with the same load resistance in the four-coil configuration WPT systems. The PTE could not reach more than 50% when the PDL is maximized for a given load resistance [Hui14]. A three-coil configuration is proposed, which can provide the high PTE as well as high PDL simultaneously for a given load resistance [Kia11]. The coupling factor of the three-coil system is higher than that of two-coil system, which leads to higher system efficiency and produces frequency bifurcation phenomenon (see 2nd paragraph below) [Moo14]. The three-coil system is also able to shift the current stress from the drive coil to the intermediate coil and maximize the coupling factor by producing larger intermediate current. Therefore, the transfer efficiency of three-coil configuration is increased over the two-coil WPT system [Zho15b].

Impedance matching for WPT systems: Matching the impedance is necessary for the *LC* circuit in order to minimize the reflection from the resonators to the source [Beh10]. In the equivalent circuit for the impedance matching (IM) system, the source is defined as Z_{source}, the load is defined as Z_{load}. The delivered power achieves the maximal value when Z_{source} is equal to the conjugate of Z_{load} [Beh13]. The parameters of the IM circuit are changed to adjust resonant frequency to 13.56 MHz for different transfer distances, so as to reach the maximal transfer

efficiency [Beh10,Beh13,Wat12]. The *L*-matching network has the advantage of simplicity, while the π-matching network allows the freedom to choose at high quality factor *Q* so as to increase the WPT systems efficiency [Beh13]. The automated impedance matching system adopts the *L*-matching network on the transmitter side [Beh13]. The WPT systems efficiency could be increased by minimizing the parameter *S*11, which is the ratio of power reflected from the resonator back to the power source [Beh13]. The π-matching network is used for reducing the reflection as presented in [Wat12]. As well as parasitic matching optimization is proposed to maximize the transmission scattering parameter *S*21 [Wat12], which is defined in [Sam11].

When the WPT system operates at several MHz, the frequency bifurcation will occur if the coupling factor between transmitter secondary coil and receiver primary coil k_{23} increases to high enough. The author names this point as k_{critical}, which is the demarcation point between the over coupled and under coupled regime [Sam11]. When k_{23} is smaller than k_{critical}, this is called the under coupled region, and if k_{23} is bigger than k_{critical}, the system is at over coupled [Sam11]. The system parameters can be modified for maximum power transfer [Sam11]. This is accomplished by decreasing coupling factors between the transmitter primary/secondary coil, receiver primary/secondary coil to satisfy the condition given in equation (1.2) [Sam11]. The resonant frequency splits in two (bifurcates) with one frequency is increasing and the other decreasing. Except when the system parameters are adjusted for maximum transfer efficiency, the automatic split resonant frequency tuning method can be used for maximum power transfer [Par11]. The author found that the input impedance is almost equal to the load impedance at the split resonant frequency in the strongly coupled region [Par11]. In this case, impedance matching can be realized by tracking the split resonant frequency and adjusting the source frequency to the split resonant frequency [Par11].

$$k_{23} = k_{\text{critical}} \tag{1.2}$$

Authors in [Che10,Duo11] also proposed that the maximum efficiency can be improved by adjusting coupling factors among resonators, transmitter primary coil and receiver secondary coil in four-coil WPT systems. The maximum system efficiency can be reached by adjusting the transfer gap among the transmitter primary coil, transmitter secondary coil, receiver primary coil, and receiver secondary coil to unify the coupling factors [Che11]. k_{12}, k_{23} and k_{34} stand for coupling factors of the primary coil and secondary coil of transmitter, transmitter secondary coil and receiver primary coil, the receiver primary coil and secondary

coil separately. The three coupling factors are set according to (1.3), which is achieved by adjusting the transfer gap of the resonators, transmitter primary coil and receiver secondary coil [Che11].

$$k_{12} \cdot k_{34} / k_{23} = 1 \tag{1.3}$$

Energy delivered through multiple hop relay coils: Improving the transmission efficiency with longer transfer distance is an important issue for WPT systems. The relay resonators can lengthen the transmission distance and increase the WPT efficiency [Zha11]. A two-hop WPT system for motion-free capsule endoscopy inspection is presented in [Sun12]. The power relay coil in the patient's jacket has strong coupling with transmitter coils installed under the floor. Then the power relay coil in the jacket transfers energy to the capsule in the patient's body via loose coupling [Sun12]. The resonant WPT system is set up with a coaxially arranged intermediate coil and a perpendicularly arranged intermediate coil between the transmitter and the receiver [Kim11]. Experiment results show that the efficiency of the coaxially arranged intermediate WPT systems is greatly increased and the transmission distance can be extended while maintaining the same efficiency [Kim11].

A WPT system using from three up to *n* nonadjacent resonators is proposed in [Lee12b], as shown in Figure 1.4. The multiple resonator system is optimized with three parameters, that is frequency, load and transmission distance [Lee12b]. When the average distance between two resonators is fixed, the maximum efficiency can be achieved by optimizing load resistance. For an optimally spaced WPT system, the load and spacing between each two resonators are optimized parameters [Lee12b]. If the average distance is smaller, the optimal frequency will shift away from the resonant frequency [Lee12b]. With the given overall distance and number of resonators, authors noticed the efficiency is maximum if the spacing between first two resonators and last two resonators is smaller than average distance [Lee12b]. This fact can also explain the phenomenon of two coupling coils applied for both transmitter and receiver coils to increase the system efficiency effectively [Zho13]. The authors proved that more resonators can increase transfer efficiency for a fixed transfer distance, as well as the fact that a system with *n* optimally located resonators has a higher efficiency than one with *n* equally spaced resonators [Lee12b].

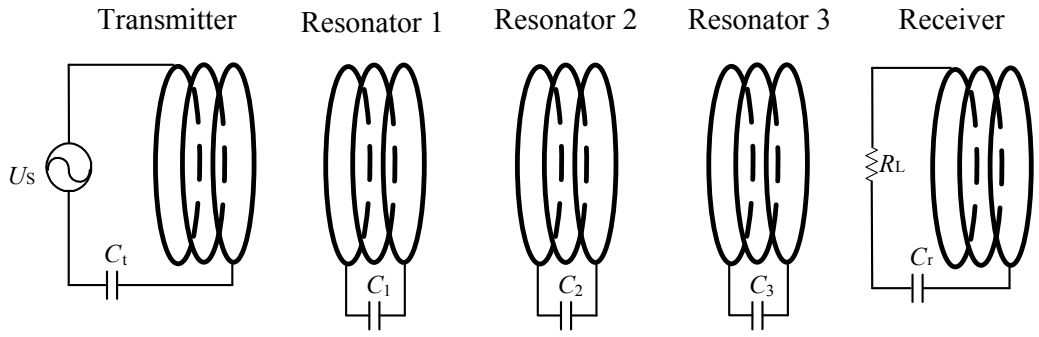

Figure 1.4 Multiple hops WPT systems (representation of resources in **[Lee12b]**)

W.X. Zhong *et al*. proposed WPT systems having a domino-resonator with non-coaxial axes and circular structures, which uses the phenomenon of current vector counteraction and reinforcement when the frequency is equal to the resonant frequency of the resonators [Zho12]. The authors also found that this effect was eliminated for circular structured WPT systems using an odd number of resonators [Zho12]. In 2013 the use of Tesla resonators in domino form for WPT systems was proposed in [Zho13]. In this paper it is proved by theory and measurement that the transmission efficiency when using unequal distance distributions between resonators has higher transmission efficiency than when using equal distance distributions. The distance between the first two resonators and the last two resonators should be smaller than the normal distance between relay resonators [Zho13].

Multiple transmitter coil and multiple receiver coil WPT systems: The MIT group proposed a magnetic resonant coupling WPT system, which has a large source coil providing power to multiple small load coils [Can09]. However, when two receiver coils are close to each other, there is strong magnetic field coupling between them, which leads to coupled mode splitting of the resonant peak [Can09]. A control circuit can be used to track the resonant frequency shift and adjust the receiver capacitors to solve this splitting problem [Can09]. Another multiple receiver geometry has the transmitter located between two receivers, which are equidistant from the source coil, as presented in Figure 1.5. The multiple receiver approach has good performance in terms of overall WPT system efficiency [Kur10]. However, the receiver coil which is further from the transmitter has lower transfer efficiency than the closer receiver. Impedance matching and power division techniques applied at the receiver side can control the amount of power delivered to the different receiver coils [Ean12].

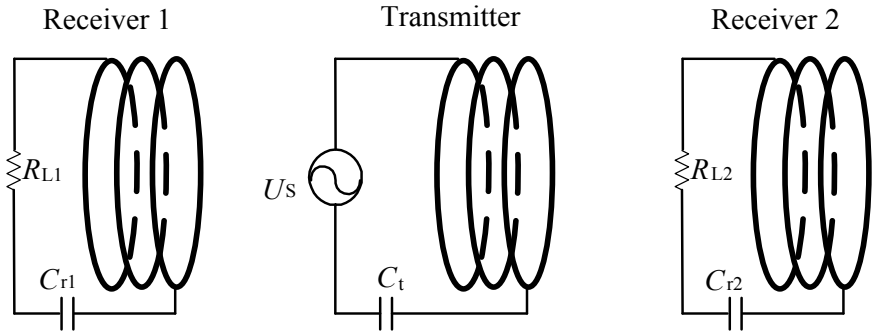

Figure 1.5 Multiple receiver coil WPT systems (representation of resources in **[Kur10]**)

Multiple transmitter coils can be used for WPT system as well as multiple receivers. Multiple transmitter coils are proposed to provide high transfer efficiency as the distance between transmitter and receiver coils increases [Lee13]. The receiver coil is placed between two transmitter coils. The advantage of this approach is the efficiency remains high even if the relative positions between transmitter and receiver coils varies including angular alignment and angular misalignment [Lee13]. Similarly, a transmitter coil array is proposed to improve the transfer efficiency for the case when the receiver coil has a rotation angle with respect to the transmitter coil array [Ood11], as shown in Figure 1.6. For this case, the transmitter power supply needs to supply power to the coils at different phase angles according to the angular orientation of the receiving coil [Ood11]. A transmitter array with four square coils in a 2×2 arrangement that has different resonant frequency because of mutual coupling between transmitter coils [Miw13], is presented in Figure 1.7. The transfer efficiency can reach 80%, independent of the receiver position, because of the homogeneous magnetic field generated by the transmitter coil array at the common resonant frequency 11.28 MHz [Miw13]. Zhong *et al*. proposed a single layer winding transmitter array providing free-positioning, having a receiver coil structure made up of cylindrical ferrite cores, for portable consumer electronic products that has efficiency in the range of 86% - 89%, for power less than 5W [Zho11], as presented in Figure 1.8. The novel winding array uses hexagonal packing of solenoids as the optimal transmitter geometry [Zho11]. A variable position WPT system through multiple cooperative flux generators is developed in [Sch11]. The advantage of this system is that the magnetic field is confined and the receiver has spatial freedom of movement in the charging area. As well as the cooperative transmitter is easy to construct and control [Sch11].

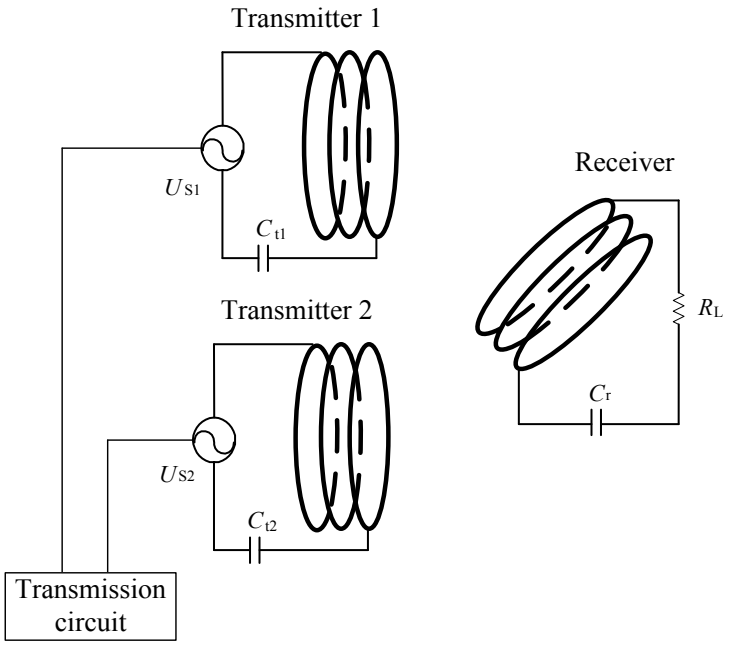

Figure 1.6 Two transmitter coils WPT systems (representation of resources in **[Ood11]**)

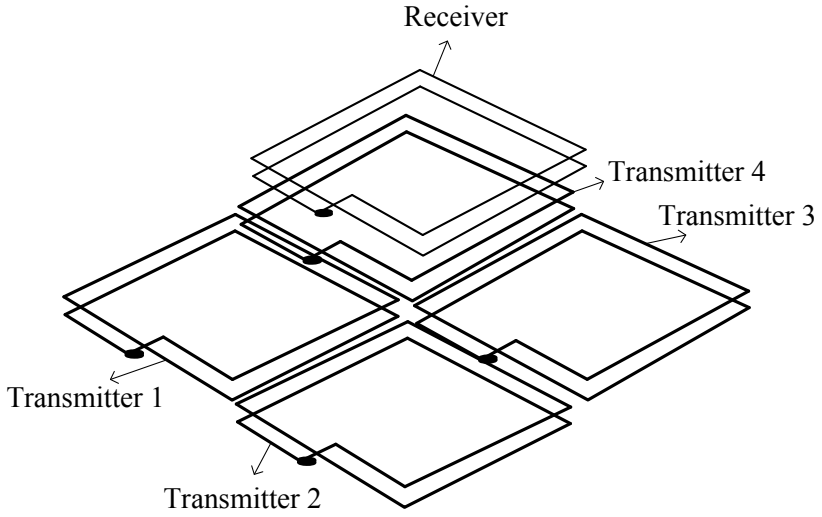

Figure 1.7 WPT systems using transmitter array (representation of resources in **[Miw13]**)

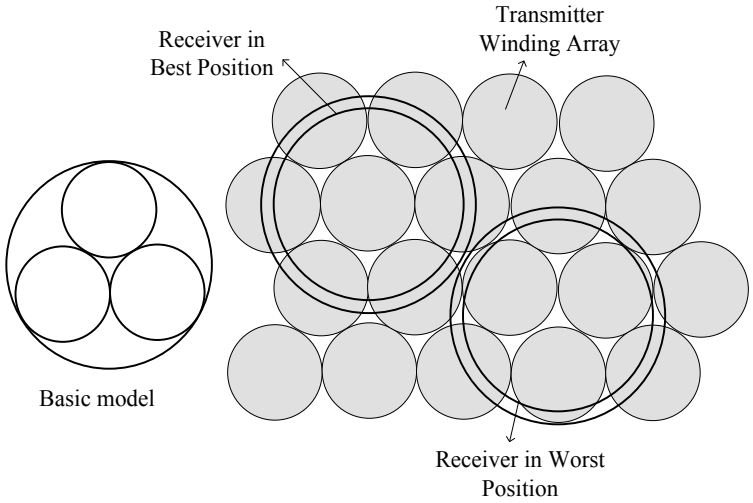

Figure 1.8 WPT systems using single layer of hexagonally packed transmitter winding array (representation of resources in **[Zho11]**)

Some authors did research on WPT systems with respect to both multiple transmitters and multiple receivers, which is shown in Figure 1.9. A rectangular spiral with blunted corners is used as the transmitter coil [Cas09b]. The space between each adjacent turns is different. That is to say, the increasing rate of radius of the transmitter coil gradually reduces. The uniform magnetic field is achieved by adjusting the space between every adjacent two turns [Cas09b]. The blunted corners are used in the rectangular spiral coil. This structure can weaken the saltation effect because of the corners, ensuring a smooth distribution at a fixed transmission distance [Cas09b]. *M* primary coils in parallel have an advantage over one single primary coil because the inductance value of the primary coils in parallel is smaller than that of a single coil. Thus, the transmitter side amplifier is less sensitive to variations [Cas09a]. In addition, the power delivered to an individual receiver coil is more stable in the system with multiple secondary coils. However, the receiver coils are not completely decoupled [Cas09a]. The results show that multiple transmitter coils are feasible and effective for supplying power to multiple receiver coils simultaneously [Cas09a]. The concept of the coupling factor between multiple transmitter coils and receiver coils is proposed by [Ahn13b]. In this case, either the driving frequency or the resonant frequency should be adjusted to maximize the transfer efficiency due to the change in resonant frequency because of the coupling in the transmitter or receiver sides [Ahn13b].

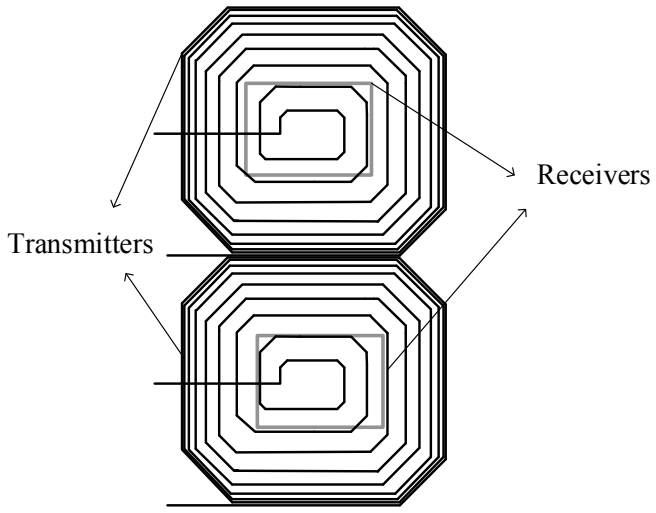

Figure 1.9 WPT systems with multiple transmitter coils and multiple receiver coils (representation of resources in **[Cas09a]**)

Localization with multiple transmitter coils: In the medical application of capsule endoscopy inspection, patients are allowed to walk freely above transmitter coils. The patient's position is detected by pressure sensors and used to switch on transmitter coils which are close to the patient [Sun12]. Position detection for capsule endoscope is also achieved by using small and flat arrayed coils which are connected in parallel [Yam13]. In this case, the capsule endoscope's position is detected by measuring the terminal voltage variation for each coil. The approach is based on the theory that the largest voltage variation occurs in the primary coil which has the shortest distance between the transmitter coil and receiver coil [Yam13]. The transmission efficiency is also improved by the large array of coils [Yam13]. The single layer winding transmitter array enables multiple receiver coils to be placed and charged on a wireless charging pad in a free-positioning manner [Zho11]. The size of the receiver is much larger than the single coil in the transmitter array. That is to say, the receiver coil covers at least one transmitter coil completely [Zho11]. The selected primary coils are switched on according to the localization of the receiver coil [Zho11].

The localization system presented in [LiH10] uses eight magnetizing coils for localization in vitro, as presented in Figure 1.10. The eight coils are activated alternately to produce an electromagnetic field that generates the voltage in the receiver load [LiH10]. The eight equations resulting from the voltages for each coil of eight coils are dependent on receiving coils' position and orientation angle which are regarded as unknown parameters. Solving the eight equations provides the location and orientation of the receiver coil [LiH10].

Not only the detecting the receiver position but also detecting the type of load has been demonstrated with a contactless wireless power desktop consisting of multiple transmitter coils [Son09], as shown in Figure 1.11. The authors propose a "scanning" method to energize each coil and measure the impedance. The type of load device is decided by the difference between calibration impedance of individual primary windings and actual measurement impendence values [Son09]. The system could successfully detect the load coil positions and distinguish different load types from the measurement results [Son09].

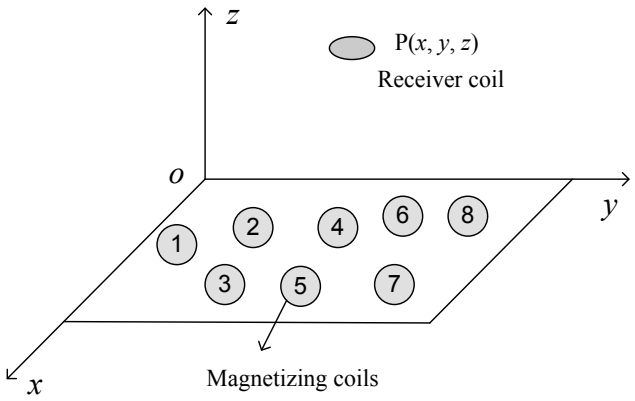

Figure 1.10 Localization model of WPT systems with eight magnetizing coils (representation of resources in **[LiH10]**)

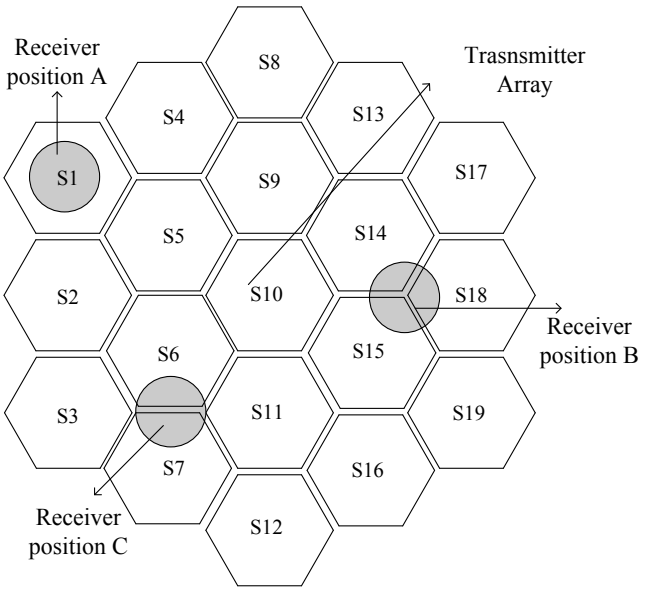

Figure 1.11 Primary hexagon spiral windings arrangement for WPT localization systems (representation of resources in **[Son09]**)

Different shielding methods: Four different shielding methods have been previously described in Section 1.2.4. For the magnetic shielding method, the magnetic material is required to have high permeability, low conductivity and, provide a low reluctance path [Ahn13a]. Therefore ceramic magnetic material Mn-Zn ferrite is a good shielding material for WPT systems [Ahn13a]. The rectangular ferrite material is used for 100 W class LED TV WPT systems in [Kim12b]. The eddy currents induced in the conductive material cancel part of the magnetic field generated by the source, therefore achieving good shielding [Ahn13a]. A lot of researchers have proposed an optimization method which combines magnetic material and metallic material for improving the efficiency and decreasing the magnetic field leakage [Kim12b,Tan02,Ahn13a], as presented in Figure 1.12.

Both active and reactive shielding methods produce the opposite magnetic field to minimize the EMF generated from the source [Kim14]. The reactive resonant loop shielding is adopted for OLEV presented in [Kim13b]. Five resonant strongly coupled loop coils are placed beside WPT systems, which reduces the magnetic field below the required limit for human exposure according to ICNIRP guidelines [Kim13b]. Active shielding is also used for OLEV, however, the active resonant loop coil requires an additional power source. What you should notice is that the current direction in the active resonant loop coil must be controlled to assure that the magnetic field direction generated by the active loop and the WPT system are in opposition [Ahn11].

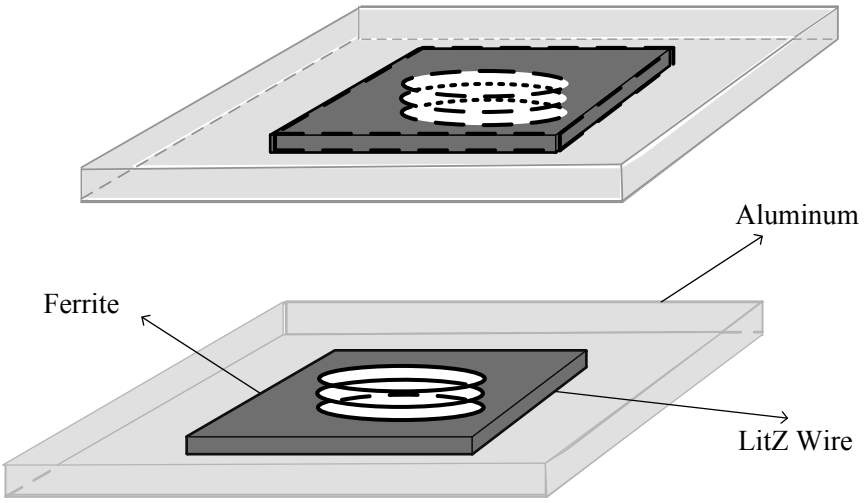

Figure 1.12 Shielding model for WPT systems with magnetic and metallic material (conceptual representation of resources in **[Son09]**)

1.4 Criticism on State of the Art

The author has elaborated on different aspects and achievements related to previous work on WPT systems with respect to efficiency, load power improvement, transfer distance, convenience and human exposure safety in Section 1.3. However, some related work of WPT systems needs further development. Therefore, it is necessary to criticize and point out shortcomings of the available research results. Leading to areas where the capability and performance of WPT systems could be further reinforced and improved.

As far as the system topology to be concerned, three-coil and four-coil WPT systems are preferred due to higher transfer efficiency than that of two-coil WPT systems [Ram11,Moo14]. However, high PDL and high PTE, which are design goals for WPT systems, could not be achieved at the same time in the four-coil WPT systems [Kia11]. It is possible to optimize the geometry and parameters of each coil in the three-coil WPT systems to achieve the best performance. Therefore, three-coil WPT systems are preferred and chosen in this thesis.

Multiple hop WPT systems are proposed so as to increase the transmission distance. However, the optimal frequency is shifted slightly from the resonant frequency because of the cross-coupling effect in multiple power paths [Lee12b]. For a fixed transfer distance, more resonators leads to smaller spacing between adjacent resonators, which results in larger cross-coupling effects [Lee12b]. Therefore, multi-hop WPT systems are not easy to establish, control and handle.

Multiple transmitters and receivers are one of the main research topics for WPT systems. Although the overall efficiency of a multiple receiver coil WPT systems is increased, the efficiency for a single receiver coil is relatively low [Kur10]. As the number of receiver coils increases, eventually the overall efficiency of a WPT system will become saturated. However, the power transfer efficiency of each individual receiver coil is reduced [Kim10]. Moreover, the coupling effect between multiple transmitters and multiple receivers results in the driving frequency or resonant frequency having to be adjusted [Ahn13b]. It is difficult to track the variable resonant frequency and complex to operate the multiple transmitter and multiple receiver WPT systems. Therefore, in author's opinion, multiple receiver WPT systems are not an effective method to increase efficiency.

There are three main advantages enabled by the use of multiple transmitters: increasing efficiency, free-positioning and localization, which is also presented in

Table 1.4. The single layer winding transmitter array permits the receiver coil to be charged while being freely placed in the charging area [Zho11]. The system is compatible with the "Qi" standard, which allows the power in the load of the receiver to reach up to 5 watts so far now. However, this WPT system is applicable only for short-range transmission [Zho11]. Therefore, the use of a multiple transmitter array results in limitations of power level and application range. This thesis is an attempt to increase the transmission distance while guaranteeing high efficiency and maintaining free-positioning of the receiver.

Localization is realized by detecting the difference between impedance amplitude calibration values and measurement values [Son09]. Although this method can determine which transmitter coil is nearest to the receiver coil, accurate position of receiver cannot be determined. This type of localization system is applicable for short-range transfer distance, restricted to distances on the order of mm. Moreover, due to the number of transmitter coils, the system is complex and difficult to establish and control [Son09]. Different magnetic field strength generated from eight coils can provide a localization solution based on theoretical analysis and solving the resulting equations [LiH10]. It seems like this method could accurately determine the receiver coil position. Nevertheless, this theory has not been verified by experiments. Hence the eight equations for coil voltages is not a reliable approach to localize the receiver with a multiple transmitter coil array WPT system. Consequently it is essential to propose a reliable and accurate localization method for improving the performance of WPT systems.

Magnetic shielding has the disadvantage of reducing the magnetic field, and conductive shielding using metallic material results in eddy currents leading to reduced mutual inductance and self-inductance and lower efficiency of WPT systems [Son16,Kim13a]. An example that uses aluminum or copper plate arranged above the receiver coil for the shielding has been tested but the efficiency was reduced as demonstrated by experiment [Tan16]. Some authors presented a combination of aluminum and ferrite plates arranged on the bottom of the transmitter and on the top of the receiver [Kim12b]. With this combination the shielding region is restricted above the top of the receiver and under the bottom of the transmitter. In designing for a practical WPT systems application, the shielding region could be adjusted by designing the shielding geometry using different shielding methods according to the desired shielding domain and required protection.

1.5 Motivation and Contribution

1.5.1 Objective and Motivation

Based on the background of the WPT development and drawbacks of WPT technology as discussed in Section 1.4, the important issues to be solved are high transmission efficiency, mid-range transmission distance, flexibility and convenience, and human exposure safety. The goals for WPT systems developed in this thesis are that mobile devices being charged are allowed to move freely above the transmitter array with 4-5 W received power in 10 cm transmission distance with more than 65% transfer efficiency. The WPT systems should be in power saving mode, that is to say, only one set of 4 overlapping coils are switched on when the receiver is close to center of that set. It is worth noting that the energized coils of the transmitter matrix are expected to have less effect on other neighboring devices. Therefore, it is essential to localize the position of mobile device to determine which transmitter coils should be in excitation mode. Above of all, the goals of high transmission efficiency, mid-range transmission distance, small influence to surroundings, localization function and free-positioning characteristics are for improving performance of WPT systems. Human exposure safety outside of the WPT systems is very important. Also the WPT systems should be EMC friendly in the shielded region. The emission values of magnetic fields and electric fields in the human accessible region should comply with IEEE and ICNIRP safety guidelines.

1.5.2 Tasks, Methodology and Contributions

To achieve the objective as described in Section 1.5.1, this thesis focuses on the improvement of system efficiency, the robustness of WPT system to position of the device to be charged and human exposure safety. First of all, SR-SR (series resonance - series resonance) topology has better performance than other topologies in terms of WPT systems' parameters in this thesis. In order to increase the transmission efficiency and received power simultaneously, three-coil WPT systems are adopted. Secondly, the author optimizes WPT systems with a single transmitter coil. The parameters of a single transmitter (TX) and receiver (RX) coils, such as radius, number of turns, thickness, are optimized to achieve maximum transmission efficiency with respect to quality factor Q and coupling factor k according to transmission distance. Thirdly, a 4-coil structure transmitter is proposed based on field forming theory. All four coils are series connected and overlapped with each other, as presented in Figure 1.13. In order to determine the

effect of field forming, the transfer efficiency of a traditional single transmitter coil is compared with that of a 4-coil structure transmitter.

Next, one of the important features of this thesis is that the receiver can move freely above the charging pad. The effective charging area is the transmitter matrix defined as 20 cm × 20 cm, which is based on using multiple 4-coil structure transmitters as presented in Figure 1.13. For 10 cm transmission distance, the radius of the single coil transmitter is optimized as 10 cm, described in Section 3.3.2. The optimized radius of each single coil in the 16 coils transmitter matrix is about 7 cm based on the weighted overall efficiency, described in Section 4.4.3.1. The size of the receiver coil should be selected so as to fit mobile or portable devices. Thus the inner radius of the receiver coil is set at about 3 cm. Therefore, the size of a traditional single coil transmitter or a single coil in the transmitter matrix is bigger than that of the receiver coil assumed in this thesis. The coil of the transmitter array presented in [Zho11] is smaller than the receiver coil, as shown in Figure 1.8. Therefore, the receiver coil would always cover several coils of the single layer transmitter array [Zho11]. However, it is possible that the vertical position of the receiver coil is located in the outer 4-coil structure. That is to say the receiver is located above at blank area of the charging area. In order to avoid this, each 4-coil structure transmitter overlaps adjacent coils. Each adjacent 4 coils, also called 4-coil structure, in the transmitter matrix is regarded as the power supply unit, which is switched on separately according to different positions of receiver. All of the analyses for the results mentioned above in this section were carried out in Matlab, COMSOL, or by experimental verification.

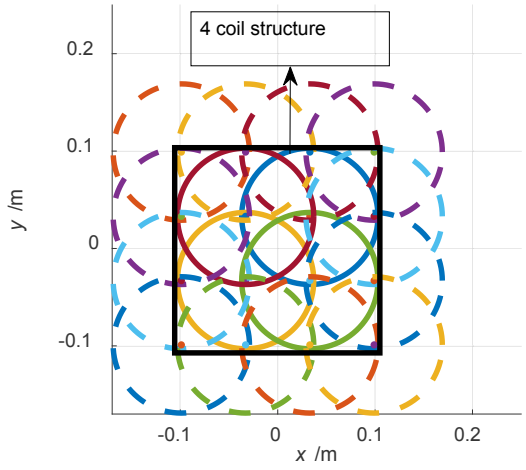

Figure 1.13 Transmitter matrix based on 4-coil structure (found by the author)

The use of a multiple coil matrix is proposed for use in WPT systems because it will enable free location of the device to be charged within a large charging area. However, in order to maintain high efficiency and power transfer, the proposed system requires knowledge of the location of the receiving coil in order to select the correct 4-coil array to activate for charging. The position of receiver coil can be detected using the grid search algorithm, reflected impedance for combined coils algorithm and the Gauss-Newton algorithm. The grid search algorithm is realized by calculating and measuring coupling factors between each coil of the transmitter matrix and the receiver located in the charging area. Each coil of the transmitter matrix is switched on one by one, and all the coupling factor values are stored in the table. All the possible positions of the receiver can be estimated coarsely by turning on the first coil of the transmitter matrix. Measurement with the second coil can narrow down the latent positions of receiver. Then switch on third coil, fourth coil and so on until the accuracy of receiver's position is in the tolerance range, as presented in Section 5.2.2.1. The reflected impedance algorithm for combined coils is based on measurement of the reflected resistance of each 4-coil structure in the transmitter matrix. Although accurate receiver position cannot be determined by this algorithm, it can determine the best 4-coil structure for charging as the one having the maximum reflected resistance. The Gauss-Newton algorithm supposes the initial position of receiver first. Then magnetic flux density nearby WPT systems is predicted by measuring the received voltage with a tiny inductance coil. The receiver coordinates are obtained by solving 16 equations based on magnetic flux density using a non-linear regression iteration method.

Consideration has been given to the electromagnetic field from the strongly coupled magnetic resonant coils in accordance with IEEE and ICNIRP human exposure safety limitation values for magnetic fields and electric fields. The target shielding region is set as the domain adjacent to the WPT systems and potential area for human occupancy. In order to improve the transmitter efficiency and reduce the magnetic field in the region to be shielded, ferrite plates are arranged under the transmitter and above the receiver. An aluminum plate is placed beside the WPT systems at 2 cm distance away. Then following the aluminum plate is a reactive shielding resonant loop coil, which can further reduce the magnetic field strength. The shielding design for the WPT systems is presented in Section 5.4.7. The shielding effect is verified by simulation of COMSOL 5.1 and efficiency improvement is proved with hardware demonstration.

Innovative ideas and contributions of this thesis include,

1. Optimize WPT systems with the traditional single coil in transmitter and two coils in the receiver (Section 3.3),

2. Design and optimize 4-coil structure transmitter based on field forming theory, which has less influence to surroundings comparing with single transmitter coil (Section 4.2),

3. Design and optimize a new overlapping multiple coil transmitter matrix based on 4-coil structure, which permits the receiver to be charged allowing free-positioning with high transfer efficiency (Section 4.4),

4. Electromagnetic localization with grid search algorithm in terms of resonant magnetic coupling factor between TX and RX, reflected impedance for combined coils algorithm, as well as Gauss-Newton algorithm (Section 5.2),

5. A composite shielding method is designed, presented and demonstrated in terms of IEEE and ICNIRP human exposure safety limits for magnetic field strength (Section 5.3).

1.6 Organization of the Dissertation

In Chapter 2, the related basic theory is introduced. Then the WPT system is described with parallel resonance (PR) and series resonance (SR) topology in the transmitter and the receiver. Four different topologies are analyzed and the best topology SR-SR is selected according to parameters in the circuit model, which are also analyzed in terms of WPT systems performance. Two-coil configuration, three-coil configuration and four-coil configuration WPT systems are analyzed and compared. In order to increase the system efficiency and load power simultaneously, the three-coil configuration WPT systems are selected by the impendence matching method.

In Chapter 3, the multi-layer helical coil model is analyzed and the parameters (wire property, radius of the coil and number of turns) of coil are optimized. The best TX and RX model is chosen based on the quality factor of the coil. The WPT efficiency is not only affected by qualify factor but also the coupling factor k_{23} between the TX and RX. The geometry of the transmitter and the receiver coils are optimized to obtain the maximal transfer efficiency for a given transmission distance. The receiver size is also taken into consideration because of the size limitation of portable devices.

In Chapter 4, a single coil structure, a 4-coil structure and a 9-coil structure are proposed based on field forming theory. The 4-coil structure is chosen because it has obvious field forming effect. A new multiple coil, 4 coils, 9 coils, 16 coils and 25 coils transmitter matrix is designed based on multiple 4 coils sub elements. First, the radius of each transmitter matrix is optimized using the weighted overall efficiency. Then the geometry of the multiple coil matrix is optimized, as well as choosing the best transmitter matrix based on cost efficiency. The mobile device has the advantage of free movement in the charging area. Only one set of 4 coils is activated corresponding to when the mobile device is close to center of that 4-coil structure. The other coils in the transmitter matrix are in standby mode.

In Chapter 5, the electromagnetic localization system and shielding for WPT systems are presented. Several methods of calculating the coupling factor between TX and RX are introduced and developed. The receiver's position is detected in the multiple coil transmitter matrix by the grid search algorithm. The reflected impedance for combined coils method is used for estimating receiver coarse position to decide which 4-coil structure can be switched on. The localization of the receiver using the Gauss-Newton algorithm is demonstrated by Matlab simulation. Electromagnetic radiation from WPT systems is reduced and the magnetic field is strengthened by a composite shielding method. COMSOL has been used to simulate the effect of shielding structures for WPT systems composed by aluminum, ferrite and reactive resonant loops.

In Chapter 6, the full H-bridge and rectifier circuit are introduced and used for generating the AC current for the transmitter and converting from AC to DC current for the load with the frequency of 100 kHz. Then SR-SR, SR-PR, PR-SR and PR-PR topology WPT systems are tested and compared. Three-coil WPT systems are verified to have better performance than two-coil WPT systems. The demonstration shows the efficiency differences that result between optimized traditional single transmitter and 4-coil structure WPT systems using field forming. The receiver position is estimated with coupling factors measured by two different methods. The Gauss-Newton algorithm is compared with the grid search algorithm with respect to position accuracy. The reflected resistance of 4-coil structure of transmitter matrix is measured with lateral misalignment between TX and RX. The 4-coil structure can be always selected correctly with all of three localization algorithms. Finally, a shielding structure for WPT systems using ferrite is presented.

In Chapter 7, the work accomplished in this thesis is concluded and the results of the research are summarized. In addition the outlook for future research is discussed.

Chapter 2

WPT Systems Modeling and Characteristic Theory Analysis

2.1 Chapter Overview

This chapter introduces basic theories about electromagnetic resonant wireless power transfer and analyzes the energy transfer mechanism. A general overview of WPT system design is presented based on circuit theory. The calculation method of transmission efficiency and load power is explained for different circuit topologies and different WPT system configurations. Parameters of quality factor, coupling factor and load resistance are analyzed which have an important effect on the performance of WPT systems. The circuit topology can be divided as SR-SR, SR-PR, PR-SR and PR-PR. By analyzing the four circuit topologies, the best circuit topology in terms of load power and system efficiency turns out to be SR-SR and is therefore chosen for further development in this thesis. The simplest basic WPT system configuration consists two coils, a transmit coil and a receive coil. This is termed the two-coil system. However resonant coupling coils can be added to improve the reliability and performance of WPT systems. In this thesis we have analyzed three configurations: (1) the simple two-coil configuration, (2) three-coil configuration having one coupling coil added on the receiver side and (3) the four-coil configuration with coupling coils added on both the transmit and receive side. The three-coil configuration is determined to be the best for providing high power transfer and efficiency simultaneously.

The chapter is organized as follows. In Section 2.2, the related basic theory in terms of WPT systems is introduced. In Section 2.3, WPT systems using the four circuit topologies mentioned above are presented and modeled and the factors that influence performance of a WPT system are analyzed. In Section 2.4, models of the different configurations of WPT system, two-coil, three-coil and four-coil, are compared and analyzed. Section 2.5 summarizes this chapter.

2.2 Related basic Theory

2.2.1 The Near Magnetic Field

The near magnetic field is also known as the reactive near field, as opposed to the radiation near field or far field. The reactive near field region is regarded as distance of 0.159 multiplied by the wavelength [Ume11]. The transmitter and the receiver react through near field by inductor or capacitor coupling. When a second device with a load is in the near field closest to the transmitter, the power source will supply power to the antenna with a load when it is needed. If the energy is not absorbed in the receiver, the emitted energy is stored and returned to the transmitter. The transmitter will not supply more power to the receiver [WIK17]. When the energy goes back to near field by electromagnetic wave, the energy is lost due to the primary coil, not because of radiation. There is a complex interrelation between magnetic field and electric field in the reactive near field, which combines as an alternating EMF wave [Ume11]. At one point in the reactive near field region, the magnetic field or electric field dominates depending on the type of antenna. For the small loop antenna, the magnetic field is likely to dominate in the reactive near field [Che07].

The characteristics of the reactive near field are as follows: There is no definite ratio relationship between the strength of the magnetic field and strength of electronic field in phase and amplitude [ITU05]. The electromagnetic field strength decreases sharply with the transmission distance ($1/d^3$), resulting in the magnetic field being inhomogeneous [ITU05]. It is obvious that the near electromagnetic field strength is larger than that of far field. From the point view of energy, the electric field and magnetic field are orthogonal, that is to say, the electric field lags behind the magnetic field by 90 degrees, which results in the real part of Poynting vector being zero [Bar10]. Thus, the energy in the reactive near field is only exchanged between the electric and magnetic fields. The reactive near field energy is not radiated outward due to these characteristics [Ume11]. However, for communications the far or radiation field is used to transmit signals

long distances. Thus, the radiation field is widely used, while the reactive near field is often neglected and avoided [Chi04].

2.2.2 Resonance Circuit Theory

2.2.2.1 *RLC* Series and Parallel Resonance

Resonance for a physical system is defined as: the natural vibration frequency of a system. When the physical system is forced to vibrate by an external source, the amplitude of the forced vibration will be increase to a maximum as the frequency of the external source approaches the inherent frequency of the physical system. Resonance phenomenon appears in different types of physical systems, such as acoustic resonance, mass-spring resonance, circuit resonance and so on [Vat16]. The WPT systems proposed in this thesis use resonant circuits. According to circuit theory, resonance can be two types, which are series resonance and parallel resonance. In the following, these two resonance circuits are analyzed.

The series resonance circuit consists of a fixed frequency sine wave excitation added in series with a resistor *R*, ideal inductance *L* and capacitor *C*. The typical series resonance circuit composed by *R L C* is shown in Figure 2.1 [Sca70].

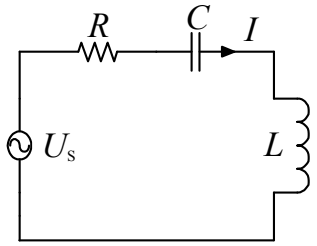

Figure 2.1 Series resonant circuit (representation of resources in **[Sca70]**)

Its equivalent impedance is shown in (2.1),

$$Z = R + j(\omega L - \frac{1}{\omega C}) \tag{2.1}$$

At the resonant frequency $\omega = \omega_0$, the inductive reactance and capacitive reactance cancel each other in the circuit. The imaginary part (IM) of (2.1) is 0 in the resonant circuit, shown in (2.2).

$$\mathrm{Im}\left[Z(j\omega_0)\right]=0 \tag{2.2}$$

Let $\omega_0 L-1/\omega_0 C=0$, the resonant angular frequency and frequency is shown as (2.3) and (2.4) separately.

$$\omega_0=\frac{1}{\sqrt{LC}} \tag{2.3}$$

$$f_0=\frac{1}{2\pi\sqrt{LC}} \tag{2.4}$$

The impendence is minimum when the circuit is resonant and equal to pure resistance, value of *R*. Meanwhile, the current in the circuit is maximum given in (2.5),

$$I_0=\frac{U_\mathrm{s}}{R} \tag{2.5}$$

The voltage across the inductor and capacitor are U_L and U_C respectively.

$$U_\mathrm{L}=j\omega_0 L I_0 \tag{2.6}$$

$$U_\mathrm{C}=-j\frac{1}{\omega_0 C}I_0 \tag{2.7}$$

Quality factor can be determined by the ratio of the voltage of the inductor or the capacitor to the resistance voltage. The phase of the inductor voltage is the inverse of the capacitor voltage. That is to say, the supply voltage is equal to the voltage across the resistor because the inductor voltage and the capacitor voltage cancel out [Sca70]. The physical significance of quality factor is the stored energy to the energy loss in the load [Sca70]. The higher the quality factor, the less energy consumed by the load in every cycle.

$$Q_\mathrm{s}=\frac{U_\mathrm{L}(\omega_0)}{U_\mathrm{R}}=\frac{U_\mathrm{C}(\omega_0)}{U_\mathrm{R}}=\frac{\omega_0 L}{R}=\frac{1}{\omega_0 CR}=\frac{1}{R}\sqrt{\frac{L}{C}} \tag{2.8}$$

Parallel resonance means that the appropriate frequency sin wave excitation is added in a circuit having a resistor, ideal inductor and capacitor in parallel. The

typical parallel resonance circuit composed by *R L C* is shown in Figure 2.2 [Sca70]. The equivalent admittance is given as

$$Y = G + j(\omega C - \frac{1}{\omega L}) \tag{2.9}$$

At resonance, the imaginary part of the circuit admittance is zero, which is shown as

$$\mathrm{Im}\left[Y(j\omega_0)\right] = 0 \tag{2.10}$$

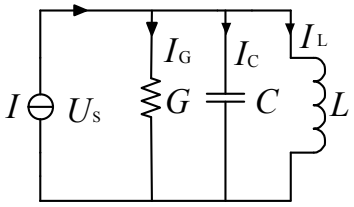

Figure 2.2 Parallel resonant circuit (representation of resources in **[Sca70]**)

Let $\omega_0 L - 1/\omega_0 C = 0$, the resonant angular frequency and frequency is shown in (2.3) and (2.4). The admittance has the minimum value of *G*. In another words, the input impendence is maximum, $Z(j\omega_0) = R$. Thus the terminal voltage (the voltage of the inductor and capacitor) is maximum. The current of the inductor and the capacitor is shown in (2.11) and (2.12) separately [Sca70].

$$I_L = \frac{U_s}{j\omega_0 L} = -j\frac{I}{\omega_0 LG} \tag{2.11}$$

$$I_C = j\omega_0 C U_s = j\frac{\omega_0 CI}{G} \tag{2.12}$$

If the circuit is resonant, the inductor current and the capacitor current have the relationship $I_L + I_C = 0$. The supply current is equal to the admittance current. Consequently, parallel resonance is also called current resonance. The quality factor is calculated as [Sca70],

$$Q_p = \frac{I_L}{I} = \frac{I_C}{I} = \frac{1}{Q_s} \tag{2.13}$$

2.2.2.2 Comparison between Series Resonance and Parallel Resonance Circuit

After comparison and analysis, the series resonant circuit and parallel resonant circuit have some similar characteristics. First, the expression for the resonant frequency is the same. Second, the equivalent impedance of these two resonant circuits is pure resistance. However, the equivalent impedance for a series resonant circuit is minimum, while the impedance of a parallel circuit is maximum. Consequently, the current is maximum in the series resonant circuit but minimum in the parallel resonant circuit. Third, for both circuits the inductor and capacitor voltage is Q times the source voltage. When the circuit is parallel resonant, the current is minimal. The inductance current and capacitor current is Q times the supply current.

2.2.2.3 The Energy Relationship in the Resonant Circuit

Take the series resonant circuit Figure 2.1 as an example. The loop current phase is same as the supply current. The angular frequency is the resonant frequency ω_0. The input loop current $i(t)$ and voltage source $u(t)$ are expressed as (2.14), where I_m, U_sm and t are peak current, peak voltage and time separately.

$$i(t) = I_\mathrm{m} \sin \omega_0 t, \quad u(t) = U_\mathrm{sm} \sin \omega_0 t \tag{2.14}$$

The consumed power in the resistor is P_R and the output power of source is defined as P_in.

$$P_\mathrm{R} = I_\mathrm{m}^2 R \sin^2 \omega_0 t \tag{2.15}$$

$$P_\mathrm{in} = U_\mathrm{sm} I_\mathrm{m} \sin^2 \omega_0 t = I_\mathrm{m}^2 R \sin^2 \omega_0 t \tag{2.16}$$

The power from the power supply is consumed completely in the load resistor. The inductance and the capacitor are energy storage elements. The magnetic energy stored in the inductance is W_L and the electric energy stored in the capacitor is W_C [Sca70].

$$W_\mathrm{L} = \frac{1}{2} L I^2 = \frac{1}{2} L I_\mathrm{m}^2 \sin^2 \omega_0 t = \frac{1}{2} L I_\mathrm{m}^2 \left(\frac{1}{2} - \frac{1}{2} \cos 2\omega_0 t \right) \tag{2.17}$$

$$W_{\mathrm{C}}=\frac{1}{2}CU_{\mathrm{C}}^{2}=\frac{1}{2}C\left[\frac{I_{\mathrm{m}}}{\omega_0 C}\sin\left(\omega_0 t-90^{\circ}\right)\right]^{2}=\frac{1}{2}LI_{\mathrm{m}}^{2}\left(\frac{1}{2}+\frac{1}{2}\cos 2\omega_0 t\right) \quad (2.18)$$

The total stored energy in the resonant loop circuit at any time is W_0,

$$W_0=W_{\mathrm{C}}+W_{\mathrm{L}}=\frac{1}{2}LI_{\mathrm{m}}^{2} \quad (2.19)$$

In one cycle T, the energy consumed in the load is W_{R}

$$W_{\mathrm{R}}=\int_0^T I_{\mathrm{m}}^{2}R\sin^{2}\omega_0 t dt=\frac{1}{2}RTI_{\mathrm{m}}^{2} \quad (2.20)$$

It is noticed that the sum of the magnetic energy and the electric energy is constant. The magnetic energy and the electric energy exchange at a rate equal to twice the frequency of the power source. Only the load resistor consumes energy in the circuit.

2.2.3 Mutual Inductive Coupled Circuit

An inductively coupled circuit transfers energy form one side to another side by using two or more closed loop circuits which have mutual coupling. The side connected to the power source is the primary circuit. Another side connected with the load, which can receive power, is called the secondary circuit. For inductive circuits the coupling is termed mutual inductance. Traditional power transformers transfer power through mutual coupling according to law of electromagnetic induction. Figure 2.3 shows the circuit diagram of an inductively coupled circuit. R_2, R_3, R_{L} are resistance of primary coil, secondary coil and load separately. L_2 and L_3 are the inductance of the primary coil and secondary coil separately. And M_{23} is the mutual inductance between the primary coil and secondary coil [Auv15].

Equation (2.21) gives the Kirchhoff Voltage Law (KVL) equations for the mutual inductive coupled circuit [Auv15].

$$\begin{cases}U_{\mathrm{s}}=I_2\left(j\omega L_2+R_2\right)-j\omega M_{23}I_3\\ 0=-j\omega M_{23}I_2+I_3\left(j\omega L_3+R_{\mathrm{L}}+R_3\right)\end{cases} \quad (2.21)$$

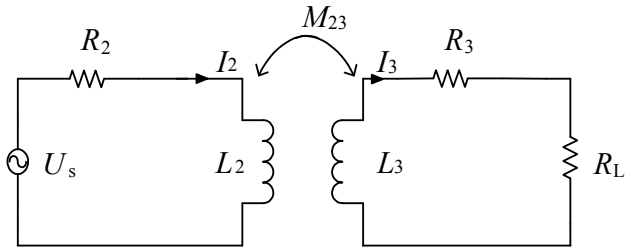

Figure 2.3 Mutual inductive coupled circuit (representation of resources in **[Auv15]**)

The current of the primary circuit I_2 and the secondary circuit I_3 is shown as

$$\begin{cases} I_2 = \dfrac{U_s}{R_2 + j\omega L_2 + \dfrac{\omega^2 M_{23}^2}{R_L + R_3 + j\omega L_3}} \\ I_3 = \dfrac{j\omega M_{23} U_s}{\left(R_2 + j\omega L_2\right)\left(R_L + R_3 + j\omega L_3\right) + \omega^2 M_{23}^2} \end{cases} \tag{2.22}$$

According to the current expressions in (2.22), the primary and the secondary decoupled circuits of Figure 2.3 can be represented as two separate circuits as shown in Figure 2.4. $Z_2 = R_2 + j\omega L_2$ is the impedance of the primary circuit. Z_r is the equivalent impedance, which reflects from the secondary circuit to the primary circuit. The equivalent reflected impedance is a function of the coupling between the transmitter and the receiver, and is used to evaluate WPT system performance [Tem10].

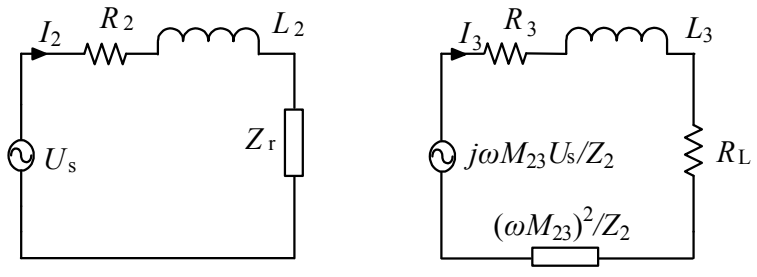

(a) Primary circuit (b) Secondary circuit

Figure 2.4 Mutual inductive decoupling circuit (conceptual representation of resources in **[Tem10]**)

The reflected impedance is shown as (2.23) [Tem10], the negative sign in X_r means the inductance in the secondary circuit becomes the capacitor in the primary circuit.

$$\begin{cases} Z_r = \dfrac{\omega^2 M_{23}^2}{j\omega L_3 + R_3 + R_L} = R_r + jX_r \\ R_r = \dfrac{\omega^2 M_{23}^2 \left(R_3 + R_L\right)}{\left(R_3 + R_L\right)^2 + \omega^2 L_3^2} \\ X_r = -\dfrac{\omega^2 M_{23}^2 L_3}{\left(R_3 + R_L\right)^2 + \omega^2 L_3^2} \end{cases} \tag{2.23}$$

2.3 Resonant WPT Systems Modeling and Analysis

2.3.1 System Overview

As mentioned in Section 2.2.2, when the inherent frequency of the resonator composed of and an inductor L and a capacitor C is the same as the external excitation frequency, the circuit is operating at resonance. The sine wave AC current generates an alternating magnetic field. While the most of the alternating electric field is constrained in the capacitor the magnetic field expands beyond the inductor. If another LC resonator with the same intrinsic frequency is placed in the effective domain of the magnetic field of the first resonator, an induced IEF is generated in the second resonator according to Faraday's Law of electromagnetic induction. That is to say, the second resonator has an excitation source with the same frequency. The secondary inductance L_3 becomes the source driving the second resonant circuit. Thus energy is transferred from the primary resonator to the secondary resonator, which is shown as Figure 2.5 [Zhe15,Tah12].

A general overview of WPT systems is shown in Figure 2.6. An AC power source is connected to the transmitter (primary coil). The receiver is assumed to be placed at a variable distance away from the transmitter, up to 10 cm to avoid the need of direct placement on some sort of the charging pad. The user can for example keep the device inside a bag or his pocket and it is still be able to be charged. The magnetic field induces power into the pick-up coil at the receiver side and powers the connected load, which could be a mobile or another portable device.

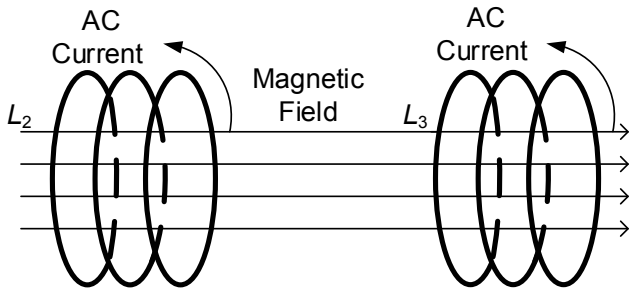

Figure 2.5 Magnetic resonance WPT principle (representation of resources in **[Zhe15]**)

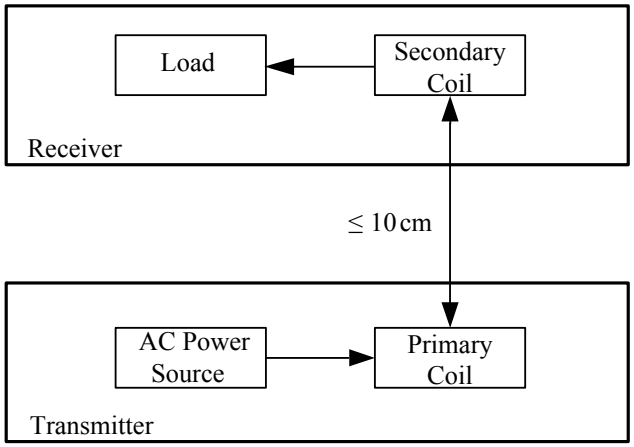

Figure 2.6 Wireless power transfer system model (derived by the author)

The design of WPT systems involves many parameters, like the shape of coils (circular, rectangular, spiral, etc), the radius of the coils, the number of windings, the circuit diagram and many other parameters that affect the performance of the system. For WPT systems the interrelated parameters of the transmitter (TX) and the receiver (RX) are adjusted so that both operate at the same frequency. The circuit is resonant to achieve higher magnetic coupling.

The efficiency of WPT systems can be defined as the ratio of the received power in the load to the delivered power from the power source. This is a strong function of the quality factor of the coils and the coupling factor between TX and RX [Kes13a]. For restricted size associated with portable devices, the attainable transmission efficiency is increased with increasing the number of turns of the receiver coil. This is because the coil resistance increases linearly with the number of turns but the inductance of the coil increases as the square of the number of turns. Thus, increasing the number of turns results in the higher Q coil, which increases the system efficiency. The frequency and load resistance also have an

obvious effect on system efficiency [Pra12]. The operational frequency for the WPT systems proposed in this thesis is 100 kHz. The induced IEF in the receiver coil is proportional to integral of the time-variant magnetic field produced by the transmitter over the area of the coil. The more the area and number of turns of the receiver, the more the induced IEF the receiver will get. This leads to an increase of the transmission efficiency and load power [Rön13]. However, the receiver coil must conveniently fit into mobile devices.

In order to understand WPT systems in-depth, it is important to analyze and compare system topology models. As well as the influence of other factors effecting WPT system performance with respect to different parameters (such as coupling factor, quality factor, inductance, load resistor), which are as presented in Section 2.3.2 and Section 2.3.3 separately.

2.3.2 System Topology Models

2.3.2.1 Overview

There are four different resonant circuit topologies that can be used in the transmitter and receiver. They are SR-SR, SR-PR, PR-SR and PR-PR separately, which are presented in Figure 2.7 [Wan05]. U_s is the power source, R_s is the inner resistance of power source. L_2 and L_3 are inductances of the primary and secondary coil. R_2 and R_3 are the inner resistances of the primary coil and secondary coil. C_2 and C_3 are the turning capacitors for the transmitter and receiver circuits. R_L is the load resistance. $I_{2series}$, $I_{3series}$, $I_{2parallel}$ and $I_{3parallel}$ are the series and parallel connection currents through the transmitter and the receiver coils, and M_{23} is the mutual inductance between the primary coil and the secondary coil [Pra12].

The series and parallel connection impedance of transmitter is presented as Z_{2s} and Z_{2p} separately [Wan05].

$$\begin{cases} Z_{2s} = R_s + R_2 + j\omega L_2 + \dfrac{1}{j\omega C_2} \\ Z_{2p} = R_s + \dfrac{1}{j\omega C_2 + \dfrac{1}{j\omega L_2 + R_2}} \end{cases} \tag{2.24}$$

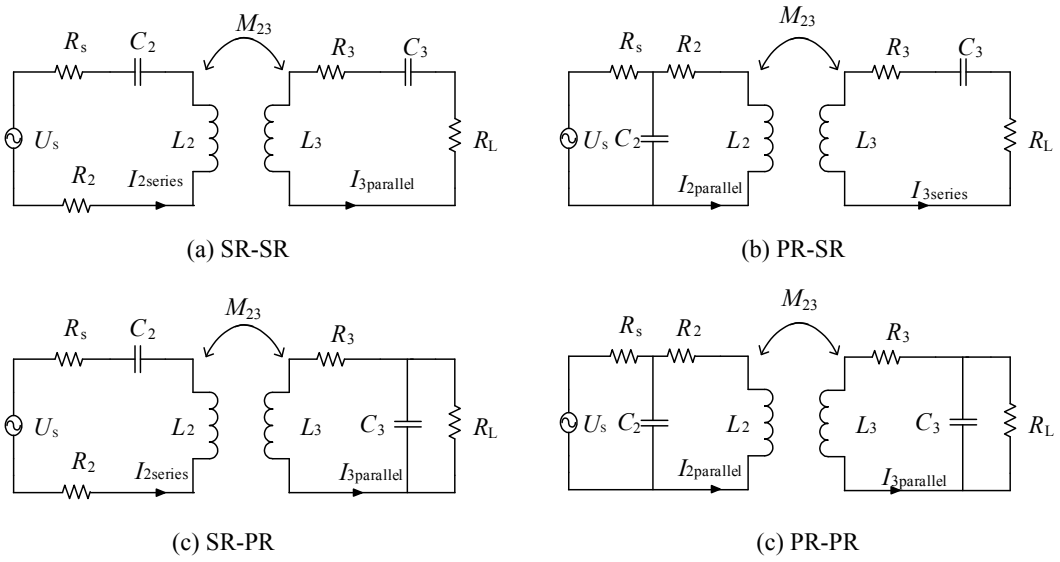

Figure 2.7 Four resonant coupling topologies of WPT systems (representation of resources in **[Auv15]**)

And the Z_{3s} and Z_{3p} are the impedance of series and parallel connection circuit at the receiver [Wan05].

$$\begin{cases} Z_{3s} = R_3 + R_L + j\omega L_3 + \dfrac{1}{j\omega C_3} \\ Z_{3p} = j\omega L_3 + R_3 + \dfrac{1}{j\omega C_3 + \dfrac{1}{R_L}} \end{cases} \tag{2.25}$$

2.3.2.2 Series Versus Parallel at the Receiver

The higher the quality factor of the receiver, the better performance a WPT system can have. Figure 2.8 (a) and (b) presents the series and parallel connection receiver circuit respectively. The impedance transformation of the parallel circuit Figure 2.8 (b) at the receiver is shown in Figure 2.8 (c) [Ram11]. The quality factor of receiver coil Q_3 is defined as $Q_3 = \omega_0 L_3 / R_3$.

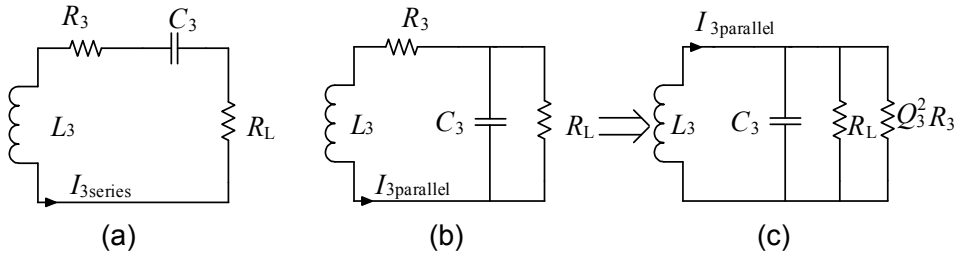

Figure 2.8 Receiver topologies (a) Series circuit (b) Parallel circuit (c) Impedance transformation of parallel circuit (representation of resources in **[Ram11]**)

The quality factor of series circuit and parallel circuit is shown as (2.26).

$$\begin{cases} Q_{3\mathrm{sc}} = \dfrac{\omega_0 L_3}{R_3 + R_\mathrm{L}} \\ Q_{3\mathrm{pc}} = \dfrac{R_\mathrm{L}\omega_0 L_3}{R_3 R_\mathrm{L} + \left(\omega_0 L_3\right)^2} \end{cases} \tag{2.26}$$

The difference of quality factor between the series and parallel circuit is given in (2.27) [Ram11].

$$Q_{3\mathrm{pc}} - Q_{3\mathrm{sc}} = \frac{\omega_0 L_3 R_\mathrm{L}^2 \left[1 - \left(\dfrac{\omega_0 L_3}{R_\mathrm{L}}\right)^2\right]}{\left(R_3 + R_\mathrm{L}\right)\left(R_3 R_\mathrm{L} + \left(\omega_0 L_3\right)^2\right)} \tag{2.27}$$

If $\omega_0 L_3 / R_\mathrm{L} > 1$, the series circuit has a higher quality factor than the parallel circuit. That is to say, the series resonance circuit in the receiver improves the efficiency with a small load resistor, while the parallel resonance in receiver is preferred with a larger load resistor. In this thesis, the operating frequency is 100 kHz, the load R_L range is from 0 to 80 Ω. The inductance of the receiver L_3 is several hundred micro Henry. So the series connection configuration at the receiver is more efficient.

The compensation capacitor for the parallel or series connection receiver circuit is shown in (2.28).

$$C_3 = \frac{1}{\omega_0^2 L_3} \tag{2.28}$$

The available power from the transmitter is affected by the reflected impedance from the receiver. The reflected resistance and reactance for both series and parallel connection in the receiver is given in (2.29) and (2.30) respectively [Liu08,Wan04].

$$Z_{23s}=\begin{cases}\dfrac{\omega^4 M_{23}^2 C_3^2\left(R_3+R_L\right)}{\omega^2 C_3^2\left(R_3+R_L\right)^2+\left(\omega^2 L_3 C_3-1\right)^2}, & \text{reflected resistance}\\ -\dfrac{\omega^3 M_{23}^2 C_3\left(\omega^2 L_3 C_3-1\right)}{\omega^2 C_3^2\left(R_3+R_L\right)^2+\left(\omega^2 L_3 C_3-1\right)^2}, & \text{reflected reactance}\end{cases} \tag{2.29}$$

$$Z_{23p}=\begin{cases}\dfrac{\left(\omega M_{23}^2\right)^2\left(R_3+R_L\right)+\omega^4 M_{23}^2 C_3 R_L^2 R_3}{\left(R_3+R_L-\omega^2 L_3 C_3 R_L\right)^2+\omega^2\left(L_3+C_3 R_3 R_L\right)^2}, & \text{reflected resistance}\\ \dfrac{\omega^3 M_{23}^2\left(C_3 R_L^2-\omega^2 L_3 C_3^2 R_L^2-L_3\right)}{\left(R_3+R_L-\omega^2 L_3 C_3 R_L\right)^2+\omega^2\left(L_3+C_3 R_3 R_L\right)^2}, & \text{reflected reactance}\end{cases} \tag{2.30}$$

As the receiver is resonant circuit, then substitute (2.28) into (2.29) and (2.30) separately. The impedance reflected to the source for both series and parallel resonance receiver coils is given in Table 2.1 [Wan04].

2.3.2.3 Series Versus Parallel at the Transmitter

For series resonance at the transmitter, the voltage of the capacitor and inductor cancel. Therefore, the high voltage required from the source is reduced. When the transmitter is parallel resonant, the current through the capacitor compensates the reactive component of the primary winding and decreases the requirement for current power supply. Thus, a low impedance, (voltage) power supply is used for the series resonant transmitter, whereas the parallel resonant circuit requires a high impedance (current) power supply [Pra12].

Transmitters in series connection and parallel connection are shown in Figure 2.9 (a) and (b) respectively. The parallel resonance configuration and impedance transformation are presented in Figure 2.9 (b) and (c). The transmission efficiency is proportional to the current through the inductance, as well as the total admittance of the transmitter circuit. The larger the current is the larger the magnetic field strength generated. For the parallel connection, the series resistance

R_2 is transformed into $Q_2^2 R_2$. Q_2 is the quality factor of the primary coil shown as $Q_2 = \omega_0 L_2 / R_2$ [Jay14].

Table 2.1 Reflected impedance of resonance receiver

Topologies of Receiver	Reflected Resistance	Reflected Reactance
Series	$\frac{\left(\omega_0 M_{23}^2\right)^2}{R_3 + R_L}$	0
Parallel	$\frac{\left(\omega_0 M_{23}^2\right)^2 \left(R_3 + R_L\right) + \omega_0^4 M_{23}^2 C_3^2 R_L^2 R_3}{R_3^2 + \omega_0^2 \left(L_3 + C_3 R_3 R_L\right)^2}$	$-\frac{\omega_0^3 M_{23}^2 L_3}{R_3^2 + \omega_0^2 \left(L_3 + C_3 R_3 R_L\right)^2}$

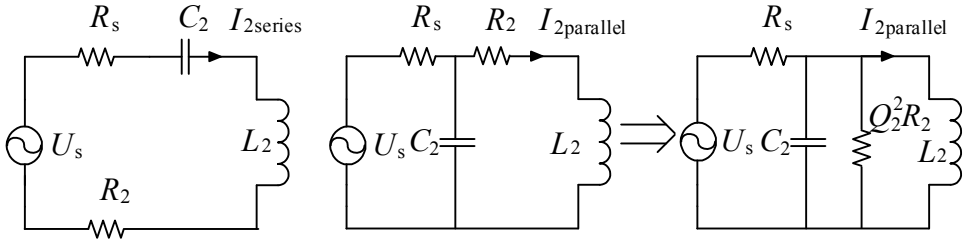

Figure 2.9 Transmitter topologies (a) Series circuit (b) Parallel circuit (c) Impedance transformation of parallel circuit (representation of resources in **[Jay14]**)

If the circuit is resonant, the inductance current $I_{2series}$ and $I_{2parallel}$ of the series circuit and parallel circuit can be written in (2.31) [Jay14].

$$\begin{cases} I_{2series} = \dfrac{U_s}{R_s + R_2} \\ I_{2parallel} = \dfrac{U_s Q_2^2 R_2}{R_s + Q_2^2 R_2} \cdot \dfrac{1}{j\omega_0 L_2} \approx \dfrac{U_s}{j\omega_0 L_2}, \quad Q_2^2 R_2 >> R_s \end{cases} \tag{2.31}$$

The unification terms $u_{2series}$ and $u_{2parallel}$ are given by the admittance G multiply by the current $I_{2series}$ and $I_{2parallel}$ respectively. The unification terms are the evaluation standard the transmitter circuit. The circuit with larger unification has

better performance. This is because the larger current I generates more magnetic field strength, resulting in more induced IEF in the receiver. Thus the load power is larger with larger current in the transmitter coil. Also, the increased admittance means the resistance is less implying lower loss. The transmitter coil resistance is the main part of the energy consumption of WPT systems.

$$\begin{cases} u_{2\text{series}} = G_{2\text{series}} \cdot I_{2\text{series}} = \dfrac{U_{\text{s}}}{\left(R_{\text{s}} + R_2\right)^2} \\ u_{2\text{parallel}} = G_{2\text{parallel}} \cdot I_{2\text{parallel}} = \dfrac{U_{\text{s}}}{R_{\text{s}} + Q_2^2 R_2} \cdot \dfrac{1}{j\omega_0 L_2} \end{cases} \tag{2.32}$$

Compare the unification $u_{2\text{series}}$ and $u_{2\text{parallel}}$, if the parameters satisfy (2.33), that means a series connection configuration would generate more magnetic field strength and have less energy consumed at the transmitter due to smaller resistance. If the inequality of (2.33) is satisfied then the efficiency of WPT systems with series connection is higher than that with parallel connection, and vice versa.

$$u_{2\text{series}} > u_{2\text{parallel}} \Rightarrow \omega_0 L_2 > \sqrt[3]{\left(R_{\text{s}} + R_2\right)^2 R_2} \tag{2.33}$$

In this thesis, the operation frequency is 100 kHz. The inductance L_2 of the transmitter is about several hundred micro Henry. The resistance R_2 is no more than 10 Ω. The internal resistance, R_{S} of the power source is about 0.5 Ω. Substituting these values in (2.33) shows that the series resonant circuit transmitter has better performance than a parallel resonant circuit.

The compensation capacitor of series and parallel circuit is shown in (2.34), where $X_{23\text{sp}}$ and $R_{23\text{sp}}$ are the reflected reactance and resistance of series and parallel receiver circuits [Wan04].

$$C_2 = \begin{cases} \dfrac{1}{\omega_0\left(\omega_0 L_2 + X_{23\text{sp}}\right)}, & \text{series connection} \\ \dfrac{\omega_0 L_2 + X_{23\text{sp}}}{\omega_0\left[R_{23\text{sp}}^2 + \left(\omega_0 L_2 + X_{23\text{sp}}^2\right)\right]}, & \text{parallel connection} \end{cases} \tag{2.34}$$

Substitute (2.34) into the reflected impedance for series and parallel resonance in Table 2.1. Resonance compensation capacitor values in the transmitter side of the

four topologies are given in Table 2.2. It is easily concluded that the primary compensation capacitor of SR-SR topology is independent of the load resistance, receiver coil resistance and mutual inductance. The transmitter circuit of SR-SR is simple to analyze and relatively immune to component variations of WPT systems.

Table 2.2 Resonance capacitor values in the transmitter

Topologies	Compensation Capacitors
SR-SR	$\frac{1}{\omega_0^2 L_2}$
SR-PR	$\frac{1}{\omega_0^2\left(L_2-\frac{\omega_0^2 M_{23}^2 L_3}{R_3^2+\omega_0^2\left(L_3+C_3R_3R_{\mathrm{L}}\right)^2}\right)}$
PR-SR	$\frac{L_2}{\left(R_2+\frac{\left(\omega_0 M_{23}\right)^2}{R_3+R_{\mathrm{L}}}\right)^2+\omega_0^2 L_2^2}$
PR-PR	$\frac{L_2-\frac{\omega_0^2 M_{23}^2 L_3}{R_3^2+\omega_0^2\left(L_3+C_3R_3R_{\mathrm{L}}\right)^2}}{\left(R_2+\frac{\left(\omega_0 M_{23}\right)^2\left(R_3+R_{\mathrm{L}}\right)+\omega_0^4 M_{23}^2 C_3^2 R_{\mathrm{L}}^2 R_3}{R_3^2+\omega_0^2\left(L_3+C_3R_3R_{\mathrm{L}}\right)^2}\right)^2+\cdots}$ $\cdots+\omega_0^2\left(L_2-\frac{\omega_0^2 M_{23}^2 L_3}{R_3^2+\omega_0^2\left(L_3+C_3R_3R_{\mathrm{L}}\right)^2}\right)^2$

2.3.3 Analysis of Energy Transfer Character for SR-SR Topology

2.3.3.1 Transmission Efficiency and Load Power

From the above analysis in Section 2.3.2.2 and Section 2.3.2.3, author chooses the SR-SR as the WPT system topology in this thesis. The energy is transferred from

the transmitter to receiver by electromagnetic induction with compensated series resonant circuits. For SR-SR topology WPT systems, KVL equations of current are shown as (2.35) [Tem10].

$$\begin{cases} U_{\mathrm{s}} = I_2\left(j\omega L_2 + \dfrac{1}{j\omega C_2} + R_{\mathrm{s}} + R_2\right) + j\omega M_{23} I_3 \\ 0 = j\omega M_{23} I_2 + I_3\left(j\omega L_3 + \dfrac{1}{j\omega C_3} + R_{\mathrm{L}} + R_3\right) \end{cases} \tag{2.35}$$

Strong magnetic coupling can be achieved when both transmitter and receiver circuits are resonant at the same frequency. If the circuit is resonant $\omega_0 = 1/\sqrt{L_2 C_2} = 1/\sqrt{L_3 C_3}$, substitute into (2.35), gives the current of the primary coil and secondary coil as

$$\begin{cases} I_2 = \dfrac{U_{\mathrm{s}}\left(R_3 + R_{\mathrm{L}}\right)}{\omega_0^2 M_{23}^2 + \left(R_{\mathrm{s}} + R_2\right)\left(R_3 + R_{\mathrm{L}}\right)} \\ I_3 = -\dfrac{j\omega_0 M_{23} U_{\mathrm{s}}}{\omega_0^2 M_{23}^2 + \left(R_{\mathrm{s}} + R_2\right)\left(R_3 + R_{\mathrm{L}}\right)} \end{cases} \tag{2.36}$$

The load power and the system efficiency is shown as (2.37) and (2.38) separately [Vil15], where P_{in} is input power.

$$P_{\mathrm{L\_SR\_SR}} = \left|I_3\right|^2 R_{\mathrm{L}} = \frac{\omega_0^2 M_{23}^2 U_{\mathrm{s}}^2 R_{\mathrm{L}}}{\left[\omega_0^2 M_{23}^2 + \left(R_{\mathrm{s}} + R_2\right)\left(R_3 + R_{\mathrm{L}}\right)\right]^2} \tag{2.37}$$

$$\eta_{\mathrm{SR\_SR}} = \frac{P_{\mathrm{L\_SR\_SR}}}{P_{\mathrm{in}}} = \left|\frac{I_3^2 R_{\mathrm{L}}}{U_{\mathrm{s}} I_2}\right| = \frac{\left(\omega_0 M_{23}\right)^2 R_{\mathrm{L}}}{\left(R_3 + R_{\mathrm{L}}\right)\left[\left(R_2 + R_{\mathrm{s}}\right)\left(R_3 + R_{\mathrm{L}}\right) + \left(\omega_0 M_{23}\right)^2\right]} \tag{2.38}$$

Let $k_{23} = M_{23}/\sqrt{L_2 L_3}$, define the quality factor of the transmitter and receiver circuits as $Q_{2\mathrm{sc}} = \omega_0 L_2/\left(R_{\mathrm{s}} + R_2\right)$, $Q_{3\mathrm{sc}} = \omega_0 L_3/\left(R_3 + R_{\mathrm{L}}\right)$, which substitute into (2.37), (2.38). The load power and the transmission efficiency could be written as (2.39) and (2.40) [Kia11].

$$P_{\mathrm{L\_SR\_SR}} = \frac{U_{\mathrm{s}}^2}{R_{\mathrm{s}} + R_2} \cdot \frac{k_{23}^2 Q_{2\mathrm{sc}} Q_{3\mathrm{sc}}}{\left(1 + k_{23}^2 Q_{2\mathrm{sc}} Q_{3\mathrm{sc}}\right)^2} \cdot \frac{R_{\mathrm{L}}}{R_3 + R_{\mathrm{L}}} \tag{2.39}$$

$$\eta_{\mathrm{SR\_SR}} = \frac{R_{\mathrm{L}}}{R_3 + R_{\mathrm{L}}} \cdot \frac{k_{23}^2 Q_{2\mathrm{sc}} Q_{3\mathrm{sc}}}{1 + k_{23}^2 Q_{2\mathrm{sc}} Q_{3\mathrm{sc}}} \tag{2.40}$$

Similarly, the transmission efficiency and the load power of SR-PR, PR-SR and PR-PR are calculated with the same methods.

2.3.3.2 The Effect of Coupling Factor

When parameters of the transmitter and receiver are fixed, the coupling factor determines the performance of the WPT system. From (2.40), it is easily to observe that the transmission efficiency monotonically increases with increasing coupling factor. The larger the coupling factor, the larger the transmission efficiency the WPT system has.

However, there is an optimum value of coupling factor for maximum load power as follows [Han10]. Calculate the derivative of (2.39) with respect to k_{23},

$$\frac{dP_{\mathrm{L\_SR\_SR}}}{dk_{23}} = 0 \tag{2.41}$$

We can get $k_{\mathrm{C\_SR\_SR}}$, which is the critical point of the coupling factor.

$$k_{\mathrm{C\_SR\_SR}} = \frac{1}{\sqrt{Q_{2\mathrm{sc}} Q_{3\mathrm{sc}}}} \tag{2.42}$$

Substitute (2.42) into (2.39) and (2.40), the maximum load power and transmission efficiency at the $k_{\mathrm{C\_SR\_SR}}$ point can be expressed as

$$P_{\mathrm{L\_C\_SR\_SR}} = \frac{U_{\mathrm{s}}^2}{4\left(R_{\mathrm{s}} + R_2\right)} \cdot \frac{R_{\mathrm{L}}}{\left(R_3 + R_{\mathrm{L}}\right)} \tag{2.43}$$

$$\eta_{\mathrm{C\_SR\_SR}} = \frac{R_{\mathrm{L}}}{2\left(R_3 + R_{\mathrm{L}}\right)} \tag{2.44}$$

The variation of load power and system efficiency with coupling factor is shown in Figure 2.10 and Figure 2.11 separately. Observing from Figure 2.10 and Figure 2.11, when the coupling factor is 0.013, the load power is maximum, while the transmission efficiency reaches 44.2% at this coupling factor point. It is

concluded that the load power and transfer efficiency cannot be maximal with the same coupling factor. The coupling factor decreases inversely with the third power of the distance between the transmitter and the receiver coils [Lee12a]. Thus the longer transmission distance has significantly lower coupling factors. However, from (2.40), transmission efficiency still increases with increasing quality factors Q_{2sc} and Q_{3sc} even if the transmission distance is large.

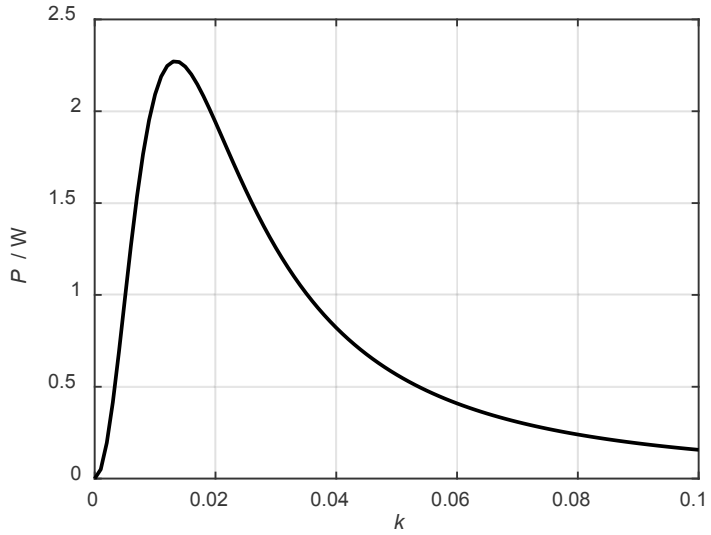

Figure 2.10 Load power versus coupling factor (conceptual representation of resources in **[Han10]**)

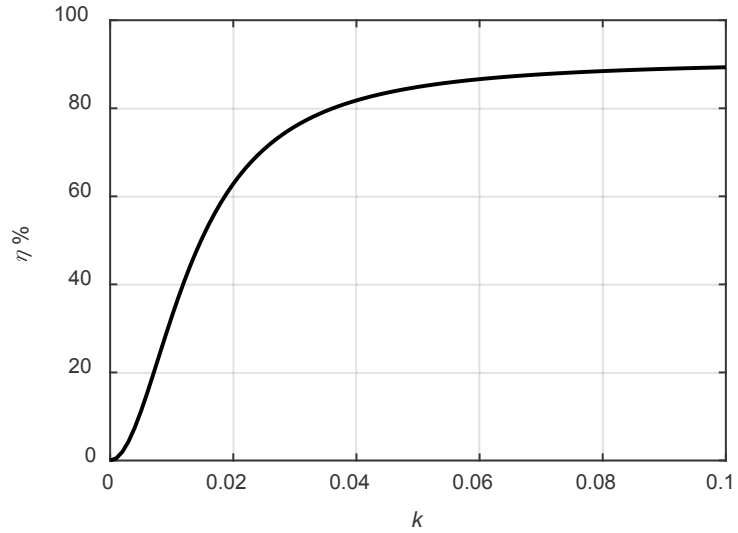

Figure 2.11 Transmission efficiency versus coupling factor (conceptual representation of resources in **[Han10]**)

2.3.3.3 The Effect of Quality Factor

Because the resistance of the receiver coil R_3 is much smaller than the load resistance R_L, the transmission efficiency is mainly decided by the factor $k_{23}^2 Q_{2sc} Q_{3sc}$ from (2.40). We define $FOM = k_{23}^2 Q_{2sc} Q_{3sc}$, which is the demarcation between strong and weak coupling. If $FOM > 1$, the WPT system is classified as using the strong coupling. While if $FOM < 1$, the energy is transferred in the weak coupling mode. This is consistent with coupled-mode theory developed by MIT [Kar07]. The strong coupling regime is regarded as the more efficient energy transfer mode, the condition of which is $\kappa^2 / \Gamma_S \Gamma_D > 1$. κ, Γ_S and Γ_D are coupling coefficient and intrinsic loss rates of the source and device respectively [Kar07,Kur07]. Figure 2.12 presents the transfer efficiency which increases with increased *FOM*. Thus, indicating that the strong coupling mode is an efficient method for WPT systems.

Quality factor is the main determinant for coil design and is affected by the resistance, capacitance and inductance of the coil [Ram11]. The optimization of the coil's parameters will be discussed in Chapter 3. What's more, the internal resistance of the power source, the operational frequency and the load resistance are important factors that influence the load power and WPT system efficiency. In this thesis, the operation frequency is fixed at 100 kHz and the internal resistance of the power source is assumed to be 0.5 Ω.

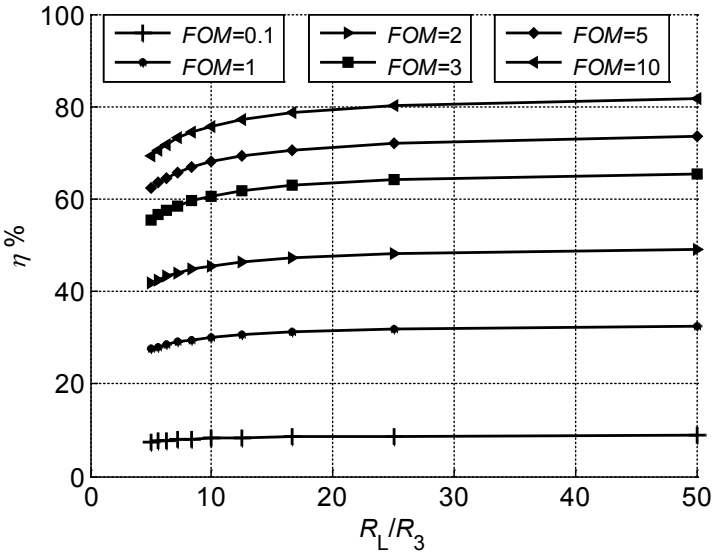

Figure 2.12 Transmission efficiency versus *FOM* (conceptual representation of resources in **[Kar07]**)

2.3.3.4 The Effect of Load Resistance

For a given set of Q_2, Q_3, and k_{23} values, there is an optimal load resistance for maximal load power and transmission efficiency. We take the derivative of (2.39) with respect to load resistance R_L [Zho15c].

$$\frac{\partial P_{L\_SR\_SR}}{\partial R_L} = 0 \tag{2.45}$$

The maximal load power is achieved with the load resistance value shown as (2.46).

$$R_{L\_P\_SR\_SR} = R_3 + \frac{\omega_0^2 M_{23}^2}{R_2 + R_s} \tag{2.46}$$

This value matches the maximum power transfer theorem. When the load is equal to the internal resistance of the source circuit, the load receives maximal power, while the transmission efficiency is just 50% [Hui14].

In order to get the maximal transmission efficiency, we take the derivative of (2.40) with respect to R_L [Zho15c].

$$\frac{\partial \eta_{SR\_SR}}{\partial R_L} = 0 \tag{2.47}$$

The maximal transmission efficiency is achieved with the load resistance value shown as (2.48).

$$R_{L\_\eta\_SR\_SR} = \sqrt{R_3^2 + \frac{R_3 \omega_0^2 M_{23}^2}{R_2 + R_s}} \tag{2.48}$$

The variation of load power and transfer efficiency with load resistance from 0 Ω to 500 Ω is shown in Figure 2.13 and Figure 2.14 separately. These figures show that when the load resistance is 122 Ω, the load power is maximum, while the transmission efficiency is just 46%. When the load resistance is 26 Ω, the transmission efficiency is maximum at about 66.22% but the load power is about half of the maximum.

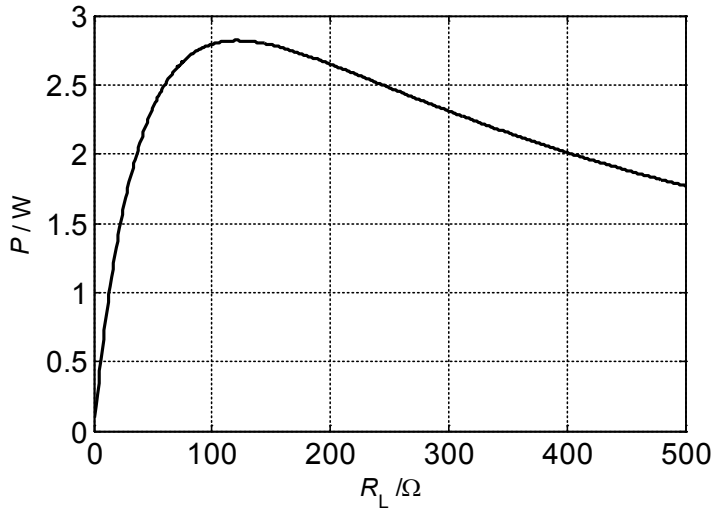

Figure 2.13 Load power versus load resistance (representation of resources in **[Can12]**)

For a resonant WPT system, when the transmitter and receiver parameters are fixed, such as transmission distance and the internal source resistance, the load resistance should be chosen carefully to match either the maximum power or the maximum WPT system efficiency. However, it is clear that for the two-coil configuration system it is impossible to achieve both maximum load power and transmission efficiency with the same load resistor value. In order to obtain high load power and high transmission efficiency simultaneously, it is necessary to consider additional resonant coupling coils in the transmitter and the receiver. So the author will discuss three-coil and four-coil systems in Section 2.4.

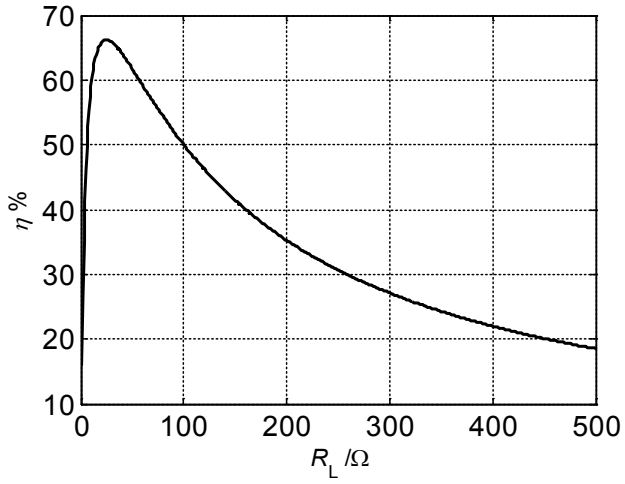

Figure 2.14 Transmission efficiency versus load resistance (representation of resources in **[Can12]**)

2.4 Multi-Coil Configuration WPT Systems Modeling and Analysis

2.4.1 Overview

In Section 2.3.3 the author has analyzed the basic two-coil configuration WPT system, and shown that load power and transmission efficiency cannot both reach maximum values with the same coupling factor and load resistor. In order to improve the performance of WPT systems, we will discuss the characteristics of three-coil and four-coil configurations WPT systems. As well as comparing the load power and transmission efficiency between two-coil, three-coil and four-coil configurations WPT systems.

2.4.2 Four-coil Configuration

In a four-coil configuration WPT system, there are two coils in both the transmitter and the receiver, which consist of a primary and secondary coil. Figure 2.15 gives the circuit diagram of a four-coil configuration WPT system. M_{12} is the mutual inductance between the primary coil and secondary coil of the transmitter. M_{23} is the mutual inductance between the secondary coil of the transmitter and the primary coil of the receiver. Let M_{34} be the mutual inductance between the primary coil and secondary coil of the receiver. Let U_s be the sinusoidal voltage of the transmitter with angular frequency ω_0. Let R_s be the resistance of the power source. Let R_1, R_2, R_3, R_4 be the internal resistances of the primary coil and the secondary coil of the transmitter and the receiver. Let R_L be the load resistance of the receiver coil. Let L_1, L_2, L_3, L_4 be the inductance of the primary coil and the secondary coil of the transmitter and the receiver. Let C_1, C_2, C_3, C_4 be compensation capacitors of the primary coil and the secondary coil of the transmitter and the receiver [Ram11]. The compensation capacitors are such that each loop is resonant.

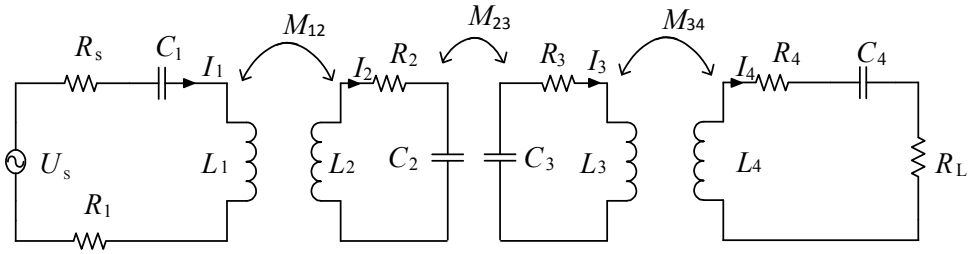

Figure 2.15 Four-coil configuration WPT system (representation of resources in **[Ram11]**)

The KVL equations of four-coil configuration WPT system can be written as (2.49) [Ram11].

$$\begin{bmatrix} I_1 \\ I_2 \\ I_3 \\ I_4 \end{bmatrix} = \begin{bmatrix} R_s + R_1 & j\omega M_{12} & 0 & 0 \\ j\omega M_{12} & R_2 & j\omega M_{23} & 0 \\ 0 & j\omega M_{23} & R_3 & j\omega M_{34} \\ 0 & 0 & j\omega M_{34} & R_4 + R_L \end{bmatrix}^{-1} \begin{bmatrix} U_s \\ 0 \\ 0 \\ 0 \end{bmatrix} \tag{2.49}$$

The solution of the equations is given in (2.50), where $k_{12} = M_{12}/\sqrt{L_1 L_2}$, $k_{23} = M_{23}/\sqrt{L_2 L_3}$, $k_{34} = M_{34}/\sqrt{L_3 L_4}$, $Q_{1sc} = \omega_0 L_1/(R_1 + R_s)$, $Q_2 = \omega_0 L_2/R_2$, $Q_3 = \omega_0 L_3/R_3$, $Q_{4sc} = \omega_0 L_4/(R_4 + R_L)$.

$$\begin{cases} I_1 = \dfrac{\left(1 + k_{23}^2 Q_2 Q_3 + k_{34}^2 Q_3 Q_{4sc}\right)}{\left(R_1 + R_s\right)\left[\left(1 + k_{12}^2 Q_{1sc} Q_2\right)\left(1 + k_{34}^2 Q_3 Q_{4sc}\right) + k_{23}^2 Q_2 Q_3\right]} U_s \\ I_2 = -\dfrac{k_{12}\sqrt{Q_{1sc} Q_2}\left(1 + k_{34}^2 Q_3 Q_{4sc}\right)}{\sqrt{\left(R_1 + R_s\right) R_2}\left[\left(1 + k_{12}^2 Q_{1sc} Q_2\right)\left(1 + k_{34}^2 Q_3 Q_{4sc}\right) + k_{23}^2 Q_2 Q_3\right]} U_s \\ I_3 = -\dfrac{k_{12} k_{23}\sqrt{Q_{1sc} Q_2}\sqrt{Q_2 Q_3}}{\sqrt{\left(R_1 + R_s\right) R_3}\left[\left(1 + k_{12}^2 Q_{1sc} Q_2\right)\left(1 + k_{34}^2 Q_3 Q_{4sc}\right) + k_{23}^2 Q_2 Q_3\right]} U_s \\ I_4 = \dfrac{k_{12} k_{23} k_{34}\sqrt{Q_{1sc} Q_2}\sqrt{Q_2 Q_3}\sqrt{Q_3 Q_{4sc}}}{\sqrt{\left(R_1 + R_s\right)\left(R_4 + R_L\right)}\left[\left(1 + k_{12}^2 Q_{1sc} Q_2\right)\left(1 + k_{34}^2 Q_3 Q_{4sc}\right) + k_{23}^2 Q_2 Q_3\right]} U_s \end{cases} \tag{2.50}$$

The load power and the transmission efficiency of the four-coil configuration WPT system is shown as (2.51) and (2.52) [Ram11].

$$P_{4\_\mathrm{coil}} = \frac{U_\mathrm{s}^2}{R_1 + R_\mathrm{s}} \cdot \frac{k_{12}^2 Q_{1\mathrm{sc}} Q_2 k_{23}^2 Q_2 Q_3 k_{34}^2 Q_3 Q_{4\mathrm{sc}}}{\left[\left(1 + k_{12}^2 Q_{1\mathrm{sc}} Q_2\right)\left(1 + k_{34}^2 Q_3 Q_{4\mathrm{sc}}\right) + k_{23}^2 Q_2 Q_3\right]^2} \cdot \frac{R_\mathrm{L}}{R_4 + R_\mathrm{L}} \tag{2.51}$$

$$\eta_{4\_\mathrm{coil}} = \frac{R_\mathrm{L}}{R_\mathrm{L} + R_4} \cdot \frac{k_{12}^2 Q_{1\mathrm{sc}} Q_2 \cdot k_{23}^2 Q_2 Q_3}{\left[\left(1 + k_{12}^2 Q_{1\mathrm{sc}} Q_2\right)\left(1 + k_{34}^2 Q_3 Q_{4\mathrm{sc}}\right) + k_{23}^2 Q_2 Q_3\right]} \cdot \frac{k_{34}^2 Q_3 Q_{4\mathrm{sc}}}{1 + k_{23}^2 Q_2 Q_3 + k_{34}^2 Q_3 Q_{4\mathrm{sc}}} \tag{2.52}$$

In the four-coil configuration WPT system, k_{34} is the key parameter which can be adjusted to achieve both maximal load power and transmission efficiency with an arbitrary load resistance R_L [Kia11]. According to analysis from (2.52), the transfer efficiency is reduced with decreasing quality factor $Q_{1\mathrm{sc}}$ and coupling factor k_{12}. The mutual inductance M_{23} between the inductance L_2 and L_3 is the dominant factor in determining the overall efficiency at a large transmission distance. According to the reflected impedance (2.23), a small distance d_{23} will cause a large reflected impedance $Z_{23\mathrm{s}}$ onto L_2, which would reduce the transmission efficiency η_{12} from primary coil to secondary coil of the transmitter. Thus, the coupling factor k_{12} should be large enough to keep a high transmission efficiency η_{12}. However, if we choose a large value of k_{12}, there is a large reflected impedance $Z_{12\mathrm{s}}$ onto L_1 which will decrease the available transferred power from L_1 as well as the load power [Kia11].

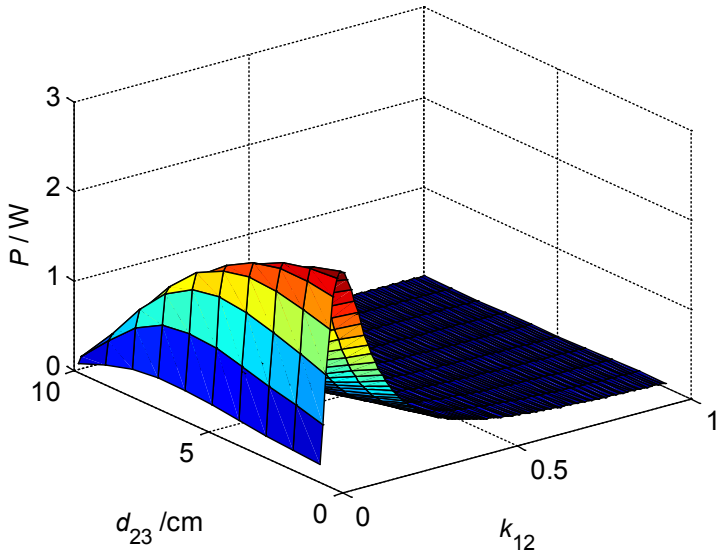

Figure 2.16 Load power versus k_{12} and d_{23} at condition U_s = 10 V, R_L = 50 Ω, k_{34} = 0.3 (conceptual representation of resources in **[Kia11]**)

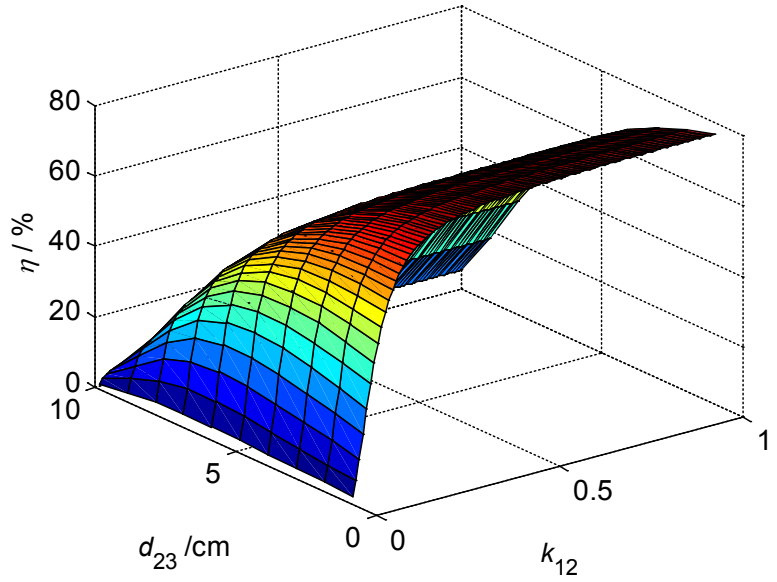

Figure 2.17 Transmission efficiency versus k_{12} and d_{23} at condition U_s = 10 V, R_L = 50 Ω, k_{34} = 0.3 (conceptual representation of resources in **[Kia11]**)

The load power has been calculated as a function of the coupling factors k_{12} and k_{23}. Figure 2.16 shows the results but for clarity one axis is shown in terms of d_{23}, which is inversely related to k_{23}.. For a given transmission distance d_{23}, there is an optimal value k_{12} for maximum load power. Figure 2.16 shows that at larger transmission distances d_{23}, the optimal value for k_{12} will be smaller. In the actual application, the primary coil and the secondary coil of the transmitter are closely coupled together so the value of k_{12} is usually greater than 0.5. In this situation, the load power decreases with the increasing coupling factor k_{12} even at small transmission distance d_{23} with constant power source U_S.

The relationship between transmission efficiency and coupling factors k_{12}, k_{23} (d_{23}) is shown in Figure 2.17. The transmission efficiency decreases sharply with smaller coupling factor k_{12}. Therefore, larger transmission efficiency can be achieved with a larger coupling factor k_{12}. We can observe from Figure 2.16 and Figure 2.17, the area of maximal load power and transmission efficiency does not overlap at all. Thus, the maximal transmission efficiency and load power cannot be achieved simultaneously for the four-coil configuration WPT system [Kia11]. To verify this for a WPT systems with four fixed coils L_1, L_2, L_3 and L_4 and certain value of coupling factors k_{12} and k_{34}, the derivative of load power (2.51) and transmission efficiency (2.52) with respect to d_{23} (k_{23}) is shown as (2.53) and (2.54) [Kia11]. Using these equations the optimal value of d_{23} can be determined for the maximum load power and transmission efficiency. However, due to the

factor $1+k_{12}^2 Q_{1sc} Q_2 > 1$, it is obvious that the optimal $k_{23\_P\_4}$ for the load power is larger than the optimal value $k_{23\_\eta\_4}$ for the transmission efficiency.

$$k_{23\_P\_4} = \left(\frac{\left(1+k_{12}^2 Q_{1sc} Q_2\right) \cdot \left(1+k_{34}^2 Q_3 Q_{4sc}\right)}{Q_2 Q_3} \right)^{1/2} \tag{2.53}$$

$$k_{23\_\eta\_4} = \left(\frac{\sqrt{1+k_{12}^2 Q_{1sc} Q_2} \cdot \left(1+k_{34}^2 Q_3 Q_{4sc}\right)}{Q_2 Q_3} \right)^{1/2} \tag{2.54}$$

2.4.3 Three-coil Configuration

In a three-coil configuration there is one coil in the transmitter and a primary coil and secondary coil in the receiver. Figure 2.18 shows the circuit diagram of a three-coil configuration WPT system. M_{23} is the mutual inductance between the transmitter and the primary coil of the receiver. Let M_{34} be the mutual inductance between the primary coil and secondary coil of the receiver. Let U_s be the sinusoidal voltage of the transmitter with angular frequency ω_0. Let R_s be the internal resistance of the power source. Let R_2, R_3, R_4 be the internal resistances of the transmitter, primary coil and the secondary coil of the receiver. Let R_L be the load resistance of the receiver coil. Let L_2, L_3, L_4 be the inductance of the transmitter, the primary coil and the secondary coil of the receiver. Let C_2, C_3, C_4 be compensation capacitors of the transmitter, the primary coil and the secondary coil of the receiver [Kia11].

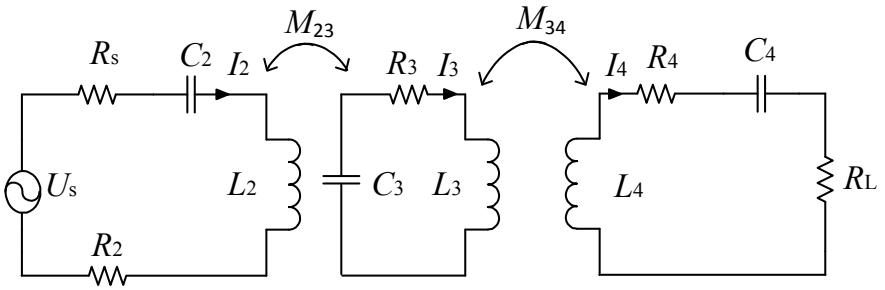

Figure 2.18 Three-coil configuration WPT system (representation of resources in **[Kia11]**)

When all the coils are resonant circuit, the KVL equations of three-coil configuration WPT system could be written as (2.55).

$$\begin{bmatrix} I_2 \\ I_3 \\ I_4 \end{bmatrix} = \begin{bmatrix} R_s + R_2 & j\omega M_{23} & 0 \\ j\omega M_{23} & R_3 & j\omega M_{34} \\ 0 & j\omega M_{34} & R_4 + R_L \end{bmatrix}^{-1} \begin{bmatrix} U_s \\ 0 \\ 0 \end{bmatrix} \tag{2.55}$$

The solution of the equations is shown in (2.56), where $k_{23} = M_{23} \big/ \sqrt{L_2 L_3}$, $k_{34} = M_{34} \big/ \sqrt{L_3 L_4}$, $Q_{2sc} = \omega_0 L_2 \big/ (R_2 + R_s)$, $Q_3 = \omega_0 L_3 / R_3$, $Q_{4sc} = \omega_0 L_4 \big/ (R_4 + R_L)$.

$$\begin{cases} I_2 = \dfrac{\left(1 + k_{34}^2 Q_3 Q_{4sc}\right)}{(R_2 + R_s)\left(1 + k_{23}^2 Q_{2sc} Q_3 + k_{34}^2 Q_3 Q_{4sc}\right)} U_s \\ I_3 = -\dfrac{k_{23}\sqrt{Q_{2sc} Q_3}}{\sqrt{(R_2 + R_s) R_3}\left(1 + k_{23}^2 Q_{2sc} Q_3 + k_{34}^2 Q_3 Q_{4sc}\right)} U_s \\ I_4 = \dfrac{k_{23} k_{34}\sqrt{Q_{2sc} Q_3}\sqrt{Q_3 Q_{4sc}}}{\sqrt{(R_2 + R_s)(R_4 + R_L)}\left(1 + k_{23}^2 Q_{2sc} Q_3 + k_{34}^2 Q_3 Q_{4sc}\right)} U_s \end{cases} \tag{2.56}$$

The load power and the efficiency of three-coil configuration WPT systems is shown as (2.57) and (2.58) [Kia11].

$$P_{3\_coil} = \frac{U_s^2}{R_2 + R_s} \cdot \frac{k_{23}^2 Q_{2sc} Q_3 k_{34}^2 Q_3 Q_{4sc}}{\left(1 + k_{23}^2 Q_{2sc} Q_3 + k_{34}^2 Q_3 Q_{4sc}\right)^2} \cdot \frac{R_L}{R_4 + R_L} \tag{2.57}$$

$$\eta_{3\_coil} = \frac{R_L}{R_L + R_4} \cdot \frac{k_{34}^2 Q_3 Q_{4sc}}{1 + k_{34}^2 Q_3 Q_{4sc}} \cdot \frac{k_{23}^2 Q_{2sc} Q_3}{1 + k_{23}^2 Q_{2sc} Q_3 + k_{34}^2 Q_3 Q_{4sc}} \tag{2.58}$$

In three-coil configuration WPT system, which is adjusted for optimum impedance match, the load resistance R_L can be any arbitrary value and still achieve maximum load power and transmission efficiency simultaneously by adjusting the coupling factor k_{34} according to (2.46) and (2.48), where the resistance of the receiver is replaced by the corresponding reflected impedance [Kia11]. The partial derivative of (2.58) with respect to load resistance for a three-coil configuration WPT system is given in (2.59). The corresponding value of optimal load resistance is derived as (2.60).

$$\frac{\partial \eta_{3\_coil}}{\partial R_L} = 0 \tag{2.59}$$

$$R_{\mathrm{L}\_\eta\_3}=\sqrt{\frac{\left(R_3R_4+\omega_0^2M_{34}^2\right)\left[\left(R_2+R_\mathrm{s}\right)R_3R_4+\omega_0^2M_{34}^2\left(R_2+R_\mathrm{s}\right)+\omega_0^2M_{23}^2R_4\right]}{\left(R_2+R_\mathrm{s}\right)R_3^2+\omega_0^2M_{23}^2R_3}} \tag{2.60}$$

Figure 2.19 and Figure 2.20 show the variation of load power and transmission efficiency with coupling factor k_{34} and transmission distance d_{23}. For a given value of k_{23}, the maximum load power and transmission efficiency can be obtained by adjusting the coupling factor k_{34}. As well as the load power is maximum if k_{23} is chosen correctly for the given k_{34} value, which is presented in Figure 2.19. The larger transmission distance d_{23} between the transmitter and receiver leads to a smaller coupling factor k_{23}, and vice versa. When the distance d_{23} increases from 0 to 10 cm, the load power reaches maximum value with optimal k_{23} (d_{23}) value. After this appropriate value d_{23}, then the load power decreases with increasing transmission distance d_{23}. When the coupling factor k_{34} is fixed, the transmission efficiency increases with decreasing transmission distance d_{23}. For the three-coil configuration WPT system maximum load power and transmission efficiency can be achieved simultaneously with proper values of k_{23} and k_{34}. As opposed to the four-coil configuration WPT system, where the high load power area is completely different from the area of high transmission efficiency [Kia11].

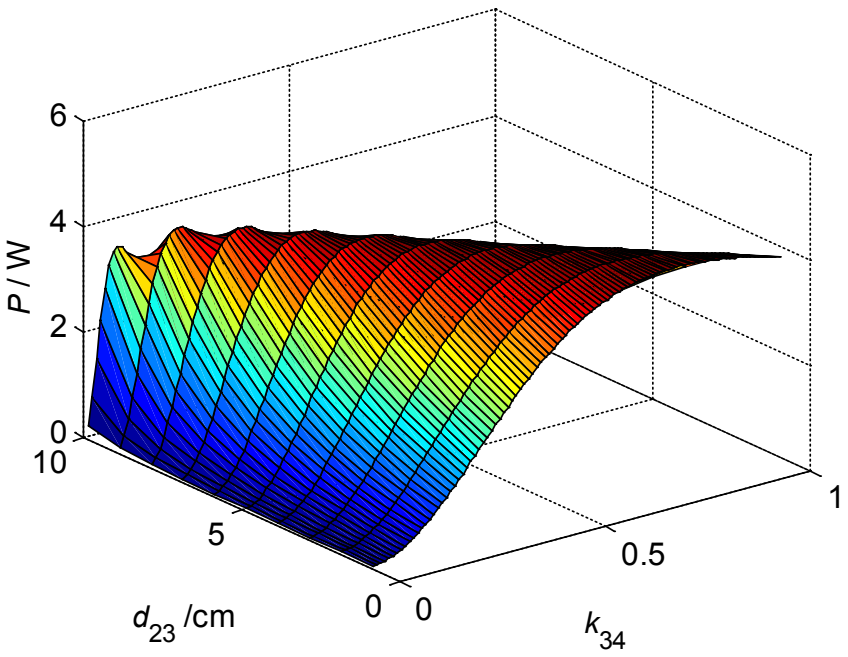

Figure 2.19 Load power versus k_{34} and d_{23} at condition U_s = 10 V, R_L = 50 Ω (conceptual representation of resources in **[Kia11]**)

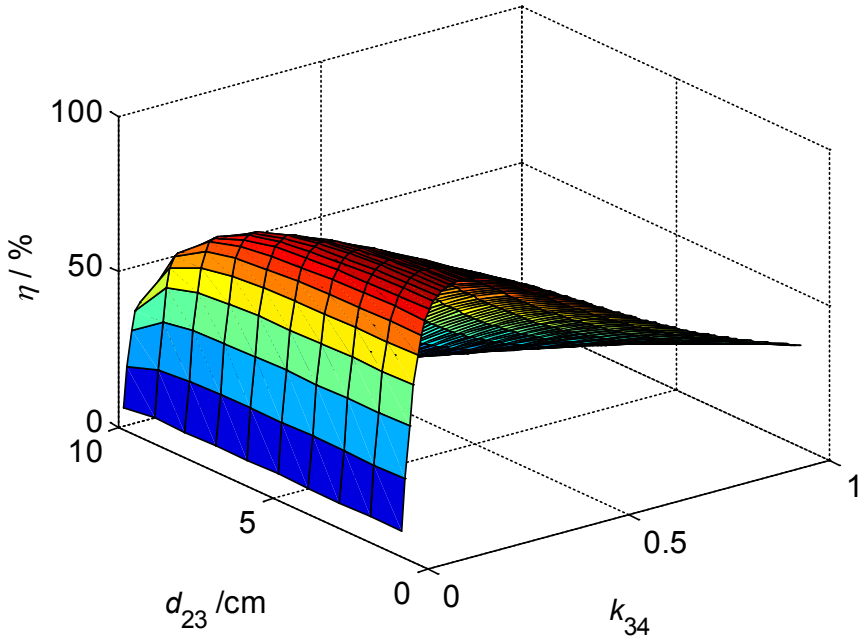

Figure 2.20 Transmission efficiency versus k_{34} and d_{23} at condition U_s = 10 V, R_L = 50 Ω (conceptual representation of resources in **[Kia11]**)

In order to obtain the maximal load power, the derivative of (2.57) with respect to k_{23} and k_{34} are shown in (2.61) and (2.62) respectively [Kia11].

$$k_{23\_P\_3} = \sqrt{\frac{k_{34}^2 Q_3 Q_{4sc} + 1}{Q_{2sc} Q_3}} \tag{2.61}$$

$$k_{34\_P\_3} = \sqrt{\frac{k_{23}^2 Q_{2sc} Q_3 + 1}{Q_3 Q_{4sc}}} \tag{2.62}$$

For the fixed transfer distance d_{23} (k_{23}), the maximum efficiency is obtained by differentiating (2.58) with respect to k_{34}. The maximum energy efficiency is achieved with the optimal load resistance shown in (2.63) [Kia11].

$$k_{34\_\eta\_3} = \left(\frac{k_{23}^2 Q_{2sc} Q_3 + 1}{Q_3^2 Q_{4sc}^2} \right)^{1/4} \tag{2.63}$$

2.4.4 Comparison of Two-coil, Three-coil and Four-coil WPT Systems

Based on the above analysis, the three-coil configuration has the advantage over the two-coil and four-coil configurations for WPT systems. Compared with the two-coil configuration, L_3, L_4 and M_{34} play an important role in impedance matching the circuit in the three-coil configuration. That is to say, the coupling factor k_{34} permits the optimal load resistance R_L to be any arbitrary value. What's more, it is possible to achieve the high load power and high transmission efficiency simultaneously by choosing proper parameters k_{23} and k_{34} in the three-coil configuration WPT system. While it is not possible to achieve high load power and transmission efficiency at the same time in a four-coil system, due to the coupling factor k_{12}. What's more, it is not necessary to consider the effect of the coupling factor k_{12}, always less than 1, on the load power and transmission efficiency of the three-coil configuration [Kia11].

Figure 2.21 shows the maximum transmission efficiency a two-coil configuration WPT system can achieve when the load resistance is properly chosen. The maximal transmission efficiency for three-coil configuration is also shown in the Figure 2.21. The maximum efficiency of the three-coil system is maintained by adjusting the coupling factor k_{34} (also shown), which permits load resistance variation [Kia11]. From the figure, it is obvious that the transmission efficiency of the three-coil configuration is always the same or higher than that of a two-coil system. The transmission efficiency of the three-coil configuration is about 20% higher than that of the two-coil configuration with 500 Ω load resistance.

In two-coil, three-coil and four-coil configurations of WPT systems, coils of L_1 and L_2, L_3 and L_4 are often coupled together in the transmitter and receiver sides respectively. The lateral and angular misalignment usually occurs between the secondary coil of the transmitter L_2 and the primary coil of the receiver L_3 [Kia11].

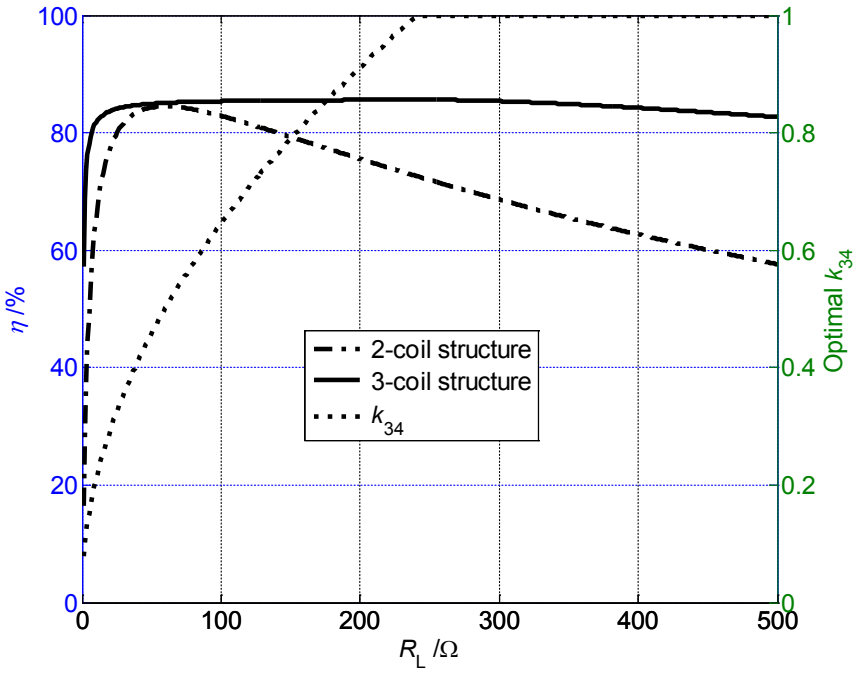

Figure 2.21 Transmission efficiency versus R_L of two-coil and three-coil configurations with k_{34} adjustment (conceptual representation of resources in **[Kia11]**)

2.5 Chapter Summary

In this chapter, the basic knowledge about resonance theory and mutual inductively coupled circuits is introduced. The general WPT system is based on coupled resonant circuits. The resonant circuit can be divided into series and parallel connected circuits, which can apply to both the transmitter and receiver respectively. Thus, there are four different topologies for the WPT system. In addition, two-coil, three-coil and four-coil configurations WPT systems are studied and compared. The influence of the factors such as load resistance, coupling factor and coil quality factor are analyzed in detail.

The analysis shows that the SR-SR topology WPT system is superior to SR-PR, PR-SR and PR-PR with respect to transfer efficiency. The simulation results presented in this thesis prove that the three-coil configuration has better performance than the two-coil and four-coil configurations WPT systems.

Chapter 3

Design and Optimization of WPT Systems

3.1 Chapter Overview

This chapter concentrates on designing an optimal 2D coil structure for the WPT transmitter and receiver. This process starts with development of a model of the power transfer coils which has been used to design a WPT system having increased efficiency and reliability. Coil models including inductance, parasitic capacitance, AC resistance, mutual inductance and quality factor calculation are introduced and analyzed. The transmitter coil is optimized with respect to quality factor. These models were used to develop a proposed WPT system design. The WPT system design takes into account application to portable devices like PDAs and cell phones. Thus, the coil parameters are chosen in such a way that they can conveniently fit into a cell phone or other portable devices. A comprehensive optimization of a single transmitter coil WPT system based on consideration of the coupling factor and quality factor is achieved in this thesis.

The chapter is organized as follows. In Section 3.2, the model for a multi-layer helical antenna coil is presented. A high quality factor helical coil is obtained using the model by adjusting the different coil parameters, such as wire cross-sectional area, coil radius and number of turns. Section 3.3 optimizes the transmitter and the receiver with respect to mutual inductance and quality factor. Section 3.4 presents optimization parameters and simulation results of an optimization WPT system. Section 3.5 summarizes this chapter.

3.2 Antenna Coil Model Design and Optimization

3.2.1 Introduction of Multi-layer Helical Coil

3.2.1.1 Multi-layer Helical Coil Description

The helical coil and spiral coil are widely used in WPT systems so far as now, because their working frequency is suitable for from several kilohertz to several megahertz [Sen13]. Since the transmission distance is 10 cm in this thesis, the multi-layer helical coil is adopted for WPT systems [Shi14]. Also, the AC resistance, self-inductance and stray capacitance of multi-layer helical coil are well known [Sen13]. Thus the multi-layer helical coil is easily constructed, analyzed, and optimized for overall performance of a WPT system [Ram11,Vil15]. Figure 3.1 shows a sketch of such a coil. The outer radius r_{out}, the inner radius r_{in} and the thickness of the coil T_{height} are the parameters to be optimized. The thickness of the coil T_{height} and wire diameter determines the number of turns per layer N_t. The difference between the inner and the outer diameter determines the number of coaxial layers N_a, which is also dependent on the wire thickness.

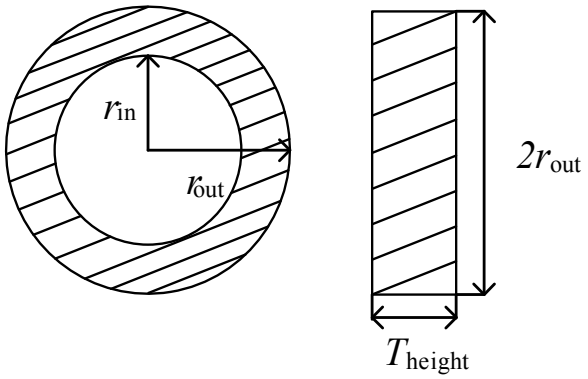

Figure 3.1 Multi-layer helical coil (derived by the author)

The ideal multi-layer helical coil can be modeled as only an inductance without the resistance and the capacitance. However, a more realistic coil model includes the inductance and the resistance in series connection, with the stray capacitance in parallel across the series RL circuit as shown in Figure 3.2 [Ram11]. The frequency where the stray capacitance resonates with the coil inductance is called the self-resonant frequency (SRF). The coil is parallel resonant at this frequency

and presents a large peak in impedance with the phase going through zero as shown in Figure 3.3. If the operating frequency is higher than the SRF, the coil impedance is capacitive. Therefore, the operating frequency of a WPT system should be smaller than the self-resonant frequency of the coil [Yan07], otherwise, the coil presents the characteristics of a capacitor, which is not useful for WPT systems.

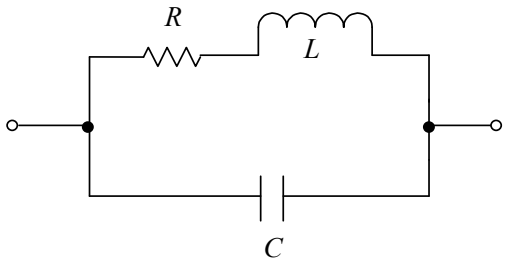

Figure 3.2 An inductor with shunt capacitance in parallel (representation of resources in **[Ram11]**)

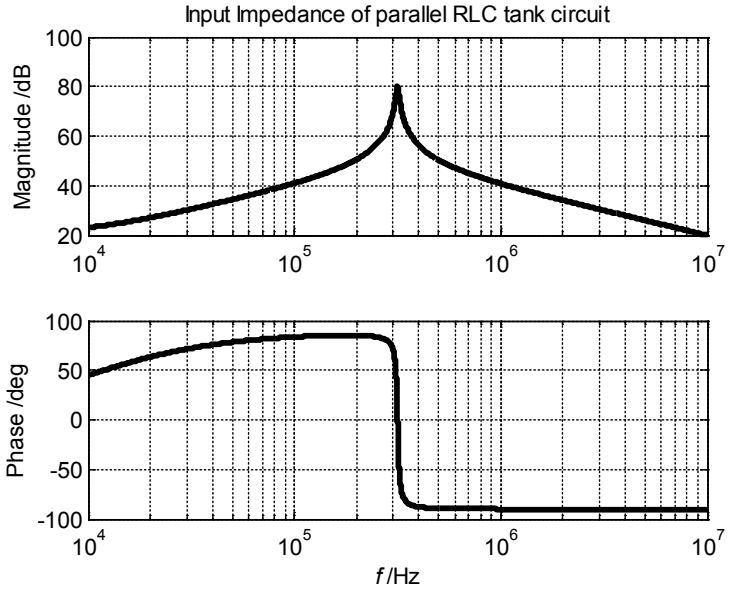

Figure 3.3 Impedance and phase of coil model at parallel resonance (simulated by the author)

3.2.1.2 Mutual Inductance

The mutual inductance between two coils is defined as the ratio of the flux linkage generated in the secondary coil to the AC current in the primary coil [Can12]. The

mutual inductance is a function of the lateral misalignment and distance between two coils. Grover's formula, for mutual inductance, derived for filamentary currents, is applied in this thesis. The radius of the primary coil and the secondary coil are r_2 and r_3. The lateral misalignment between the centers of the primary and the secondary coil is d_{mis}, the perpendicular distance between two coils is d. The formula for mutual inductance is given in (3.1) to (3.5) [Bab08].

$$M = \frac{\mu_0}{\pi}\sqrt{r_2 \times r_3} \times \int_0^{\pi} \frac{\left[1 - \frac{d_{\text{mis}}}{r_3} \times \cos\varphi\right] \times \chi(\tau)}{\sqrt{V^3}} d\varphi \tag{3.1}$$

where,

$$V = \sqrt{1 - 2\frac{d_{\text{mis}}}{r_3}\cos\varphi + \frac{d_{\text{mis}}^2}{r_3^2}} \tag{3.2}$$

$$\xi = \frac{r_3}{r_2}, \zeta = \frac{d}{r_2} \tag{3.3}$$

$$\tau^2 = \frac{4\xi V}{(1+\xi V)^2 + \zeta^2} \tag{3.4}$$

$$\chi(\tau) = \left(\frac{2}{\tau} - \tau\right)K(\tau) - \frac{2}{k}E(\tau) \tag{3.5}$$

μ_0 is the magnetic permeability of vacuum. φ is the angle of integration at any point of the secondary coil. $K(\tau)$ and $E(\tau)$ represent complete elliptic integral of the first kind and the second kind respectively. ξ is the ratio of the secondary coil radius to the primary coil radius. ζ is the ratio of distance between two coils to the primary coil radius.

The Grover formula does not directly apply to multi-layer helical coils for calculation of mutual inductance. The approach is to use the Grover filament formula for individual turns and sum the mutuals in order to accurately calculate the total. Figure 3.4 presents two laterally misaligned coils. Radiuses of the primary and the secondary coil are r_2 and r_3 respectively. The primary coil and the secondary coil have N_2 turns and N_3 turns respectively. The cross sectional area of primary coil and the secondary coil are divided into $(2N+1)\times(2K+1)$ cells and

$(2m+1)\times(2n+1)$ cells respectively. Using the Grover filament method, and summing all the mutual, formulas for the mutual inductance between two circular coils with cross sectional division into cells as shown can be written as follows [Bab08],

$$M=\frac{N_2N_3\sum_{g=-K}^{g=K}\sum_{h=-N}^{h=N}\sum_{l=-n}^{l=n}\sum_{p=-m}^{p=m}M(g,h,l,p)}{(2K+1)(2N+1)(2n+1)(2m+1)} \tag{3.6}$$

$$M(g,h,l,p)=\frac{\mu_0}{\pi}\sqrt{r_2(h)r_3(l)}\int_0^{\pi}\frac{\left[1-\frac{d_{\text{mis}}}{r_3(l)}\times\cos\varphi\right]\times\chi(\tau)}{\sqrt{V^3}}d\varphi \tag{3.7}$$

where,

$$\xi(h,l)=\frac{r_3(l)}{r_2(h)} \tag{3.8}$$

$$\zeta(h,g,p)=\frac{d(g,p)}{r_2(h)} \tag{3.9}$$

$$\tau^2(h,l,g,p)=\frac{4\xi(h,l)V(l)}{\left(1+4\xi(h,l)V(l)\right)^2+\zeta^2(h,g,p)} \tag{3.10}$$

$$V=\sqrt{1-2\frac{d_{\text{mis}}}{r_3(l)}\cos\varphi+\frac{d_{\text{mis}}^2}{r_3^2(l)}} \tag{3.11}$$

$$\chi(\tau)=\left(\frac{2}{\tau}-\tau\right)K(\tau)-\frac{2}{\tau}E(\tau) \tag{3.12}$$

$$r_2(h)=r_2+\frac{h_2}{2N+1}h,\ \ h=-N\ldots0\ldots N \tag{3.13}$$

$$r_3(l)=r_3+\frac{h_3}{2n+1}l,\ \ l=-n\ldots0\ldots n \tag{3.14}$$

$$r_2=\frac{r_{2\text{in}}+r_{2\text{out}}}{2},h_2=r_{2\text{out}}-r_{2\text{in}} \tag{3.15}$$

$$r_3 = \frac{r_{3\text{in}} + r_{3\text{out}}}{2}, h_3 = r_{3\text{out}} - r_{3\text{in}} \tag{3.16}$$

$$\begin{aligned} d(g,p) &= d + \frac{T_{2\text{height}}}{2K+1} g + \frac{T_{3\text{height}}}{2m+1} p, \\ g &= -K \ldots 0 \ldots K \quad p = m \ldots 0 \ldots m \end{aligned} \tag{3.17}$$

r_{in2} and r_{out2} are the inner radius and outer radius of the primary coil of rectangular cross section respectively. r_{in3} and r_{out3} are the inner radius and outer radius of the secondary coil of rectangular cross section respectively. In order to compute the mutual inductance more accurately, the primary and the secondary coil are divided into sub-rectangles. Each sub-rectangle represents one intersecting surface of the filamentary circular coil. $M(g,h,l,p)$ represents every condition of mutual inductance between two inductively coupled filamentary coils. Matlab simulation is used to do the calculations. The more sub-rectangles there are, the more accurate the mutual inductance calculation, however, the Matlab simulation will take longer [Bab08].

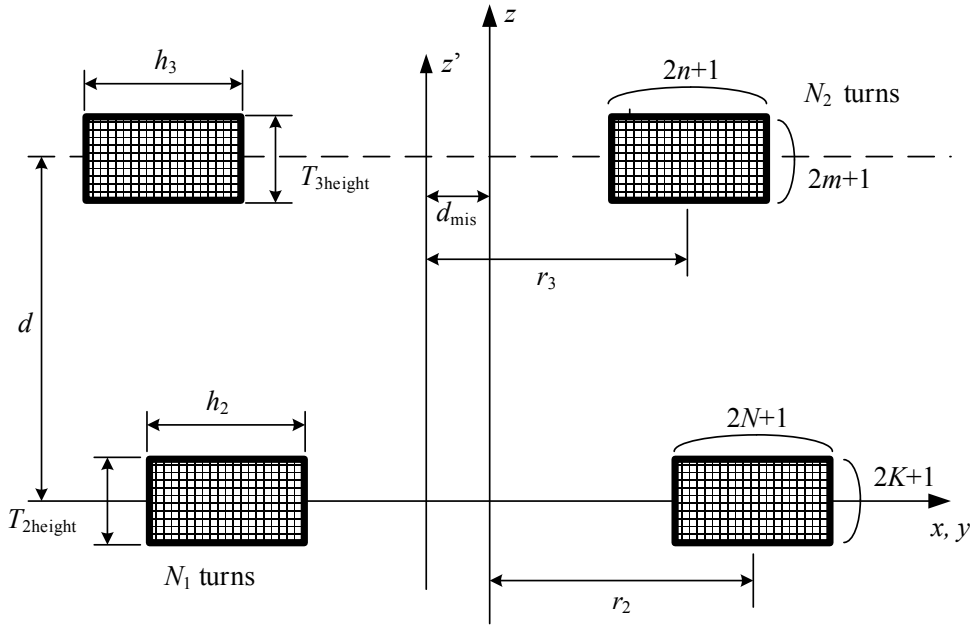

Figure 3.4 Cross-sectional view of two non-coaxial circular coils (representation of resources in **[Bab08]**)

3.2.1.3 Inductor Model

Self-inductance is a measure of magnetic flux passing through the area enclosed by a current carrying coil [Auv15]. For the case of circular coil radius r and conducting-wire radius a, the self-inductance of a single circular loop is shown in (3.18) when $a/r<<1$ [Ram11]. The self-inductance of a number of single circular loops of approximately equal diameter is the self-inductance derived in (3.18) multiplied by the square of the number of turns together with the total mutual inductance between each pair of single circular loops. Mutual inductance is a measure of the extent of magnetic linkage between current-carrying coils. The mutual inductance of two non-coaxial and parallel filamentary coils is expressed as (3.6).

$$L(r,a) = \mu_0 r(\ln(\frac{8r}{a}) - 2) \tag{3.18}$$

For helical coil with number of turns per layer N_t and number of coaxial layers N_a, the total inductance can be expressed as (3.19) [Ram11].

$$\begin{aligned} L_{\text{self}} &= N_t \sum_{ii=1}^{N_a} L(r_{ii}, a) + \\ &\sum_{ii=1}^{N_a}\sum_{jj=1}^{N_a}\sum_{k=1}^{N_t}\sum_{l=1}^{N_t} M(r_{iik}, r_{jjl}, \rho = 0, d = d_{\min}\left|k-l\right|) \times (1-\delta_{iijj})(1-\delta_{kl}) \end{aligned} \tag{3.19}$$

where δ_{iijj} (or δ_{kl}) =1 for ii=jj (or k=l) and δ_{iijj} (or δ_{kl}) = 0 otherwise. $D_{\min}$ is the minimum distance between coaxial layers.

3.2.1.4 Parasitic Capacitance

The coil is made from parallel conductors; this causes an unwanted distributed capacitance between the turns of the coil due to their proximity. This unwanted capacitance is called parasitic capacitance and acts as if there is a parallel capacitance connected across the coil. This will pose a limitation on the resonance frequency of the WPT systems depending on the value of the inductance of the coil [Ram11]. Generally speaking, the efficiency increases with increasing number of turns [Man14]. However, with increasing number of turns, the value of the inductance and parasitic capacitance of the coil also increases significantly. Thus, the number of turns should be increased only to the point where the parasitic capacitance of the coil is still negligible [Yan06,Yan07].

For a multilayer tightly wound coil with N_a layers and N_t turns per layer, stray capacitance is approximated as (3.20) [Yan07].

$$C_{self} = \frac{1}{N^2}\left[C_b \left(N_t - 1\right) N_a + C_m \sum_{i=1}^{N_t} \left(2i-1\right)^2 \left(N_a - 1\right) \right] \tag{3.20}$$

where N is the total number of turns, C_b is parasitic capacitance between two nearby turns in the same layer, and C_m is parasitic capacitance between different layers, which are shown as (3.21) and (3.22).

$$C_b = \varepsilon_0 \varepsilon_r \int_0^{\pi/4} \frac{\pi D_{ave} a}{\varsigma + \varepsilon_0 \varepsilon_r (1-\cos\theta)} d\theta \tag{3.21}$$

$$C_m = \varepsilon_0 \varepsilon_r \int_0^{\pi/4} \frac{\pi D_{ave} a}{\varsigma + \varepsilon_0 \varepsilon_r (1-\cos\theta) + 0.5\varepsilon_r d_l} d\theta \tag{3.22}$$

where D_{ave}, a, ς, ε_0, ε_r, d_l are the average diameter of coil, wire radius, thickness of insulation layer, permittivity of free space, relative permittivity of strand insulation and separation between two layers respectively. The SRF of coil is determined from the self-inductance and parasitic capacitance of the coil, as shown in (3.23) [Yan07].

$$f_{self} = \frac{1}{2\pi\sqrt{L_{self} C_{self}}} \tag{3.23}$$

3.2.1.5 AC Resistance

With increasing frequency, the proximity effect and skin effect increase the effective series resistance (ESR). Therefore, the quality factor of the coil decreases [Ram11]. Litz wire, consisting of many single insulated strands, is designed to reduce the losses caused by the skin and proximity effects [Yan06]. The strands are twisted in such a way that their position within the wire varies along the wire, being at each position within the wire about an equal length. In this way the current distribution remains nearly uniform over the wire cross section. Using multi-strand litz wire in the appropriate frequency range, results in the AC resistance being very close to the DC resistance [Ram11]. Therefore, multi-strand litz wire is chosen for the transmitter and receiver coils of the WPT systems in this thesis.

The AC resistance of circular coils made of multi-strand litz wires including skin effect and proximity effect can be approximated as (3.24) [Yan07].

$$R_{ac} = R_{dc}\left(1+\frac{f^2}{f_h^2}\right) \tag{3.24}$$

where R_{dc} is the dc resistance. f is the operating frequency, f_h is the frequency at which power dissipation is twice dc power dissipation and is calculated as (3.25).

$$f_h = \frac{2\sqrt{2}}{\pi r_s^2 \mu_0 \sigma \sqrt{N N_s \eta_a \eta_b}} \tag{3.25}$$

where r_s is the radius of each single strand, μ_0 is the permeability of free space, σ is conductivity of the wire, N is number of turns, N_s is the number of strands per bunch. η_a is the area efficiency of the coil with thickness T_{height} and width h_w and is shown in Figure 3.5. η_b is the area efficiency per bunch.

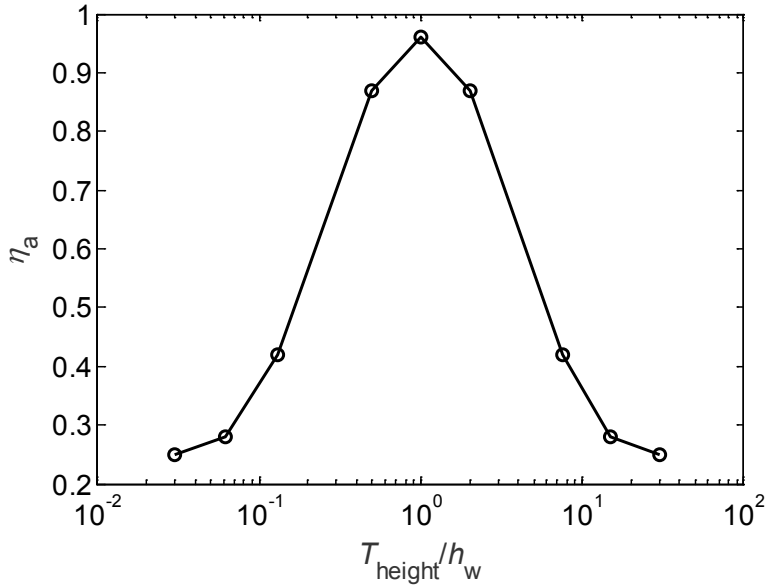

Figure 3.5 Area efficiency versus thickness over width (representation of resources in **[Yan07]**)

The DC resistance of the coil is calculated as (3.26). ρ is resistivity of the conductive material. D_i is the diameter of each layer. Cross-section area of each bunch is a [Ram11].

$$R_{\mathrm{dc}} = \sum_{i=1}^{N_{\mathrm{a}}} \rho \frac{N_{\mathrm{t}} \pi D_i}{a} \tag{3.26}$$

3.2.1.6 Quality Factor

The quality factor Q of the coil is an important parameter, which quantifies the loss of an inductive coil. The antenna coil should be designed to have a high quality factor at the working frequency. For this thesis, a circular coil is adopted for the transmitter and the receiver antenna design. The geometry of the coil should be selected with the aim of maximizing the quality factor. The coil circuit model is already presented in Figure 3.2. Based on that model the impedance of the coil including the parasitic capacitor in parallel with the series AC resistance and inductance is given in (3.27) [Ram11].

$$Z = \left(R_{\mathrm{ac}} + j\omega L_{\mathrm{self}}\right) \left\| \frac{1}{j\omega C_{\mathrm{self}}} \right. \tag{3.27}$$

At a given frequency, the coil impedance can be modeled as an equivalent series inductance and resistance. The effective value of inductance and resistance are given in (3.28) and (3.29) separately [Ram11].

$$L_{\mathrm{eff}} = \frac{L_{\mathrm{self}}}{\left(1 - \frac{f^2}{f_{\mathrm{self}}^2}\right)} \tag{3.28}$$

$$R_{\mathrm{eff}} = \frac{R_{\mathrm{ac}}}{\left(1 - \frac{f^2}{f_{\mathrm{self}}^2}\right)^2} \tag{3.29}$$

The quality factor of the coil is shown as (3.30) [Ram11].

$$Q = \frac{\omega L_{\mathrm{eff}}}{R_{\mathrm{eff}}} = \frac{2\pi f L_{\mathrm{self}} \left(1 - \frac{f^2}{f_{\mathrm{self}}^2}\right)}{R_{\mathrm{dc}} \left(1 + \frac{f^2}{f_h^2}\right)} \tag{3.30}$$

3.2.2 Quality Factor Optimization of Transmitter Coil

3.2.2.1 Wire Property

As the author presented in Section 2.3.3.3, the power transfer efficiency of a resonant WPT system depends on the quality factor of the resonant circuit. To obtain a resonant circuit with a high quality factor, the resistance of the resonant circuit should be minimized and the inductance should be maximum according to (3.30). From equation (3.26) the DC resistance of a conducting wire will decrease with increasing radius of the wire. However, the result in [Fer92] shows that keeping all other factors the same and just increasing the wire diameter, the AC resistance only decreases up to a certain point, after which the resistance increases. One available option for further reduction of the resistance of a conducting wire is to strand the conductors and form litz wires. Litz wire is commonly used to reduce the AC resistance of wire, leading to a higher quality factor of the coil [Ram11]. The minimum diameter of each strand is approximately the same order as the skin depth at the operating frequency. The skin depth δ is shown as (3.31), and the value of skin depth for copper is around 0.2 mm at the operating frequency of 100 kHz. Interpolating the results from Table 3.1, a 0.1 mm diameter litz wire (gauge AWG38) is found to be the suitable strand size to use for litz wire operating in the frequency range of 100 kHz.

$$\delta = \sqrt{2/\mu_0 \sigma \omega} \tag{3.31}$$

The magnetic field due to the currents in the strands of litz is the the same as would be generated by a single turn with the same total current. Therefore, according to Faraday's Law, the induced voltage in the receiver coil is also the same. For a given total number of strands, thickness and width of the coil, the number of strands per bundle should be optimized to improve the quality factor of the coil. Using litz wire with a fixed total number of strands of 2400, the coil quality factor for 30, 60, 120 strands per bundle has been calculated and given in Table 3.2. The last entry in the table has the highest quality factor and corresponds to litz wire of type CLI 200/120 with diameter of 120×0.1 mm, which the author selected for use in this thesis.

Table 3.1 Litz Wire parameters for different frequency (representation of resources in **[New17]**)

Recommended Wire Gauge	Frequency	Nominal Diameter Over Copper (inch)	Maximum DC Resistance Ohms/m	Single Strand R_{ac}/R_{dc} "H"
28 AWG	60 Hz to 1 kHz	0.0126	66.37	1.0000
30 AWG	1 kHz to 10 kHz	0.0100	105.82	1.0000
33 AWG	10 kHz to 20 kHz	0.0071	211.70	1.0000
36 AWG	20 kHz to 50 kHz	0.0050	431.90	1.0000
38 AWG	50 kHz to 100 kHz	0.0040	681.90	1.0000
40 AWG	100 kHz to 200 kHz	0.0031	1152.30	1.0000
42 AWG	200 kHz to 350 kHz	0.0025	1801.0	1.0000
44 AWG	350 kHz to 850 kHz	0.0020	2873.0	1.0003
46 AWG	850 kHz to 1.4 MHz	0.0016	4544.0	1.0003
48 AWG	1.4 MHz to 2.8 MHz	0.0012	7285.0	1.0003

Table 3.2 Quality factor versus strands per bundle

Strands per bundle	Number of turns	Inner Radius (cm)	Outer Radius (cm)	Thickness (mm)	Quality Factor
30	80	2.9	4.15	3.5	84
60	40	2.9	4.25	3.5	103
120	20	2.8	4.4	3	143

3.2.2.2 Number of Turns of Coil

To optimize the quality factor of the coil, the effect of the number of turns per layer N_t is analyzed. Using the derivative of (3.30) with respect to the parameter of N_t ($N_a \gg 1$), the quality factor can be maximized by (3.32) [Ram11].

$$\frac{dQ}{dN_t} = 0 \Rightarrow 1 - 4\frac{\omega^2}{\omega_{self}^2} - 3\frac{\omega^2}{\omega_{self}^2}\frac{\omega^2}{\omega_h^2} = 0 \tag{3.32}$$

where, $\omega_{self} = 1/\sqrt{L_{self}C_{self}}$, $\omega_h = 2\pi f_h$ and the operating frequency $\omega = 2\pi f$. L_{self}, R_{dc}, f, f_h and f_{self} are the function of N_t. The higher value of f_h is, the less power loss from proximity effect will be based on (3.25). Let the operating frequency f be less than $2\times f_h$ to ensure the power efficiency is not declining sharply. That is to say, $\omega \le 2\omega_h \Rightarrow \omega^2 \le 4\omega_h^2$, which substitutes into (3.32). The quality factor is increased if the operating frequency satisfies (3.33). Therefore, the optimum N_t could be obtained when $\omega \le \omega_{self}/4$.

$$1 - 16\frac{\omega^2}{\omega_{self}^2} \ge 0 \tag{3.33}$$

Figure 3.6 shows Matlab simulation results for quality factor of a coil with 10 cm inner radius as a function of the number of turns per layer (N_t) and the number of coaxial layers (N_a). When the N_a is larger than 14, the quality factor increases to the maximum value with optimal N_t and then decreases with the increasing value of N_t. The quality factor increases rapidly as N_t increases when value of N_a is smaller than 5. Based on these results and from Figure 3.6 it is clear that, for $N_a \gg 1$, the quality factor will be maximum if N_t is chosen as the optimum value 2.

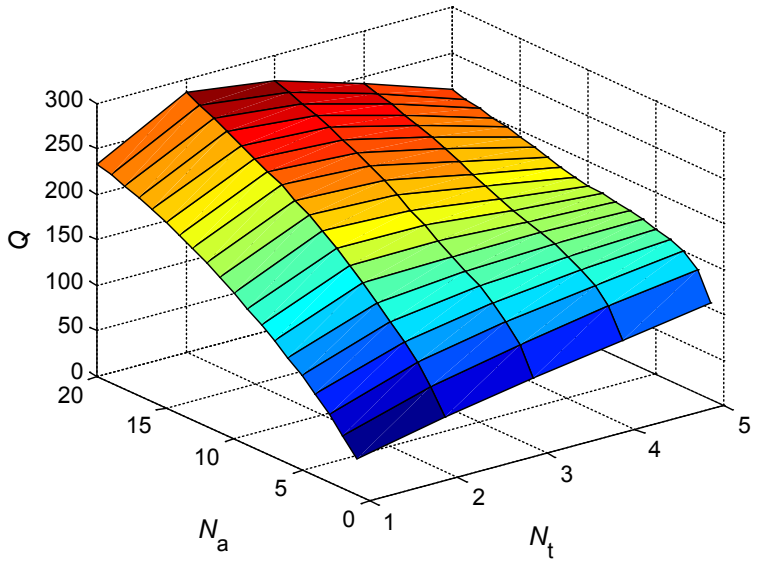

Figure 3.6 Maximum quality factor with optimum N_t (simulated by the author)

3.2.2.3 Radius of Coil

Qualitatively, increasing the number of turns improves the quality factor of a coil because the inductance increases as square of number of turns, while the resistance increases linearly with number of turns based on (3.19) and (3.24). Similarly, the quality factor improves with increasing coil radius because the inductance increases as the square of coil radius and resistance increases linearly with coil radius as shown in (3.19) and (3.24). Therefore, a high quality factor coil will have a large radius and a lot of turns. Figure 3.7 shows simulation results for the quality factor of a coil as a function of the number of turns and the radius of the coil. When the number of turns per layer is 2, optimum according to Figure 3.6, Figure 3.7 shows that the rate of increasing of the quality factor as a function of N becomes larger when the radius is larger. When the number of turns is less than 10, the variation of radius has little influence on the quality factor. However, for larger number of turns the quality factor increases rapidly with increasing coil radius.

3.2.3 Receiver Coil Choice

3.2.3.1 Primary Coil

As discussed in Section 2.4, the receiver consists of a resonant tuned primary coil and a resonant tuned secondary coil connected to the load. The size of the receiver

coil is restricted by the application, thus the total number of strands is determined. For the types of litz wire considered, 30×0.1 mm, 60×0.1 mm, and 120×0.1 mm, the 30×0.1 mm litz wire is chosen for the primary and the secondary coil of the receiver. The reason is that, for a fixed number of strands, fewer strands per bundle leads to more turns in the receiver. Thus for a given magnetic flux density generated by the transmitter, the induced voltage in the receiver when using litz wire with 30 stands per bundle is higher than that of the same radius receiver with 60 or 120 strands per bundle according to Faraday's Law. The main purpose for the choice of 30 strands per bundle litz wire is that the load power is increased due to the higher induced voltage. The induced voltage can also be increased by using a receiver coil with larger effective area. The number of layers should be as few as possible with a fixed outer radius for the primary coil, so that the effective area intercepting the magnetic field is larger. As the WPT system application is for mobile devices, the outer radius of the receiver coil should not be larger than 4 cm. The quality factor as a function of number of layers and number of turns per layer has been calculated using Matlab as shown in Figure 3.8. The number of layers and number of turns per layer are chosen as 8 and 10 separately by overall consideration of quality factor and effective receiving coil area.

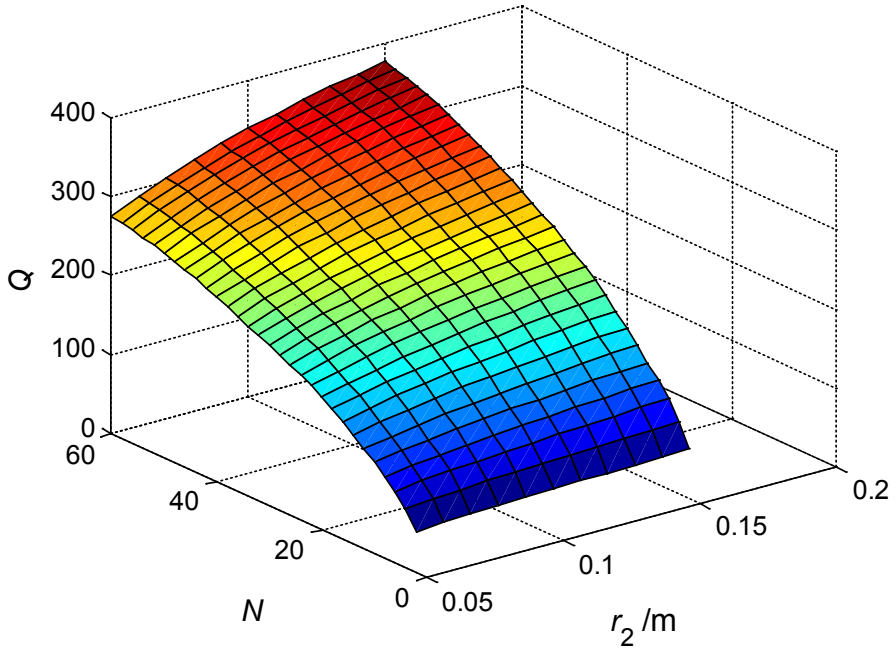

Figure 3.7 Quality factor versus total number of turns and radius (simulated by the author)

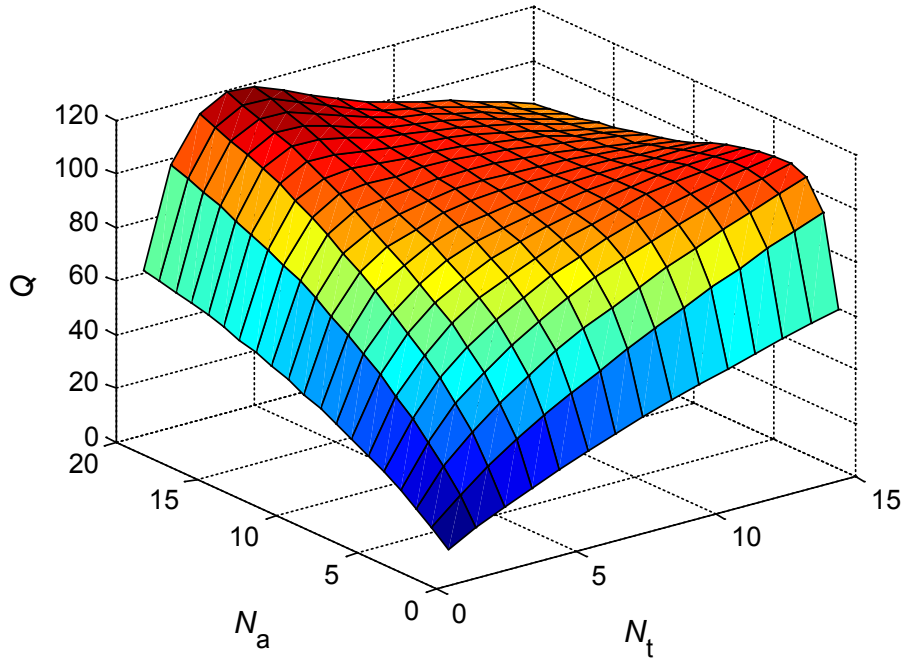

Figure 3.8 Quality factor versus N_t and N_a (simulated by the author)

3.2.3.2 Secondary Coil

The WPT system optimization for this thesis assumes that the load resistance in the secondary coil of the receiver is set to 80 Ω. Thus the quality factor of the secondary coil circuit will be small. However, the WPT system efficiency mainly depends on the quality factor of the transmitter coil and the primary receiver coil. Therefore the quality factor of the secondary coil should be designed and adjusted based on (2.62) and (2.63), which improves the load power and system efficiency of WPT systems with the optimum coupling factor k_{34}. Due to the application, the overall size of the receiver in a three-coil configuration should be same as that of two-coil configuration. For a fixed number of turns per layer, which is set to 1 in this thesis, the quality factor of the coil depends on the number of layers. The outer radius of the secondary coil is same as the primary coil. The coupling factor k_{34} is fixed when the radiuses of the primary coil, secondary coil, misalignment distance and the space between primary and secondary coil are defined. The quality factor of the secondary coil by itself without the influence of the load resistance is shown in Figure 3.9. The quality factor increases with increasing number of layers.

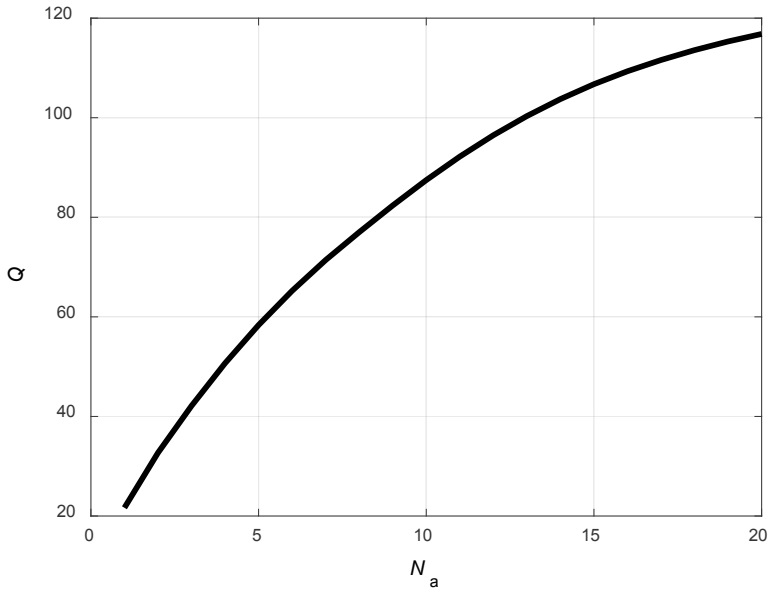

Figure 3.9 Quality factor of secondary coil of receiver (simulated by the author)

3.3 Comprehensive Optimization

3.3.1 Initial Values and Range of Parameters

For the single circular coil transmitter with radius r, the magnetic field strength H at the distance d along the z-axis is shown in (3.34), where I is the transmitter coil current.

$$H(x,r)=\frac{I\cdot r^2}{2\sqrt{\left(r^2+d^2\right)^3}} \tag{3.34}$$

The magnetic field strength along the z-axis achieves the maximum value when the radius r meets the condition of $r=\sqrt{2}d$ [Ram11]. The transmission distance is defined as 10 cm in this thesis, so the radius of the transmitter coil should be smaller than about 15 cm to result in a strong magnetic field at the location of the receiver. Larger radius coils will result in both less magnetic field at that distance and the flux being spread over a larger area. The proposed WPT system is to be used for charging mobile devices, so the receiver coil must fit in the mobile device. As mentioned in Section 3.2.3, the maximum outer radius allowed for the receiver primary coil and secondary coil is 4 cm.

3.3.2 Optimization Procedure

3.3.2.1 Coupling Factor

The coupling factor between two coils is defined as (3.35), where M is the mutual inductance between two inductively coupling coils presented in (3.6), L_2 and L_3 are self-inductance of the coils shown in (3.19).

$$k = \frac{M}{\sqrt{L_2 L_3}} \tag{3.35}$$

It is obvious that the coupling factor is independent of frequency and number of turns, but dependent on the size and shape of coils and their relative location. The estimated value of the coupling factor between the transmitter and the primary coil of the receiver is about 0.033 by simulation results according to (3.35). For the receiver, the outer radiuses of the primary and the secondary coil are same. The average distance between these two coils is about 5 mm. Therefore, the coupling factor between primary and secondary coils is about 0.65.

3.3.2.2 Operating Distance with Optimum Radius of Transmitter Coil

In three-coil configuration WPT system, the efficiency is proportional to the square of the coupling factor k_{23} multiplied by quality factors Q_{2sc} and Q_3 based on (2.58). That is to say, the larger the value of $k_{23}^2 Q_{2sc} Q_3$, the larger efficiency the WPT system can obtain. Figure 3.10 shows simulations results of the variation of $k_{23}^2 Q_{2sc} Q_3$ for different number of turns and radiuses of the transmitter at 10 cm transmission distance. For all values of the total number of turns, the factor $k_{23}^2 Q_{2sc} Q_3$ reaches the maximum when the inner radius of the transmitter coil is 10 cm. For all values of inner radius considered the variation of $k_{23}^2 Q_{2sc} Q_3$ increases with the increasing total number of turns.

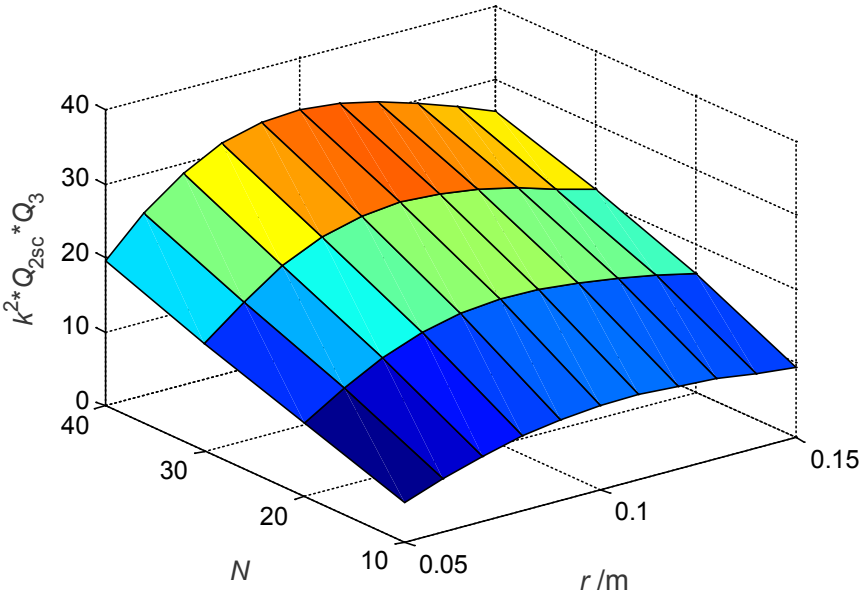

Figure 3.10 Combined optimization versus number of turns and radius in transmitter (simulated by the author)

3.3.2.3 Design Flow and Optimization

The power transfer is accomplished by resonant inductive coupling using transmitting and receiving coils. Thus the optimization procedure has to include both transmitter and the receiver coils. The design goals are to transfer high power to the load with high transfer efficiency. The radius of the receiver primary and secondary coils is determined by a size constraint due to the application. For a given outer radius of the primary coil, the number of turns per layer is determined when the maximum quality factor is achieved with minimum layers. The quality factor of the transmitter coil is maximized by optimizing the number of layers, number of turns per layer and radius. First, the number of turns per layer of the transmitter coil is optimized to obtain the maximum quality factor. Second, the radius of the transmitter coil is optimized according to the combination of coupling factor and quality factors $k_{23}^2 Q_{2sc} Q_3$. In order to decrease the effect of self-resonant frequency (SRF) on the quality factor according to (3.30), the SRF should be 10 times larger than the operating frequency (OF) [Gre01]. If the SRF is not large enough, it can be increased by decreasing the total number of turns or number of layers in the coil. The receiver secondary coil has the same outer radius as the primary coil. The number of turns per layer is set to 1, the number of layers determines the quality factor, which should be optimized with respect to (2.62) and (2.63). The flowchart of WPT system design used in this thesis is shown in Figure 3.11.

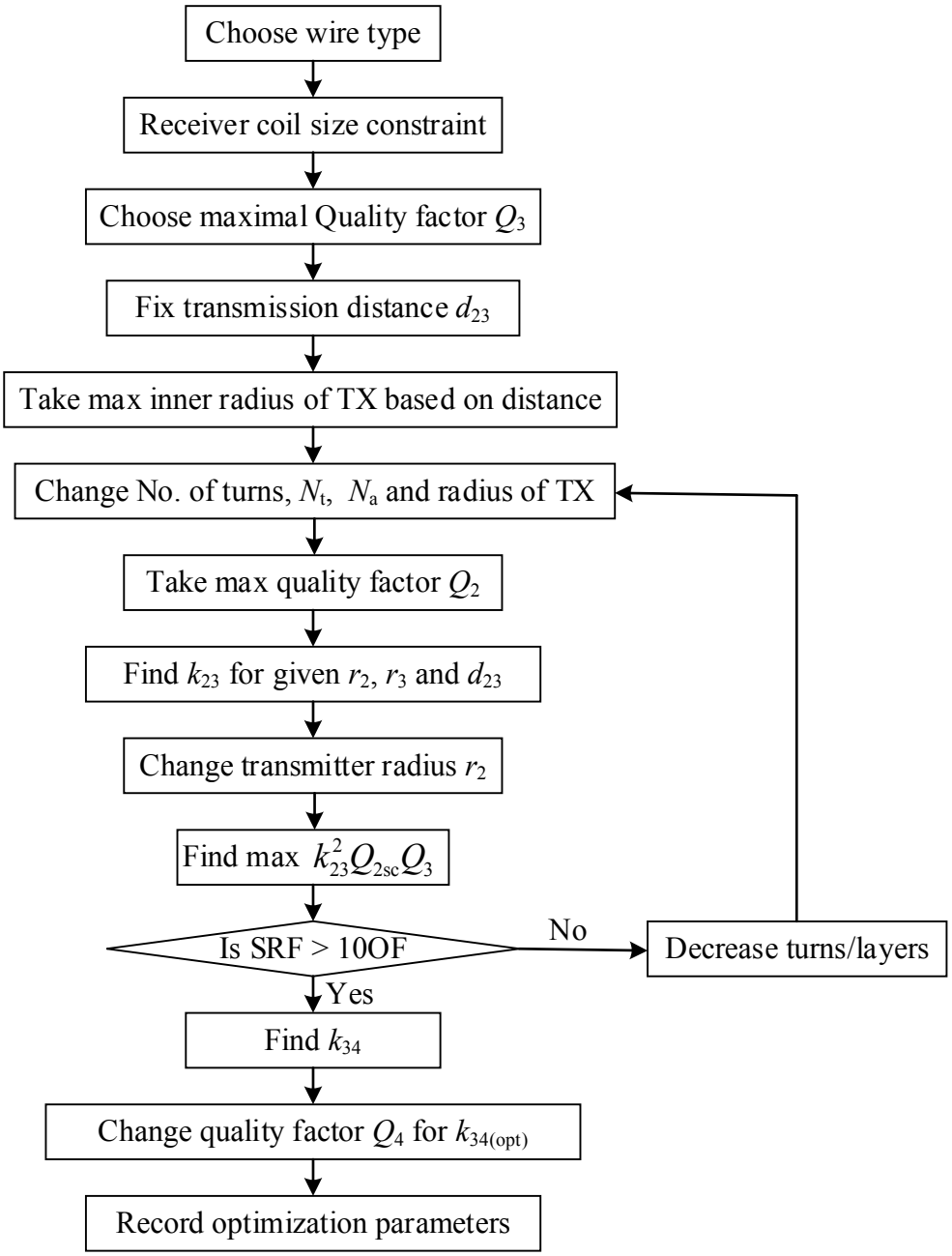

Figure 3.11 Flowchart for coils dimension optimization of WPT systems (derived by the author)

3.4 Performance Evaluation for Optimized WPT Systems

3.4.1 Parameters Determination

3.4.1.1 Parameters of Transmitter Coil

In the three-coil configuration WPT system, there is only one coil in the transmitter side. All parameters of the transmitter were optimized according to Figure 3.11, and are given in Table 3.3. The resistance, inductance and quality factor were measured with Agilent U1733C Handheld LCR Meter at the frequency of 100 kHz. The self-resonant frequency of the coil, as measured by the network analyzer, is 10 times larger than the operating frequency of 100 kHz. The coil configuration should be carefully designed to minimize shunt capacitance to prevent the coil from becoming capacitive.

Table 3.3 Parameters for transmitter coil

Parameters	Symbols	Design Values
Inner Radius (cm)	r_{in}	10
Number of turns per layer	N_t	2
Number of Layers	N_a	10
Resistance (Ω)	R_2	0.64
Inductance (μH)	L_2	183.38
Quality factor	Q_2	180
Self-resonant frequency(MHz)	SRF	1.6

3.4.1.2 Parameters of Receiver Coil

The receiver coils are optimized separately from the transmitter. For a three-coil WPT system, the receiver consists of two coils, a primary coil and secondary coil. The optimized parameters are given in Table 3.4. The quality factor of the primary coil should be as large as possible to achieve the maximum efficiency. For the secondary coil, the optimization of the quality factor with load resistor is 0.09, which satisfies the conditions determined by (2.62) and (2.63).

3.4.2 Simulation Results

Both transmitter and receiver coils have been optimized to achieve better WPT system performance in Section 3.3 above. The 2D configuration having maximum efficiency can be easily extended to a 3D configuration and the performance analyzed by simulation. The receiver is assumed to be located within the transmission area between -10 cm to 10 cm in both *x*-axis and *y*-axis, which corresponds to the area of the transmitter coil. The transmission distance is 10 cm. Figure 3.12 and Figure 3.13 show the power transfer efficiency at 100 kHz as a function of location within the 20 cm × 20 cm area above the transmitter coil in a 3D plot and a contour plot respectively. The power transfer efficiency of the optimized WPT system has a symmetric distribution centered about the center of the transmitter coil. The contour map clearly shows the area where the receiver can get high efficiency values. The area with over 60% efficiency is circular with a radius of 5 cm.

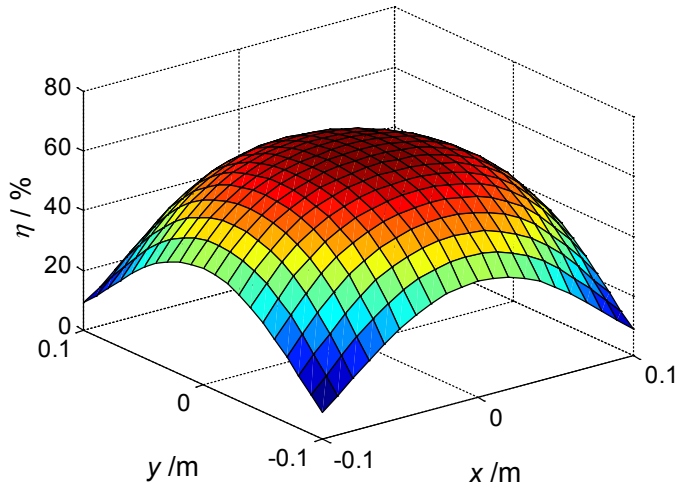

Figure 3.12 Efficiency of optimized WPT systems in 3D (simulated by the author)

Table 3.4 Parameters for receiver coil

Coils Types	Parameters	Symbols	Design Values
Primary Coil	Outer Radius (cm)	r_{out}	3.75
	Number of turns per layer	N_t	10
	Number of Layers	N_a	8
	Resistance (Ω)	R_3	4.3
	Inductance (μH)	L_3	693.1
	Quality factor	Q_3	101.3
Secondary Coil	Outer Radius (cm)	r_{out}	3.75
	Number of turns per layer	N_t	1
	Number of Layers	N_a	10
	Resistance (Ω)	R_4	0.09
	Inductance (μH)	L_4	12.66
	Quality factor	Q_4	88.38
	Coupling Factor	k_{34}	0.74

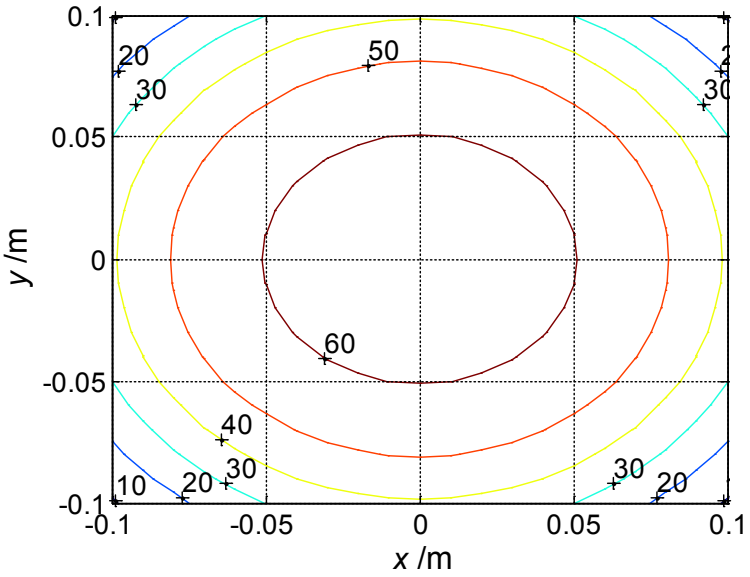

Figure 3.13 Efficiency of optimized WPT systems in contour (simulated by the author)

3.5 Chapter Summary

This chapter mainly contains the optimization process and results for the application of optimized transmitter and receiver coils in a three-coil WPT system. In this thesis, a multi-layer helical coil model is introduced and proposed for the WPT system. Multi-strand litz wire has been used to reduce losses due to skin and proximity effect, with 120 strands and 30 strands for transmitter and receiver coils respectively. As previously mentioned in Section 2.4.3, the efficiency of the WPT system is increased by maximizing the quality factor of the transmitter coil and receiver primary coil. The quality factor of the coils has been optimized based on parameters, such as radius, number of layers and number of turns per layer of coils. For the given load resistance, the quality factor of the receiver secondary coil is adjusted to achieve maximum load power and transmission efficiency simultaneously. Finally, all parameters are further optimized with respect to the coupling-quality factor $k_{23}^2 Q_{2sc} Q_3$, as well as keeping the SRF more than 10 times larger than the operating frequency. A WPT system with the optimized parameters has been simulated by Matlab and the maximum power transfer efficiency reaches about 65%, and is greater than 60% over an area with 5 cm radius.

Chapter 4

Magnetic Field Forming with Multiple Antennas for WPT System

4.1 Chapter Overview

In Chapter 3, the transmitter coil, the primary and the secondary coils of the receiver have been designed and optimized. Traditional WPT systems consist of just one transmitter coil and one receiver coil. The author presents a transmitting structure consisting of a matrix of overlapping coils which improves transmission efficiency and allows the receiver coil to be freely placed and charged above a relatively large wireless charging pad. The pad has a controller which can select the appropriate coils for charging depending on the location of the mobile device being charged. The optimum radius of the transmitter coils is determined for different transmitter matrixes based on field forming.

In Section 4.2 the WPT transmitter structure based on field forming is introduced and designed. Different multiple coil structures are presented and a structure with four overlapping coils (4-coil structure) is chosen as the best configuration for the transmitter. Theoretical analysis using the circuit model of the 4-coil structure transmitter is presented in Section 4.3. In Section 4.4, a multiple coil transmitter matrix is designed using the 4-coil structure as the basis. The best transmitter matrix is determined based on cost efficiency. The performance of the traditional single coil transmitter system is compared with the proposed 4-coil structure and the transmitter matrix by simulation. In Section 4.5 the chapter is summarized.

4.2 Transmitter Structure Based on Concept of Field Forming

4.2.1 Description of Field Forming

WPT systems have the challenge of generating a strong electromagnetic field at the charging device and at the same time elimination electromagnetic field interference to other devices in the vicinity of the transmitter [Sch11]. The magnetic near field in the vicinity of the transmitting coil falls off rapidly with distance leading to severe reduction in transferred power with increasing distance. The electromagnetic field in the vicinity of a WPT system must be kept low to minimize interference with nearby electronic devices and to comply with human safety requirements, while still supplying sufficient power to the charging devices. Field forming in introduced and applied to WPT systems in order to achieve high efficiency power transfer over longer distances. Field forming uses multiple antennas to spatially focus the electromagnetic field for dedicated power delivery to charging devices while keeping the field level minimal in all the other locations.

Field forming uses the combined magnetic fields from a set of non-directional coils to shape the near field to be concentrated in a certain region. Field forming can provide enhanced fields in one area with reduced fields in other areas. The approach is to design a system where the fields are focused in the area where the receiver will be located. The novelty in this proposal is the different transmitter structures used for field forming. Field forming takes advantage of constructive and destructive interference to change the shape of the near field. A technique similar to field forming can also be used for receiving by combining multiple receivers to achieve spatial selectivity. The transmitting field former controls the phase and relative amplitude of the signals at each transmitter coil in order to create a pattern of constructive and destructive interference. When receiving, the signals from different sensors are combined in such a way to receive radiation from a preferred direction. Magnetic field forming enables spatially focused or dedicated power delivery to charging devices, while reducing the fields at all other locations by controlling the phase shift and amplitude of the currents in the transmitting antennas.

Field forming is more significant for WPT transmitting systems than receiving systems for at least two reasons. First, the receiving antennas size is limited by the device, resulting in receiving antennas necessarily smaller than the transmitting

antenna. Second, the transmitted field is strong and needs to be controlled to minimize interference and human hazards. An array of multiple overlapping coils can be used change the magnetic field strength distribution (field forming). Placing the receiver in an area where the fields are concentrated by field forming will increase the WPT system efficiency. The aim is to determine the best structure for the transmitter to maximize energy transfer to the receiver. In the following sections magnetic field forming using multiple coils in various configurations in presented and analyzed [Che13].

4.2.2 Transmitter Structures

4.2.2.1 Overview

The transmitter consists of multiple overlapping coils, which are symmetrically distributed in an area of a 2D space. There are many different structures that can be used to generate various sorts of magnetic field distributions. It is possible to use single coil, 4-coil, 9-coil structures and so on for the transmitter. For now, only s^2 numbers of coil structures are chosen for the design, where s is limited to the positive integers 1, 2 and 3 because single coil, 4-coil and 9-coil structures are symmetric and easy to compare with the each other. Figure 4.1, Figure 4.2 and Figure 4.3 show examples for the single coil, 4-coil and 9-coil structures, respectively [Zha12].

4.2.2.2 Single Coil Structure

Figure 4.1 shows a single circular coil transmitter structure centered in a spherical coordinate system. The magnetic induction in any point in space for a single winding is shown in (4.1) [Sim01]. B_z is the magnetic induction in the z-axis direction. The space coordinates of point P are expressed as (d_o, θ, ϕ). d_o is the distance between point P and the center of the transmitter coil, which is in the origin of the coordinate system. r_ρ is the distance between the center of the transmitter coil and the projected point of P in the xy-plane. θ is the included angle between d_o and the z-axis and ϕ is the included angle between r_ρ and the x-axis. μ_0 is the vacuum permeability, the alternating electric current of the coil is I and the radius of the circular coil is r. $K(v)$ and $E(v)$ are complete elliptic integrals of the first and the second kind, defined in (4.2) and (4.3). The parameter k is the coefficient to calculate $K(v)$ and $E(v)$ and is defined in (4.4). The components B_x and B_y of the magnetic induction are not given because only magnetic induction in z-direction is effective for the receiver.

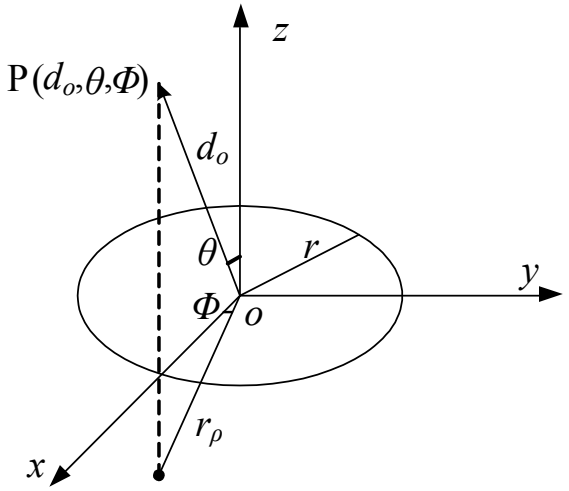

Figure 4.1 Single coil transmitter structure (conceptual representation of resources in **[Sim01]**)

$$B_z = \frac{\mu_0 I}{2\pi} \cdot \frac{1}{\sqrt{(r_\rho + r)^2 + (d_o \cos\theta)^2}} \cdot [K(\nu) + \frac{r^2 - r_\rho^2 - (d_o \cos\theta)^2}{(r_\rho - r)^2 + (d_o \cos\theta)^2} E(\nu)] \quad (4.1)$$

$$K(\nu) = \int_0^{\pi/2} \frac{d\phi}{\sqrt{1 - \nu^2 \sin^2 \phi}} \quad (4.2)$$

$$E(\nu) = \int_0^{\pi/2} \sqrt{1 - \nu^2 \sin^2 \phi} d\phi \quad (4.3)$$

$$\nu = \sqrt{\frac{4 \cdot r \cdot d_o \cdot \sin(\theta)}{d_o^2 + r^2 + 2 \cdot r \cdot d_o \cdot \sin(\theta)}} \quad (4.4)$$

Then the *z*-component of the magnetic induction of a single coil with a given number of turns of *N* is shown in (4.5).

$$B_z^n = \frac{\mu_0 I N}{2\pi} \cdot \frac{1}{\sqrt{(r_\rho + r)^2 + z^2}} \cdot [K(\nu) + \frac{r^2 - r_\rho^2 - z^2}{(r_\rho - r)^2 + z^2} E(\nu)] \quad (4.5)$$

4.2.2.3 4-Coil Structure

Figure 4.2 shows a 4-coil transmitter structure, where all four coils are connected in series. r is the radius of each coil and d_{dia} is the maximum diagonal line distance of the opposite coils. It is important to note that these coils are

overlapping. The coordinate of point P in the 3D space is (x_P,y_P,z_P). Point B shown in Figure 4.2 is the vertical projection of point P in the *xy*-plane. The magnetic induction of point P is calculated as follows. Let the center coordinates of the four coils be (x_1, y_1), (x_2, y_2), (x_3, y_3) and (x_4, y_4), respectively. Since the magnetic conduction caused by one coil is shown in (4.5), the magnetic induction of each coil in the 4-coil structure can be deduced by analogy in (4.6). The index m represents the sequence number of the coils from 1 to 4. N is number of turns of each coil and is the same for each coil in the 4-coil structure.

$$B_{z,m}^{n} = \frac{\mu_0 IN}{2\pi} \cdot \frac{1}{\sqrt{(\sqrt{(x_P - x_m)^2 + (y_P - y_m)^2} + r)^2 + z_P^2}} \cdot \left[K(\nu_m) + \frac{r^2 - ((x_P - x_m)^2 + (y_P - y_m)^2) - z_P^2}{(\sqrt{(x_P - x_m)^2 + (y_P - y_m)^2} - r)^2 + z_P^2} E(\nu_m)\right] \tag{4.6}$$

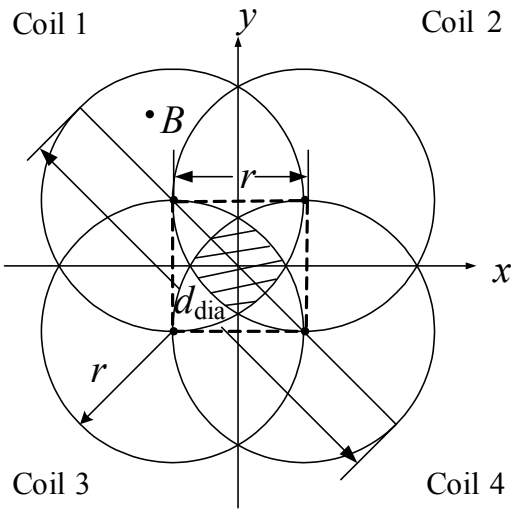

Figure 4.2 4-coil transmitter structure (found by the author)

The $K(\nu_m)$ and $E(\nu_m)$ calculation methods can be found in (4.2) and (4.3). The ν_m calculation method for all coils with m = 1, 2, 3 or 4 is shown in (4.7).

$$\nu_m = \sqrt{\frac{4r\sqrt{(x_P - x_m)^2 + (y_P - y_m)^2}}{(r + \sqrt{(x_P - x_m)^2 + (y_P - y_m)^2})^2 + z_P^2}} \tag{4.7}$$

Then the total magnetic induction $B_{z,tot}^{n}$ at point P generated by the transmitter is calculated by vector addition of the magnetic induction from each coil as shown

in (4.8). In the intersecting part (Figure 4.2 shadow area), the lines of magnetic induction are nearly parallel with each other so that the vector addition of the magnetic induction is larger in that area. Therefore, the power transfer efficiency will be maximum for a receiver located in that area.

$$B_{z,tot}^{n} = B_{z,1}^{n} + B_{z,2}^{n} + B_{z,3}^{n} + B_{z,4}^{n} \tag{4.8}$$

The coupling between each pair of transmitter coils results in mutual inductances in the transmitter antenna inductance. The total inductance of the transmitter antenna includes the self-inductance and the mutual inductance between each pair of coils. The current in each transmitter coil is the same, since the 4 coils are connected in series. When resonated by a capacitor, the coil impedance is just equal to the coil resistance. So that for a given source voltage, the current at resonance is not affected by the change in reactance due to mutual coupling. Since the magnetic induction is a function of the current, as shown in (4.1), the total magnetic induction of the 4 coils can be added directly.

The coordinates of (x_1,y_1), (x_2,y_2), (x_3,y_3), and (x_4,y_4) can be expressed by d_{dia} and r, which is shown in (4.9). Figure 4.2 presents the scenario with the 4-coil structure set with the distance between coil centers equal to the radius r. For this case the parameter d_{dia} is expressed in (4.10).

$$\begin{aligned}
x_1 &= \frac{d_{\text{dia}} - 2\cdot r}{2\sqrt{2}}, y_1 = \frac{d_{\text{dia}} - 2\cdot r}{2\sqrt{2}} \\
x_2 &= -\frac{d_{\text{dia}} - 2\cdot r}{2\sqrt{2}}, y_2 = \frac{d_{\text{dia}} - 2\cdot r}{2\sqrt{2}} \\
x_3 &= -\frac{d_{\text{dia}} - 2\cdot r}{2\sqrt{2}}, y_3 = -\frac{d_{\text{dia}} - 2\cdot r}{2\sqrt{2}} \\
x_4 &= \frac{d_{\text{dia}} - 2\cdot r}{2\sqrt{2}}, y_4 = -\frac{d_{\text{dia}} - 2\cdot r}{2\sqrt{2}}
\end{aligned} \tag{4.9}$$

$$d_{\text{dia}} = 2r + \sqrt{2}r \tag{4.10}$$

4.2.2.4 9-Coil Structure

Figure 4.3 shows the 9-coil structure transmitter where all of the coils are symmetrically distributed with the same total area as for the 4-coil structure. The calculation for the magnetic induction from the 9-coil structure transmitter is similar to that for the single coil structure and 4-coil structure transmitter.

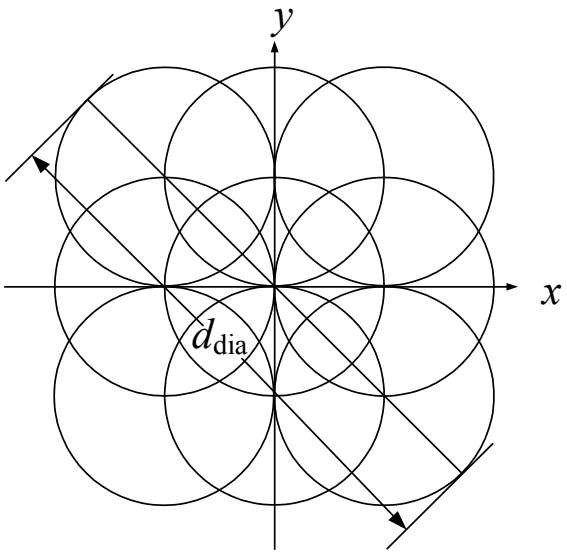

Figure 4.3 9-coil transmitter structure (found by the author)

4.2.3 Comparison between the Single Coil and the Proposed Transmitter Structure

Figure 4.4 shows a plot comparing the magnetic field generated by a single coil, a 4-coil structure and a 9-coil structure transmitter, based on the geometric construction shown in Figure 4.1, Figure 4.2 and Figure 4.3. Figure 4.4 is based on the assumption that the multiple overlapping coil configurations and the single coil transmitter have the same area and the receiver is placed the same transmission distance from the transmitter. Both the proposed transmitter and the traditional transmitter have the highest efficiency when the centers of the receiver and the transmitter are coaxial from Figure 4.4. The proposed multiple overlapping coil structures present a viable and simple method resulting in forming the magnetic field of the transmitter such that the magnetic field is strengthened in the central zone and weakened on the margins of the transmitter structure.

There are two potential advantages of magnetic field forming. One is that the maximum efficiency of the proposed transmitter will be greater than that for the single coil transmitter since there will be more magnetic induction at the receiver. The other is that since the magnetic induction is more nearly uniform in the high field area, the area where high efficiency power transfer occurs is larger for the overlapping coil transmitter than for the single coil transmitter. Furthermore, in the fringing field area, the efficiency of the multiple coil transmitter declines more

quickly than that for the single coil transmitter because the field generated by the multiple coil structure is focused in a certain area while decreased in the remaining space. It is observed from Figure 4.4, that the 4-coil structure appears to have the best field forming of the structures considered since the field at the center is stronger over a larger region and the field outside that area is smaller.

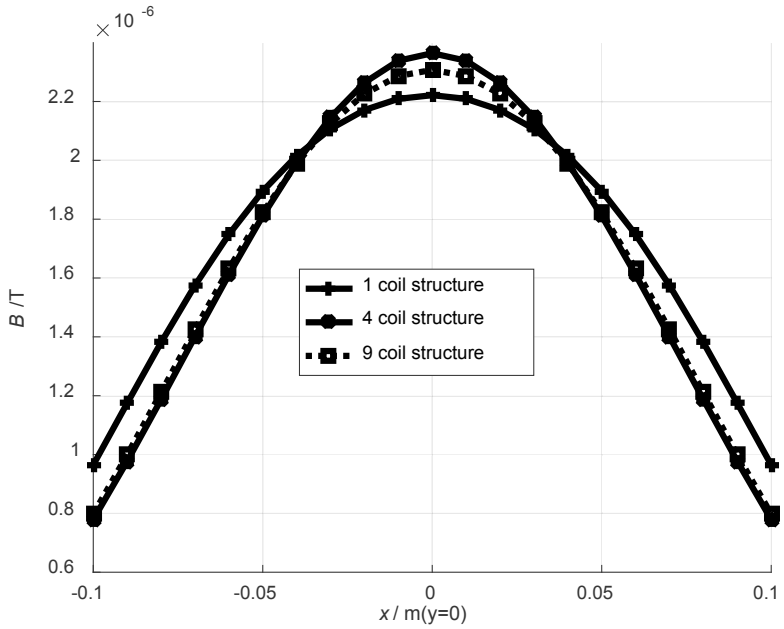

Figure 4.4 Field forming based on different coil structures (simulated by the author)

4.3 Theoretical Analysis for 4-Coil Structure

4.3.1 Circuit Diagram of Resonant WPT Systems

Figure 4.5 shows the circuit diagram for the WPT system with a 4-coil structure transmitter and two coils in the receiver [Che13]. The coils are connected in series so that each coil carries the same current, that is the same amplitude, same phase and same frequency. Assume that the resistance, the inductance and capacitance values are the same in all 4 coils of the transmitter. As in [Ram11], the efficiency of a WPT system having coupling coils in both the transmitter and the receiver is higher than that without them. As [Ram11] elaborates, the efficiency of a WPT system depends mainly on the quality factors of the transmitter secondary coil and receiver primary coil. The internal resistance of the power source is assumed

small (0.5 Ω) in this WPT system demonstration so that circuit quality factor of the single in the transmitter is kept at a high value.

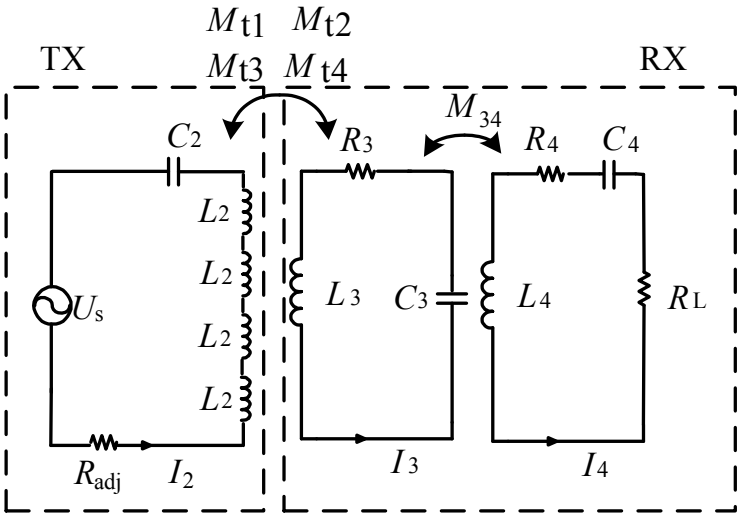

Figure 4.5 Wireless power transfer system for 4-coil structure (derived by the author)

Let M_{t1}, M_{t2}, M_{t3}, M_{t4} be the mutual inductance between each transmitter coil and the primary coil of the receiver. Let M_{34} be the mutual inductance between the primary coil and the secondary coil in the receiver. Let U_s be the sinusoidal voltage of the transmitter with angular frequency ω_0. Let R_2, R_3 and R_4 be the internal resistances of a single transmitter coil, the primary coil and the secondary coil of the receiver, respectively. Let R_L be the load resistance on the receiver secondary coil. Let L_2, L_3 and L_4 be the inductance of a single transmitter coil, the primary coil and the secondary coil of the receiver, respectively. C_2, C_3 and C_4 are the capacitors of the transmitter, the primary coil and the secondary coil of the receiver. All capacitors should be adjusted for appropriate values to make the system (transmitter and receiver) work at resonance with the same frequency as shown in (4.11) to achieve maximum power transfer. R_{adj} is the total resistance of the four series connected transmitter coils. L_{adj} is the total inductance of the four series connected transmitter coils, including mutual inductance as shown in (4.12) . m is the number of coils in the transmitter. M is the mutual inductance between each two coils in the transmitter, which is calculated in (3.6). Plus and minus signs stand for in-phase and out-phase connection between each two coils in the transmitter side. The magnitude of the quality factor is directly proportional to inductance. Thus, large inductance is preferred. Therefore, all the coils in the

transmitter should be series connected in-phase, which leads to maximal inductance.

$$\omega_0 = \frac{1}{\sqrt{L_{\text{adj}}C_2}} = \frac{1}{\sqrt{L_3C_3}} = \frac{1}{\sqrt{L_4C_4}} \tag{4.11}$$

$$L_{\text{adj}} = 4L_2 \pm \sum_{i=1}^{m}\sum_{j=1\neq i}^{m} M_{ij} \tag{4.12}$$

4.3.2 Analysis of Power Transfer Efficiency

The efficiency of the WPT systems can be defined as the ratio of the received power in the load to the delivered power from the electric power source. The circuit model is used to analyze the performance of the proposed WPT systems using magnetically coupling resonators. The mutual inductance between the transmitter and the secondary coil of the receiver has been neglected in the following analysis. Then, the current in each resonant circuit is determined from (4.13) to (4.16) by using Kirchhoff's voltage law.

$$I_2\left(R_{\text{adj}} + j\omega L_{\text{adj}} + \frac{1}{j\omega C_2}\right) - I_3 j\omega M_{\text{tot}} = U_{\text{s}} \tag{4.13}$$

$$I_3\left(R_3 + j\omega L_3 + \frac{1}{j\omega C_3}\right) - I_2 j\omega M_{\text{tot}} - I_4 j\omega M_{34} = 0 \tag{4.14}$$

$$I_4\left(R_4 + j\omega L_4 + \frac{1}{j\omega C_4} + R_{\text{L}}\right) - I_3 j\omega M_{34} = 0 \tag{4.15}$$

$$M_{\text{tot}} = \sqrt{M_{\text{t1}}^2 + M_{\text{t2}}^2 + M_{\text{t3}}^2 + M_{\text{t4}}^2} \tag{4.16}$$

The efficiency of the WPT systems model is calculated in (4.17), which shows that larger values of system angular frequency ω and M_{tot} increase transfer efficiency, where $R_{4\text{L}} = R_4 + R_{\text{L}}$. Also, smaller values of R_{adj}, R_3 and R_4 give higher efficiency for the 4-coil structure transmitter WPT system. The efficiency can also be expressed as (4.18), which is with respect to coupling coefficient and quality factor of the transmitter and receiver, where $Q_{4\text{sc}} = \omega_0 L_4 / R_{4\text{L}}$, $Q_{2\text{sc}} = \omega_0 L_{\text{adj}} / R_{\text{adj}}$, $Q_3 = \omega_0 L_3 / R_3$, $k_{23} = M_{\text{tot}} / \sqrt{L_{\text{adj}} L_3}$, $k_{34} = M_{34} / \sqrt{L_3 L_4}$.

$$\eta_{4str} = \frac{\omega_0^4 M_{tot}^2 M_{34}^2 R_L}{(R_{adj} R_3 R_{4L} + R_{4L}\omega_0^2 M_{tot}^2 + R_{adj}\omega_0^2 M_{34}^2)\cdot(R_3 R_{4L} + \omega_0^2 M_{34}^2)} \tag{4.17}$$

$$\eta_{4str} = \frac{R_L}{R_{4L}} \cdot \frac{k_{34}^2 Q_3 Q_{4sc}}{1 + k_{34}^2 Q_3 Q_{4sc}} \cdot \frac{k_{23}^2 Q_{2sc} Q_3}{1 + k_{23}^2 Q_{2sc} Q_3 + k_{34}^2 Q_3 Q_{4sc}} \tag{4.18}$$

Equation (4.18) is similar to the efficiency of single coil transmitter shown in (2.58) because the receiver side is the same for both the single coil and 4-coil structure transmitters. The field forming effect realized by the 4-coil structure WPT system depends on the key parameters k_{23} and Q_{2sc}.

4.3.3 Optimization Criterion

The author has already optimized the total number of turns and number of layers of a single transmitter coil based on quality factor in Section 3.2.2. Each coil in the 4-coil structure uses the optimum values determined for the single coil transmitter. For the 4-coil structure transmitter WPT system, there are three methods to maximize the efficiency for each receiver position. First, set the radius of each coil of 4-coil structure transmitter to the same as that for the optimized single coil structure. Then adjust the center to center distance d_{cc} between each two coils for optimum, as shown in (4.19). The variation of d_{cc} leads to increasing or decreasing the parameters Q_{2sc} and k_{23}, which have significant effect on the transfer efficiency.

$$\eta_{4str\_max} = \frac{\partial \eta_{4str}}{\partial d_{cc}} = 0 \tag{4.19}$$

The radius of a single transmitter coil has been optimized for WPT system power transfer efficiency at 10 cm transmission distance in Section 3.3. Second, the maximum efficiency for each receiver position is achieved by using the optimized radius r of the coils of the 4-coil structure transmitter for the fixed transmission distance and center to center distance d_{cc}, as shown in (4.20) [Che13].

$$\eta_{4str\_max} = \frac{\partial \eta_{4str}}{\partial r} = 0 \tag{4.20}$$

Third, the 4-coil structure WPT system is optimized with respect to the radius or center to center distance given the fixed parameter d_{dia}, which is the maximum diagonal across the coils shown in Figure 4.2. The fixed relationship of coil

radius, d_{cc} and d_{dia} is presented in (4.9). The system efficiency of a 4-coil structure WPT system can be improved by increasing the number of turns of the transmitter and receiver coils as well as their radiuses. However, the number of turns and the radiuses cannot be too large otherwise they will exceed the design constraints.

4.4 Cooperative Coil Transmitter Matrix for Position Independent Positioning WPT Systems

4.4.1 Transmitter Matrix Based on 4-Coil Structure

Here the author proposes a matrix of coils creating a large area and operated in such a way as to allow free placement of the device to be charged anywhere in the charging area. In Section 4.2.3, the 4-coil structure is proved to be more efficient than the single coil and 9-coil transmitter structures due to field forming. The proposed cooperative transmitter matrix consists of multiple coils which are arranged symmetrically [Che14a]. There can be 4 coils, 9 coils, 16 coils and 25 coils arrayed to form a multiple coil transmitter matrix. For now, only s^2 numbers of coils are chosen for the design, where s is limited to the positive integers 2, 3, 4 and 5, because 4 coils, 9 coils, 16 coils and 25 coils are symmetric and easy to analyze for comparison. Coordinates of the coil circle centers constitute the overall charging area (OCA), which is assumed to be the same for all transmitter matrixes considered. The novel concept is that the transmitter matrix will activate a single sub-charging zone, consisting of at most four coils, when the location of the receiver has been detected by the transmitter matrix controller. In the case studied here each sub-charging zone (SCZ) is formed from the fields generated by four adjacent coils. The center of the sub-charging zone (CSCZ) consists of the area defined by the coordinates of the circle centers of the four adjacent coils forming the SCZ.

The optimum coil radius for the coils will be determined for each of the configurations. The formula for calculation of the initial (minimum) coil radius, r, that is to be optimized for the cooperative transmitter matrix is shown in (4.21). That means two adjacent coils are tangent to each other in the initial multiple coil transmitter matrix. L_{sl} is the side length of the OCA and n_c is the number of coils in the matrix.

$$r = \frac{L_{\mathrm{sl}}}{2 \times \left(\sqrt{n_{\mathrm{c}}} - 1 \right)} \tag{4.21}$$

Figure 4.6 (a), (b), (c) and (d) shows 4 coils, 9 coils, 16 coils and 25 coils with the minimum radius given by (4.21) respectively in the cooperative transmitter matrix with the same OCA of 20 cm × 20 cm. When the receiver is located in the CSCZ, the 4 coils whose circle center coordinates constitute this CSCZ will be switched on. That is to say, the 4 coils having their circle center coordinates are closest to the position of the vertical projection of the mobile device center. Take Figure 4.6 (b) as example, when the receiver is placed at (7 cm, 7 cm), the 4 coils with circle center coordinates (0 cm, 0 cm), (0 cm, 10 cm), (10 cm, 0 cm), (10 cm, 10 cm) respectively would be switched on to charge the receiver coil. Obviously the CSCZ is different for different numbers of coils in the transmitter matrix. For example, the CSCZ is 5 cm × 5 cm in the rectangular coordinate system shown in Figure 4.6 (d).

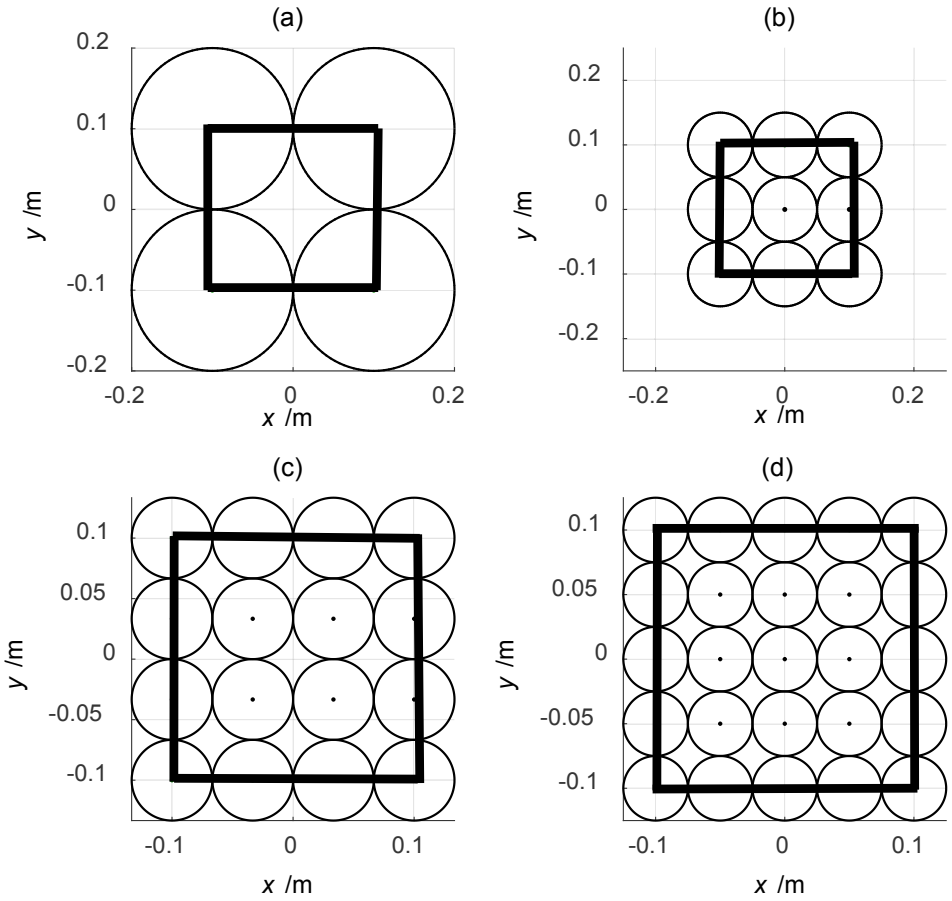

Figure 4.6 Different number of coils for initial transmitter matrix (found by the author)

4.4.2 Design Process for the Multiple Coil Transmitter Matrix

Let the radius of each coil be the same for all coils in the transmitter matrix. The radiuses should be optimized to gain higher transfer efficiency in the CSCZ and lower efficiency on the margins of the SCZ for each transmitter matrix based on field forming theory. Using the optimized 4-coil structure in transmitter matrixes having more than 4 coils, the optimal numbers of coils in the transmitter matrix should be determined also. That is to say, author would choose the best transmitter matrix from 4 coils, 9 coils, 16 coils or 25 coils. A transmitter matrix controller is assumed to select the appropriate set of 4 coils within the matrix depending upon the device location. The final aim of this design is to make the OCA (20 cm × 20 cm) such that high efficiency wireless power transfer is available independent of location with a shorter total length of litz wire winding.

4.4.3 Optimization of Transmitter Matrix

4.4.3.1 Radius Optimization

The weighted average efficiency has been developed to evaluate the performance as a function of coil radius. Note that for this optimization, as the coil radius increases from the minimum given in (4.21), the coils overlap as per Figure 4.2 and Figure 4.3. The average efficiency is calculated in two areas, the CSCZ and in the marginal area around the SCZ as given in (4.23). The average is calculated by taking the sum of the receiver transfer efficiency at several sample locations in the associated area and dividing by the number of samples. Then the weighted average efficiency is defined as the weighted sum of the receiver average efficiency in the CSCZ and the reciprocal of the receiver average efficiency in the marginal area around the SCZ. This function is maximized in order to obtain maximum average efficiency for the CSCZ and at the same time minimum average efficiency in the margin around the SCZ. The weighted average efficiency is calculated by (4.22). r_ρ is the distance between center of transmitter matrix and projection of receiver center, $r_{\rho\text{avg\_center}}$ and $r_{\rho\text{avg\_edge}}$ are lateral misalignment distance when the projection of the receiver center is in the CSCZ and the marginal area of SCZ separately. m_p and n_p are number of testing positions in CSCZ and edge of SCZ separately. r is the radius of the coil. α and β are the weighting coefficients applied to the average efficiency in the CSCZ and inverse of the average efficiency in the SCZ fringe area respectively. The weighting coefficients α and β are set as 0.45 and 0.55 respectively.

$$\eta\left(r,r_\rho\right)_{\text{weighted\_ave}} = \alpha\cdot\eta\left(r,r_{\rho\text{avg\_center}}\right)_{\text{average}} + \beta\cdot \Big/ \eta\left(r,r_{\rho\text{avg\_edge}}\right)_{\text{average}} \qquad (4.22)$$
$$\alpha+\beta=1$$

$$\begin{aligned}\eta\left(r,r_{\rho\text{avg\_center}}\right)_{\text{average}} &= \sum_{ii=1}^{m_\text{p}}\eta\left(r,r_{\rho ii}\right)\Big/ m_\text{p}\\ \eta\left(r,r_{\rho\text{avg\_edge}}\right)_{\text{average}} &= \sum_{jj=1}^{n_\text{p}}\eta\left(r,r_{\rho jj}\right)\Big/ n_\text{p}\end{aligned} \qquad (4.23)$$

In addition, the difference between the average efficiency in the CSCZ and the average efficiency in the marginal area of the SCZ is an important indicator for coil radius optimization, which is presented in (4.24). The larger the difference, the more effective is the field forming effect. The weighted overall efficiency is a measure of the influence on the field forming effect of the weighted average

efficiency and average difference efficiency shown in (4.25). α and β are the weighting coefficients for weighted average efficiency and average difference efficiency of the CSCZ and edge of SCZ respectively, as shown in (4.22). The values of α and β are set as 0.7 and 0.3 respectively.

$$\eta\left(r,r_{\rho}\right)_{\text{average\_diff}}=\eta\left(r,r_{\rho\text{avg\_center}}\right)_{\text{average}}-\eta\left(r,r_{\rho\text{avg\_edge}}\right)_{\text{average}} \tag{4.24}$$

$$\eta\left(r,r_{\rho}\right)_{\text{weighed\_overall}}=\alpha\cdot\eta\left(r,r_{\rho}\right)_{\text{weighted\_ave}}+\beta\cdot\eta\left(r,r_{\rho}\right)_{\text{average\_diff}} \tag{4.25}$$

At a fixed transmission distance, the areas of maximum and minimum magnetic field are a function of the transmitter coil radiuses. Magnetic field forming can be used to make some area have high efficiency while other areas have low efficiency. To achieve the objective of higher transfer efficiency in the CSCZ, with lower efficiency in the marginal area of the SCZ, the weighted overall efficiency of the transmitter should be maximum according to (4.25). The optimal coil radius needs to be determined to give the best 4-coil structure for different transmitter matrixes. Figure 4.7, Figure 4.8, Figure 4.9 and Figure 4.10 show the efficiency curves of the 4-coil structure for 4 coils, 9 coils, 16 coils and 25 coils transmitter matrixes with the same number of turns respectively. Each figure presents the efficiency as a function of the transmitter coil radius. Each figure has efficiency curves for 11 different receiver center coordinates labeled RCC (*x* cm, *y* cm), average efficiency in RC, average efficiency in RE, weighted average efficiency and weighted overall efficiency by different transmitter radiuses. RC and RE represent the receiver in the center and receiver on the edge of the SCZ respectively.

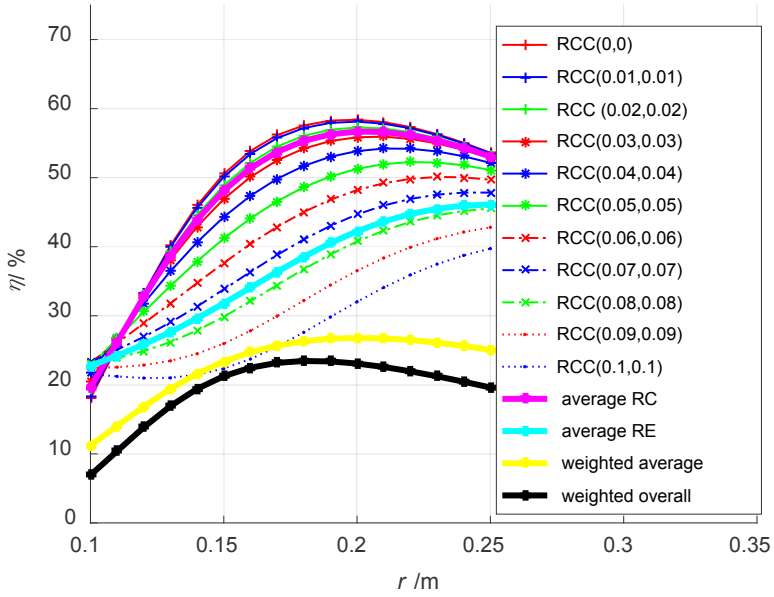

Figure 4.7 Efficiency with different receiver positions of 4 coils matrix (simulated by the author)

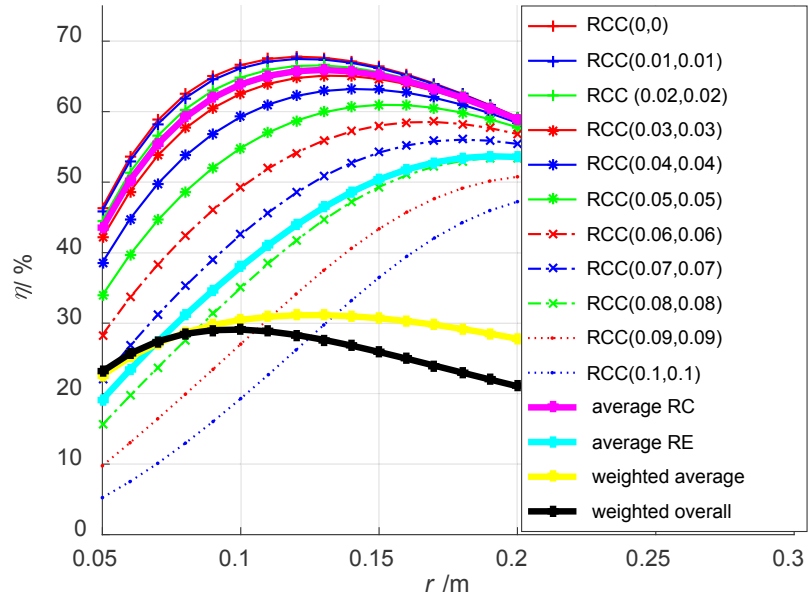

Figure 4.8 Efficiency with different receiver positions of 9 coils matrix (simulated by the author)

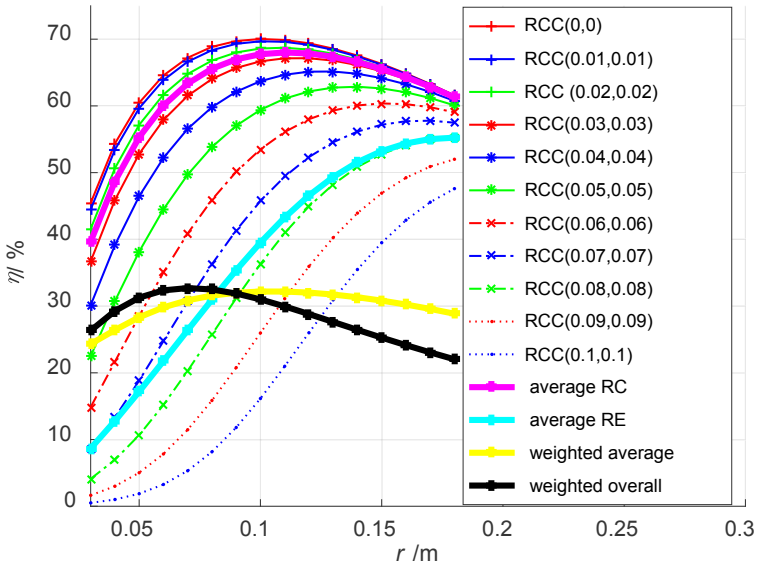

Figure 4.9 Efficiency with different receiver positions of 16 coils matrix (simulated by the author)

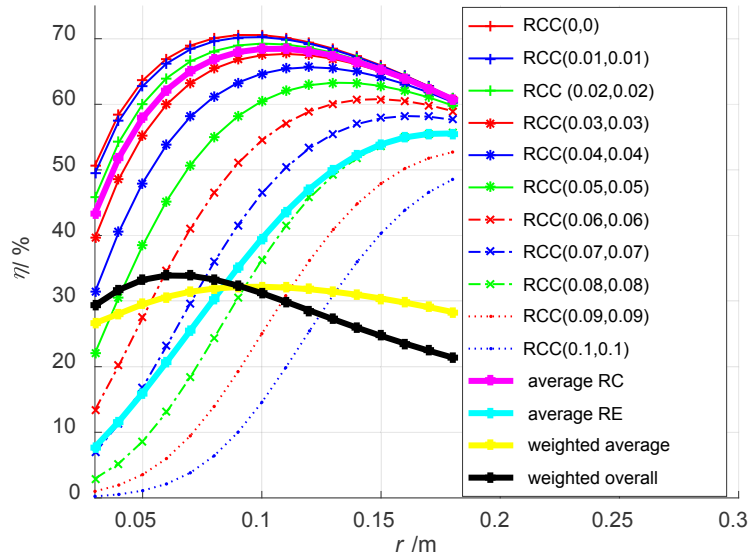

Figure 4.10 Efficiency with different receiver positions of 25 coils matrix (simulated by the author)

Observing the weighted overall efficiency curve from Figure 4.7, Figure 4.8, Figure 4.9 and Figure 4.10, the optimal radius of 4 coils, 9 coils, 16 coils and 25 coils transmitter matrixes are 0.18 m, 0.1 m, 0.07 m and 0.06 m separately in our simulation model. Using the optimum radius for each transmitter matrix will

strengthen the effect of field forming and provide a WPT system having high efficiency and low external fields.

4.4.3.2 Transmitter Matrix Selection Based on Cost Efficiency

Section 4.4.3.1 presents different four transmitter coil matrixes each having different optimal radius for the coils. First of all, we define the concept of a weighted overall efficiency gain ratio which is given in (4.26). η_{ratio} means the weighted overall efficiency of WTP system per unit length of transmitter coil. The radius is optimized based on considering every possible 4-coil structure. N is the number of turns for each coil, r_{opt} is the optimal radius for the particular transmitter matrix being considered. $\eta_{\text{weighed\_overall}}$ is the weighted overall efficiency of SCZ. From Figure 4.7, Figure 4.8, Figure 4.9 and Figure 4.10, the 4-coil structure with the 25 coils transmitter matrix with has the maximum η_{ratio}. That means the weighted overall efficiency will achieve a higher value with same length of windings. In other words, the 4-coil structure in a 25 coils transmitter matrix uses the least winding length while achieving the same weighted overall efficiency as that of 4-coil structure configured as of 4 coils, 9 coils and 16 coils transmitter matrixes.

$$\eta_{\text{ratio}} = \frac{\eta_{\text{weighed\_overall}}}{2 \times \pi \times r_{\text{opt}} \times N \times 4} \tag{4.26}$$

The cost efficiency (CE) η_{CE} takes into account both the efficiency gain ratio of the weighted overall efficiency and the total expense for building the transmitter coil matrix, shown in (4.27), where n_{c} is the number of coils of different transmitter matrixes. Then the best transmitter matrix can be selected on the basis of maximum cost efficiency, which is a tradeoff between efficiency gain ratio and cost of windings. From the simulation results shown in Table 4.1, the 16 coils transmitter matrix has the highest cost efficiency. Therefore, the results of this thesis indicate that the 16 coils transmitter matrix will make the best WPT system given the constraints used.

$$\eta_{\text{CE}} = \eta_{\text{ratio}} \cdot \frac{1}{2 \times \pi \times r_{\text{opt}} \times N \times n_{\text{c}}} \tag{4.27}$$

Table 4.1 Performance of different transmitter matrix

Transmitter Matrix	$\eta_{\text{weighted\_overall}}$ (%)	η_{ratio} (%)	η_{CE} (%)
4 coils	23.4718	0.2497	0.0027
9 coils	28.9041	0.5374	0.0044
16 coils	32.499	0.8397	0.0054
25 coils	33.8967	1.0065	0.0048

4.4.3.3 Efficiency Comparison for Single Coil and 16 Coils Matrix with Optimized Parameters in OCA

In the 16 coils transmitter matrix, the receiver is assumed to be placed from -0.1 m to 0.1 m in both *x*-axis and *y*-axis. The height of the receiver above the transmitter is 0.1 m. The transfer efficiency for the 16 coils matrix using the 4-coil sub structure having the optimal coil radius and operating at 100 kHz is given as a 3D plot in Figure 4.11 and as a contour map in Figure 4.12. For each 4-coil structure, the area with over 65 % efficiency is circular with a radius of 0.03 m. Simulation results in Figure 4.12 show that the 16 coils matrix transmitter is able to transfer power with greater than 63 % efficiency, for a transmission distance of 10 cm, at any location within the 0.2 m × 0.2 m pad area.

The author has presented optimum value of number of turns per layer is 2 in Section 3.2.2, as well as the optimal inner radius of single coil structure WPT system of 0.1 m for a 10 cm transfer distance in Section 3.3. Figure 4.13 shows the receiver efficiency as it moves along the *x*-axis from -0.1 m to 0.1 m, while the position on the *y*-axis is always 0 m for the 4-coil structure configured in a 16 coils matrix. This is compared with the same receiver moving above a single coil structure. Both the traditional single coil and proposed 4-coil structure used in a 16 coils transmitter matrix have more than 65 % efficiency when the receiver is located at the center of the transmitter. The 16 coils transmitter matrix guarantees the CSCZ area where the receiver is located has high efficiency with more than 65 %, while the efficiency in other zones of the matrix decreases rapidly. That means that high efficiency is achieved as well as reducing the magnetic field strength in the marginal area of the SCZ so as to have little effect on other electronic devices located nearby.

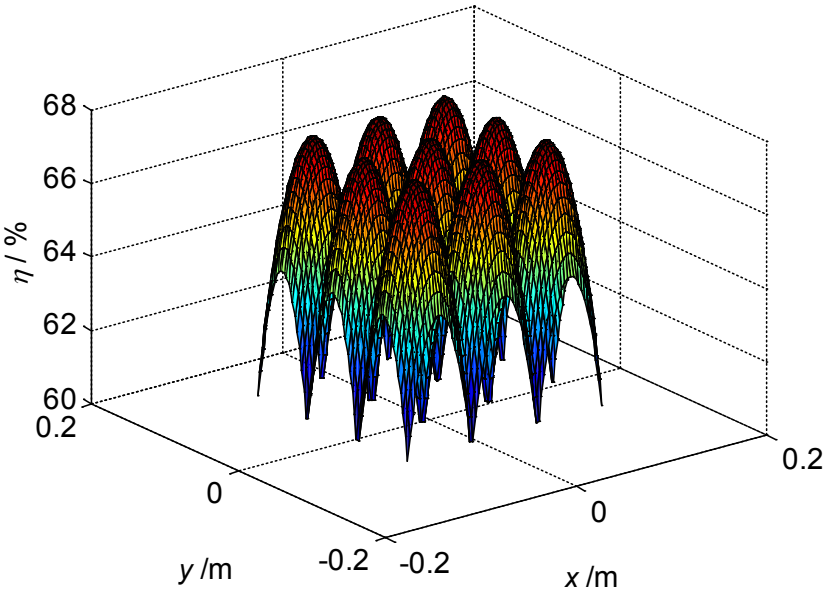

Figure 4.11 16 Coils transmitter matrix efficiency (simulated by the author)

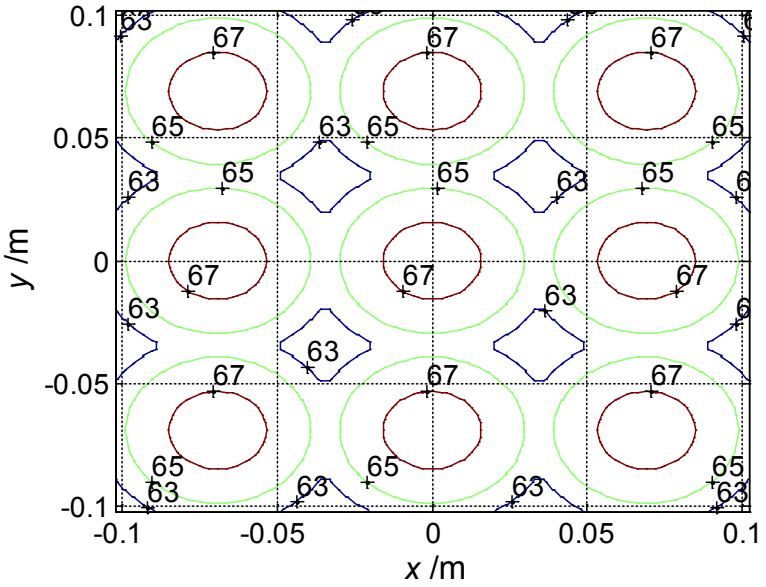

Figure 4.12 Efficiency of contour maps for 16 coils matrix (simulated by the author)

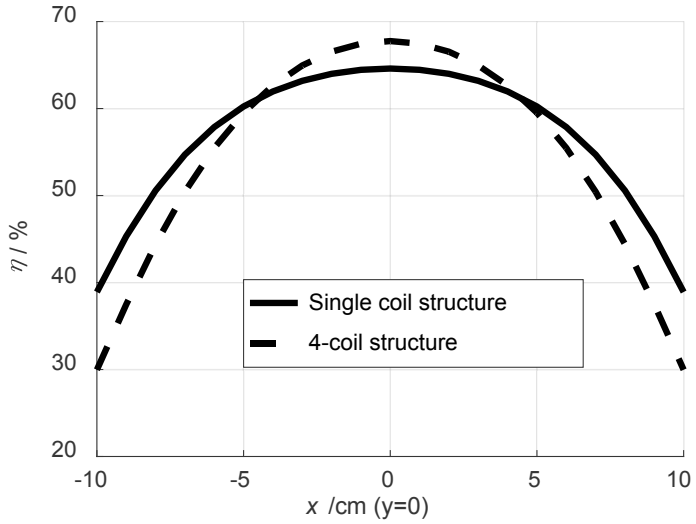

Figure 4.13 Efficiency comparison of single coil structure and 4-coil structure in a 16 coils transmitter matrix (simulated by the author)

4.5 Chapter Summary

In this chapter, the author focuses on the use of a transmitter matrix compared with the traditional transmitter configuration. The design goal is that lateral misalignment between the transmitter and the receiver is tolerated while still maintaining high transmission efficiency and at the same time minimizing the fringing field so as to have little effect on nearby electronic equipment.

A basic 4-coil structure transmitter has been designed using the concept of field forming. The center of area of the 4-coil transmitter strengthens the magnetic field while at the same time part of the magnetic field around the edges of the 4-coil structure is cancelled out. Therefore, a multiple coil transmitter matrix is proposed based on 4-coil structure elements, which are switched on or off depending on the location of the receiver coil. The 16 coils transmitter matrix, which provides high efficiency transmission to a mobile device at any location within a charging area 20 cm × 20 cm, is the best choice for the WPT system according to the criterion of cost efficiency. The optimal radius of the coils in the 4-coil structure placed in a 16 coils transmitter matrix is about 7 cm. The simulation results show significant advantages for the multiple coil transmitter structure with respect to the field forming effect which keeps the external fields small, as well as the fact that the 16 coils transmitter matrix provides a large area of high transfer efficiency.

Chapter 5

Localization and EMC for WPT Systems

5.1 Chapter Overview

As mentioned in Section 4.4, the appropriate transmitter coils within the transmitter coil matrix are activated according to the location of the mobile device to allow free placement of the device within the large charging area. The field forming controller can detect the location of the receiver by measuring the coupling factor between the transmitter and receiver coils. Three different localization algorithms are proposed in this work, which are a grid search algorithm, the Gauss-Newton method and the reflected impedance for combined coils method. The magnetic field strength for a practical WPT system must be compatible with human exposure safety standards. In this chapter different shielding methods and materials are investigated. Shielding materials and configurations have been found that reduce emissions thereby lowering exposure levels to humans as well as nearby electronic devices as well as improve the WPT system efficiency.

In Section 5.2 the position detection method is investigated. Different calculation methods for coupling factor between the transmitter and the receiver are presented. In particular, the author proposes a method for estimation of the magnetic flux density by measuring the receiver voltage. In Section 5.3, different magnetic field shielding methods are presented and the WPT system shielding is

designed using a combination of shielding methods and materials. In Section 5.4, the effectiveness of the different shielding methods are determined by simulation with COMSOL. In Section 5.5 the chapter is summarized.

5.2 Position Detection Method Based on Multiple Coil Matrix

5.2.1 Coupling Factor Criterion

5.2.1.1 Direct Definition

The coupling factor is quantitatively described as the amount of coupling between two coils, which is related to the coil shape, relative geometrical location and the magnetic medium [Dep52]. The value of the coupling factor is between 0 and 1. If the coupling factor is 1, that means two coils are perfectly coupled without leakage flux. Mutual inductance M_{12} is a measure of the extent of magnetic linkage between current-carrying coils. The method for calculation mutual inductance is introduced in Section 3.2.1.2. L_1 and L_2 are the self-inductance of coil 1 and coil 2 respectively. The self-inductance of the coil is calculated in Section 3.2.1.3. The coupling factor is defined as the geometric mean of the ratio of mutual inductance magnetic flux linkage to self-inductance magnetic flux linkage, shown in (5.1) [Boy07].

$$k = \sqrt{\frac{|\psi_{12}|}{\psi_{11}} \cdot \frac{|\psi_{21}|}{\psi_{22}}} \tag{5.1}$$

where $\psi_{11} = L_1 I_1$, $|\psi_{12}| = M_{12} I_2$, $\psi_{22} = L_2 I_2$, $|\psi_{21}| = M_{12} I_1$, which are substituted into (5.1), then (5.2) is obtained by derivation [Sve13].

$$k = \frac{M_{12}}{\sqrt{L_1 L_2}} \tag{5.2}$$

5.2.1.2 Coupled Inductance Measurement Method

When the transmitter and the receiver coils are series connected, the current direction in the two coils could be in phase or out phase. Figure 5.1 shows both scenarios of series connection. U_{L1} is the voltage of coil 1, which consists of two

parts, voltage U_{L11} generated by its own coil and U_{L12} generated by coil 2. Similarly voltage of coil 2 U_{L2} consists of U_{L22} and U_{L21}, which are caused by coil 2 and coil 1 separately. According to the Lenz law, the voltage U_{L11}, U_{L12}, U_{L22} and U_{L21} could be expressed by (5.3) [Sve13].

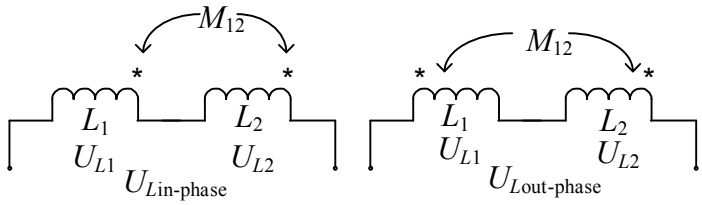

Figure 5.1 Series connection of in phase and out phase (conceptual representation of resources in **[Dep52]**)

$$\begin{aligned} U_{\mathrm{L11}} &= L_1 \frac{dI_1}{dt}, \quad U_{\mathrm{L12}} = M_{12} \frac{dI_2}{dt} \\ U_{\mathrm{L22}} &= L_2 \frac{dI_2}{dt}, \quad U_{\mathrm{L21}} = M_{21} \frac{dI_1}{dt} \end{aligned} \tag{5.3}$$

Therefore the voltage across the series connected inductances $U_{\mathrm{Lin\text{-}phase}}$ and $U_{\mathrm{Lout\text{-}phase}}$, are the sum or the difference of U_{L1} and U_{L2}, shown in (5.4). Since reciprocity requires $M_{12} = M_{21}$, the effective total inductance of the series connected coils can be express as (5.5), where positive and negative signs mean in phase and out phase connection respectively [Dep52].

$$\begin{aligned} U_{\mathrm{Lin\text{-}phase}} &= U_{\mathrm{L1}} + U_{\mathrm{L2}} = L_1 \frac{dI_1}{dt} + M_{12} \frac{dI_2}{dt} + L_2 \frac{dI_2}{dt} + M_{21} \frac{dI_1}{dt} \\ U_{\mathrm{Lout\text{-}phase}} &= U_{\mathrm{L1}} + U_{\mathrm{L2}} = L_1 \frac{dI_1}{dt} - M_{12} \frac{dI_2}{dt} + L_2 \frac{dI_2}{dt} - M_{21} \frac{dI_1}{dt} \end{aligned} \tag{5.4}$$

$$L_{\mathrm{adj}} = L_1 + L_2 \pm 2M_{12} \tag{5.5}$$

The total inductance L_{adj}, and the self-inductance L_1 and L_2 of the two coils can be measured with the Agilent U1733C a Handheld LCR Meter. The mutual inductance M_{12} between two coils is given in (5.6) by derivation from (5.5). The coupling factor can be determined by substituting the values determined for M_{12}, L_1 and L_2 into (5.2).

$$M_{12} = \pm \frac{L_{\text{adj}} - (L_1 + L_2)}{2} \tag{5.6}$$

5.2.1.3 Open Loop Voltage Measurement Method

If the transmitter and receiver coils are coupled without loss and connected with nothing else, such as inductors, resistor and capacitor, the general equations of the lossless coupling can be expressed as (5.7) [Dua14].

$$\begin{cases} L_1 \dfrac{dI_1}{dt} + M_{12} \dfrac{dI_2}{dt} = U_{\text{L1}} \\ L_2 \dfrac{dI_2}{dt} + M_{21} \dfrac{dI_1}{dt} = U_{\text{L2}} \end{cases} \tag{5.7}$$

When a voltmeter is connected to the receiver coil, I_2 is reduced to 0 and U_{L2} is the open loop voltage. The coupling factor k can be deduced from (5.8), which describes the relationship between the transmitter voltage and the open loop voltage of receiver coils U_{L1} and U_{L2} separately, as well as the inductance of transmitter and receiver coils L_1 and L_2. The voltage source has low impedance and the voltage measurement device has high impedance [Ben12]. If the inductance of the transmitter and receiver are the same, the coupling factor is simply equal to the ratio of the transmitter voltage and measured open loop receiver voltage.

$$\frac{U_{\text{L2}}}{U_{\text{L1}}} = k \sqrt{\frac{L_2}{L_1}} \tag{5.8}$$

5.2.1.4 Short Circuit Measurement Method

In this case, the transmitter is connected to the power source, and the receiver is shorted. The corresponding equation of the coupling circuit is shown as (5.9) [Dua14].

$$\begin{cases} L_1 \dfrac{dI_1}{dt} + M_{12} \dfrac{dI_2}{dt} = U_{\text{L1}} \\ L_2 \dfrac{dI_2}{dt} + M_{21} \dfrac{dI_1}{dt} = 0 \end{cases} \tag{5.9}$$

Let L_s be $L_1 - M^2/L_2$, the coupling factor k is deduced as (5.10). L_1 is the inductance measured across transmitter without the receiver coil. L_S is the inductance measured across the transmitter when the receiver coil is short circuit [Ben12].

$$k = \sqrt{1 - L_S / L_1} \tag{5.10}$$

5.2.1.5 Reflected Impedance Method

As the WPT system works at resonance, the reflected impedance is reduced to pure resistance. As previously described, the three-coil configuration WPT system is the best choice for the assumptions used in this thesis. The circuit diagram for the three-coil configuration WPT system is given in Figure 2.18. (5.11) gives the resistance reflected from the secondary coil to the primary coil of the receiver. The total resistance in the primary coil of the receiver is described as (5.12).

$$R_{34} = \frac{(\omega_0 M_{34})^2}{R_4 + R_L} \tag{5.11}$$

$$R_{3\_34} = R_3 + R_{34} = R_3 + \frac{(\omega_0 M_{34})^2}{R_4 + R_L} \tag{5.12}$$

For the transmitter side, the total impedance consists of two parts: the resistance from the transmitter itself and the reflected impedance from the receiver to the transmitter. The equivalent resistance R_{23} from the receiver coil reflected to the transmitter is shown in (5.13). The voltage U_{L2} and the current I_2 in the transmitter can be measured and the transmitter resistance R_2 can be expressed as (5.14).

$$R_{23} = \frac{(\omega_0 M_{23})^2}{R_{3\_34}} \tag{5.13}$$

$$R_2 = \frac{U_{L2}}{I_2} - R_{23} \tag{5.14}$$

Substitute (5.13) into (5.14), the coupling factor k_{23} between the transmitter and the receiver is given in (5.15) according to (5.2).

$$k_{23} = \sqrt{\left(\frac{U_{L2}}{I_2} - R_2\right) R_{3\_34} \Big/ \left(\omega_0^2 L_2^2 L_3^2\right)} \tag{5.15}$$

5.2.2 Localization Algorithm for WPT Systems

5.2.2.1 Grid Search Algorithm with Coupling Factor Calibration

In Section 5.2 four methods for determining the coupling factor by measurement have been presented: coupled inductance, open loop, short circuit method and reflected impedance method. The first three methods are useful to determine the coupling factor prior to the WPT system being operational. However, only the reflected impedance method is suitable for real time use in an operational system. The proposed approach is the WPT transmitting system controller estimates the coupling factor for each transmitter coil based on the reflected impedance (5.15). The algorithms described below localize the receiver coil using the measured coupling factors as input.

The coupling factor varies with both the transmission distance *d*, defined to be the distance between the planes containing the transmitter and receiver coils, and the lateral misalignment distance r_ρ between the centers of the transmitter and the receiver coils. The coupling factor has been calculated as shown in Figure 5.2 as a function of lateral misalignment and parametric in transmission distance. The parameters of the WPT system in Table 3.3 and Table 3.4 are used for calculating coupling factors. For decreasing transmission distance, the magnitude of the coupling factor generally increases. For a fixed transmission distance of more than 6 cm, the coupling factor decreases with the increasing lateral displacement. When the distance between the transmitter and the receiver coils is smaller (less than 6 cm), the coupling factor is positive for small lateral displacement but then goes through 0 to negative through a peak and then coming back towards 0 as the misalignment distance increases. The region having negative coupling is the result of negative magnetic linkage passing through the receiver when the misalignment distance is more than the transmitter coil radius. As shown in Figure 5.3, the direction of magnetic field is opposite between the internal and external positions of the transmitter coil. Therefore, the coupling factor is negative when the direction of the magnetic flux external to the transmitter coil is in the opposite direction to the internal magnetic flux.

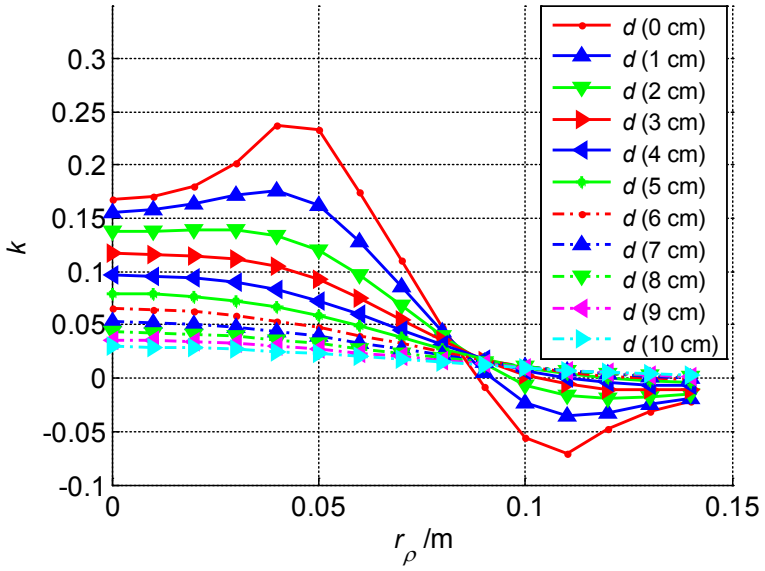

Figure 5.2 Coupling factor between transmitter and receiver coil parametric in transmission distance (simulated by the author)

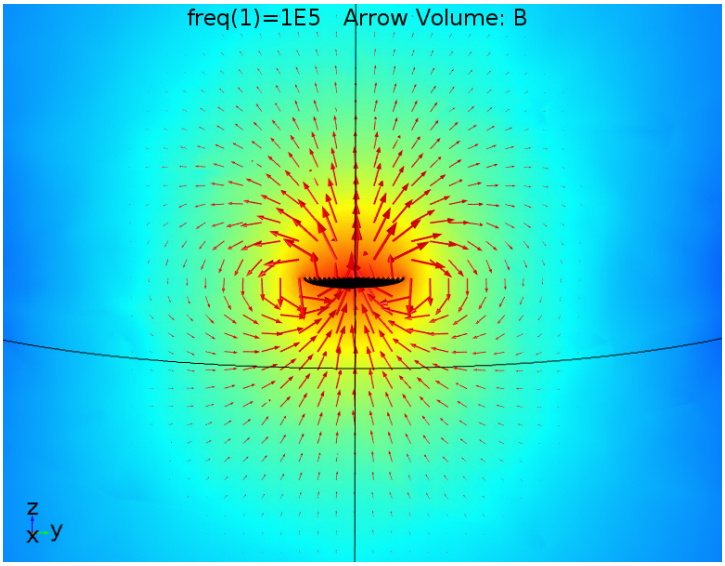

Figure 5.3 Magnetic field distribution of single coil (simulated by the author)

For a given transmission distance and coils parameters, the coupling factor k is only a function of the lateral misalignment, r_ρ, between transmitter and receiver coils. For the case considered in this thesis, the transmission distance is 10 cm, and the coupling factor always decreases with increasing r_ρ according to Figure 5.2. The coupling factor is estimated from the reflected impedance for each coil of the transmitter matrix using (5.15), and the lookup table is used to get the

corresponding value r_ρ. There are two grid search scenarios depending on the accuracy of the estimated r_ρ. If the values are nearly exact, precise localization (ideal), the circles defining the location will cross at a point. However, if the estimates have some error, fuzzy localization, (practical situation) the circles will not cross at a point. These cases are presented conceptually in Figure 5.4. The circles represent the estimated lateral misalignment of the receiver from three transmitting coils (1, 2, 3). The point A is the actual location of the receiver coil center. The solid line circle means the actual r_ρ between the transmitter and receiver. While dashed line (Mea b) stands for the case when the estimated lateral misalignment is bigger than the actual r_ρ and dot dashed line (Mea s) stands for the case when the estimated lateral misalignment is smaller than the actual r_ρ.

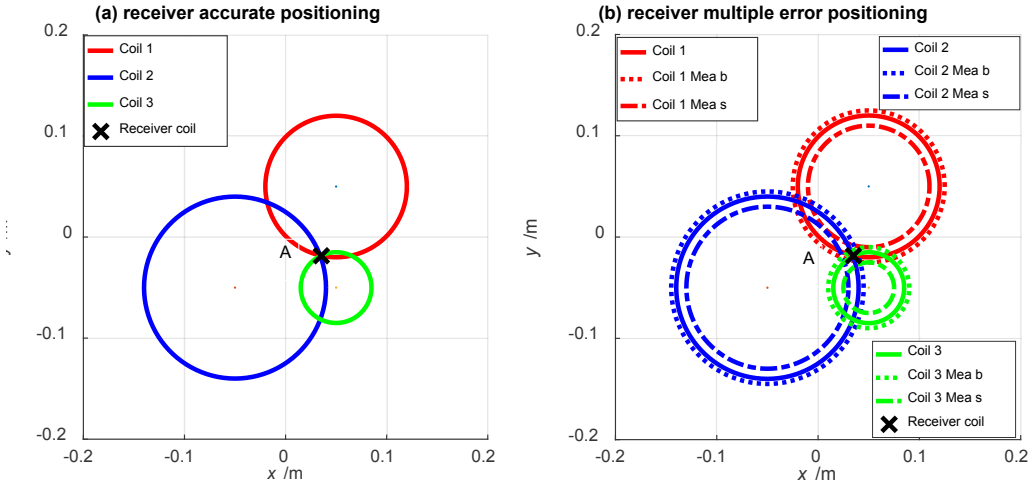

Figure 5.4 Receiver localization based on r_ρ estimation from measured coupling factor between the transmitter coils (1, 2 & 3) and the receiver coil (center represented by the x) (found by the author)

Details of grid search algorithm are given by the following steps [Che15]:

- Step 1: Establish a table of coupling factors for all positions of the receiver coil in three-dimensional space. A lookup table stores the coupling factor data which varies with the two variables, transfer distance and lateral misalignment distance. A lookup table matrix having dimension of 100 × 100 has been developed based on the data in Figure 5.2, a portion of which is shown in Table 5.1.

Table 5.1 Coupling factor lookup table developed for the grid search algorithm

Transmission Distance (cm)	Lateral Misalignment (cm)	Coupling Factor
1	0	0.156
2	1	0.138
3	2	0.115
4	3	0.09
5	4	0.066
6	5	0.048
7	6	0.033
8	7	0.024
9	8	0.0167
10	9	0.015

- Step 2: Assuming the receiver's height above the transmitter coil (transfer distance) is known, the lateral misalignment distance between the receiver and the first transmitter coil is estimated according to the measured coupling factor using the lookup table. The coupling factor gives an estimate of the lateral misalignment distance. In the ideal situation, this constitutes a circle defining all possible receiver positions where the coupling factor would be equal to the value measured. The radius of the circle is the lateral misalignment distance between the centers of the transmitter and receiver coils and the circle center is at first transmitter coil center.

- Step 3: Similarly, the second transmitter coil is used to estimate the lateral misalignment distance with the same method in step 2. The two intersecting circles generate two feasible solutions for the receiver coil position. Similarly, the third transmitter is used to generate another circle containing the receiver's position. Then the intersection point of three circles from transmitter coil 1,

transmitter coil 2 and transmitter coil 3 is the estimated receiver position. This scenario requires very high measurement accuracy for the coupling factors with respect to lateral misalignment. Figure 5.4 (a) illustrates the results for an accurate grid search method which enables all three circles to intersect exactly at the receiver's position point A.

- Step 4: However, the estimated value $\acute{r}_\rho$ of lateral misalignment may be larger or smaller than the actual value of r_ρ. Therefore, the third circle of coupling factor may not intersect the first and second circle at a single point. As Figure 5.4 (b) shows, the three circles shown as dot and dashed lines which have estimation errors define either a common intersection area or no intersection area. In order to avoid the situation with no intersection area, the estimated measurement value $\acute{r}_\rho$ of each circle is extended by 0.5 cm. The increased value for $\acute{r}_\rho$ may be larger than the actual value of r_ρ as shown by the dashed line circles in Figure 5.4 (b). In this case, the enlarged circles represented by the dashed lines generate a larger intersection area. Nevertheless, the actual receiver location is in the intersection area enclosed by the three dashed line circles.

- Step 5: From step 4, we know the receiver coil position is within the intersection area of the three circles. The coupling factor estimation is allowed to have a certain error tolerance. In this thesis, the error tolerance (ERT) for the receiver location is defined to be no more than 1 cm^2 (ERT≤1). If the first three circles give an ambiguous position estimate with intersection area greater than the ERT, then the fourth, fifth, sixth transmitter coils, and so on, in sequence are used to estimate receiver's position. Again, the estimated radius from each additional coil includes the added 0.5 cm. Including the additional coils will reduce the size of the intersection area. The more transmitter coils are used, the smaller the intersection area until the overlapping area is smaller than ERT and so on. The average of the positions determined by using all transmitter coils provides a very good estimate of the actual receiver positon. The intersection area overlapped by the three dot dashed line circles in Figure 5.4 (b) is consistent with the ERT condition and is an example of the effectiveness of the multiple coil positioning method.

5.2.2.2 Gauss-Newton Algorithm

The Gauss-Newton algorithm is used to solve the non-linear least squares problem (NLSP). The basic idea of Gauss-Newton algorithm is to modify the regression

coefficient by minimizing the non-linear squares until the coefficient approaches the optimum regression value [WIK16b,Smy98]. The Gauss-Newton method solves NLSP approximation problem with a series linear least squares regressions and it does not require the second derivative. Therefore, it is more efficient method for NLSP problems [Gra14]. The *n* non-linear regression coefficients are defined as $\gamma = (\gamma_1, \gamma_2, ...\gamma_{n-1}, \gamma_n)$ with the function of $f(x_1, x_2, ...x_m) = y$, where $x_1, x_2, ...x_m$ are *m* variables. The residual function is $\chi = f(x_1, x_2, ...x_m) - y$. And the residual vectors are $\boldsymbol{\chi}$ with $\chi_i = f(x_{i,1}, x_{i,2}, \ldots x_{i,\mathrm{m}}) - y_i,\ i = 1...k$. The partial derivatives of the residual vectors $\boldsymbol{\chi}$ with respect to regression coefficients γ is shown as (5.16) [WIK16b].

$$\chi_1' = \frac{\partial \chi}{\partial \gamma_1}, \quad \chi_2' = \frac{\partial \chi}{\partial \gamma_2}, \quad \cdots, \quad \chi_n' = \frac{\partial \chi}{\partial \gamma_n} \tag{5.16}$$

The Jacobian matrix **D**, the matrix of residual vectors $\boldsymbol{\chi}$ as well as the coefficients γ are defined in (5.17).

$$D = \begin{pmatrix} \chi_{1,1}' & \chi_{1,2}' & \cdots & \chi_{1,n}' \\ \chi_{2,1}' & \chi_{2,2}' & \cdots & \chi_{2,n}' \\ \vdots & \vdots & \vdots & \vdots \\ \chi_{k,1}' & \chi_{k,2}' & .... & \chi_{k,n}' \end{pmatrix}; \quad \chi = \begin{pmatrix} \chi_1 \\ \chi_2 \\ \vdots \\ \chi_k \end{pmatrix}; \quad \gamma = \begin{pmatrix} \gamma_1 \\ \gamma_2 \\ \vdots \\ \gamma_n \end{pmatrix} \tag{5.17}$$

The idea of the iterative Gauss-Newton algorithm is to determine the minimal sum of residual vectors, which is shown in (5.18) [WIK16b].

$$\min\left[\sum_{i=1}^{k}\left(f(x_{i,1}, x_{i,2}, ...x_{i,m}) - y_i\right)^2\right] \tag{5.18}$$

Therefore, the iteration can be expressed as a matrix for with the given initial approximation as shown in (5.19). Here the vector γ includes the parameters which will gradually approach the desired solution as the number of iterations increase [WIK16b].

$$\gamma_{p+1} = \gamma_p - \left(D^T \cdot D\right)^{-1} \cdot D^T \cdot \chi \quad p = 0,1 \cdots k-1 \tag{5.19}$$

The Gauss-Newton algorithm is a typical localization method applied for a single point, or a set of data points [CCR15]. In real applications, Ad-hoc networks and

wireless sensor networks (WSN) are localized based on the Gauss-Newton algorithm [Che05,Bej10]. In this thesis, the Gauss-Newton algorithm is applied for localization of the receiver for WPT systems. The position of the receiver is defined as (x_p, y_p, z_p) in rectangular coordinate system, which is refined by iteration. To get the solution of x_p, y_p, z_p, at least four equations of magnetic flux density with respect to the unknowns (x_p, y_p, z_p) are necessary. A transmitter matrix consisting of 16 coils is proposed in this thesis. Therefore, normally 16 equations are available to estimate the receiver position (x_p, y_p, z_p) with Gauss-Newton algorithm.

The magnetic near fields used for WPT systems are highly non-uniform and fall off rapidly with distance. Therefore in order to measure the magnetic field strength accurately at a point in the space the measurement device should be as small as possible. The induced IEF is a function of the magnetic flux density over the surface of the sensor. The receiver is installed with the small test inductance coil whose radius is 0.05 cm with 1000 turns. The measured magnetic field strength at the sensor is regarded to be homogeneous if the test coil is small enough. The homogeneous magnetic flux density is defined as $B = A\sin(\omega \cdot t)$, which could be estimated from the induced IEF in the small inductance coil according to Faraday's Law of induction. ω is the angular frequency of the transmitted signal, and A is the amplitude of the magnetic flux density from the transmitter. The expression for induced IEF with respect to the homogeneous magnetic flux density is given in (5.20).

$$\varepsilon_{in} = -\frac{d\psi}{dt} = -\frac{d(B \cdot S)}{dt} = -NAS\omega\cos(\omega \cdot t) \tag{5.20}$$

Where N is the number of turns of the small sensor coil and S is the effective area of the sensor coil. Therefore, the amplitude of magnetic flux density A is easily estimated with given values ε_{in}, N, S and ω according to (5.20).

The magnetic flux density at the receiver as a function of position in the 3D space is given in (5.21) in rectangular coordinate system, which is deduced from equation (4.1). A set of coordinates for the centers of the 16 coils are defined as (x_k, y_k, z_k), where $z_k = 0$, k = 1,2,3,…16. N is the number of turns of each transmitter coil.

$$B_{z,k} = \frac{\mu_0 IN}{2\pi} \cdot \frac{1}{\sqrt{\left(\sqrt{\left(x_\mathrm{P} - x_k\right)^2 + \left(y_\mathrm{P} - y_k\right)^2} + r\right)^2 + z_\mathrm{P}^2}} \cdot \left[K\left(\nu_k\right) + \frac{r^2 - \left(\left(x_\mathrm{P} - x_k\right)^2 + \left(y_\mathrm{P} - y_k\right)^2\right) - z_\mathrm{P}^2}{\left(\sqrt{\left(x_\mathrm{P} - x_k\right)^2 + \left(y_\mathrm{P} - y_k\right)^2} - r\right)^2 + z_\mathrm{P}^2} E\left(\nu_k\right) \right] \tag{5.21}$$

The first and the second elliptic integrals $K(v)$ and $E(v)$ are shown in (4.2) and (4.3). The argument ν for the elliptic integrals is given in (5.22).

$$\nu_k = \sqrt{\frac{4r\sqrt{(x_\mathrm{P} - x_k)^2 + (y_\mathrm{P} - y_k)^2}}{(r + \sqrt{(x_\mathrm{P} - x_k)^2 + (y_\mathrm{P} - y_k)^2})^2 + z_\mathrm{P}^2}} \tag{5.22}$$

The receiver's position can be found by minimizing the sum of the squares of the residuals. The aim is to minimize the function of (5.23).

$$S(\gamma) = \sum_{k=1}^{16} \chi_k^2(\gamma) \tag{5.23}$$

where χ_k is given in (5.24).

$$\chi_k = A_k - B_{z,k} \tag{5.24}$$

Let Γ and Υ be equivalent to (5.25) and (5.26), respectively.

$$\Gamma = \frac{\mu_0 IN}{2\pi} \cdot \frac{1}{\sqrt{\left(\sqrt{\left(x_\mathrm{P} - x_k\right)^2 + \left(y_\mathrm{P} - y_k\right)^2} + r\right)^2 + z_\mathrm{P}^2}} \tag{5.25}$$

$$\Upsilon = \frac{r^2 - \left(\left(x_\mathrm{P} - x_k\right)^2 + \left(y_\mathrm{P} - y_k\right)^2\right) - z_\mathrm{P}^2}{\left(\sqrt{\left(x_\mathrm{P} - x_k\right)^2 + \left(y_\mathrm{P} - y_k\right)^2} - r\right)^2 + z_\mathrm{P}^2} \tag{5.26}$$

The Gauss-Newton method requires the Jacobian matrix **D** of partial derivatives for the residual vector χ_k with k lines and 3 columns which is shown in (5.27).

$$D=\begin{pmatrix} \chi_{1,x_\mathrm{p}}' & \chi_{1,y_\mathrm{p}}' & \chi_{1,z_\mathrm{p}}' \\ \chi_{2,x_\mathrm{p}}' & \chi_{2,y_\mathrm{p}}' & \chi_{2,z_\mathrm{p}}' \\ \vdots & \vdots & \vdots \\ \chi_{k,x_\mathrm{p}}' & \chi_{k,y_\mathrm{p}}' & \chi_{k,z_\mathrm{p}}' \end{pmatrix} \tag{5.27}$$

The calculation of partial derivate of χ with respect to x_p, y_p and z_p is shown in (5.28).

$$\begin{bmatrix} \frac{\partial\chi}{\partial x_\mathrm{p}} \\ \frac{\partial\chi}{\partial y_\mathrm{p}} \\ \frac{\partial\chi}{\partial z_\mathrm{p}} \end{bmatrix} = \begin{bmatrix} \Gamma_{xp}'\left(K(\nu)+\Upsilon E(\nu)\right)+\Gamma\left(K_{xp}'(\nu)+\Upsilon_{xp}'E(\nu)+\Upsilon E_{xp}'(\nu)\right) \\ \Gamma_{yp}'\left(K(\nu)+\Upsilon E(\nu)\right)+\Gamma\left(K_{yp}'(\nu)+\Upsilon_{yp}E(\nu)+\Upsilon E_{yp}'(\nu)\right) \\ \Gamma_{zp}'\left(K(\nu)+\Upsilon E(\nu)\right)+\Gamma\left(K_{zp}'(\nu)+\Upsilon_{zp}E(\nu)+\Upsilon E_{zp}'(\nu)\right) \end{bmatrix} \tag{5.28}$$

The derivative of the first and the second complete elliptic integral with respect to ν is given in (5.29) and (5.30) respectively.

$$\frac{\partial K(\nu)}{\partial\nu}=\frac{E(\nu)}{\nu\left(1-\nu^2\right)}-\frac{K(\nu)}{\nu} \tag{5.29}$$

$$\frac{\partial E(\nu)}{\partial\nu}=\frac{E(\nu)-K(\nu)}{\nu} \tag{5.30}$$

(5.19) shows the estimated position of the receiver coil γ, which is determined by the Jacobian matrix after iteration. The initial approximations for the receiver's location could be defined as (0, 0, 0). This was simulated using Matlab and it was found that after 16 iterations, the resulting position estimate approached the actual position within the desired precision.

5.2.2.3 Reflected Impedance for Combined Coils

The grid search algorithm and Gauss-Newton algorithm are proposed by the author to accurately determine the receiver position. The accurate position of receiver is required because which 4 coils can be determined to switch on for the mobile device charging. However, for charging with the proposed 4-coil structure

sub units of the transmitter array, what is required is the knowledge of which 4-coil structure is used for charging. As the reference [Son09] described, the reflected impedance method can be used to detect which coils should be switched on in the primary winding matrix. The author proposes using the reflected impedance method applied to each of the available 4-coil structures made up from the coils in the transmitting matrix in turn. The 4-coil structure with the maximum reflected impedance is the best one for charging. There are nine 4-coil structure transmitters in the 16 coils transmitter matrix. The controller can check nine possibilities one by one to detect the maximum reflected impedance. Since the transmitter and receiver coils are resonant, the measured impedance will actually be the reflected resistance R_{ref}.

The optimized 4-coil structure in the 16 coils transmitter matrix is shown in Figure 5.5, the receiver is moving along the arrow line (lateral misalignment) at 10 cm transmission distance. The reflected resistance is changed with lateral misalignment between the 4-coil structure transmitter and the receiver, which is shown in Figure 5.6. Section 5.2.1.5 presents the details of reflected resistance calculation method. The reflected resistance from receiver to the 4-coil structure is given in equation (5.13). In this situation, the mutual inductance between 4-coil structure and primary coil of receive is calculated in (4.16). The larger the reflected resistance in the 4-coil structure, the shorter distance is between the transmitter and the receiver. When the receiver center is located at the border line between two coils centers, the reflected impedance is the same for both and either 4-coil structure transmitter can be selected as providing identical charging for the mobile device.

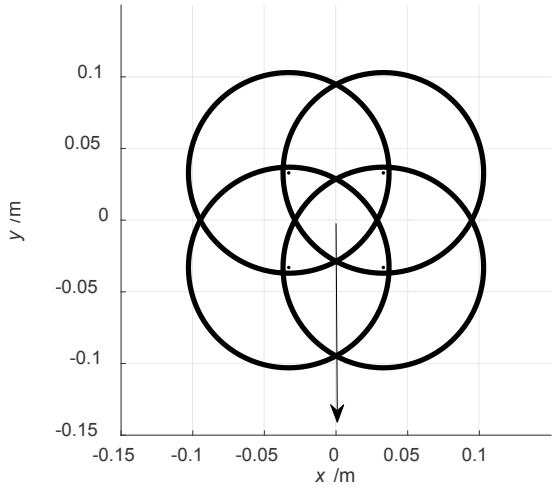

Figure 5.5 Optimized 4-coil structure (simulated by the author)

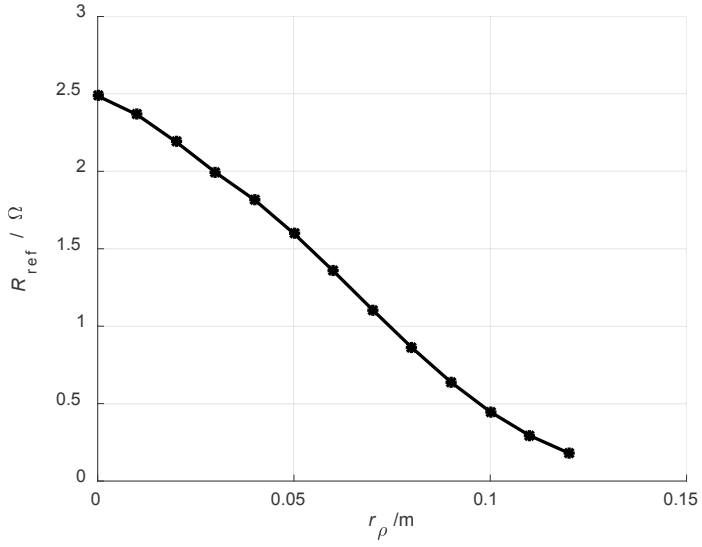

Figure 5.6 4-coil structure reflected resistance with lateral misalignment (simulated by the author)

5.3 Shielding Issues for WPT Systems

5.3.1 Overview

As Section 1.2.2 presents, the ICNIRP guidelines limit the magnetic field for human exposures to less than 27 μT for the general public at frequency 100 kHz. In order to reduce the magnetic flux density of a specified domain below the required limit, near field shielding is necessary for WPT systems. The shielding methods are required to counteract the magnetic field emission from the transmitter. In general, shielding techniques are classified as the compensation method and the thin shielding materials.

5.3.2 Shielding Methods

5.3.2.1 Active Shielding

Compensation shielding includes both active shielding and passive shielding (introduced in Section 5.3.2.2) using a compensation coil. The active shielding method makes use of a coil series connected with the power source. The magnetic field generated by the compensation active coil has the opposite direction of the magnetic field from the WPT system transmitter coil, and therefore reduces the field from the transmitter in some region. The power supply can adjust the

magnitude and phase of the current of the active coil, which influences the magnetic field strength. A schematic diagram showing active shielding is given in Figure 5.7. For the active shielding method, an additional power source is necessary for the shielding loop coil. In this case it is difficult to control the phase of the active coil power supply to be the same as the phase of WPT system power supply [Kim13b]. Another disadvantage of active shielding is the active coil also generates magnetic field emission to other electronic devices in the vicinity [Kim14].

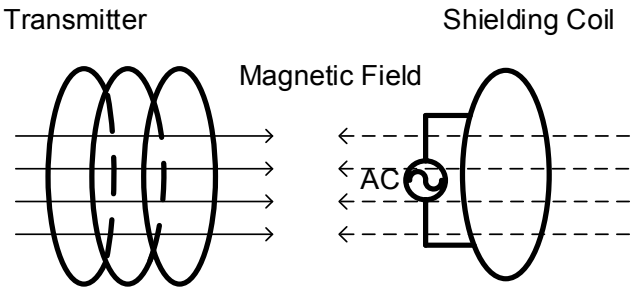

Figure 5.7 Active shielding method (representation of resources in **[Kim14]**)

5.3.2.2 Passive Shielding

For passive shielding no separate power source is required. The reactive coil is tuned by a capacitor by adjusting the value of the capacitor for resonance, so that the current is maximum in the compensation coil. Therefore, the magnetic field strength from the resonant compensation coil is large enough to neutralize the magnetic field generated from the transmitter. Figure 5.8 shows a capacitor replacing the power source in the passive shielding compensation coil. Passive shielding eliminates the disadvantage of an additional power source required for the active shielding method [Kim14,Kim13b].

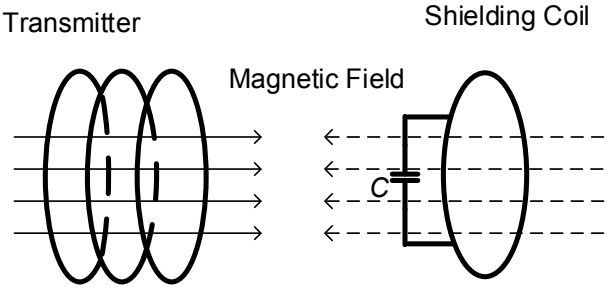

Figure 5.8 Passive shielding method (representation of resources in **[Kim14]**)

5.3.2.3 Magnetic Shielding

The magnetic shielding method makes use of ferromagnetic material to guide the magnetic field. As a result, the incident magnetic field concentrates in the ferromagnetic material. Usually the ferromagnetic material has high relative permeability. For example the relative permeability of the ferrite is more than 1000 ($\mu_r > 1000$) and low conductivity ($\sigma \ll 10^2$ S/m) [Kim12a]. Also ferrite has relatively low eddy current loss. The magnetic field along the path of the ferromagnetic material is coupled to the magnetic field from the transmitter. Both the self-inductance and the mutual inductance of the coils can be increased by adding ferromagnetic material under or above the coils. What is more, leakage of the magnetic field can be reduced with the addition of appropriate magnetic shielding. In another words, the magnetic shielding method can concentrate the magnetic field from coils in the domain between the transmitter and the receiver [Kim13b,Kim12a]. Figure 5.9 shows that the magnetic field chooses the path of the ferrite shielding plate. The advantage of magnetic shielding is that the magnetic field is concentrated and thus strengthened by the presence of the ferromagnetic material. Therefore the performance of a WPT system can be improved with the use of magnetic panels. However, the shielding effectiveness may be limited and the weight of the magnetic material is heavier than other metallic material [Son16].

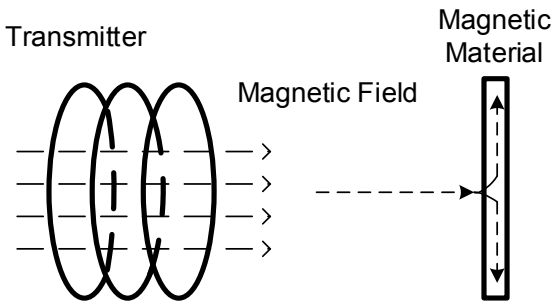

Figure 5.9 Magnetic shielding method (representation of resources in **[Kim14]**)

5.3.2.4 Conductive Shielding

Aluminum and copper are commonly used as conductive material for shielding [Tan02,Kim12b]. Even though the conductivity of aluminum is less than that of copper, aluminum is often preferable for the conductive shielding because it is cheaper and lighter than copper. At the higher frequencies, the skin depth of

aluminum is almost the same as for copper. Therefore, aluminum is chosen as the preferred conductive shielding material for WPT systems.

Eddy currents are induced in conductive material exposed to the time-variable magnetic field from the transmitter according to Faraday's Law of electromagnetic induction. A conductive material board, such as copper or aluminum, has high conductivity. The eddy currents induced in the metal panels produce a cancelling magnetic field, having the opposite direction of the transmitter magnetic field [Kim12a]. Figure 5.10 shows the schematic diagram of conductive shielding. However, when the conductive panel is close to the WPT system, the eddy current may reduce the desired magnetic field being used for WPT and therefore may reduce the transfer efficiency and received power [Son16].

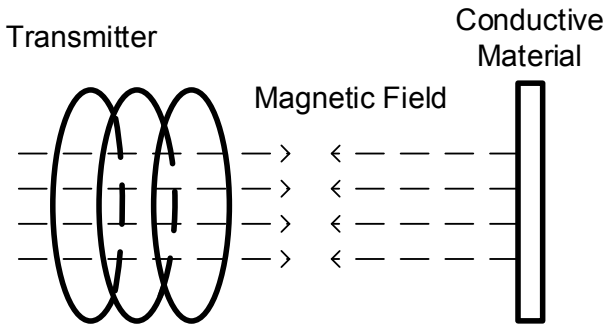

Figure 5.10 Conductive shielding method (representation of resources in **[Kim14]**)

5.3.3 EMF Shielding Design for WPT Systems

In this thesis, the shielding region considered is mainly the side of the WPT system to protect human exposure. Thus, the WPT shielding system is designed using a combination of magnetic shielding, resonant loop shielding and conductive shielding. As introduced in Section 5.3.2, different shielding methods are presented and compared with separate merits and demerits. Unfortunately, magnetic shielding has the disadvantage of limited shielding effectiveness. Nevertheless, better performance was obtained for the ferromagnetic material which provides a controlled path for the magnetic field. Therefore, it can strengthen the magnetic coupling between the transmitter and receiver and decrease the magnetic field emission in the shielding region. Ferromagnetic material close to the coils can concentrate the magnetic field and has low loss.

Therefore, ferromagnetic material panels are used at the bottom of the transmitter and above the receiver.

A passive resonance coil is placed around the WPT system at the horizontal distance. Finally, the aluminum shielding panel is placed outside a passive resonance coil. The horizontal distance between the resonance coil and aluminum panel is 3 cm. Aluminum panels have high conductivity resulting in high shielding effectiveness. The eddy current generated in the aluminum panels produces the reverse magnetic field to reduce the magnetic field generated from the transmitter. For this reason, aluminum panels further reduces the magnetic field leakage. Figure 5.11 gives the schematic diagram of the combination shielding design. With aluminum and reactive resonant loop shielding, the magnetic flux density on the user's side of the WPT is reduced below the limit defined by ICNIRP guidelines. Therefore, the composite shielding method proposed by the author improves the WPT system performance, reduces the magnetic field strength in the shielding domain. What's more, this structure designed insures the safety from exposure for humans in the vicinity of the WPT system.

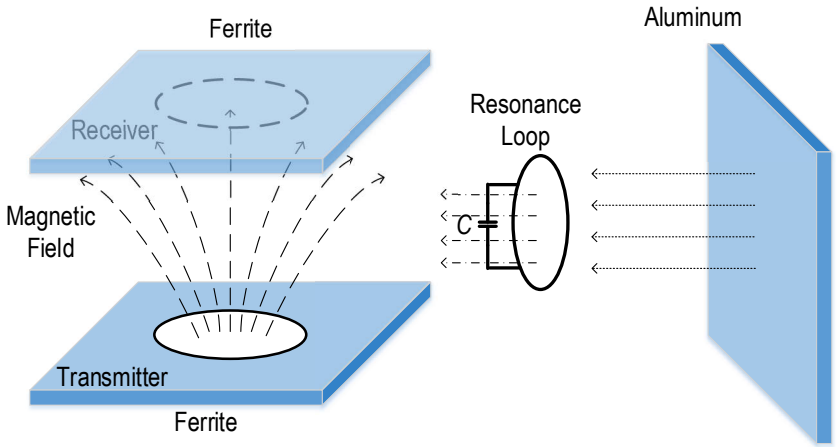

Figure 5.11 WPT systems optimized shielding design (designed by the author)

5.4 Simulation Results with COMSOL

5.4.1 Simulation Setup

COMSOL is the one of simulation tools for simulating electromagnetic models to test and verify EMC criteria. The WPT systems model is built up with finite

element method (FEM) using COMSOL Multiphysics 5.1 [Sin09]. In addition, the simulation of this project is set up using magnetic fields from the AC/DC interface model [Com17]. The coil geometry is built in 3D space. In the modeling domain, the boundary conditions were set such that the magnetic field waves pass through without reflection. Therefore, the impedance boundary condition is set to specified values to avoid refection so as to not influence energy transfer in the computational domain. The relative permittivity ε_r and relative permeability μ_r are set to 1, while electrical conductivity is 0. In other words, the boundary of the modeling domain is transparent for outgoing electromagnetic field.

The COMSOL software has components of geometry, materials, physics, mesh and study. For this project, using the geometry part of COMSOL, we define the transmitter and receiver coils to have the same size and other parameters. All the simulations in this chapter use the same transmitter and receiver coils as described below. In order to show the geometry of the coils clearly, the 2D coil geometry is presented in Figure 5.12. The coil has 10 turns, whose outer radius is 10 cm and inner radius is 0.4 cm. The radius of each turn is 0.2 cm. The material of the coil is copper. Air is used for all other space in the 3D spherical modeling domain. In the magnetic field part of "Physics" in COMSOL, a lumped port is defined for power excitation, and a lumped element capacitor is used in the coil circuit. The free tetrahedral mesh method is selected for the power transfer domain. In order to assure the accuracy of the calculation, small fine or finer mesh is used for the coil model, the rest of the modeling domain surrounding of the coil has a normal triangular mesh. The frequency set to 100 kHz in the study component. The BiCGStab was selected to be the stationary solver in the solver configurations.

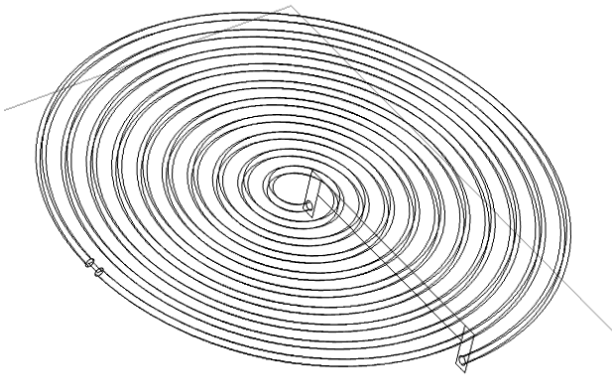

Figure 5.12 Geometry of coils model (simulated by the author)

5.4.2 Basic Model of WPT

The transmission distance between the transmitter coil and receiver coil is 10 cm. Figure 5.13 presents the modeled WPT system.

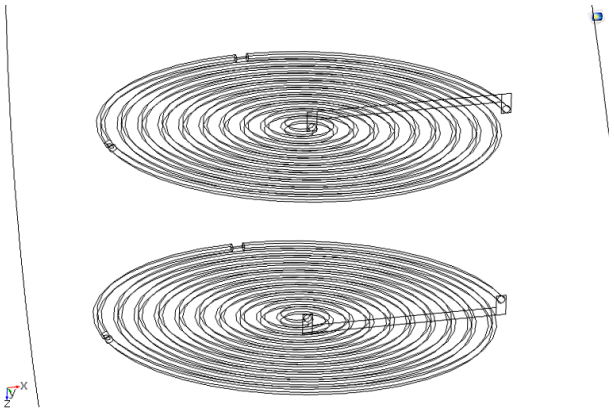

Figure 5.13 WPT model in COMSOL (simulated by the author)

The working frequency domain in the COMSOL simulation is set from 80 kHz to 150 kHz. When the capacitance of the lumped element is chosen as 3 μF, the imaginary part of the impedance is 0 at 100 kHz, as shown in Figure 5.14. That is to say, the coils of the WPT system become resonant at 100 kHz.

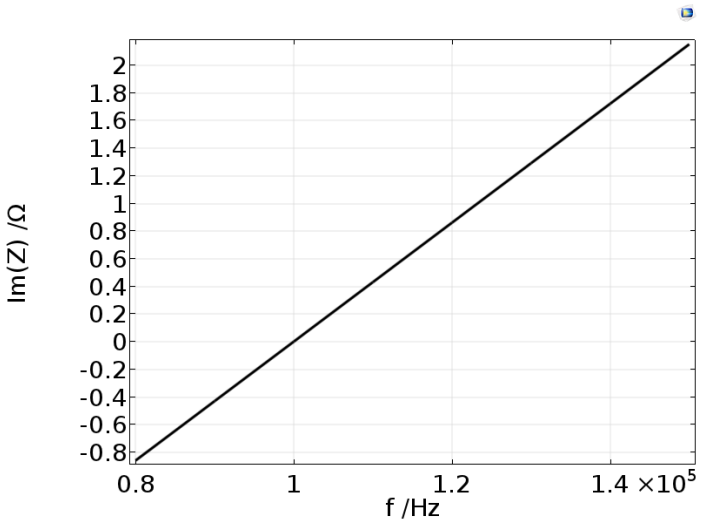

Figure 5.14 Reactance of coil model (simulated by the author)

Figure 5.15 gives COMSOL simulation results for the normalized magnetic flux density (B_n) in the WPT system at 100 kHz. The quantity plotted in the figure and

shown in the legend is $20\times\log 10\left(|B|/\sqrt{P_{\text{port}}}\right)$ in dB, where $|B|$ is the magnitude of the magnetic flux density ($\sqrt{B_x^2+B_y^2+B_z^2}$) in Tesla and P_{port} is the input power in watts, where B_x, B_y, B_z are the magnetic flux density in x, y, z axes in the 3D domain. All the magnetic flux density results presented in this thesis are normalized to the square root of the power input and simply referred to as magnetic flux density. From the figure it is clear that the magnetic flux density is maximum close to the transmitter coil. Some of the magnetic field lines generated by the transmitter go through the receiver coil, so as to induce the IEF which drives the current in the receiver.

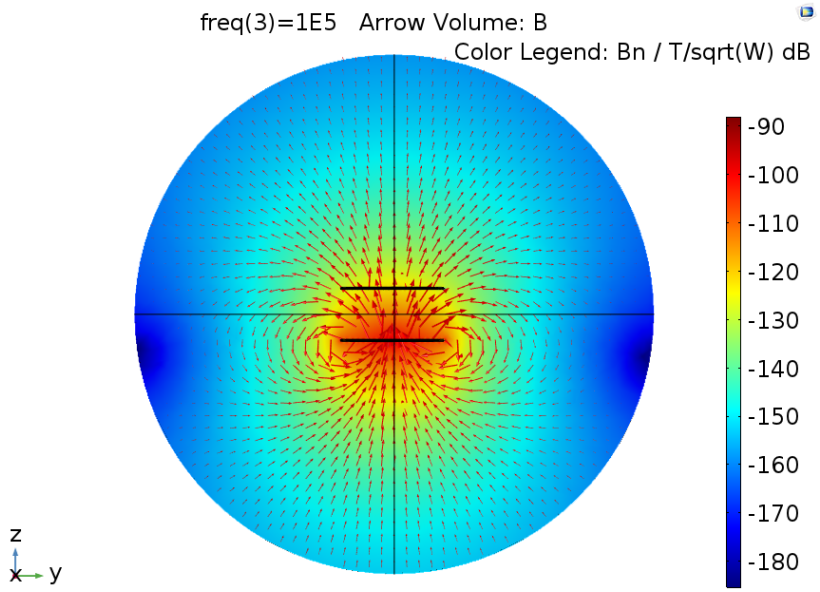

Figure 5.15 Normalized magnetic flux density distribution of WPT system at 100 kHz (simulated by the author)

5.4.3 Active Shielding of WPT

As presented in Section 5.3.2.1, the active shielding method is introduced and analyzed. The geometry of a WPT system with active shielding coil is shown in Figure 5.16. The plane of the shielding coil is perpendicular to the planes of the transmitter and receiver coils. The coordinates (x, y, z) of the active shielding coil center is set as (0, 12cm, 0). The shielding coil has 10 turns. Diameter of each turn is 0.2 cm. The inner radius and outer radius of the shielding coil is 0.4 cm and 5 cm separately. The material of the active shielding coil is also copper. A lumped port, which is considered to be the additional power source, is added in the circuit of the active shielding coil.

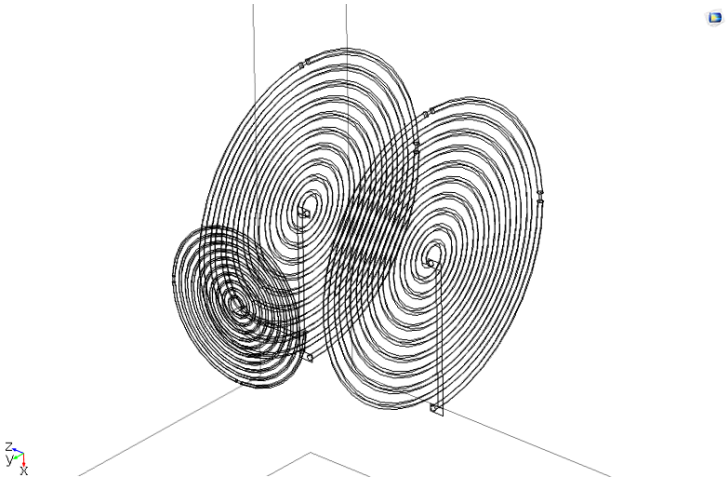

Figure 5.16 Active WPT shielding COMSOL model (simulated by the author)

Active shielding generates a magnetic field in the opposite direction of the magnetic field from the transmitter coil. The effect is that the total magnetic field strength is decreased in the vicinity of the shielding coil due to cancellation. In Figure 5.17, the magnetic field at the active shielding coil is reduced but still in the same direction as the field from the transmitter coil because the magnetic field strength of the transmitter is stronger than that produced by the active shielding coil.

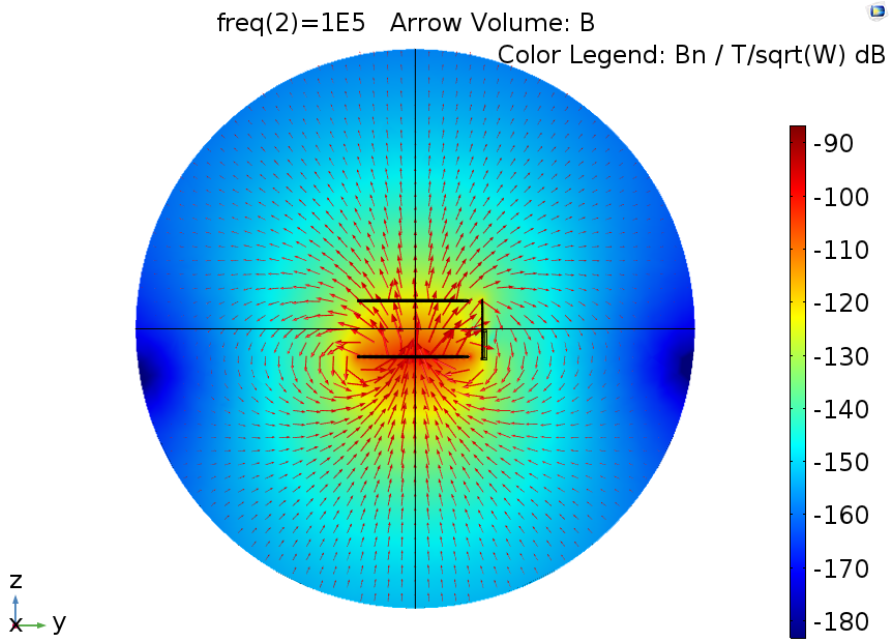

Figure 5.17 Normalized magnetic flux density distribution in WPT system with active shielding at 100 kHz (simulated by the author)

The effect of active shielding is presented in Figure 5.18. The 1D plot shows the magnetic flux density along a line between two terminal points, whose coordinates (x, y, z) are (-2 cm, -15 cm, 0) and (-2 cm, 15 cm, 0) respectively. The lumped element current of the transmitter is around 0.12 ampere. As the center of active shielding coil is located at 12 cm in the positive y-axis, the magnetic field strength from 12 cm to 15 cm is obviously smaller than that from -15 cm to -12 cm in y-axis according to Figure 5.18.

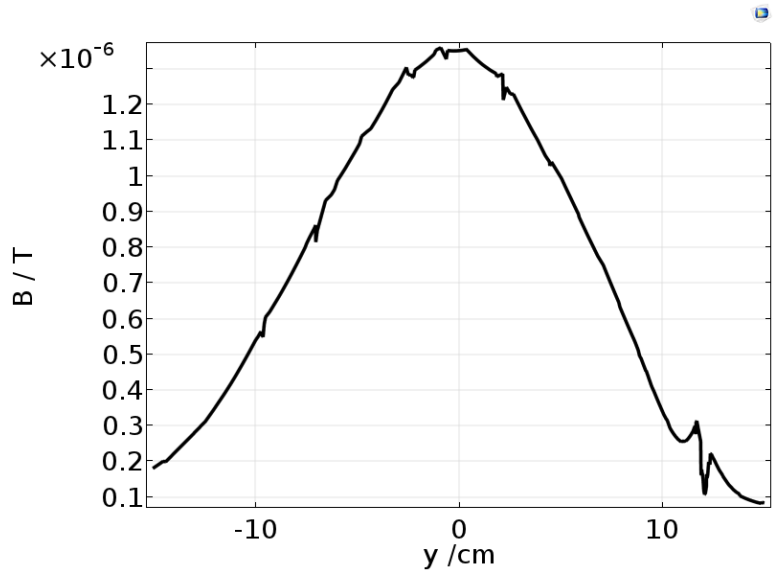

Figure 5.18 Magnetic flux density with active shielding method at 100 kHz (simulated by the author)

5.4.4 Passive Shielding of WPT

The geometry of WPT systems with a passive reactive resonant shielding coil is similar to that of Figure 5.16. The only difference between active shielding and passive shielding is the lumped port is supplied with power for active shielding, while passive shielding is a resonant coil without any power supply. The power source is replaced by the capacitor which is required to resonant the coil. Accordingly, the lumped port is defined as a capacitor.

It is worth noting that the outer diameter of the passive shielding coil is the same as, or smaller than the distance between the transmitter and receiver coils. This is because the direction of magnetic field generated by the WPT transmitter should be same when going through the reactive resonant coil. This strategy will prevent magnetic field cancellation in the area of the shielding coil. Therefore, the

magnetic flux of the shielding coil can reach the maximum. The magnetic flux density distribution is similar to that of the active shielding method given in Figure 5.17, in which the magnetic field through the area of the shielding coil has the same direction. The magnetic field strength with and without passive shielding is given in Figure 5.19. The magnetic field strength measurement positions are the same as used for the active shielding method data. The input current of transmitter is about 0.12 ampere. The magnetic flux density in coordinates (2 cm, 15 cm, 0) is smaller than that from (-2 cm, -15 cm, 0) along the *y*-axis. The shielding effectiveness of passive shielding is not as good as that of active shielding locally. Active shielding can lead to stronger external fields in some areas. The result is that the passive shielding method has less influence on devices in the surroundings due to less external fields.

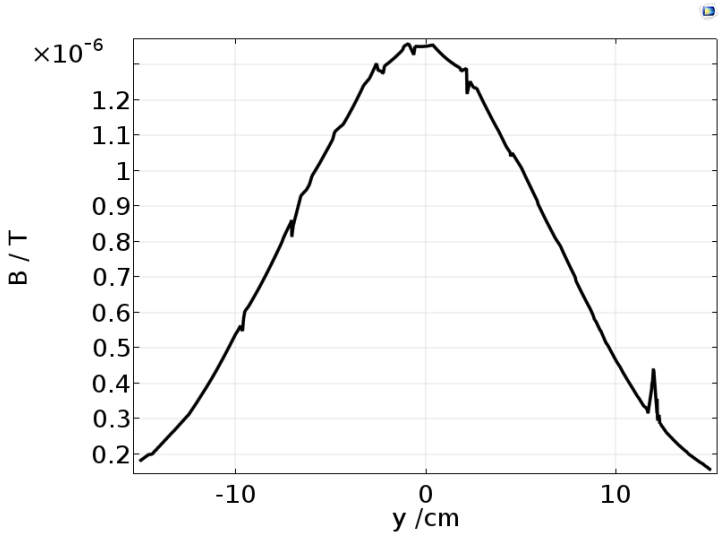

Figure 5.19 Magnetic flux density with passive shielding method at 100 kHz (simulated by the author)

5.4.5 Magnetic Shielding of WPT

Since magnetic material concentrates the magnetic field ferrite plates have been designed to be placed at the bottom of the transmitter coil and on the top of the receiver coil in order to concentrate the field in the desired area and reduce it in the outside regions. The geometry of the WPT system with magnetic shielding material as modeled in COMSOL is shown in Figure 5.20. The upper and lower ferrite plates are identical. The width and depth of the ferrite plate is 25 cm, and the height of ferrite plate is set as 0.5 cm. The gap between the coil and ferrite plate is about 1.3 cm.

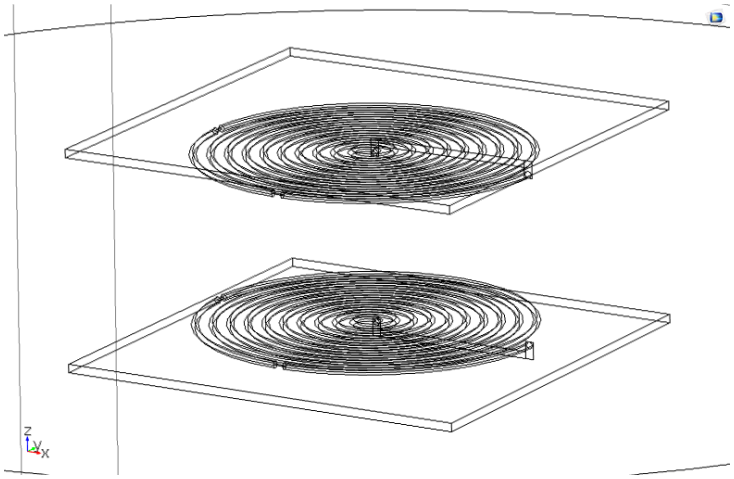

Figure 5.20 Magnetic shielding model in COMSOL (simulated by the author)

Figure 5.21 presents the magnetic flux density with magnetic shielding. It is clearly seen that the magnetic flux density is concentrated in the energy transfer domain between the transmitter and the receiver due to the ferrite plates.

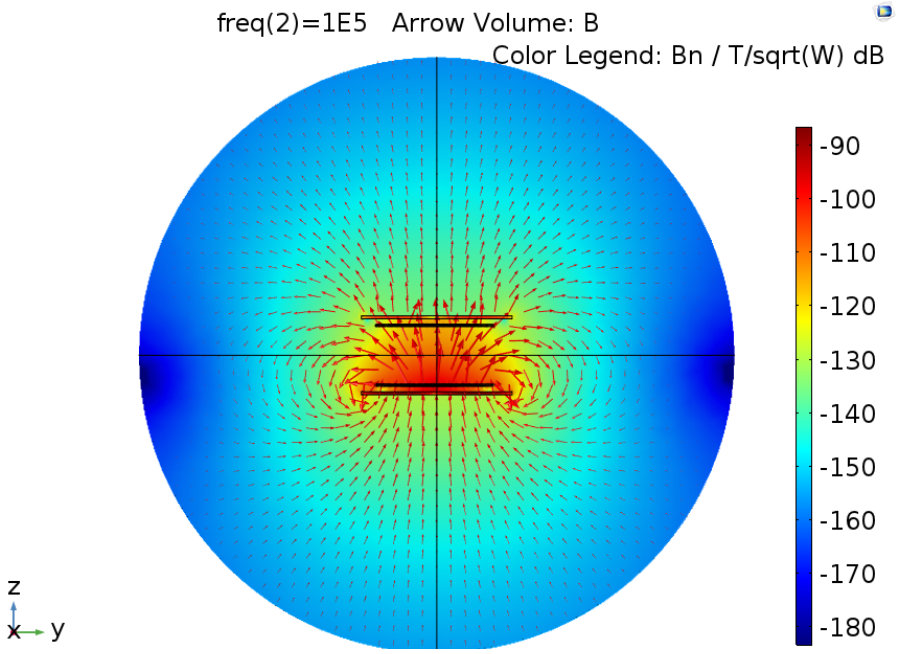

Figure 5.21 Normalized magnetic flux density distribution with magnetic shielding at 100 kHz (simulated by the author)

Therefore, magnetic shielding should increase the energy transfer efficiency of WPT systems. COMSOL can provide power transfer results in terms of S-parameters and has been used to calculate $S11$ and $S21$ for a normal WPT

system (single transmit coil and single receiver coil) with and without magnetic shielding. The simulation was done at the self-resonant frequency of 6 MHz because it is impossible to adjust the exact compensation capacitor for resonant circuit in COMSOL. Nevertheless, the results are indicative of the performance at 100 kHz. The results for 5-7 MHz are shown in Figure 5.22 and Figure 5.23. The S-parameters describe the power transfer and reflection between two ports in a power transfer system. For this case there are two ports, Port 1 is the transmitter and Port 2 is the receiver. *S*11 corresponds to the power reflected back to the source from to the transmitter coil. *S*11 is also named the input reflection coefficient. *S*21 represents the energy transferred from Port 1 to Port 2. *S*21 is the positive transfer coefficient, which corresponds to the gain in the power transfer system [Bev08].

For instance, if *S*11 is 0 dB, that implies all the power is reflected from the transmitter antenna and no power is transferred to the system. When *S*21 is equal to 0 dB, this means all the power from the transmitter is delivered to the receiver. Compare Figure 5.23 with Figure 5.22, at resonance *S*11 for the WPT system with magnetic shielding is smaller than *S*11 in the system without magnetic shielding. While *S*21 for the magnetic shielding WPT system at resonance is slightly larger than *S*21 in normal WPT system. Therefore, the system with magnetic shielding has less power reflected from the transmitter and more power is transferred to the receiver.

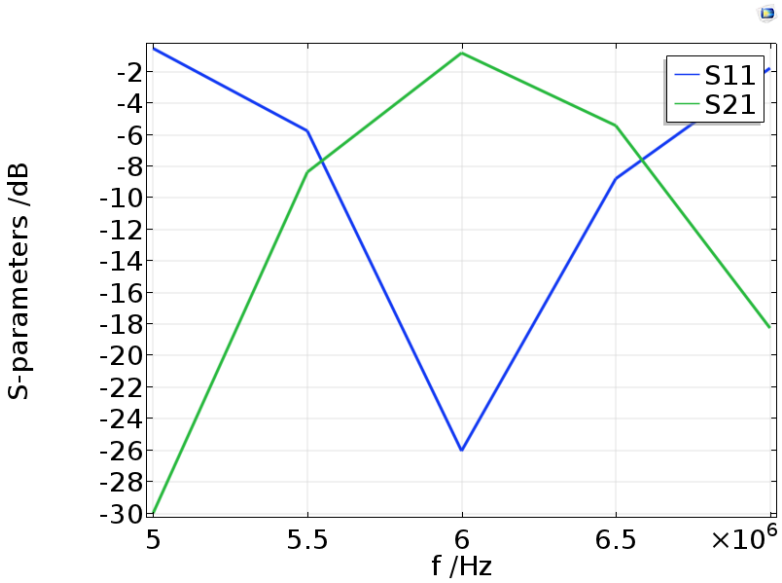

Figure 5.22 S-Parameters of normal WPT systems without magnetic shielding (simulated by the author)

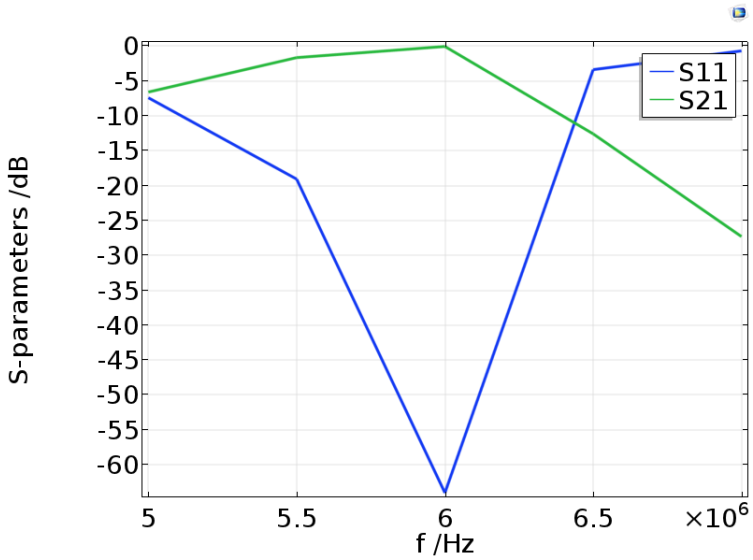

Figure 5.23 S-Parameters of WPT systems with magnetic shielding (simulated by the author)

This can be demonstrated in the same COMSOL model at 100 kHz with resonant coils by calculating the magnetic flux density along the *z*-axis. The results for the cases with and without ferrite are given in Figure 5.24 and Figure 5.25 respectively. The lumped element current of transmitter for both shielding and without shielding model is 0.12 ampere. The coordinates for the two end points of the magnetic strength test line is (0, 0, -10 cm) and (0, 0, 10 cm) respectively.

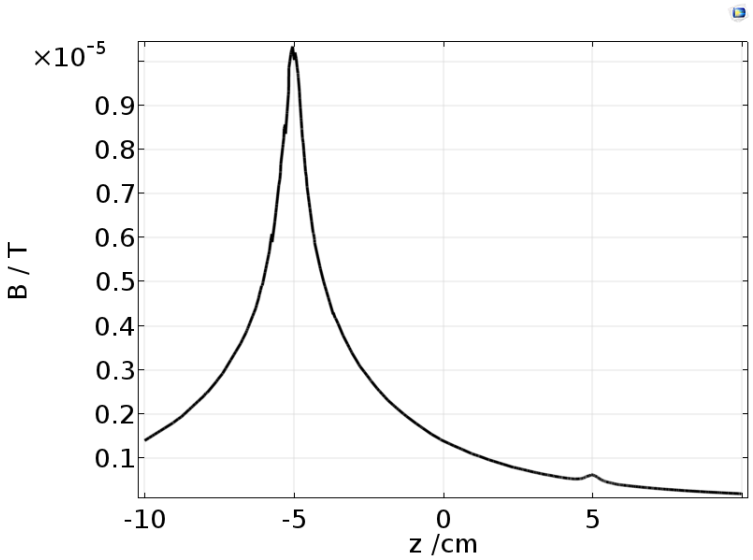

Figure 5.24 Magnetic flux density of normal WPT system at 100 kHz without magnetic shielding (simulated by the author)

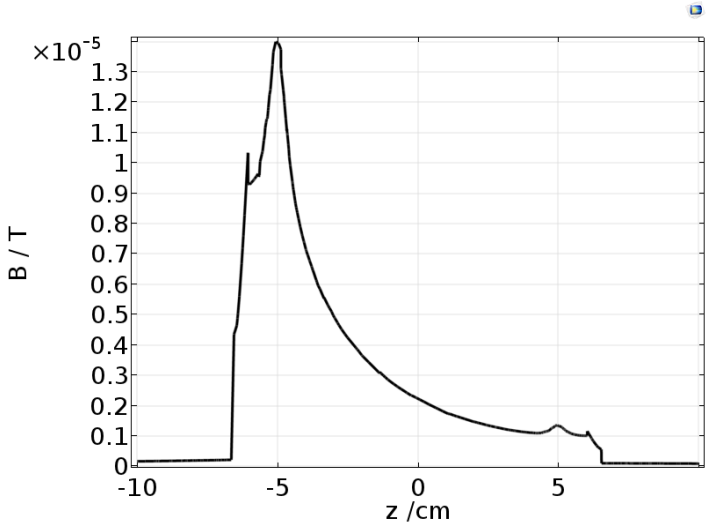

Figure 5.25 Magnetic flux density of WPT system at 100 kHz with magnetic shielding (simulated by the author)

The transmitter coil center is located at -5 cm on the *z*-axis so the magnetic flux density is maximum there. Figure 5.23 gives the magnetic field without ferrite shielding. Note that the field falls off slowly away from the maximum. The normalized field at the location of the receiver coil (+5 cm) is about 5 μT. Figure 5.24 gives the results when two ferrite plates are placed at -6.3 cm and 6.3 cm on the *z*-axis, under the transmitter and above the receiver respectively. In this case, the magnetic flux density decreases dramatically to nearly 0 T outside the domain between the ferrite plates. The flux density at the location of the receiver field is increased by more than a factor of 2. Thus the shielding successfully restricts the field between the two ferrite plates achieving the desired shielding effect. In addition, the magnetic flux density is strengthened in the location of the receiver, which leads to increased power and transfer efficiency for the WPT system.

5.4.6 Conductive Shielding of WPT

As the analysis in Section 5.3.2.4, aluminum is the material chosen to be used for conductive shielding for the WPT system. The plane of the shielding plate is perpendicular to the plane of transmitter and receiver coils. The geometry used in COMSOL to investigate the WPT system with metallic material is presented in Figure 5.26. The coordinate (*x*, *y*, *z*) of aluminum plate center is set as (0, 12 cm, 0). Both the width and depth of the aluminum plate is 25 cm and the thickness is 0.5 cm.

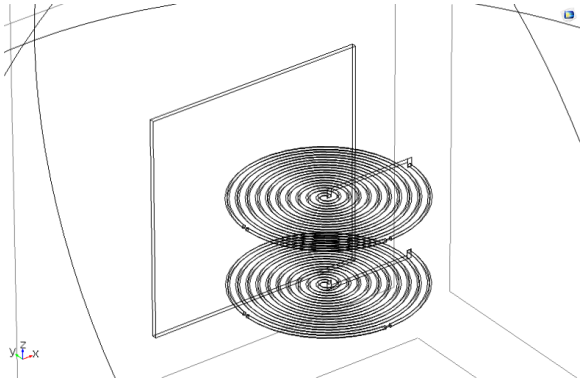

Figure 5.26 Conductive shielding COMSOL model (simulated by the author)

Figure 5.27 shows the magnetic flux density distribution for the WPT system with aluminum plate shielding. It can be seen that the magnetic field strength is much smaller beyond the aluminum plate. Almost no magnetic field from the transmitter can go through the aluminum plate. The shielding effect with aluminum is better than that for either the active coil or reactive resonant coil.

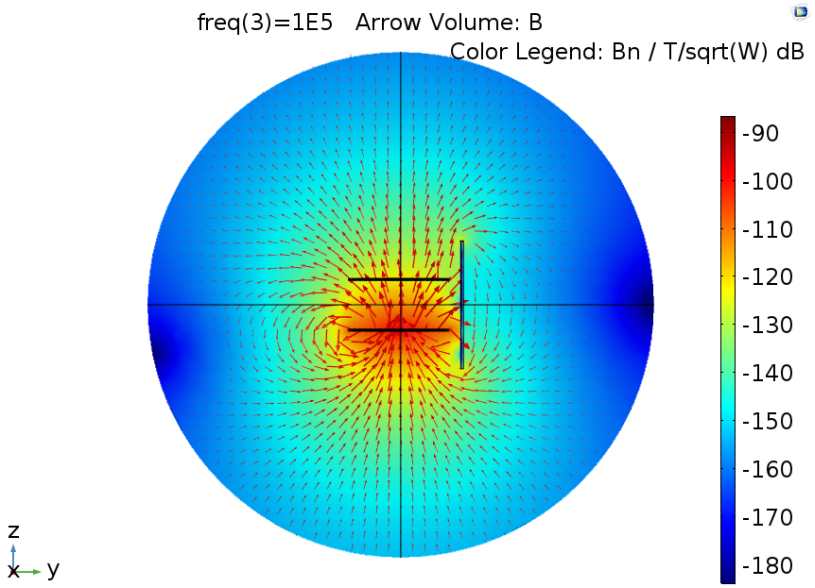

Figure 5.27 Magnetic flux density distribution with conductive shielding at 100 kHz (simulated by the author)

The simulation results 1D plot of magnetic flux density is shown in Figure 5.28. The input current of the transmitter is about 0.12 ampere. Coordinates of two terminal points of the magnetic field strength testing line are (0, -15 cm, 0) and (0, 15 cm, 0) respectively. The magnetic flux density is decreased dramatically to nearly 0 T beyond the aluminum plate, which is placed at 12 cm on the *y*-axis.

Figure 5.28 shows that aluminum shielding is very effective for magnetic field reduction for human exposure. Some ripples shown in Figure 5.18, Figure 5.19, Figure 5.24, Figure 5.25 and Figure 5.28 are caused by artifact that is related to finite element mesh. Each point on the element of the modeling domain is approximated calculated by triangular mesh which causes unwanted artifact in the visualization. That is to say, the magnetic flux density computation results by COMSOL simulation are estimated values in the WPT model domain. The calculation accuracy depends on the mesh size. The self-intersection also results in the artifact if the edge length is smaller than the certain threshold length. The self-intersection is from two mesh elements overlapping each other in the triangular mesh [Yam09]. Therefore, it is impossible to choose an appropriate length size of mesh to overcome the artifact.

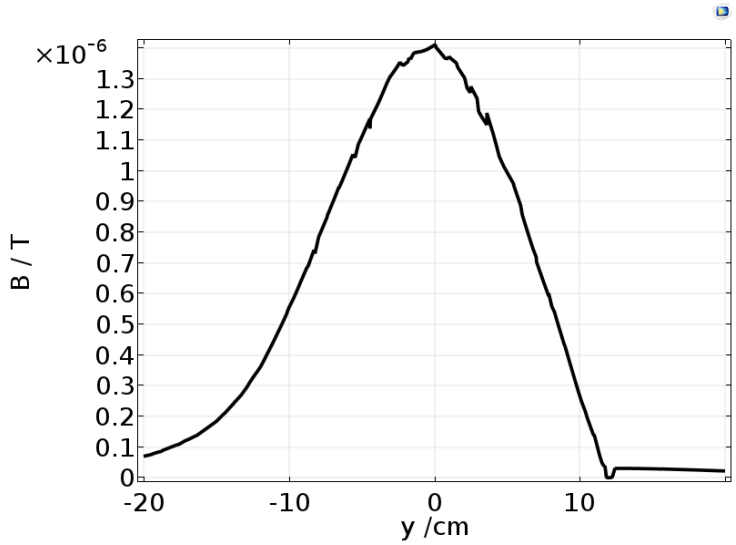

Figure 5.28 Magnetic flux density with conductive shielding at 100 kHz (simulated by the author)

5.4.7 Composite Shielding for WPT Systems

Different shielding methods have been introduced, discussed and corresponding simulation results presented. Increasing efficiency while lowering external fields to meet human exposure safety limits and reduce the impact on surrounding electronic devices are ultimate aims for WPT systems. With this in mind, passive shielding, magnetic shielding and inductive shielding methods have been combined to optimize the WPT system, which is presented in Section 5.3.3. The composite shielding configuration modeled in COMSOL is shown in Figure 5.29. The ferrite plates are placed under and above the transmitter and receiver coils

respectively. The conductive shielding plate and reactive resonant loop coil are placed at the side of the WPT system, parallel to the *xz*-plane. The coordinate of the shielding coil center is (0, 15 cm, 0). The aluminum plate is placed behind the passive shielding coil in the *y*-axis. The coordinate of the aluminum plate center is (0, 18 cm, 0). The parameters of the WTP system, ferrite plates, aluminum plate and reactive shielding coil are the same as presented from Section 5.4.1 to Section 5.4.6.

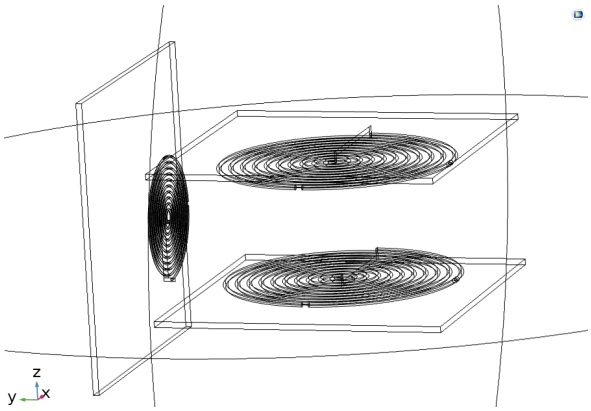

Figure 5.29 Optimized shielding of WPT system in COMSOL model (simulated by the author)

Figure 5.30 presents the distribution of the magnetic induction lines in the *yz*-plane. The resonant frequency of the WTP system with composite shielding is set as 100 kHz. The magnetic flux density is concentrated in the energy transfer domain between the transmitter and receiver coils. The magnetic flux density is strengthened due to the ferrite plates. Therefore, the S-parameter power gain coefficient *S*21 is also increased. According to Figure 5.30, the magnetic induction lines are restricted inside the borders formed by the two ferrite plates. With the additional aluminum plate and the reactive resonant coil, the leakage magnetic field is clearly reduced in the areas where there is the potential that the human body, electronic devices or animals could be present.

Figure 5.31 shows the normalized magnetic flux density contours visualized on a vertical plane cut through the center of the WPT system. The lumped element power of the transmitter is about 0.36 W. The magnetic flux density is maximum in the vicinity of the transmitter coil and decreases gradually from the transmitter to receiver. Outside of the shielding boundaries, the magnetic flux density is nearly 0 T. From Figure 5.31, it is seen that the ferrite shielding plates under the transmitter and above the receiver provide the path that contains most of the

magnetic field generated from the transmitter. The composite shielding method reduces the external magnetic flux density that will be in the vicinity of human beings, animals or electric devices to be much smaller than the limit of 27 μT for the general public at the frequency of 100 kHz.

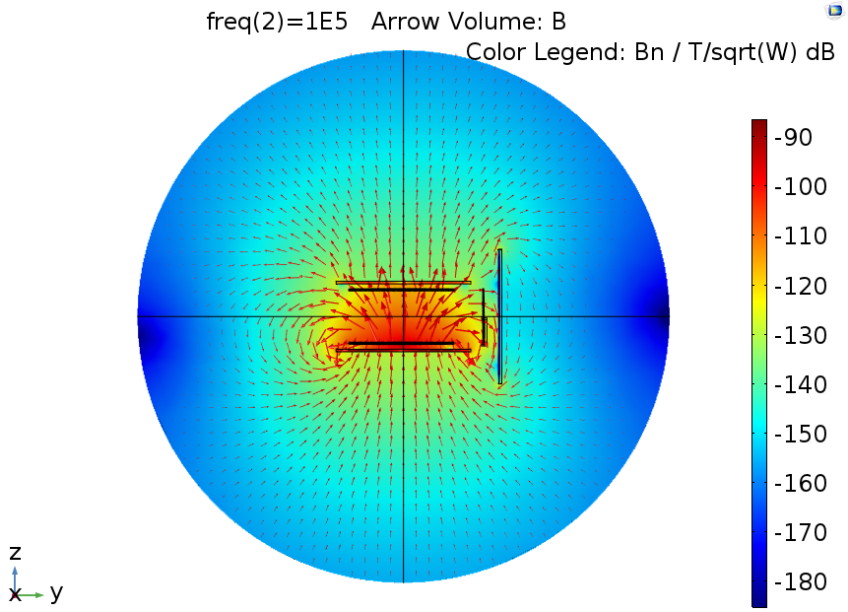

Figure 5.30 Magnetic flux density distribution of composite shielding at 100 kHz (simulated by the author)

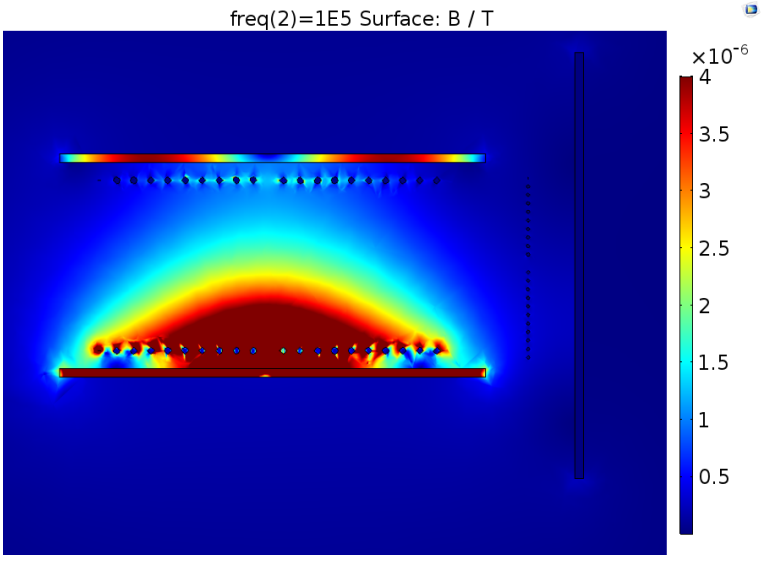

Figure 5.31 Magnetic flux density of composite shielding (simulated by the author)

5.5 Chapter Summary

A 16 coils transmitter has been proposed that operates a single 4-coil sub structure for charging depending on the location of the receiver. For this system it is essential that the system controller be able to determine the receiver location. In order to accomplish this, several different localization methods are invented, presented and explained in detail. This is essential to obtain effective power transfer and charging efficiency while allowing free placement of the device within the large charging area of the 16 coils transmitter matrix.

Secondly, to be practical the WPT system must be EMC friendly in the shielding region outside of the WPT system. To this end a composite shielding system has been designed including ferrite plates, aluminum plates and a passive resonant coil that meets all the requirements.

Chapter 4 proves that a 16 coils transmitter matrix can be used to enlarge the charging area while still providing high transmission efficiency. The position of receiver determines which 4-coil structure is switched on of the 16 coils matrix transmitter. Therefore, localization of the receiver is essential for energy conservation and to charge the mobile device effectively. Three different localization algorithms are presented in this chapter. The grid search algorithm makes use of a lookup table which stores coupling factors simulated and measured a-priori by different methods. The measurement methods are the mutual inductance method, open loop voltage method, short circuit current method and reflected impedance method respectively. The second localization method is the Gauss-Newton algorithm, which utilizes the measured received magnetic field strength values generated by the individual coils in the 16 coils matrix transmitter. The Gauss-Newton algorithm has been simulated in Matlab, which iterates from preset initial values to approximate the optimal regression coefficient by minimizing the target function. The last localization method is applied to the 4-coil structures. In this case the resistance of each available 4-coil structures is measured and the one with the largest reflected resistance is switched on for charging. In the case of ambiguity, that is to say two or more 4-coil structures having equally high reflected resistance, any one of them can be chosen with equal charging efficiency.

The magnetic field emission outside of the WPT must comply with ICNIRP guidelines and EU directives on EM fields. The reference values or limits for human exposure are: 100 μT for workers and 27 μT for the general public at

100 kHz. In order to meet these requirements and reduce the influence on other electric devices in the vicinity, magnetic shielding is necessary for WPT systems. The shielding geometry for WPT systems depends on the type of shielding material used. In this thesis, passive resonant inductive shielding, magnetic shielding and conductive shielding are combined and optimized to improve the efficiency of WPT systems and decrease the magnetic field emission. Ferrite plates are placed at the bottom of the transmitter and on the top of the receiver respectively. This geometry of magnetic shielding concentrates the magnetic field in the transmission domain and improves the efficiency of WPT systems. Combined shielding using a resonant coil and conductive shielding with an aluminum board are used to reduce the field in the desired shielding region. The combined shielding methods have been simulated with COMSOL Multiphysics 5.1. The simulation results show that the efficiency was significantly improved and the external magnetic field was reduced to less than 27 μT by using a combination of the three shielding methods.

Chapter 6

Hardware Platform Setup and Demonstration of WPT Systems

6.1 Chapter Overview

This chapter validates by laboratory demonstration the relevant aspects of WPT systems theory, which have been presented from Chapter 2 to Chapter 5. Various experimental demonstrations of WPT systems have been constructed in the reactive near field using a signal generator, full H-bridge in the transmitter and an AC/DC rectifier in the receiver.

For these demonstrations, coils with different windings have been constructed using the optimized parameters determined from the theory. The relative geometric positions of the transmitter and receiver coils, and multiple coils in the transmitter are set according to the design optimization. The chapter is organized as follows. In Section 6.2, the hardware of WPT systems is introduced, which includes the full H-bridge and rectifier design. In Section 6.3, different topologies of WPT systems including the two-coil configuration and three-coil configuration are presented and compared. In Section 6.4, experiments are described and documented to compare the performance of a traditional transmitter coil with the proposed transmitter matrix. In addition, the computer simulation results are compared with the experimental results. In Section 6.5 different coupling factor measurement methods are discussed and measured results are presented. The localization accuracy is verified by experiment and compared with simulation

results by the Gauss-Newton algorithm. Finally, the use of ferrite plates, as introduced in Section 6.5.4, is investigated by experiment and shown to significant improve efficiency because the magnetic field is concentrated between two ferrite plates and should be adopted for use in WPT systems.

6.2 Hardware Block Description and Experiments Setup

The complete WPT system block diagram includes a power source, controller, inverter (H-Bridge), transmitter coil (TX), coupling circuit between transmitter and receiver (RX_P), receiver coil (RX_S), rectifier and the mobile device (Figure 6.1). The AC current is applied to the transmitter coil, which generates the variable magnetic field in the space. The H-bridge is an electronic switching circuit that converts DC to AC. The H-Bridge consists of two n-channel and p-channel Metal-Oxide-Semiconductor Field-Effect Transistors (MOSFET). The breakover switches are S1, S2, S3 and S4 separately, when S1 and S4 are on with S2 and S3 off and vice versa. The controller connected between the H-Bridge and high level signal IN_H low level signal IN_L is a high frequency H-Bridge driver, such as HIP4081A, which drives the gates of switches. The input triggering signals, IN_H and IN_L, are driven by the microcontroller (μC). The H-Bridge is designed for use with a biomedical implant, for example pacemaker, which is developed by Kommunikationstechnik institute of Duisburg-Essen University [Ric16]. The H-Bridge can operate at frequencies up to 150 kHz with supply voltage from 3 V to 28V. The internal resistance of the H-bridge is roughly 0.5 Ω. When the H-brdige is series connected to a resistor of external circuit, the internal resistance can be measured according to maximum power transmission theorem, which states the power of external circuit resistor reaches maximum when the internal resistance is equal to the resistance of external circuit. The loss during switching is minimized by choke inductors and timing delay. The resonant circuit of the transmitter side is connected between the breakpoints A and B, as shown in Figure 6.1.

The load in the receiver could be the battery in an electric drill, model aircraft, electric robot, cell phone and so on requiring DC for charging. Thus, it is necessary to have the AC/DC rectifier bridge circuit at the receiver. The diode bridge rectifier circuit shown in Figure 6.1, composed of four diodes, produces the desired DC output voltage. When the AC current goes into two diodes D1 and D2, the other two diodes D3 and D4 are reverse biased in the half cycle. The current direction through the load is always same regardless of the AC voltage direction

from the receiver. The frequency of the rectified voltage is twice the frequency of input voltage source, which is given in Figure 6.2. In the practice, the peak to peak rectified voltage has 1.4 V voltage drop in very half cycle, as there is 0.7 V voltage drop across each diode [Doy15].

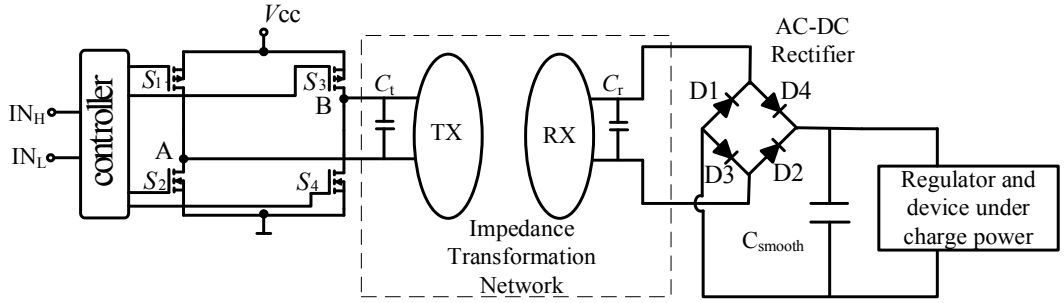

Figure 6.1 Block diagram of WPT systems (representation of resource in **[Ric16,Ric13]**)

In order to get more smooth output waveform a smoothing capacitor connected across the output of the bridge circuit converts the rectified ripple into a smooth DC voltage. Normally the smoothing capacitor is an aluminum electrolytic type with value of 100 μF or more [Doy15]. Figure 6.2 gives the smooth DC voltage output with smoothing capacitor.

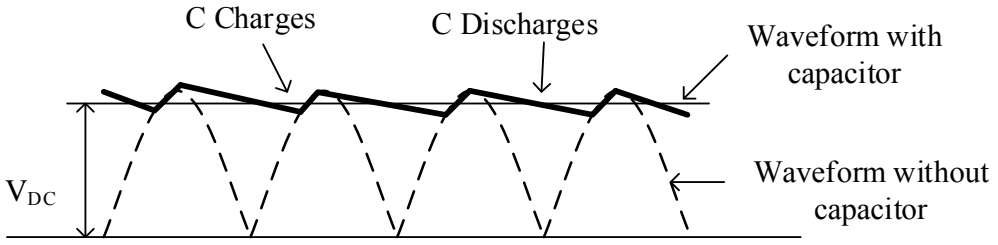

Figure 6.2 Output waveform with smoothing capacitor (representation of resources in **[Ele17]**)

The maximum superimposed ripple voltage (U_{ripple}) is determined by the output frequency (f), the smoothing capacitor (C_{smooth}) and current of the load (I_{load}), which is calculated in (6.1). Users should be sure the smoothing capacitor chosen has the proper value in order to obtain the desired peak to peak ripple voltage. Normally the peak to peak ripple voltage should be less than 100 mV [Doy15].

$$U_{\text{ripple}} = \frac{I_{\text{load}}}{f \times C_{\text{smooth}}} \tag{6.1}$$

To demonstrate the validity of the WTP system which the author proposed in this thesis, the WPT test system platform was setup. The comparison of different topologies modeling, two-coil and three-coil WPT systems are implemented, as well as implementing the transmitter coil matrix proposed for the WPT system. A microcontroller and H-bridge are adopted for use as the signal generator in the transmitter side, as shown in Figure 6.3. The H-bridge is designed to generate a rectangular signal for the power supply. The power source voltage supplied to the WPT system was 3.3V at a frequency of 100 kHz. In order to measure the current of the transmitter circuit, a test resistance with value of 0.1 Ω is connected between the output of H-bridge and the transmitter coil, which is shown in Figure 6.3. Since the test resistance is very small, the effect of the resistor can be neglected. The oscilloscope displays, and can measure input voltage, input current and output voltage, from which the WPT system efficiency can be calculated. According to the requirement for different practical applications, the AC-DC rectifier is connected in the secondary coil of the receiver, which is shown in Figure 6.4.

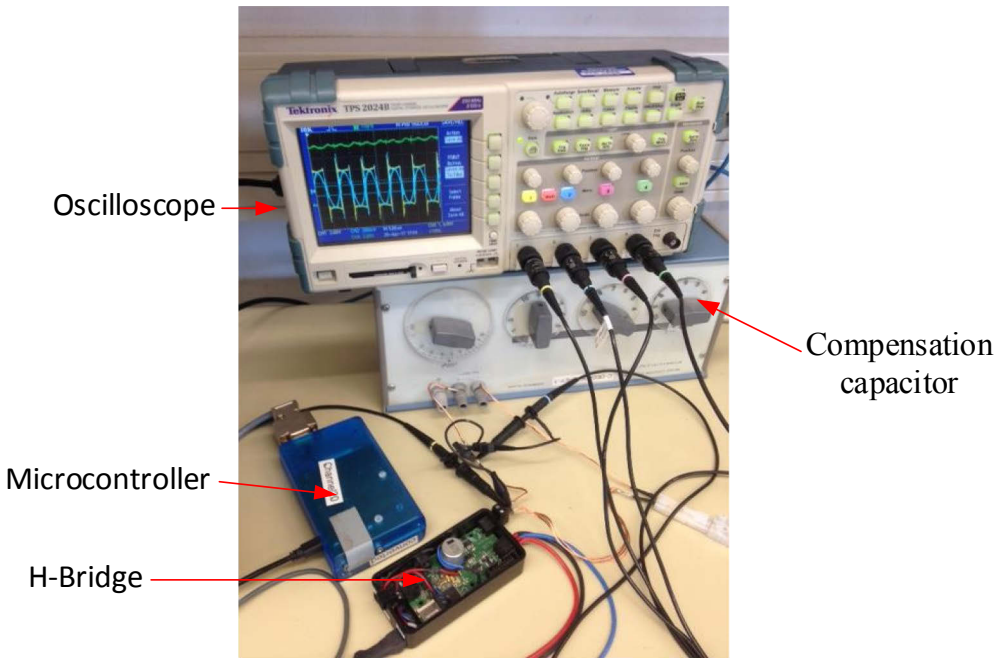

Figure 6.3 Hardware setup with microcontroller and H-bridge (H-bridge and microcontroller developed resource in **[Ric16]**, demonstration setup by the author)

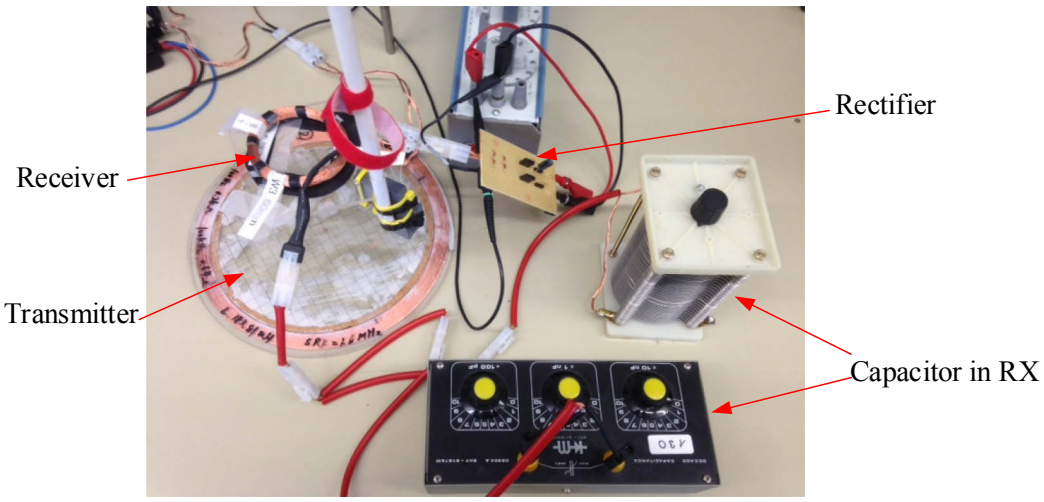

Figure 6.4 Receiver with rectifier circuit (demonstration setup by the author)

6.3 Different Topologies and Models of WPT Systems Comparison

6.3.1 Topology Modeling Comparison

Section 2.3.2 gives theoretical analysis showing that series-series topology is the best choice for mobile device applications of WPT systems. The physical transmitter and receiver coils developed for testing are shown in Figure 6.5. These coils are wound with Litz wire, which is designed for reducing skin effect and proximity effect. The inner diameter of transmitter coil is 10 cm, with 20 turns (0.1mm diameter × 120). Measured values of inductance and resistance of the transmitter coil are 66.4 μH and 0.26 Ω respectively. The quality factor of transmitter coil is about 160.5. The inner and outer radius of the receiver coil is 2.5 cm and 3 cm respectively. The type of litz wire is 0.1 mm × 30, with 80 turns windings. The measured inductance and resistance values are 528.9 μH and 3.7 Ω respectively. Therefore, the quality factor of the receiver coil is roughly 89.8. All the resistance and inductance values are measured at frequency of 100 kHz. The transmission distance is about 5 cm, and load resistance value in the receiver side is set as 50 Ω.

To compare the performance of SR-SR, SR-PR, PR-SR and PR-PR WPT systems, circuits with all four topologies are set up. The circuit diagram of the four topologies is presented in Figure 2.7. What should be noticed is the output of the

signal generator for a parallel resonance circuit should be in the high-impedance state. Then a high value resistance is series connected in the parallel circuit. With this high value resistor, the power supply can provide constant current to the parallel resonance circuit. Very little of the current in a parallel resonant circuit is carried by the internal resistance of the power source and the additional high value resistor. Thus the energy loss is restricted in the resistor of the *LC* parallel circuit. In this case, a high value resistor R_H 100 Ω resistor is connected in series with the source, which is given in Figure 6.6. R_{te} is the test resistor for measuring current with value of 0.1 Ω. R_2 and L_2 are the resistance and inductance of the coil. And R_s is the internal resistance of the power source.

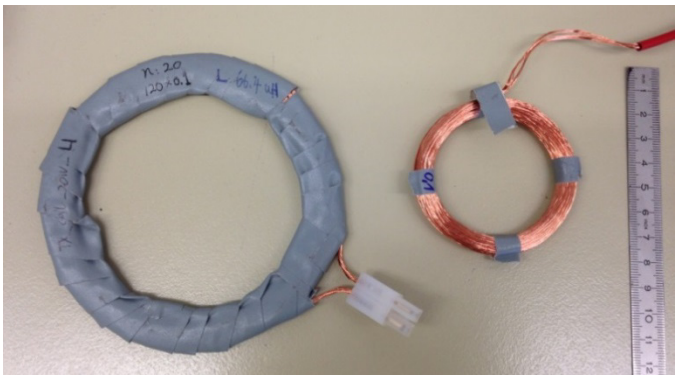

Figure 6.5 Structures of transmitter and receiver coils (demonstrated by the author)

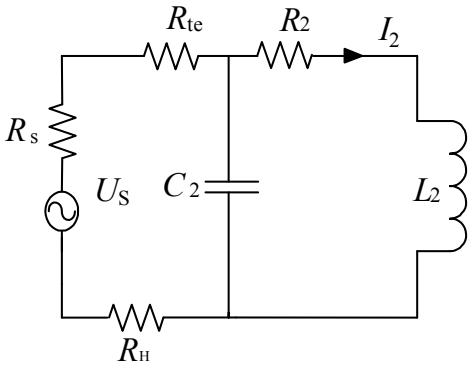

Figure 6.6 Transmitter parallel circuit diagram with high resistor (representation of resources in **[Mie17]**)

The power source voltage and input current measured through test resistor R_{te} will be in-phase when the circuit is resonant. In SR-SR and PR-PR WTP systems, the

load voltage has a 90 degree phase shift with respect to the power source. While load voltages for SR-PR and PR-SR WPT systems have no phase shift from the power source. Figure 6.7 presents experimental results using a SR-SR WPT system, showing the waveform and measured value of input voltage (blue), input current (yellow) and load voltage (green).

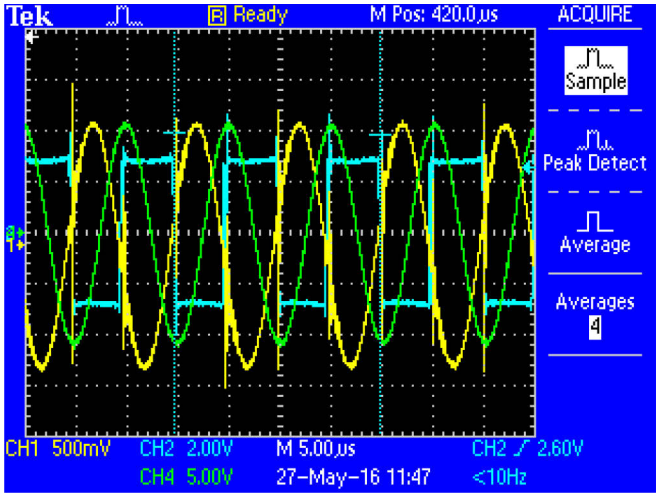

Figure 6.7 Phase and measured value of SR-SR WPT systems (demonstrated by the author)

Capacitances are adjusted to the resonance state in both transmitter and receiver coils. Capacitor values of transmitter and receiver in all four WPT systems topologies are given in Table 6.1.

Table 6.1 Capacitance of transmitter and receiver in four topologies WPT systems

Topologies / TX/RX	SR-SR	SR-PR	PR-SR	PR-PR
Transmitter	37.7nF	37.4nF	37.9nF	38.6nF
Receiver	4.7nF	4.7nF	4.7nF	4.7nF

The efficiency of the WPT system is defined as the ratio of the received power in the load to the delivered power from the electric power source. Table 6.2 gives the measured value of input voltage, input current and load voltage in the four WPT

systems topologies. All measured values from the oscilloscope in Table 6.2 are peak-peak value. The table shows that the SR-SR topology WPT system has by far the highest measured efficiency.

Table 6.2 Efficiency comparison of four topologies WPT systems

Topologies	Input Voltage (V)	Input Current (A)	Load Voltage (V)	Efficiency (%)
SR-SR	5.28	2.68	21.2	70.06
SR-PR	5.04	5.28	7.04	10.16
PR-SR	24.2	0.048	4.56	25.32
PR-PR	25.4	0.136	1.64	1.1

6.3.2 Comparison of Different Configurations WPT Systems

In this thesis, only the two-coil and three-coil configurations of WPT systems are compared and verified by experiment. The four-coil configuration having two coupled coils in the transmitter side is applied for a power supply having a large internal resistance [Ram11]. In this project an H-Bridge power supply is used having an internal resistance that is only 0.5 Ω. Therefore, the four-coil configuration has not been tested. The coils for the two-coil system, consisting of one transmitter coil and the primary coil of the receiver are already shown in Figure 6.5. The receiver secondary coil, wound with 20 turns of Litz wire of 0.1mm diameter × 30 strands, is shown in Figure 6.8. The outer radius of the receiver secondary coil is 3 cm. The inductance and resistance of the secondary coil receiver are 46.68 uH and 0.31 Ω respectively at 100 kHz.

The receiver secondary coil is connected directly to the load without compensation capacitance. The measured efficiency from experiment with two-coil and three-coil WPT systems is given in Figure 6.9. From the figure it is seen that the efficiency reaches maximum value when the load resistor is about 55 Ω for the two-coil system and 80 Ω for the three-coil system respectively. As the theory in section 2.4.4 indicates and Figure 6.9 shows, the three-coil

configuration has more stable performance than that of the two-coil configuration WPT system. By adjusting the coupling factor between the primary and secondary coil of the receiver, the efficiency of the three-coil WPT keeps a high value over a wide range of load resistance. While the efficiency of the two-coil configuration decreases sharply with increasing load resistance after reaching the maximum. Consistent with the theoretical analysis in Section 2.4, the three-coil configuration has greater maximum efficiency as a result of impedance matching with the two coils in the receiver.

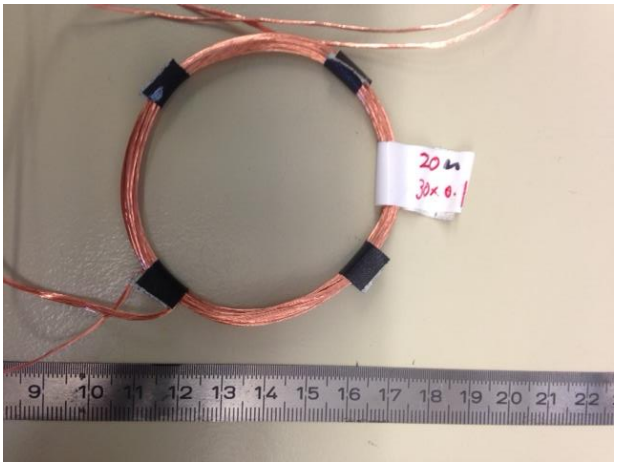

Figure 6.8 Secondary coil of receiver (demonstrated by the author)

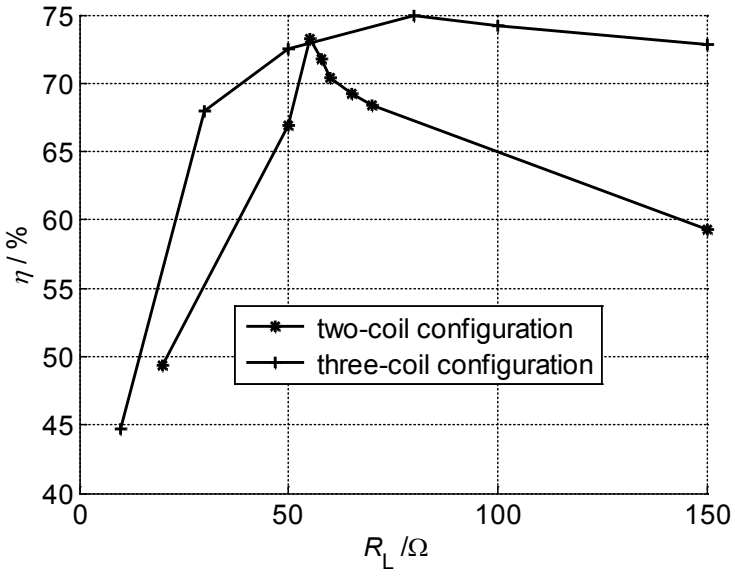

Figure 6.9 Measured Efficiency of two-coil and three-coil configuration WPT systems (simulated by the author)

6.4 Optimum Single Coil and 4-Coil Structure Transmitter WPT Systems Experiment

6.4.1 WPT Systems with Single Transmitter

Chapter 3 presented the optimization for a single coil transmitter WPT system. The physical model of the optimum transmitter coil is shown in Figure 6.10. Included in the figure are the receiver primary and secondary coil also constructed with optimum parameters. For the single coil structure WPT system, the transmitter coil is fixed between two glass sides about 4 mm thick. Since the glass does not affect the magnetic field, the effect of glass in the experiment can be neglected. SR-SR topology is used for the transmitter and primary coil of the receiver. As the inductance and resistance of the receiver secondary coil is quite small, then the 10 turn coil can be directly connected to the load, which is set as 80 Ω in this demonstration. Detailed optimized parameters of the WTP system are given in the Table 3.3 and Table 3.4 of Section 3.4.1.

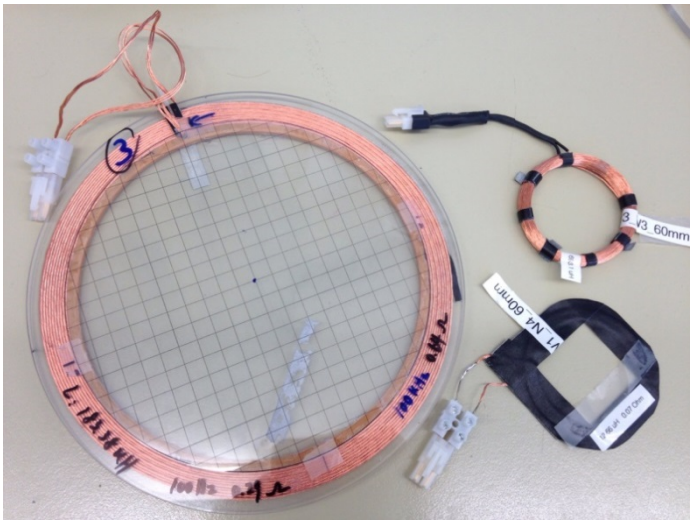

Figure 6.10 Optimized single coil structure WPT system (demonstrated by the author)

In this experiment, the receiver is placed 10 cm above the transmitter, and the center of the receiver moves along *x*-axis away from the center of the transmitter area. The size of transmission area is defined as 20 cm × 20 cm. The range of the *x*-axis is from -10 cm to 10 cm, and the position on the *y*-axis is 0 cm. In general, it can be shown that the transfer efficiency is maximum when the center of the

transmitter and receiver are coaxial. The results for experimental and simulated power transfer efficiency are given in Figure 6.11 at 100 kHz. From Figure 6.11, it is seen that the efficiency of the WPT system is maximum, reaching almost 65%, when the receiver is located at the in the center of the transmitter ($x = 0$) and falls off as the distance from the center increases.

The simulated and experiment results agree very well, with the experimental results being a little higher when the receiver is located in the center of the and a little lower when the receiver is at the edge of the transmitter. The data shown in Figure 6.11 validate simulation results. Therefore, the simulation approach is reliable for use in predicting performance of the WPT systems modeled in this thesis.

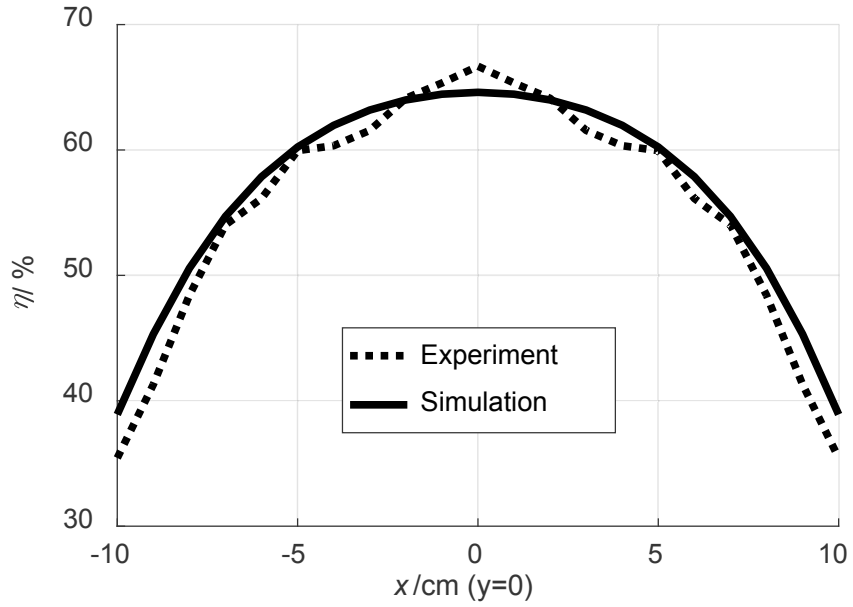

Figure 6.11 Efficiency versus receiver position (simulated by the author)

6.4.2 WPT Systems with 4-Coil Structure Transmitter

In the demonstration of the transmitter matrix validity, series circuits are used in both the transmitter and the receiver. In the 4-coil structure the 4 coils are overlapping as shown in Figure 5.5. Thus when the receiver is centered on the 4-coil structure it has lateral misalignment with respect to all 4 transmitter coils. However the receiver, primary coil and secondary coil are always alignments. The simulation results given in Section 4.4.3 showed that a 16 coils transmitter matrix

is the best choice. The 16 coils structure is composed of 4-coil structures. The simulation results have shown that the optimal radius of the 4-coil structure is 7 cm. Each single coil of a 4-coil structure has 20 turns. The measured resistance, inductance and quality factor of single coil at 100 kHz are 0.35 Ω, 131.7 μH and 236.4 respectively. The constructed 4-coil structure is shown in Figure 6.12. Circle centers coordinates of each coil are (3.3 cm, 3.3 cm), (-3.3 cm, 3.3 cm) (-3.3 cm, -3.3 cm) and (3.3 cm, -3.3 cm) respectively. Since the 4-coil structure is composed of four single coils connected in series, the resistance, inductance and quality factor of the 4-coil structure are 4 Ω, 806 μH and 126.6 respectively.

In the following, WPT systems using optimized parameters for the traditional single coil transmitter and the 4-coil structure are compared when used in a 16 coils transmitter matrix. The receiver coil is placed 10 cm above the 4-coil structure transmitter. The receiver moves along the *x*-axis away from the center of the transmission area, whose size is about 20 cm × 20 cm. The range of the *x*-axis is from -10 cm to 10 cm, and the position on the *y*-axis is 0 cm. The measurement method used for the 4-coil structure is same as for the traditional single coil system. The experimental and simulation results for the single coil system have already been presented in Section 6.4.1.

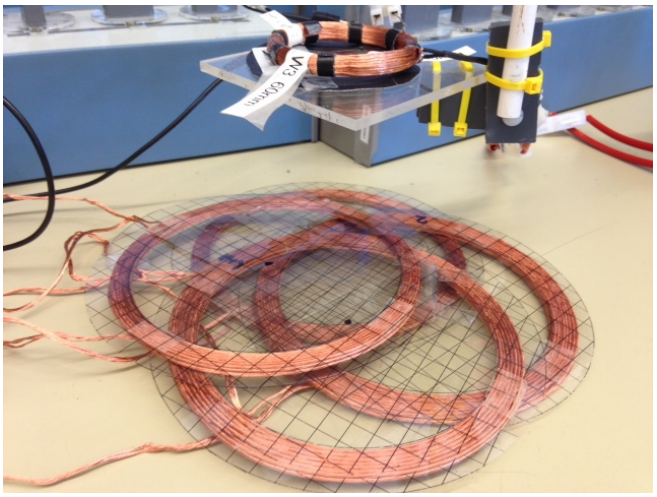

Figure 6.12 Optimized 4-coil structure for demonstrator (demonstrated by the author)

Figure 6.13 presents a comparison of the efficiency of the single coil structure and 4-coil structure by simulation and demonstration. It is seen from Figure 6.13, the simulation results have good agreement with the experiment results. The 16 coils matrix transmitter is made up of 4-coil structures. The concept is that the

appropriate 4-coil structure transmitter will be switched on depending on the position of the receiver. For both single coil structure and 4-coil structure, the efficiency is reduced when the receiver moves along a radial away from the center of the transmission area. Figure 6.13 shows that the 4-coil structure transmitter has higher efficiency than the single coil transmitter when the receiver is near the center of transmitter. When the receiver is near the edge of the transmitter area, the single coil transmitter has a little higher efficiency than the 4-coil structure transmitter. This is caused by the field forming resulting from the multiple transmitter coils. The 4-coil structure transmitter concentrates the magnetic field at the center of the transmitter, while the magnetic field is weakened at the edge of the transmitter.

It can be concluded that the 4-coil structure is more efficient than single coil. The lower efficiency near the edge of the 4-coil structure is due the fact that the magnetic flux density of the 4-coil structure transmitter is decreased more than that of the single coil transmitter along the radial direction of transmission area. Therefore, the magnetic field from the 4-coil system will have less effect on human body and neighboring electronic devices. At the same time, the receiver can be charged with high efficiency in the effective charging area of transmitter matrix, consisting of the area enclosed by the centers of the 4-coil structure transmitter.

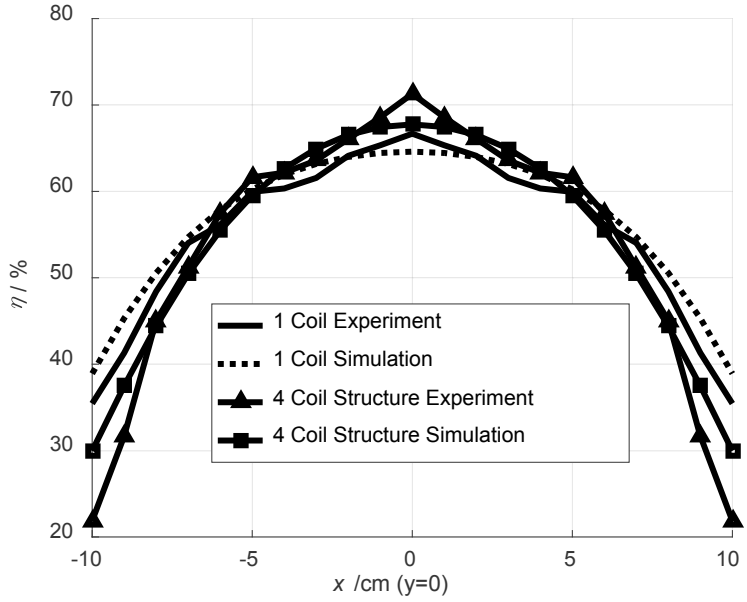

Figure 6.13 Efficiency of different transmitter structure for different receiver position (simulated by the author)

6.5 Localization and Shielding Structure for WPT Systems with Higher Efficiency

6.5.1 Coupling Factor Measurement

The 16 coils transmitter matrix operated in 4-coil structure subsets enables high efficiency charging with free placement of the device anywhere in the large charging area defined by the matrix. However, this requires localization of the receiver coil so that the appropriate 4-coil structure can be activated for charging. Therefore, the author has performed measurements that simulate a 16 coils transmitter matrix for validation of the grid search localization algorithm proposed in Section 5.2.2.1. The parameters and relative position of each transmitter coil are presented in Section 6.4.2. In order to simplify the coupling factor measurement, there is only one coil in the receiver side, parameters of which are presented in Table 3.4 of primary coil. As Section 5.2.1 presented, four coupling factor measurement methods are described, such as coupled inductance method, open loop voltage method, short circuit current method and reflected impedance measurement method. When the transmitter and receiver coils have lateral misalignment of 14 cm or more, then the coupling coefficient is smaller than 0.05 as shown in Figure 5.2. In order to measure more easily and get more accurate results, only the coupled inductance and reflected impedance methods are easier to measure and provide more accurate results and are therefore adopted for the demonstration in this section.

The Agilent U1733C Handheld LCR Meter is used to measure the self-inductance and coupled inductance of the transmitter and receiver coil separately. Since the transmitter and receiver are series connected, the mutual inductance is calculated with (5.5) and the coupling factor is estimated with (5.2). For the reflected impedance measurement, the transmitter circuit is shown in Figure 2.7 (a), where the power source is composed of the microcontroller and H-bridge. The total impedance of the transmitter is obtained by measuring the resonance circuit current and input voltage. The reflected impedance from receiver to transmitter is obtained by (5.14). With the known reflected impedance, (5.13) shows the calculation of mutual inductance between transmitter and receiver coils. Therefore the coupling factor is easily calculated with the measured mutual inductance as shown in (5.2).

The measurement results for the two different methods are shown in Figure 6.14, from which it is easy to observe that the variation of the measured coupling factor

is consistent within the margin of measurement errors. The distance between transmitter and receiver is about 10 cm. The misalignment distance reaches to 14 cm which is twice of inner radius of transmitter coil. When the receiver is located above the center of transmitter, the coupling factor reaches the maximum value 0.033. Then the coupling factor decreases till to almost 0 with the receiver moving along the radial distance away from the center of transmitter.

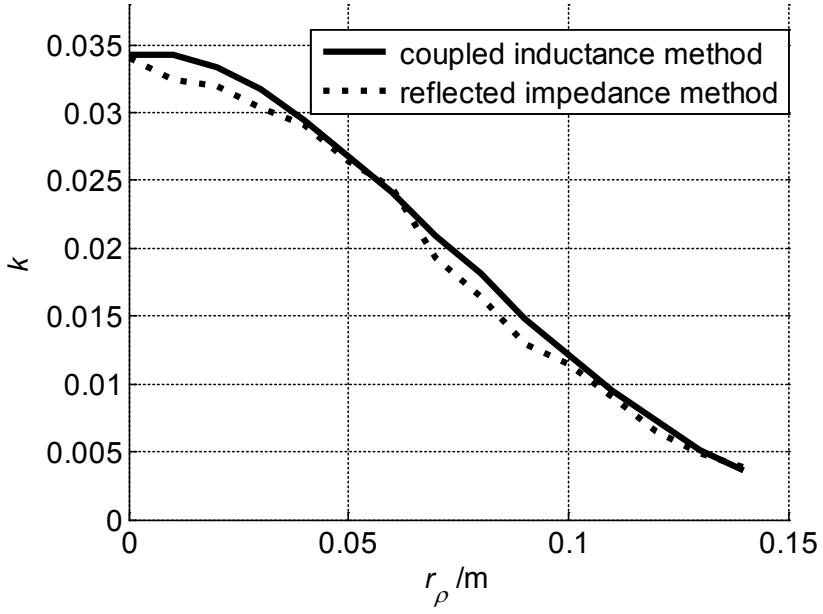

Figure 6.14 Coupling factor measurement results (demonstrated by the author)

6.5.2 Reflected Impedance for Combined Coils Measurement

The reflected impedance for combined coils algorithm is described in Section 5.2.2.3. One set of optimized 4-coil structures (Figure 5.5) in the 16 coils transmitter matrix is switched on to measure the resistance reflected from the receiver coil, as shown in Figure 6.15. The figure shows that the reflected resistance from the receiver to the 4-coil structure transmitter decreases monotonically with increasing lateral misalignment. The simulation results of reflected resistance are basically in accord with the measurement results. Therefore, the reflected impedance for combined coils algorithm is reliable for coil localization for the transmitter matrix. The 4-coil structure with the highest value of reflected resistance is closest to the receiver coil. So this 4-coil structure is selected to be activated for charging the mobile device.

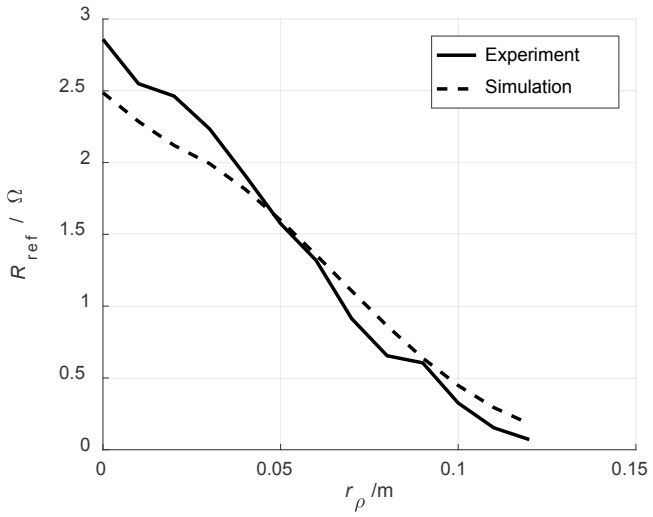

Figure 6.15 Reflected resistance of 4-coil structure (demonstrated and simulated by the author)

6.5.3 Localization Accuracy

In this section, three different localization methods of grid search algorithm, reflected impedance for combined coils algorithm, and Gauss-Newton algorithm are validated and compared by demonstration and simulation separately. Two different coupling factor measurement methods are given and compared by demonstration in Section 6.5.1, which validates the reliability of the coupled inductance and reflected impedance measurement methods. For the case when the receiver is located at 10 cm height above the transmitter, the coupling factors as a function of radial misalignment between each coil of the transmitter matrix and receiver are saved in a lookup table, which is shown in Figure 6.14. The position of the receiver coil can be localized using the values stored in the lookup table, which is denominated grid search algorithm presented in Section 5.2.2.1.

The second method of localization of receiver coil is Gauss-Newton algorithm, which estimates the position of the receiver using the known magnetic flux density of the different transmitter coils based on Matlab simulation. The magnetic field strength from the WPT systems is determined by measurement of the induced voltage in a tiny inductance coil. The received voltages from each of the 16 coils in the matrix are measured by switching on each coil individually. Because the diameter of the test coil is very small, with value of 0.1 cm, the magnetic field strength going through coil is assumed as to be homogenous. Therefore, the magnetic flux density at the receiver generated by each coil of the 16 coils in the transmitter matrix, can be calculated according to (5.20). The

center coordinates of each coil in the 16 coils transmitter matrix is shown in Table 6.3 along with the received voltage and estimated magnetic flux density for the case when the test coil is located at (2 cm, 1 cm, 10 cm). Using the estimated magnetic flux density at the test coil from each of the 16 coils in the transmitter matrix, the unknown receiver's *x,y* coordinates can be estimated with the Gauss-Newton algorithm. Coordinates of the initial estimate are set (0.001 cm, 0.001 cm) in the Matlab simulation. The Gauss-Newton algorithm realized in Matlab iterates to get the minimum target function to obtain the correct regression coefficient.

The combination reflected impedance algorithm uses the measured input impedance of the 4-coil structures to determine which 4-coil structure should be switched on for charging. There are nine 4-coil sub structures within the 16 coils matrix. The 4-coil structure transmitters are checked one by one with reflected resistance test. This method would be checked periodically in order to detect if the receiver had moved or been removed. Although this method cannot detect the exact receiver position, it can easily select the correct 4-coil structure by choosing the one having the highest reflected resistance. It is possible for two of the 4-coil structures to have the same reflected impedance when the receiver is located at the border of two coil centers. In this situation, either of 4-coil structure transmitters can be switched on for charging mobile device.

In order to verify the three different localization methods, the measurement results of the grid search algorithm and reflected impedance for combined coils algorithm are compared with the simulation results from the gauss-newton algorithm. Figure 6.16 shows a diagram with 10 different examples for the receiver's positions in the 10 cm × 10 cm charging area. For each position the diagram includes the actual position of the receiver coil, as well as the estimated position of receiver for both the grid search and gauss-newton algorithms. It can be concluded from Figure 6.16 that the error range of the grid search algorithm is less than 1 cm, while the gauss-newton algorithm has better performance with error on the order of 0.5 cm. When the receiver coil is located in position 1 in transmitter matrix shown in Figure 6.16, the four coils of black color are selected to be switched on because of they had the maximum reflected impedance. Similarly, the red four coils are chosen to be activated when the receiver coil is in position 2. If the receiver coil is at the border between two coils centers, for example position 3, either the four black coils or two black coils together with the adjacent two pink coils are switched on. Thus, the grid search algorithm, Gauss-Newton algorithm and reflected impedance for combined coils algorithms can all successfully localize the position of the receiver coil.

Table 6.3 Parameters for estimating position of receiver

Coil Number	Center Coordinates of Transmitter Matrix (cm)	Received Voltage (mV)	Magnetic Field Strength (μT)
1	(3.3, 3.3)	5.4	34.54
2	(-3.3, -3.3)	3.4	21.69
3	(3.3, -3.3)	4.7	29.88
4	(-3.3, 3.3)	4.0	25.57
5	(-9.9, 9.9)	0.17	1.10
6	(-9.9, 3.3)	0.79	5.01
7	(-9.9, -3.3)	0.63	4.00
8	(-9.9, -9.9)	0.02	0.14
9	(-3.3, 9.9)	1.5	9.32
10	(-3.3, -9.9)	0.79	5.01
11	(3.3, 9.9)	2.1	13.66
12	(3.3, -9.9)	1.2	7.63
13	(9.9, 9.9)	0.86	5.47
14	(9.9, 3.3)	2.6	16.40
15	(9.9, -3.3)	2.1	13.66
16	(9.9, -9.9)	0.43	2.73

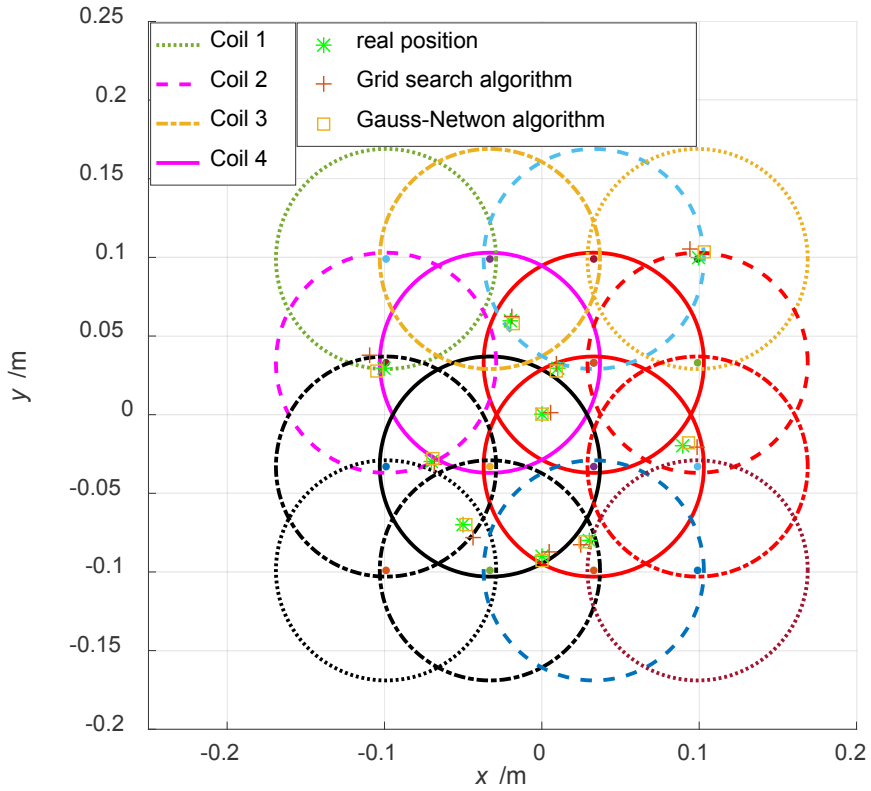

Figure 6.16 Localization accuracy of grid search, Gauss-Newton algorithm and reflected impedance for combined coils algorithm (demonstrated and simulated by the author)

6.5.4 Improvement of WPT Systems Efficiency with Ferrite

In Section 5.3.2.3 and 5.3.3, the author analyzes the advantage by using ferrite for WPT systems, as well as presents the desired location of ferrite plates for transmitter and receiver coils. Section 5.4.5 gives the simulation results describing the shielding effect with respect to decreasing external EMF emission and concentration of the internal magnetic field. In this section, only the efficiency improvement of the WPT system is verified by demonstration. Figure 6.17 presents a picture of the shielded WPT system constructed with ferrite plates under the transmitter and above the receiver respectively.

The ferrite material DMR40 made from Manganese-Zink was chosen as the ferrite plate in this thesis. DMR 40 has the following characteristics at 25˚C: initial permeability is about 2300, the saturation flux density is 510 mT, and 100 kHz is in the range of its proper working frequency. The dimensions, length, width and

thickness of the ferrite plate at the transmitter are 24.5 mm × 24.5 mm × 10 mm and at the receiver side 12.2 mm × 9.2 mm × 10 mm respectively. The self-inductance, resistance and mutual inductance of the transmitter and receiver coils are increased due to the ferrite plates, as shown in Table 6.4 quality factor of the transmitter is decreased from 180 to 145.1. However, the quality factors of the primary and secondary coil of the receiver are increased from 101.3 to 115.4 and from 88.38 to 108.7 respectively. The self-inductance of the transmitter and receiver coils is increased with the ferrite plate and the mutual inductance between the transmitter and receiver is also increased. Thus, the coupling factor between transmitter and receiver, which is calculated according to (5.2), is increased from 0.03 without ferrite to 0.07 with ferrite at 10 cm transmission distance. This demonstration proves that the efficiency of the WPT system with ferrite plates is increased to 74.28 % compared with 66.9 % efficiency without ferrite. From the analysis in Section 5.3.2.3, the performance is improved due to the stronger coupling factor resulting from the guidance and concentration of the magnetic field between the transmitter and receiver coils due to the ferrite plates.

Table 6.4 Parameters of WPT systems with ferrite

Transmitter/Receiver	Without Ferrite	With Ferrite
Inductance of transmitter	183.38 μH	284.1 μH
Resistance of transmitter	0.64 Ω	1.23 Ω
Inductance of primary coil of receiver	693.1 μH	1028.4 μH
Resistance of primary coil of receiver	4.3 Ω	5.6 Ω
Inductance of secondary coil of receiver	12.66 μH	20.76 μH
Resistance of secondary coil of receiver	0.09 Ω	0.12 Ω
Mutual inductance between TX and RX	10.96 μH	39.7 μH

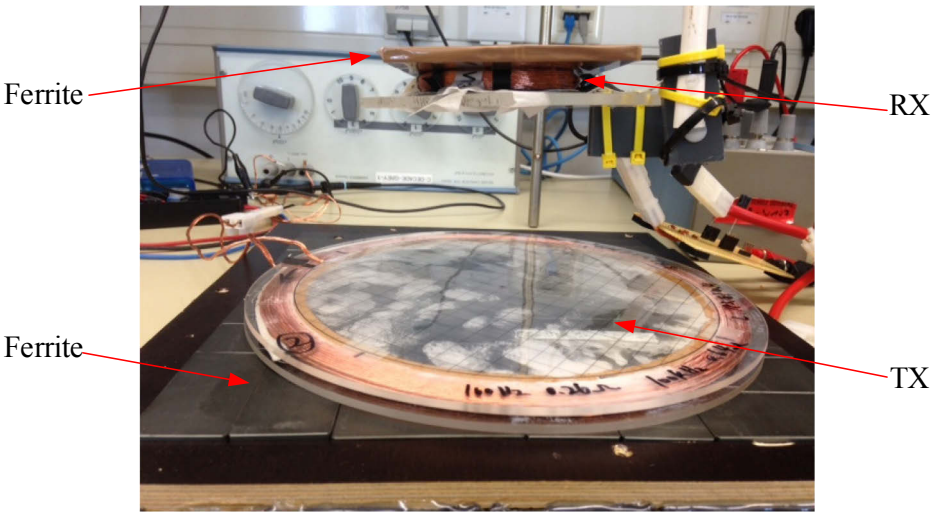

Figure 6.17 WPT systems with ferrite (demonstrated by the author)

6.6 Chapter Summary

This chapter mainly focuses on the laboratory demonstration of WPT systems by comparison of the measured performance of different topologies and configurations, the optimized single coil and 4-coil structure transmitter. Included are coupling factor measurements between transmitter and receiver, demonstration of receiver localization using with the 16 coils transmitter matrix, and measurements of the system with the ferrite shielding structure. All experiments are carried out by reacting between the resonant transmitter and resonant receiver in the near field.

In the hardware design, the full H-bridge is used as the sine wave signal generator for the transmitter side, which is developed by Kommunikationstechnik institute of Duisburg-Essen University. The AC-DC rectifier circuit is used in the load coil because the application of this work is to charge batteries in mobile devices. The SR-SR topology and three-coil configuration are proved to have the best performance in efficiency by comparison with other configurations for the application chosen in this thesis. Therefore, SR-SR topology and three-coil configuration are constructed and used in laboratory demonstrations of single and multiple coil transmitter design, localization of receiver and WPT systems shielding structure. In addition, WPT systems for single transmitter and 4-coil structure transmitters with optimized parameters based on theoretical Matlab simulations are constructed and validated by experiment. The localization methods of the grid search algorithm by coupling factor measurement and the Gauss-Newton algorithm by Matlab simulation are shown to be able to detect the

position of receiver coil. Both localization methods have less than 1 cm error range. The choice of which 4-coil structure to activate can be determined by the reflected impedance for combined coils algorithm, which localizes the receiver position by measuring the reflected resistance of the 4-coil structure. Gauss-Newton, reflected impedance for combined coils and grid search algorithms are accordant and proved to be appropriate for localization of the receiver in a WPT system by simulation and laboratory demonstration.

To verify the performance with ferrite shielding structure, a WPT system was designed and implemented with two ferrite plates placed above and under the receiver and transmitter respectively. The measured results show that mutual inductance and coupling factor between transmitter and receiver are increased leading to improved performance. Even though the resistance of the transmitter and receiver coils increased, the efficiency of the WPT system constructed with ferrite structure has at more than 7 % improvement in efficiency at the 10 cm transmission distance.

Chapter 7

Conclusion and Outlook

7.1 Conclusion of This Thesis

This thesis focuses on solving existing problems of the application of wireless charging technology for mobile and portable devices, such as limited transmission distance, low transfer efficiency, inconvenience for placement and human exposure safety. In allusion to the problems mentioned above, the author proposes specific solutions, which enable practical WPT techniques to charge mobile devices.

As part of this thesis it was necessary to examine the basic WPT system models. There are four different topologies for WPT systems which are SR-SR, SR-PR, PR-SR and PR-PR. After evaluating these topologies based on the parameters selected , such as working frequency, inductance, resistance of transmitter and receiver coils, and load resistor, SR-SR is selected as the best topology for the systems modeled in this thesis. In the demonstration, SR-SR topology had the highest efficiency. Four different configurations using this topology were examined. For a two-coil WPT system there is only one coil in both transmitter and receiver. Both three-coil and four-coil WPT systems have an additional coupling coil in the receiver. For a four-coil WPT system there is an additional coupling coil on the transmit side. By adjusting the coupling factor (k_{34}) between the primary and secondary coil of receiver, the efficiency of a WPT system can be kept high regardless of load resistance. In contrast with the two-coil system, the three-coil and four-coil WPT systems maintain high efficiency with variation of

load resistance. In four-coil WPT systems, the value of coupling factor (k_{12}) between the primary and secondary coils of transmitter can be optimized for either high transfer efficiency or high power received but not both. That is to say, high efficiency and high received load power could not be achieved for the four-coil WPT system. In a word, with high Q value for the transmitter coil and primary coil of receiver, while using series connection circuit diagram structure, three-coil WPT systems can provide high efficiency and high power transfer simultaneously with varying load resistance. Therefore, three-coil WPT system can provide stable system performance and has been chosen for investigation in this thesis.

The design and optimization steps for WPT systems at increasing distance have been investigated and are an important part of this thesis. The required efficiency for charging mobile and portable devices is greater than 65 %. The transmission distance is fixed at 10 cm which is regarded as middle range for magnetic resonance WPT systems. For this distance a system using, multi-layer helical coils is chosen. The author considers the effect of the coupling factor between transmitter and receiver k_{23}, the quality factor of the transmitter coil Q_{2sc} and the receiver primary coil Q_3 in a comprehensive optimization for a traditional single transmitter coil. The resulting transmitter coil number of turns per layer, number of layers and inner radius was 2, 10 and 10 cm respectively. For the receiver side, the quality factor and size restriction of the mobile devices are considered as the optimization criteria. The outer radius of the receiver coil is limited to 4 cm, the number of turns per layer and number of layers are fixed as 10 and 8 respectively. The quality factor of the receiver secondary coil is decided according to the optimum coupling factor (k_{34}) between the primary and secondary coil of the receiver. The result is that the secondary coil of the receiver has one turn per layer and 10 layers, which is in accord with equation (2.63).

In addition to the optimization of the single transmitter coil WPT system, the author proposes a 4-coil structure transmitter using four overlapping coils based on field forming theory. The design of the 4-coil structure is such that the magnetic field is concentrated in the area between the transmitter and receiver and reduced elsewhere. This results in improved efficiency when the receiver coil is located in the central zone of a 4-coil structure, while reducing the magnetic field strength at the margin of the 4-coil structure compared with that of a single coil WPT system. In order to enable mobile and portable devices to move freely in the charging area, a transmitter matrix consisting of multiple 4-coil structures is proposed. For this approach, the appropriate set of 4 adjacent coils is switched on to provide maximum charging depending upon the location of the mobile device. A transmitter matrix consisting of 16 coils is selected in terms of maximal cost

efficiency, which is determined by efficiency gain ratio of the weighted overall efficiency and total expense of Litz wire winding. An optimum inner radius for each coil in the 16 coils transmitter matrix is determined to be roughly 7 cm using the maximum weighted overall efficiency. The optimization procedure provides the maximum magnetic field strength in the center of a sub-charging zone (CSCZ) and minimal magnetic field strength in the fringe of a sub-charging zone (SCZ). In addition, there is a significant difference of magnetic field strength between CSCZ area and the SCZ margin. The 16 coils transmitter matrix provides a 20 cm × 20 cm charging area while maintaining transfer efficiency more than 65 % by switching on the appropriate 4-coil structure transmitter depending on the position of the mobile and portable devices. In other words, the system has the advantage of high efficiency and convenience wherever the receiver coil is located in the charging area.

As mentioned in Section 4.4, the receiver coil's position determines which 4-coil structure of the transmitter matrix is activated. Therefore, it is necessary to estimate the location of the receiver coil. The author proposes three different positioning methods which are: a grid search algorithm, a Gauss-Newton algorithm and the reflected impedance for combined coils algorithm. Details of the grid search algorithm are presented in Section 5.2.2.1. The approach is to use the intersection area or a single point defined by several intersecting circles. Each circle stands for the coupling factor value between each coil of the transmitter matrix and the receiver coil. The coupling factor between TX and RX coils is measured using the coupled inductance and reflected impedance methods. The position of the receiver can be predicted from coupling factor circles determined by switching on each coil of the transmitter matrix separately. The second positioning method is the Gauss-Newton algorithm using non-liner regression. In this method an initial value is selected and then the regression coefficient is modified iteratively, until it approximates the optimum regression coefficient of a non-linear regression model. In the end, the residual sum of squares of original model reaches minimal value. The Gauss-Newton algorithm for WPT systems positioning is implemented by Matlab simulation. The third method is reflected impedance for combined coils algorithm presented in Section 5.2.2.3. The reflected resistance is measured for each of the nine possible 4-coil structures which are switched on in turn. The 4-coil structure having the maximum reflected resistance is chosen for charging the mobile device.

For a complete WPT system, the effect on external systems should be considered with respect to shielding so as to be EMC friendly and, comply with ICNIRP guidelines. According to ICNIRP guidelines The magnetic flux density limit for

human exposure of the general public is 27 μT at 100 kHz in the neighborhood of WPT systems. There are several shielding methods, including active shielding, passive shielding, magnetic shielding and conductive shielding, which could reduce the magnetic field emissions and exposure levels to ensure human exposure safety. The design objective of shielding structure for WPT systems is a shielded region around the WPT complying with ICNIRP regulations while maintaining the WPT system efficiency requirements. The sides of the transmitter are regarded as the target shielding region. Thus, aluminum plate and reactive resonant coil shielding is symmetrically placed around the WPT system. The analysis of these shields has taken into account the merits and demerits of conductive shielding and passive shielding methods. Ferrite plates are used under and above the TX and RX coils respectively because ferrite has the advantage of increasing the coupling factor and reducing the loss and emission from the transmitter. The COMSOL simulation results show the magnetic field strength in the shielding region is greatly reduced with the aluminum plate and reactive resonant loop coil. The transfer efficiency is improved by usage of ferrite material as well, which has been validated by COMSOL simulation and demonstration. Moreover, the magnetic field is restricted in the domain between the two ferrite plates, therefore, the magnetic fields in the region under and above the TX and RX coils is also reduced. From the analysis above, we can conclude that WPT systems using the 4-coil structure transmitter and additional ferrite plates can increase the transfer efficiency by concentration of the magnetic field strength in the desired region, and reduction of the magnetic field strength in the undesired regions.

7.2 Outlook and Open Issues

Wireless charging chips, which include hardware, software protocols and power management systems, as well as having modular design are being developed rapidly by many companies in the electronic consumer markets. The integrated circuit (IC) for this application has strict requirements on its size, accuracy control and stability. Therefore, a specialized IC design is proposed to act as the transmitter controller for a WPT system as described in this thesis. This controller would be used to detect the position of mobile device by measuring the coupling factors, opening-closing every 4-coil structure in turn for reflected resistance measurement, as well as activating the appropriate coils of the 16 coils transmitter matrix according to the location of the receiver coil.

The proposed 16 coils system has many advantages including convenience and high efficiency and can meet the human safety requirements. As a new system the development and initial costs may be significant. However, in mass production it is likely to become relatively inexpensive and with the solid state controllers it will be extremely reliable. The system is so convenient that it is anticipated WPT systems like the one proposed in this thesis will receive wide acceptance in the near future.

References

[Agb13] Agbinya, Johnson Ihyeh : Investigation of Near Field Inductive Communication System Models, Channels and Experiments, *Progress in Electromagnetics Research B*, vol. 49, pp. 129-153, 2013.

[Ahn11] Ahn, Seungyoung ; Kim, Joungho : Magnetic Field Design for High Efficient and Low EMF Wireless Power Transfer in On-Line Electric Vehicle, in *The 5th European Conference on Antennas and Propagation (EUCAP 2011)*, Rome, 2011, pp. 3979-3982.

[Ahn13a] Ahn, Seungyoung ; Hwang, Chulsoon ; Park, Hyun Ho : Optimized Shield Design for Reduction of EMF from Wireless Power Transfer Systems, *IEICE Electronics Express*, vol. 11, no. 2, pp. 1-9, 2013.

[Ahn13b] Ahn, Dukju ; Hong, Songcheol : Effect of Coupling Between Multiple Transmitters or Multiple Receivers on Wireless Power Transfer, *IEEE Transactions on Industrial Electronics*, vol. 60, no. 7, pp. 2602-2612, July 2013.

[Aje14] Ajey, Kumar.R ; Gayathri, H.R ; Bette, Gowda.R ; Yashwanth, B : WiTricity:Wireless Power Transfer By Non-radiative Method, *International Journal of Engineering Trends and Technology*, vol. 11, no. 6, pp. 290-295, May 2014.

[Aug14] Augustine, Mystica ; Duke, Michael : Wireless Power Transmission, *International Journal of Scientific & Engineering Research*, vol. 5, no. 10, pp. 125-129, October 2014.

[Auv15] Auvigne, Christophe Bruno : Electrical and Magnetical Modeling of Inductive Coupled Power Transfer Systems, ÉCOLE POLYTECHNIQUE FÉDÉRALE DE LAUSANNE, Écublens, Dissertation 6593, 2015.

[Aya02] Ayano, Hideki ; Yamamoto, Kouki ; Hino, Noriaki ; Yamato, Ikuo : Highly Efficient Contactless Electrical Energy Transmission System, in *IECON 2002 28th Anuual Conference of the IEEE Industrial Electronics Society* , vol. 148, Sevilla, 2002, pp. 1364-1369.

[Aza14] Azahar, Ahmad Faiz Bin Ahmad : Wireless Power Transfer Monitoring, Universiti Teknikal Malaysia Melaka, Malacca, Project 2014.

[Bab08] Babic, Slobodan I. ; Akyel, Cevdet : Calculating Mutual Inductance Between Circular Coils with Inclined Axes in Air, *IEEE Transactions on Magnetics*, vol. 44, no. 7, pp. 1743-1750, July 2008.

[Bar10] Barker, D.J. ; Summerer, L. : Analysis of near-field wireless power transmission for fractionated spacecraft applications, in *62nd International Astronautical Congress*, Cape Town, 2010, pp. 1-8.

[Bar15] Barman, Surajit Das ; Reza, Ahmed Wasif ; Kumar, Narendra ; Karim, Md. Ershadul ; Munir, Abu Bakar : Wireless Powering by Magnetic Resonant Coupling: Recent Trends in Wireless Power Transfer System and its Applications, *Elsevier*, pp. 1525-1552, July 2015.

[Beh10] Beh, TeckChuan ; Kato, Masaki ; Imura, Takehiro ; Hori, Yoichi : Wireless Power Transfer System via Magnetic Resonant Coupling at Fixed Resonance Frequency - Power Transfer System Based on Impedance Matching, *World Electric Vehicle*, vol. 4, pp. 744-753, 2010.

[Beh13] Beh, Teck Chuan ; Kato, Masaki ; Imura, Takehiro ; Oh, Sehoon ; Hori, Yoichi : Automated Impedance Matching System for Robust Wireless Power Transfer via Magnetic Resonance Coupling, *IEEE Transactions on Industrial Electronics*, vol. 60, no. 9, pp. 3689-3698, Sep. 2013.

[Bej10] Bejar, Benjamin ; Belanovic, Pavle ; Zazo, Santiago : Distributed Gauss-Newton method for localization in AD-hoc networks, in *2010 Conference Record of the 44 Asliomar conference on signal, systems and computers*, Pacific Grove, 2010, pp. 1452-1454.

[Ben12] Benko, Larry. (2012, June) Coupling between coils or coefficient of coupling. W0QE.

[Bev08] Bevelacqua, Peter Joseph. (2008) Antenna Theory. [Online]. http://www.antenna-theory.com/definitions/sparameters.php

[Bit14] Bito, J ; Cook, B.S ; Tentzeris, M.M : A Multi-Coil Wireless Power Transfer System Utilizing Dynamic Matching for In-Vivo and Biomedical Applications, in *Proceedings of Asia-Pacific Microwave*, Sendai,Japan, 2014, pp. 680-682.

[Bom05] Bomber, Andrew : Wireless Power Transmission An Obscure history and a Bright Future, Project PH 464 Applied Optics, 2005.

[Bom13] Bombardier. (2013) Primove. [Online]. http://primove.bombardier.com/fileadmin/primove/content/MEDIA/Publications/BT_Brochure_PRIMOVE_210x280_2013_final_upd_110dpi_SP.pdf

[Bom16] Bombardier. (2016, June) Primove. [Online].

http://primove.bombardier.com/en/media/news/news-detail-page/article/2016/06/30/298.html

[Boy00] Boys, J.T ; Covic, G.A ; Green, A.W : Stability and control of inductively coupled power transfer systems, *IEE Proceedings Electric Power Applications*, vol. 147, no. 1, pp. 37-43, Janarury 2000.

[Boy07] Boys, John T. ; Elliott, Grant A.J. ; Covic, Grant A. : An Appropriate Magnetic Coupling Co-Efficient for the Design and Comparison of ICPT Pickups, *IEEE Transactions on Power Electronics*, vol. 22, no. 1, pp. 333-335, January 2007.

[Bre14] Brecher, Aviva ; Arthur, David : Review and Evaluation of Wireless Power Transfer for Electric Transit Applications, U.S.Department of Transportation, FTA Report No.0060, 2014.

[Bro66] Brown, W.C ; Mims, J.R ; Heenan, N.I : An Experimental Microwave-Powered Helicopter, *IEEE International Convention Record*, vol. 13, no. 5, pp. 225-235, 1966.

[Bro81] Brown, William C : Status of the Microwave Power Transmission Components for the Solar Power Satellite, *IEEE Transactions on Microwave Theory and Techniques*, vol. MIT-29, no. 12, pp. 1319-1327, Dec. 1981.

[Bro84] Brown, William C : The history of power transmission by radio waves, *IEEE Transactions on Microwave Theory and Techniques*, vol. 32, no. 9, pp. 1230-1242, 1984.

[Bro89] Brown, William C. (1989) History and Status of Beamed power Technology and Applications at 2.45 Gigahertz. Ntrs.Nasa.

[Bro96] Brown, William C : The history of wireless power transmission, *Solar Energy*, vol. 56, no. 1, pp. 3-21, 1996.

[Can09] Cannon, Benjamin L ; Hoburg, James.F ; Stancil, Daniel D ; Goldstein, Seth Copen : Magnetic Resonant Coupling as a Potential Means for Wireless Power Transfer to Multiple Small Receivers, *IEEE Transactions on Power Electronics*, vol. 24, no. 7, pp. 1819-1825, July 2009.

[Can12] Cano, Raquel Montalvo : Wireless Power Transfer, Chalmers University of Technology, Göteborg, Project 2012.

[Car15] Carolus, Ken : Making Conducted and Radiated Emissions Measurements for EMI Pre-Compliance Test, Keysight Technologies, 2015.

[Cas09a] Casanova, Joaquin J ; Ning, Zhen ; Lin, Jen shan : A Loosely Coupled Planar Wireless Power System for Multiple Receivers, *IEEE Transactions on Industrial Electronics*, vol. 56, no. 8, pp. 3060-3068, Aug. 2009.

[Cas09b] Casanova, Joaquin J. ; Low, Zhen Ning ; Lin, Jenshan ; Tseng, Ryan : Transmitting Coil Achieving Uniform Magnetic Field Distribution for Planar Wireless Power Transfer System, in *Radio and Wireless*

Symposium, San Diego, 2009, pp. 530-533.

[CCR15] CCRMA. (2015, October) Applications of the Gauss-Newton method. Stanford University.

[Che05] Cheng, Bing Hwa ; Hudson, Ralph E. ; Lorenzelli, Flavio ; Vandenberghe, Lieven ; Yao, Kung : Distributed Gauss-Newton method for node localization in wireless sensor networks, in *IEEE 6th Workshop on signal prcessing advances in wireless communications*, New York, 2005, pp. 915-919.

[Che07] Chen, Zhi Ning : *Antennas for portable devices*, 1st ed. London, England: John Wiley & Sons Ltd, 2007.

[Che10] Chen, Chih-Jung ; Chu, Tah-Hsiung ; Lin, Chih-Lung ; Jou, Zeui-Chown : A Study of Loosely Coupled Coils for Wireless Power Transfer, *IEEE Transactions on Circuits and Systems*, vol. 57, no. 7, pp. 536-540, July 2010.

[Che11] Cheon, Sanghoon et al.: Circuit-Model-Based Analysis of a Wireless Energy-Transfer System via Coupled Magnetic Resonance, *IEEE Transactions on Industrial Electronics*, vol. 58, no. 7, pp. 2906-2914, July 2011.

[Che13] Chen, Wei et al.: Optimization Spatial Multiple Coil Transmitter Structure for Wireless Power Transfer, in *Antennas and Propagation Society International Symposium (APSURSI), 2013 IEEE*, Orlando, 2013, pp. 854-855.

[Che14a] Chen, Wei ; Bai, Zijian ; Rickers, Sebastian ; Bruck, Guido H. ; Jung, Peter : Transmitter with Cooperative Coils Matrix for robust Wireless Power Transfer Systems, in *International Symposium on Electromagnetic Compatibility (EMC Europe)*, Gothenburg, 2014, pp. 48-52.

[Che15] Chen, Wei ; Rickers, Sebastian ; Bruck, Guido H. ; Jung, Peter : Localization System Using Resonant Magnetic Coupling Factor for Improving Efficiency in Wireless Power Transfer, in *9th European Conference on Antennas and Propagation*, Portugal, 2015, pp. 1-2.

[Chi04] Chitode, J.S. : *Communication Systems - I*, 3rd ed., Shri Avinash Wani and Shri Ravindra Wani, Eds. Pune, India: Technical Publications, 2004.

[Cho11] Choudhary, Vikash ; Singh, Satendar Pal ; Kumar, Vikash ; Prashar, Deepak : Wireless Power Transmission: An innovative Idea, *International Journal of Educational Planning & Administration*, vol. 1, no. 3, pp. 203-210, 2011.

[CIS10] CISPR. (2010) International Electrotechnical Commission. [Online]. https://webstore.iec.ch/publication/76

[CLC16] CLC/TC 69X Electrical Systems for Electric road vehicles. (2016) CENELEC. [Online]. https://www.cenelec.eu/dyn/www/f?p=104:7:1282482009054201:FS

P_ORG_ID:1258145

[Com17] Comsol. (2017) Comsol. [Online]. https://www.comsol.com/acdc-module

[Cov06] Covic, G.A ; Boys, J.T ; Lu, H.G : A Three-Phase Inductively Coupled Power Transfer System, in *2006 1ST IEEE Conference on Industrial Electronics and Applications*, Singapore, 2006, pp. 1-6.

[Cov07] Covic, Grant.A ; Boys, John.T ; Kissin, Michael L.G ; Lu, Howard G : A Three-phase Inductive Power Transfer System for Roadway-Powered Vehicles, *IEEE Transactions on Industrial Electronics*, vol. 54, no. 6, pp. 3370-3378, December 2007.

[Cov10] Covic, Grant : Inductive Power Transfer (IPT) Powering our Future, The University of Auckland, Seminar 2010.

[Del01] Delaballe, Jacques. (2001) Cahier Technique no.149 EMC: Electromagnetic Compatibility. Schneider Electric.

[Dep52] Department of the Army,. Washington, D.C., USA: United States Government Printing Office, 1952, ch. chapter 2.

[Doy15] Doyle, Charles Lee. (2015, October) Single phase, uncontrolled rectification. overleaf.

[Dry04] Dryden Flight Research Center. (2004, March) Beamed Laser Power For UAVs. NASA.

[Dua14] Duarte, Rafael Mendes ; Felic, Gordana Klaric : Analysis of the coupling coefficient in inductive energy transfer systems, *Hindawi Publishing Corporation: Active and Passive Electronic Components*, vol. 2014, pp. 1-6, 2014.

[Duk14] Duke, Mystica Augustine Michael : Wireless Power Transmission, *International Journal of Scientific & Engineering Research*, vol. 5, no. 10, pp. 125-129, October 2014.

[Duo11] Duong, Thuc Phi ; Lee, Jong-Wook : Experimental Results of High-Efficiency Resonant Coupling Wireless Power Transfer Using a Variable Coupling Method, *IEEE Microwave and Wireless Components Letters*, vol. 21, no. 8, pp. 442-444, August 2011.

[Ean12] Ean, Koh Kim ; Chuan, Beh Teck ; Imura, Takehiro ; Hori, Yoichi : Novel band-pass filter model for multi-receiver wireless power transfer via magnetic resonance coupling and power division, in *IEEE 13th Annual Wireless and Microwave Technology Conference (WAMICON)*, Cocoa Beach, 2012, pp. 1-6.

[ECC16] ECC. (2016) CEPT. [Online]. http://www.cept.org/ecc/groups/ecc/cpg/page/cept-briefs-and-ecps-for-wrc-19/

[ECF16] ECFR. (2016) GPO. [Online]. http://www.ecfr.gov/cgi-bin/text-idx?SID=a315462c679e8555c3097bd8d82fac2d&mc=true&tpl=/ecfrbrowse/Title47/47cfrv1_02.tpl#0

[Ele17] ElectronicsTutorials. (2017) [Online]. http://www.electronics-

tutorials.ws/diode/diode_6.html

[Ell06] Elliott, Grant A.J ; Covic, Grant A ; Kacprzak, Dariusz ; Boys, John T : A New Concept: Asymmetrical Pick-Ups for Inductively Coupled Power Transfer Monorail Systems, *IEEE Transactions on Magnetics*, vol. 42, no. 10, pp. 3389-3391, October 2006.

[Ell95] Elliott, G.A.J ; Boys, J.T ; Green, A.W : Magnetically coupled systems for power transfer to electric vehicles, in *Proceedings of 1995 International Conference on Power Electronics and Drive Systems*, Singapore, 1995, pp. 797-801.

[Elm96] Elmo Motion Control. (1996) Electromagnetic Compatibility (EMC) Users Guide for ELMO Motor Drives.

[ETS15] ETSI. (2015, March) ETSI. [Online]. http://www.etsi.org/deliver/etsi_en/300300_300399/30033001/01.08.01_60/en_30033001v010801p.pdf

[ETS16] ETSI. (2016, October) ETSI. [Online]. http://www.etsi.org/deliver/etsi_tr/103400_103499/103409/01.01.01_60/tr_103409v010101p.pdf

[Fer92] Ferreira, J.A. : Analytical computation of AC resistance of round and rechangular litz wire windings, in *IEE PROCEEDINGS-B*, 1992, pp. 21-25.

[Goo13] Goodman, Luke ; Karp, Alexander ; Shorrock, Peter ; Walker, Thomas : The feasibility of wireless energy, Worcester Polytechnic, Project IQP_ERT_1212, 2013.

[Got14] Goto, Daisuke ; Yoshida, Hiroyuki ; Suzuki, Hiroaki ; Arimoto, Yoshinori : The Overview of JAXA Laser Eneergy Transmission R&D Activities and the Orbital Experiments Concept on ISS-JEM, in *International Conference on Space Optical Systems and Applications(ICSOS)*, Kobe, 2014, pp. S5-2.

[Gra14] Gratton, S. ; Lawless, A.S. ; Nichols, N.K. : Approximate Gauss-Newton methods for nonlinear least squares problems, Cerfacs, Toulouse, Report 2014.

[Gra99] Graichen, Friedmar ; Bergmann, Georg ; Rohlmann, Antonius : Hip Endoprosthesis for in Vivo Measurement of Joint Force and Temperature, *Journal of Biomechanics*, vol. 32, no. 10, pp. 1113-1117, October 1999.

[Gre01] Green, Leslie. (2001, September) RF-inductor modeling for the 21st century.

[Gre94] Green, A.W ; Boys, J.T : 10 kHz inductively coupled power transfer-concept and control, in *Fifth International Conference on Power Electronics and Variable-Speed Drives*, London, 1994, pp. 694-699.

[Han10] Han, Sangwook ; Wentzloff, David D. : Wireless power transfer using resonant inductive coupling for 3D integrated ICs, in *2010 IEEE International 3D Systems Integration Conference (3DIC)*, Munich,

2010, pp. 1-5.

[Has15] Hassan, Mohamed A ; Elzawawi, A : Wireless Power Transfer Through Inductive Coupling, *Recent Advances in Circuits*, pp. 115-118, 2015.

[Hay98] Hayes, J.G : Battery Charging Systems for Electric Vehicles, in *Electric Vehicles-A Technology Roadmap for the Future, IEE Colloquium on*, London, 1998, pp. 1-8.

[Hir08] Hirabayashi, Katsuji ; Hanamoto, Hideo : Efforts toward EMC Design (I), *Fujitsu Ten Technichal Journal*, vol. 30, pp. 53-59, 2008.

[Hly13] Hlyoon,. (2013, August) KAIST's Wireless Online ELectric Vehicle (OLEV) Runs Inner City Roads. KAIST.

[Hui14] Hui, S.Y.R ; Zhong, Wen Xing ; Lee, C.K : A Critical Review of Recent Progress in Mid-Range Wireless Power Transfer, *IEEE Transactions on Power Electronics*, vol. 29, no. 9, pp. 4500-4511, September 2014.

[ICN10] ICNIRP: ICNIRP Guidelines, *Health Physics*, vol. 99, no. 6, pp. 1-20, 2010.

[IEE06] IEEE: IEEE Standard for Safety Levels with Respect to Human Exposure to Radio Frequency Electromagnetic Fields, IEEE International Committee on Electromagnetic Safety (SCC39), New York, IEEE Std C95.1, 2006.

[Irs13] Irshad, Sabeel : Electromagnetic Interference & Electromagnetic Compatibility, Seminar 2013.

[Ite15] Item Media. (2015, January) Magnetic Resonance System Could Signal Breakthrough in Wireless Charging. Interference Technology.

[ITU05] ITU: Evaluating fields from terrestrial broadcasting transmitting systems operating in any frequency band for assessing exposure to non-ionizing radiation , ITU, Recommendation BS.1698, 2005.

[ITU15] ITU-R: Wireless Power Transmission Using Technologies other than Radio Frequency Beam, ITU, SM.2303-1, 2015.

[Jay14] Jay, Rajiv ; Palermo, Samuel : Resonant coupling analysis for a two-coil wireless power transfer system, in *2014 IEEE Dallas Circuits and Systems Conference (DCAS)*, Richardson, 2014, pp. 1-4.

[Jon13] Jonah, Olutola ; Georgakopoulos, Stavros V ; Tentzeris, Manos M : Orientation Insensitive Power Transfer by Magnetic Resonance for Mobile Devices, in *IEEE Wireless Power Transfer (WPT)*, Perugia, 2013, pp. 1-4.

[KAI15] KAIST Wireless Power Transfer Research Center. (2015) KAIST OLEV Transport System. smfir.

[Kal14] Kalialakis, Christos ; Georgiadis, Apostolos : The Regulatory Framework for Wireless Power Transfer Systems, *Wireless Power Transfer*, vol. 1, no. 2, pp. 108-118, November 2014.

[Kar06] Karalis, Aristeidis ; Joannopoulos, John.D : Wireless Non-Radiative Energy Transfer, *Arxiv preprint physics*, 2006.

[Kar07] Karalis, Aristeidis ; Joannopoulos, John.D ; Soljačić, Marin : Efficient wireless non-radiative mid-range energy transfer, *Annals of Physics*, vol. 323, no. 2008, pp. 34-48, Apr. 2007.

[Kay86] Kaya, Nobuyuki et al.: Nonlinear interation of strong microwave beam with the ionosphere MINIX rocket experiment, in *Space Power*, 1986, pp. 181-186.

[Kes13a] Kesler, Morris : Highly Resonant Wireless Power Transfer:Safe, Efficient, and over Distance, WiTricity Corporation, 2013. [Online]. http://www.witricity.com/assets/highly-resonant-power-transfer-kesler-witricity-2013.pdf

[Kha15] Khayrudinov, Vladislav : Wireless Power Transfer System Development and Implementation, Helsinki Metropolia University of Applied Sciences, Bachelor Thesis 2015.

[Kia11] Kiani, Mehdi ; Jow, Uei-Ming ; Ghovanloo, Maysam : Design and Optimization of a 3-Coil Inductive Link for Efficient Wireless Power Transmission, *IEEE Transactions on Biomedical Circuits and Systems*, vol. 5, no. 6, pp. 579-591, Dec. 2011.

[Kim10] Kim, Jin-Wook ; Son, Hyeon-Chang ; Kim, Do-Hyun ; Kim, Kwan-Ho ; Park, Young-Jin : Analysis of Wireless Energy Transfer to Multiple Devices Using CMT, in *Proceedings of Asia-Pacific Microwave Conference*, Yokohama, 2010, pp. 2149-2152.

[Kim11] Kim, Jin Wook ; Son, Hyeon Chang ; Kim, Kwan Ho ; Park, Young Jin : Efficiency Analysis of Magnetic Resonance Wireless Power Transfer with Intermediate Resonant Coil, *IEEE Antennas and Wireless Propagation Letter*, vol. 10, 2011.

[Kim12a] Kim, Hongseok ; Song, Chiuk ; Kim, Jonghoon ; Kim, Jiseong ; Kim, Joungho : Shielded Coil Structure Suppressing Leakage Magnetic Field from 100W-Class Wireless Power Transfer System with Higher Efficiency, in *2012 IEEE MTT-S International Microwave Workshop Series on Innovative Wireless Power Transmission: Technologies, System, and Applications (IMWS)*, Kyoto, 2012, pp. 83-86.

[Kim12b] Kim, Hongseok ; Cho, Jonghyun ; Ahn, Seungyoung ; Kim, Jonghoon ; Kim, Joungho : Suppression of leakage magnetic field from a wireless power transfer system using ferrimagnetic material and metallic shielding, in *IEEE International Symposium on Electromagnetic Compatibility (EMC)*, Rome, 2012, pp. 640-645.

[Kim13a] Kim, Sukjin et al.: Electromagnetic Interference Shielding Effects in Wireless Power Transfer using Magnetic Resonance Coupling for Board-to-Board Level Interconnection, in *IEEE International Symposium on Electromagnetic Compatibility (EMC)*, Denver, 2013, pp. 773-778.

[Kim13b] Kim, Jiseong et al.: Coil Design and Shielding Methods for a

Magnetic Resonant Wireless Power Transfer System, *Proceedings of the IEEE*, vol. 101, no. 6, pp. 1332-1342, June 2013.

[Kim14] Kim, Minho ; Kim, Sunghwan ; Ahn, Seungyoung ; Chun, Yangbae ; Park, Seongwook : Low Frequency Electromagnetic Compatibility of Wireless Powered Elecric Vehicles, in *2014 International Symposium on Electromagnetic Compatibility*, Tokyo, 2014, pp. 426-429.

[Kra95] Kraz, Vladimir : Near-Field Methods of Locating EMI Sources, *Compliance Engineering Magazine*, pp. 1-7, May 1995.

[Kum09] Kumar, Anil ; Mirabbasi, Shahriar ; Chiao, Mu : Resonance-based Wireless Power Delivery for Implantable Devices, in *IEEE Biomedical Circuits and Systems Conference, BioCAS 2009*, Beijing, 2009, pp. 25-28.

[Kur07] Kurs, André et al.: Wireless Power Transfer via Strongly Coupled Magnetic Resonances, *Science*, vol. 317, no. 83, pp. 83-86, 2007.

[Kur10] Kurs, Andre ; Moffatt, Robert ; Solijacic, Marin : Simultaneous mid-range power transfer to multiple devices, *Applied Physics Letters*, pp. 1-3, 2010.

[Lan05] Landis, Geoffrey.A , "Charging of Devices by Microwave Power Beaming," Grant US6967462 B1, November 22, 2005.

[Lea16] Learning Center. (2016) Celectronics. [Online]. https://celectronics.com/training/learning/method/EN55011.html

[Lee12a] Lee, C.K ; Zhong, W.X ; Hui, S.Y.R : Recent Progress in Mid-Range Wireless Power Transfer, in *The 4th Annual IEEE Energy Conversion Congress and Exposition*, Raleigh, 2012, pp. 3819-3824.

[Lee12b] Lee, Chi Kwan ; Zhong, Wen Xing ; Hui, S.Y.Ron : Effects of Magnetic Coupling of Nonadjacent Resonators on Wireless Power Domino-Resonator Systems, *IEEE Transactions on Power Electronics*, vol. 27, no. 4, pp. 1905-1916, Apr. 2012.

[Lee13] Lee, Kisong ; Cho, Dong-Ho : Diversity Analysis of Multiple Transmitters in Wireless Power Transfer System, *IEEE Transactions on Magnetics*, vol. 49, no. 6, pp. 2946-2952, June 2013.

[Ley08] Leyh, G.E ; Kennan, M.D : Efficient Wireless Transmission of Power using Resonators with Coupled Electric Fields, in *Power Symposium,2008. NAPS 08. 40th North American*, Calgary, 2008.

[LiH10] Li, H ; Yan, G ; Gao, P : A method for improving the wireless power transmission efficiency of an endoscopic capsule based on electromagnetic localization and synthesis of magnetic field vector, *Journal of Mechanical Engineering Science*, vol. 224, pp. 1463-1471, July 2010.

[Liu07] Liu, Xun ; Hui, S.Y.(Ron) : Simulation Study and Experimental Verfication of a Universal Contactless Battery Charging Platform with Localized Charging Features, *IEEE Transactions on Power Electronics*, vol. 22, no. 6, pp. 2202-2210, November 2007.

[Liu08] Liu, Xun ; Ng, W.M. ; Lee, C.K. ; Hui, S.Y. : Optimal operation of contactless transformers with resonance in secondary circuits, in *23 th Annual IEEE Applied Power Electronics Conference and Exposition APEC 2008*, Austin, 2008, pp. 645-650.

[Liu14] Liu, Jin Feng ; Wang, Xu Dong ; Yan, Mei Cun : Optimized Parameter of Contactless Energy Transmission System Realized by Optimum Energy-Efficiency Prduct, *International Journal of Hybrid Information Technology*, vol. 7, no. 2, pp. 39-48, 2014.

[LiX12] Li, Xiu Han et al.: A Wireless Magnetic Resonance Energy Transfer System for Micro Implantable Medical Sensors, *Sensors*, pp. 10292-10308, July 2012.

[LuR10] Lu, Ren gui ; Wang, Tian yu ; Mao, Yin hua ; Zhu, Chun bo : Analysis and design of a wireless closed-loop ICPT system working at ZVS mode, in *2010 IEEE Vehicle Power and Propulsion Conference*, 2010.

[LuX15] Lu, Xiao ; Wang, Ping ; Niyato, Dusit ; Kim, Dong In ; Han, Zhu : Wireless Charging Technologies: Fundamentals, Standards, and Network Applications, *IEEE Communications Surveys and Tutorials*, vol. 18, no. 2, pp. 1413-1452, November 2015.

[LYO01] LYONS, Timothy Augustine : *A treatise on electromagnetic phenomena, and on the compass and its deviations aboard ship. Mathematical, Theoretical and Practical*, 1st ed., John Wiley & Sons, Ed. New York: Chapman & Hall, Limited, 1901.

[Man06] Mandal, Tanuj Kumar : Wireless Transmission of Electricity - Development and Possibility, in *Sixth International Symposium Nikola Tesla*, Belgrade, 2006.

[Man13] Manivannan, P ; Bharathiraja, S : Qi Open Wireless Charging Standard-A Wireless Technology for the Future, *International Journal of Engineering and Computer Science*, vol. 2, no. 3, pp. 573-579, March 2013.

[Man14] Manez, Alejandro Llop : Optimization of Inductive Resonant Coupling Links for Low Power and Mid-Range Wireless Power Transfer, Technical University of Madrid, Madrid, Spain, Master Thesis 2014.

[Maq13] Maqsood, M ; Nasir, M Nauman : Wireless Electricity (Power) Transmission Using Solar Based Power Satellite Technology, in *6th Vacuum and Surface Sciences Conference of Asia and Australia*, Islamabad, 2013, pp. 1-8.

[MaS02] MaSpadden, James O ; Mankins, John C : Space Solar Power Programs and Microwave Wireless Power Transmission Technology, *IEEE Microwave Magazine*, vol. 3, no. 4, pp. 46-57, Dec. 2002.

[Mie17] Mietke, Detlef. (2017) Informations- und Kommunikationstechnik. [Online]. http://elektroniktutor.de/analogtechnik/par_swkr.html

[Mik06] Mikail, Rajib : Fundamentals of Electric Motors and Transformers, Bangladesh University of Engineering and Technology , Dhaka, Short Course 984-32-1803-6 , 2006.

[Miw13] Miwa, Keishi ; Mori, Hisamichi ; Kikuma, Nobuyoshi : A Consideration of Efficiency Improvement of Transmitting Coil Array in Wireless Power Transfer with Magnetically Coupled Resonance, in *IEEE Wireless Power Transfer*, Perugia, 2013, pp. 13-16.

[Moo14] Moon, SangCheol ; Kim, Bong-Chul ; Cho, Shin-Young ; Ahn, Chi-Hyung ; Moon, Gun-Woo : Analysis and Design of a Wireless Power Transfer System with an Intermediate Coil for High Efficiency, *IEEE Transactions on Industrial Electronics*, vol. 61, no. 11, pp. 5861-5870, November 2014.

[Mou15] Mou, Xiao Lin ; Sun, Hong Jian : Wireless Power Transfer: Survey and Roadmap, in *IEEE 81st Vehicular Technology Conference*, Glasgow, 2015, pp. 1-5.

[Nag09] Naggi, R.K : *Solar Energy & its Uses*, 1st ed., Mahaveer&Sons, Ed. New Delhi, India: Smt.Seema Sharma, 2009.

[Nag86] Nagatomo, Makoto ; Kaya, nobuyuki ; Matsumoto, Hiroshi : Engineering aspect of the microwave ionosphere nonlinear interaction experiment (MINIX) with sounding rocket, *Acta Astronautica*, vol. 13, no. 1, pp. 23-29, January 1986.

[Nam15] Nambiar, Shyam Chandrasekhar : Design of a Wireless Power Transfer System using Electrically Coupled Loop Antennas, Faculty of the Virginia Polytechnic Institute and State University, Blacksburg, Master Thesis 2015.

[Nar16] Narda. (2016) Safety Evaluation Within a Magnetic Field Environment. Narda.

[New17] New England Wire Technologies. (2017) [Online]. https://www.newenglandwire.com/product-selection-guide/litz-wire-and-formed-cables/litz-wire-theory.aspx

[Oba14] Obayashi, Shuichi ; Tsukahara, Hitoshi : EMC Issues on Wireless Power Transfer, in *2014 International Symposium on Electromagnetic Compatibility*, Tokyo, 2014, pp. 601-604.

[Ood11] Oodachi, Noriaki ; Ogawa, Kenichiro ; Kudo, Hiroki ; Morooka, Tasuku : Efficiency Improvement of Wireless Power Transfer via Magnetci Resonance Using Transmission Coil Array, in *IEEE International Symposium on Antennas and Propagation (APSURSI)*, Washington, 2011, pp. 1707-1710.

[Ozo15] Ozovehe, A ; Usman, A.U ; Hamdallah, A : Electromagnetic Radiation Exposure from Cellular Base Station: A Concern for Public Health, *Nigerian Journal of Technology*, vol. 34, no. 2, pp. 355-358, April 2015.

[Par11] Park, Jongmin ; Tak, Youndo ; Kim, Yoongoo ; Kim, Youngwook ;

Nam, Sangwook : Investigation of Adaptive Matching Methods for Near-Field Wireless Power Transfer, *IEEE Transactions on Antennas and Propagation*, vol. 59, no. 5, pp. 1769-1773, May 2011.

[Ped99] Pedder, Don A.G ; Brown, Andrew D ; Skinner, J.Andrew : A Contactless Electrical Energy Transmission System, *IEEE Transactions on Industrial Electronics*, vol. 46, no. 1, pp. 23-30, Feb. 1999.

[Pet13] Peterson, Gary. (2013, August) Wardenclyffe How does Tesla's tower work. teslainfo.

[PMA16] PMA. (2016) Power Matters Alliance. [Online]. http://www.merger.powermatters.org/index.php

[Pow10] Power Electronics Research Department of Electrical & Computer Engineering: Possibilities in Inductive Energy Transfer, The Univerisy of Auckland, 2010.

[Pow16] (2016) Power Electronics. [Online]. http://www.ece.auckland.ac.nz/en/about/our-research/research-areas/powerelectronicsresearch.html

[Pra12] Prasanth, Venugopal : Wireless Power Transfer for E-Mobility, Delft University of Technology, Delft, Master Thesis 2012.

[Pra15] Prashansa, ; Duggal, Aditya ; Srivastava, Manish Kumar : An Innovative Design of Wireless Power Transfer by High Frequency Resonant Coupling, *International Journal of Innovative Research in Science, Engineering and Technology*, vol. 4, no. 7, pp. 6031-6037, July 2015.

[Ram11] RamRakhyani, Anil Kumar ; Mirabbasi, Shahriar ; Chiao, Mu : Design and Optimization of Resonance-Based Efficient Wireless Power Delivery Systems for Biomedical Implants, *IEEE Transactions on Biomedical Circuits and Systems*, vol. 5, no. 1, pp. 48-63, Feb. 2011.

[Ram16] Rampradesh, T ; Vignesh, R ; Nivedha, A : Analysis of Various Inductor Core Materials for Wireless Power Transfer, *Middle-East Journal of Scientific Research*, vol. 24, no. 4, pp. 1283-1288, April 2016.

[Rao16] Rao, T.S.Chandrasekar ; Geetha, K : Categories, Standards and Recent Trends in Wireless Power Transfer: A Survey, *Indian Journal of Science and Technology*, vol. 9, no. 20, pp. 1-11, May 2016.

[Red13] Reddy, M.Venkateswara ; Hemanth, K.Sai ; Mohan, CH.Venkat : Mircrowave Power Transmission - A Next Generation Power Tranmission System, *IOSR Journal of Electrical and Electronics Engineering*, vol. 4, no. 5, pp. 24-28, Februray 2013.

[Ric13] Rickers, Sebastian et al.: Wireless Power Transfer H-Bridge Design with Serial Resonance and Varying Supply Voltage, in *IEEE International Symposium on Circuits and Systems (ISCAS)*, Beijing,

2013, pp. 630-633.

[Ric16] Rickers, Sebastian : Entwurf eines sondenlosen Herzschrittmachersystems mit drahtloser, induktiver Energieübertragung, Duisburg-Essen University, Duisburg, Dissertation 2016.

[Rob13] Robbins, Allan H ; Miller, Wilhelm C , "Transformer and Coupled Circuits," in *Circuit Analysis with Devices:Theory and Practice*, Dave Garza, Ed. Del Mar, USA, 2013, pp. 829-860.

[Roh01] Rohde&Schwarz. (2001) [Online]. https://cdn.rohde-schwarz.com/pws/dl_downloads/dl_common_library/dl_brochures_and_datasheets/pdf_1/HZ-10_22.pdf

[Rön13] Rönnbäck, Oskar : Optimization of Wireless Power, Lulea University of Technology, Lulea, Master Thesis 2013.

[Sah11] Sahoo, Priyabrata : Wireless Electricity(Witricity), Indira Gandhi institute of technology, Sarang, Seminar ODISHA-759146, 2011.

[Sai14] Saifuddin, Md ; Saha, Tushar ; Islam, Monirul ; Akhand, Md. Mujammel Hossain : Wireless Power Transmission Compare and Contrast with the Form of Resonance Frequency, Mutual Inductance and Solar Energy, *International Journal of Engineering Research and Applications*, vol. 4, no. 10, pp. 66-96, October 2014.

[Sam11] Sample, Alanson P ; Meyer, David A ; Smith, Joshua R. : Analysis, Experimental Results, and Range Adaptation of Magnetically Coupled Resonators for Wireless Power Transfer, *IEEE Transactions on Industrial Electronics*, vol. 58, no. 2, pp. 544-554, February 2011.

[Sca70] Scanlan, J.O. ; LEVY, R. : *Circuit Theory volume one*, 1st ed., P.J.B. Clarricoats and P.J. Lawrenson, Eds. Edinburgh, Scotland: Oliver and Body, 1970.

[Sch10] Schneider, Jesse. (2010, December) Wireless Charging of Electric and plug-in Hybrid Vehicles. SAE International.

[Sch11] Schwannecke, J ; Umenei, A.E ; Leppien, T ; Baarman, D : Variable Position Wireless Power Transmitter through Multiple Cooperative Flux Generators, in *Telecommunications Energy Conference,2011 IEEE 33rd International*, Amsterdam, 2011.

[Sch88] Schlesak, Joseph J ; Alden, Adrian ; Ohno, Tom : A Microwave Powere High Altitude Platform, *IEEE MIT-S Digest*, pp. 283-286, 1988.

[Sen13] Senjuti, Shawon : Design and optimization of efficient wireless power transfer link for implantable biotelemetry systems, The Univeristy of Western Ontario, London, Master thesis 2013.

[Shi12] Shin, Wonseok ; Fan, Shan Hui : Choice of Perfectly Matched Layer Boundary Condition for Frequency-Domain Maxwell's Equation Solvers, *Journal of Computational Physics*, vol. 231, pp. 3406-3431, 2012.

[Shi14] Shi, Xinzhi et al.: Effects of coil shapes on wireless power transfer via magnetic resonance coupling, *Journal of Electromagnetic Waves and Applications*, vol. 28, no. 11, pp. 1316-1324, May 2014.

[Shu15] Shukyn, Murray ; Krull, Achim K , "Honing Your Science Skills and Knowledge," in *Get Science For Dummies*, John Wiley, Ed. Canda, 2015, p. 131.

[Sim01] Simpson, James ; Lane, John ; Immer, Christopher ; Youngquist, Robert : Simple Analytic Expressions for the Magnetic Field of a Circular Current Loop, NASA, 20010038494, January 2001.

[Sin09] Singh, Gagandeep. (2009, November) Short Introduction to Finite Element Method. Norwegian University of Science and Technology.

[Sin12] Singh, Sagolsem Kripachariya ; Hasarmani, T.S ; Holmukhe, R.M : Wireless Transmission of Electrical Power Overview of Recent Research & Development, *International Journal of Computer and Electrical Enginerring*, vol. 4, no. 2, pp. 207-211, April 2012.

[Sin16] Sinha, Priyanka ; Diwan, Ritesh : Review Paper on Wireless Power Transmission for Energy Havrvesting System, *International Journal of Science and Research*, vol. 5, no. 5, pp. 181-186, May 2016.

[Smy98] Smyth, Gordon K. : *Optimization and nonlinear equations*, Peter Armitage and Theodore Colton, Eds. Chichester, England: John Wiley & Sons, Ltd, 1998.

[Son09] Sonntag, C.L.W ; Duarte, J.L ; Pemen, A.J.M : Load Position Detection and Validation on Variable-phase Contactless Energy Transfer Desktops, in *Energy Conversion Congress and Expositon*, San Jose, 2009, pp. 1818-1825.

[Son16] Song, Kai et al., "A Review of Dynamic Wireless Power Transfer for In-motion Electric Vehicles," in *Wireless Power Transfer-Fundamentals and Technologies*.: INTECH, 2016, ch. 6, pp. 109-128.

[Spi15] Spizzi, Stefano ; Campatelli, Gianni ; Roy, Johansson ; Fiedler, Jens : Wireless Charging for ELEctric Vehicles, Project Unplugged 314126, 2015.

[Sri15] Sripodok, P ; Jettanasen, C : Mitigation of Conducted and Radiated EMI Generation in High-Frequency Switching Devices, in *Proceedings of the International MultiConference of Engineers and Computer Scientists (IMECS 2015)*, Hong Kong, 2015, pp. 1-4.

[Sum09] Summerer, Leopold ; Purcell, Oisin. (2009) Concepts for Wireless Energy Transmission via Laser. ESA-Advanced Concepts Team.

[Sun12] Sun, Tian Jia ; Xie, Xiang ; Li, Guo lin ; Gu, Ying ke : A Two-Hop Wireless Power Transfer System with an Efficiency-Enhanced Power Receiver for Motion-Free Capsule Endoscopy Inspection, *IEEE Transactions on Biomedical Engineering*, vol. 59, no. 11, pp. 3247-3254, Nov. 2012.

[Sve13] Svensson, Alexander : Inductive Energy Transfer Vehicular

application, Division of Industrial Electrical Engineering and Automation Faculty of Engineering, Lund Universiyt, Lund, Master Thesis 2013.

[Tah12] Tahsin, Naim Muhammad ; Siddiqui, Md.Murtoza ; Zaman, Md.Anik ; Kayes, Mirza Imrul : Wireless Charger for Low Power Devices using Inductive Coupling, Faculty of Engineering American International University Bangladesh, Dhaka, Project 2012.

[Tan00] Tang, S.C ; Hui, S.Y.(Ron) ; Chung, Henry Shu-Hung : Coreless Planar Printed-Circuit-Board(PCB) Transformers-A Fundamental Concept for Signal and Energy Transfer, *IEEE Transactions on Power Electronics*, vol. 15, no. 5, pp. 931-941, September 2000.

[Tan02] Tang, S.C ; Hui, S.Y.(Ron) ; Chung, Shu-Hung : Evaluation of the Shielding Effects on Printed-Circuit-Board Transformers Using Ferrrite Plates and Copper Sheets, *IEEE Transactions on Power Electronics*, vol. 17, no. 6, pp. 1080-1088, November 2002.

[Tan16] Tan, Linlin et al.: Analysis and Performance Improvement of WPT Systems in the Environment of Single Non-Ferromagnetic Metal Plates, *Energies*, vol. 9, no. 8, pp. 1-16, 2016.

[Tan99] Tang, S.C ; Hui, S.Y.(Ron) ; Chung, Henry Shu-Hung : Coreless Printed Circuit Board (PCB) Transformers with Multiple Secondary Windings for Complementary Gate Drive Circuits, *IEEE Transactions on Power Electronics*, vol. 14, no. 3, pp. 431-437, May 1999.

[Tec12] Technical Committee 100 - Audio, video and multimedia systems and equipment. (2012) International ELectrotechnical Commission. [Online]. http://www.iec.ch/dyn/www/f?p=103:23:0:FSP_ORG_ID,FSP_LANG_ID:1297,25

[Tec16] Technical Committee 69 - Electric road vehicles and electric industrial trucks. (2016) International Electromagnetic Commission. [Online]. http://www.iec.ch/dyn/www/f?p=103:7:0:FSP_ORG_ID:1255

[Tek13] Tektronix. (2013) Farnell. [Online]. http://www.farnell.com/datasheets/1760371.pdf?_ga=1.187338347.2105220102.1478792336

[Tem10] Temürlenk, Nuri : Investigation of maximum wireless power transfer conditions in the near field, Yeditepe University, Istanbul, Master Thesis 2010.

[Tes00] Tesla, Nikola , "System of transmission of electrical energy," US645576A, March 20, 1900.

[Tes04] Tesla, Nikola , "The Transmission of Electrical Energy without Wires," *Electrical World and Engineer*, pp. 566-572, Mar. 1904.

[Tes27] Tesla, Nikola , "World System of Wireless Transmission of Energy," *Telegraph and Telegraph Age*, pp. 1510-1515, Oct. 1927.

[Tom12] Tomar, Anuradha ; Gupta, Sunil : Wireless Power Transmission Applications and Components, *International Journal of Engineering Research & Technology*, vol. 1, no. 5, July 2012.

[Ume11] Umenei, A.E.. (2011) Understanding low frequency non-radiative power transfer. Fulton Innovation.

[URS07] URSI Inter-commission Working Group on SPS: URSI White paper on Solar Power Satellite Systems and Report of the URSI Inter Commission Working Group on SPS, URSI, 2007.

[Vae09] Vaessen, Peter. (2009, September) Leonardo ENERGY Wireless Power Transmission. [Online]. http://www.leonardo-energy.com/sites/leonardo-energy/files/root/pdf/2009/WirelessPower.pdf

[Val02] Valone, Thomas : *Harnessing the Wheelwork of Nature*. Kempton, United States of America: Adventures Unlimited Press, 2002.

[Vat16] Vatankhahan, Farshad ; Mahmoudi, Moeinoddin ; Dorali, Mohammad Reza : Vibrational analysis of perforated composite plate with 3-layered galss, boron and graphite fibre/expoxy, in *3rd International Conference on Recent Innovations in Industrial Engineering & Mechanical Engineering*, Tehran, 2016, pp. 1-11.

[Vil15] Vilathgamuwa, D.M ; Sampath, J.P.K , "Wireless Power Transfer (WPT) for Electric Vehicles (EVs)-Present and Future Trends," in *Plug in Electric Vehicles in Smart Grids*, Sumedha Rajakaruna, Farhad Shahnia, and Arindam Ghosh, Eds. Singapore: Springer, 2015, pp. 33-60.

[Wad16] Wade, Therese. (2016, April) Waking Times. [Online]. http://www.wakingtimes.com/2016/04/12/shaman-within-channeling-universal-life-force-heal-body/

[Wan04] Wang, Chwei-Sen ; Covic, Grant A. ; Stielau, Oskar H. : Power Transfer Capability and Bifurcation Phenomena of Loosely Coupled Inductive Power Transfer Systems, *IEEE Transactions on Industrial Electronics*, vol. 51, no. 1, pp. 148-157, February 2004.

[Wan05] Wang, Chwei-Sen ; Stielau, Oskar H ; Covic, G.A : Design considerations for a contactless electric vehicle battery charger, *IEEE Transactions on Idustrial Electronics*, vol. 52, no. 5, pp. 1308-1314, Oct. 2005.

[Wan12a] Wang, B ; Teo, K.H. (2012, March) Matamaterials for Wireless Power Transfer. Mitsubishi Electric Research laboratories.

[Wan12b] Wang, Jun Hua et al.: Lateral and Angular Misalignments Analysis of a New PCB Circular Spiral Resonant Wireless Charger, *IEEE Transactions on Magnetics*, vol. 48, no. 11, pp. 4522-4525, November 2012.

[Was00] Waser, Andre. (2000, August) Nikola Tesla's Wireless Systems. Andre-waser.

[Wat12] Waters, Benjamin H ; Sample, Alanson P ; Smith, Joshua R : Adaptive Impedance Matching for Magnetically Coupled Resonators, in *PIERS Proceedings*, Moscow, 2012, pp. 694-701.

[Wei14] Wei, Xue Zhe ; Wang, Zhen Shi ; Dai, Hai Feng : A Critical Review of Wireless Power Transfer via Strongly Coupled Magnetic Resonance, *Energies*, vol. 7, no. 7, pp. 4316-4341, July 2014.

[WIK16a] WIKIPEDIA,. (2016) WIKIPEDIA. [Online]. https://en.wikipedia.org/wiki/Electromagnetic_compatibility

[WIK16b] WIKIPEDIA. (2016) [Online]. https://de.wikipedia.org/wiki/Gau%C3%9F-Newton-Verfahren

[WIK17] WIKIPEDIA. (2017) [Online]. https://en.wikipedia.org/wiki/Near_and_far_field

[Wir16] Wireless Power Consortium. (2016) Qi. [Online]. http://www.wirelesspowerconsortium.com/

[WuT16] Wu, Tzong Lin. (2016) Overview of EMC Regulations and Testing. NTU EMC Lab.

[Yam09] Yamakawa, Soji ; Shimada, Kenji : Removing self intersecionts of a triangular mesh by edge swapping, edge hammering, and face lifting, in *18th International Meshing Roundtable*, Salt Lake City, October 2009, pp. 13-29.

[Yam11] Yamanaka, Yukio ; Sugiura, Akira : Possible EMC Regulations for Wireless Power Transmission Equipment, in *2011 IEEE MTT-S International Microwave Workshop Series on Innovative Wireless Power Transmission: Technologies, Systems, and Applications(IMWS)*, Kyoto, 2011, pp. 97-100.

[Yam13] Yamamoto, T ; Koshiji, K : Position Detection for Transcutaneous Energy Transmission System for Capsule Endoscope, in *Wireless Power Transfer, 2013 IEEE*, Perugia, 2013, pp. 210-213.

[Yan06] Yang, Zhi ; Wang, Guo Xing ; Liu, Wen Tai : Analytical calculation of the self-resonant frequency of biomedical telemetry coils, in *Proceedings of the 28th IEEE EMBS Annual International Conference*, New York, 2006, pp. 5880-5883.

[Yan07] Yang, Zhi ; Liu, Wen Tai ; Basham, Eric : Inductor Modeling in Wireless Links for Implantable Electronics, *IEEE Transactions on Magnetics*, vol. 43, no. 10, pp. 3851-3860, October 2007.

[Zha11] Zhang, Fei et al.: Relay Effect of Wireless power Transfer Using Strongly Coupled Magnetic Resonances, *IEEE Transactions on Magnetics*, vol. 47, no. 5, pp. 1478-1481, May 2011.

[Zha12] Zhao, Duan et al.: Magnetic Field Forming of Spatial Multiple Antennas for Wireless Power Transfer, in *International Symposium on Antennas and Propagation (ISAP)* , Nagoya, 2012, pp. 1204-1207.

[Zha15] Zhang, Yi Ming et al.: Wireless Power Transfer to Multiple Loads Over Various Distances Using Relay Resonators, *IEEE Microwave*

and Wireless Componets Letters, vol. 25, no. 5, pp. 337-339, May 2015.

[Zhe15] Zheng, Cong : Loosely Coupled Transformer and Tuning Network Design for High-Efficiency Inductive Power Transfer Systems, Faculty of the Virginia Polytechnic Institute and State University, Virginia, Dissertation 2015.

[Zho11] Zhong, W.X ; Liu, Xun ; Hui, S.Y.Ron : A Novel Single-layer Winding Array and Receiver Coil Structure for Contactless Battery Charging Systems with Free-Positioning and Localized Features, *IEEE Transactions on Industrial Electronics*, vol. 58, no. 9, pp. 4136-4144, Sep. 2011.

[Zho12] Zhong, Wen Xing ; Lee, Chi Kwan ; Hui, S.Y.Ron : Wireless Power Domino-Resonator Systems with Noncoaxial Axes and Circular Structures, *IEEE Transactions on Power Electronics*, vol. 27, no. 11, pp. 4750-4762, Nov. 2012.

[Zho13] Zhong, Wen xing ; Lee, Chi Kwan ; Hui, S.Y.Ron : General Analysis on the Use of Tesla's Resonators in Domino Forms for Wireless Power Transfer, *IEEE Transactions on Industrial Electronics*, vol. 60, no. 1, pp. 261-270, Jan. 2013.

[Zho15a] Zhong, Wen Xing ; Hui, S.Y.R : Auxiliary Circuits for Power Flow Control in Multifrequency Wireless Power Transfer Systems with Multiple Receivers, *IEEE Transactions on Power Electronics*, vol. 30, no. 10, pp. 5902-5910, October 2015.

[Zho15b] Zhong, W.X ; Zhang, C ; Liu, Xun ; Hui, S.Y.Ron : A Methodology for Making a Three-Coil Wireless Power Transfer System More Energy Efficient Then a Two-Coil Counterpart for Extened Transfer Distance, *IEEE Transactions on Power Electronics*, vol. 30, no. 2, pp. 933-942, February 2015.

[Zho15c] Zhong, W.X. ; Hui, S.Y.R. : Maximum Energy Efficiency Tracking for Wireless Power Transfer Systems, *IEEE Transactions on Power Electronics*, vol. 30, no. 7, pp. 4025-4034, July 2015.

[Zhu08] Zhu, Chunbo ; Liu, Kai ; Yu, Chun lai ; Ma, Rui ; Cheng, He Xiao : Simulation and Exoerimental Analysis on Wireless Energy Transfer Based on Magnetic Resonances, in *IEEE Vehicle Power and Propulsion Conference(VPPC)*, Harbin, Sep. 2008.

[Zhu15] Zhu, Bin ; Li, Jincheng ; Hu, Wenshan ; Gao, Xingran : Review of Magnetic Coupling Resonance Wireless Energy Transmission, *International Journal of Service, Science and Technology*, vol. 8, no. 3, pp. 257-272, 2015.

List of Figures

List of Tables

List of Symbols

A	Amplitude of magnetic flux density
a	Conducting wire of cross-sectional radius
B	Magnetic induction intensity
B_z	Magnetic induction intensity in z-axis
$B_{\mathrm{z,tot}}$	Magnetic induction vector addition in z-axis
B_{n}	Normalized magnetic flux density
B_x	magnetic flux density
B_y	magnetic flux density
B_z	magnetic flux density
C	Capacitance
C_1	Compensation capacitors of primary coil of transmitter
C_2	Compensation capacitors of secondary coil of transmitter
C_3	Compensation capacitors of primary coil of receiver

C_4	Compensation capacitors of secondary coil of receiver
C_b	Parasitic capacitance between two nearby turns in the same layer
C_m	Parasitic capacitance between different layers
C_{self}	Parasitic capacitor
C_{smooth}	Smoothing capacitor
d	Transmission distance of EMF
D	Jacobian matrix
D	Diode
d_{23}	Distance between primary coil and secondary coil
D_{ave}	Average diameter of coil
d_{cc}	Center to center distance of two coils
d_{dia}	Maximum diagonal line distance of the opposite coils
D_i	Diameter of each layer
d_l	Separation between two layers
d_{min}	Minimum distance between coaxial layers
d_{mis}	Lateral misalignment of the primary and the secondary coil
d_o	Distance between point P and the center of the transmitter coil
E	Complete elliptic integral of the second kind
f	Frequency
f_0	Resonant frequency

f_h	Frequency of power dissipation twice dc power dissipation
f_{self}	Self-resonant frequency
G	Admittance
$G_{2parallel}$	Parallel admittance of primary coil circuit
$G_{2series}$	Series admittance of primary coil circuit
H	Magnetic field strength
h_W	Width of coil
I	Supply current
I_0	Resonant current
I_C	Current of capacitor
I_L	Current of inductance
I_1	Current of primary coil of transmitter
I_2	Current of secondary coil of transmitter
$I_{2parallel}$	Parallel connection current of primary coil
$I_{2series}$	Series connection current of primary coil
I_3	Current of primary coil of receiver
$I_{3parallel}$	Parallel connection current of secondary coil
$I_{3series}$	Series connection current of secondary coil
I_4	Current of secondary coil of receiver
I_{load}	Current of the load

I_m	Peak current
K	Complete elliptic integral of the first kind
k_{12}	Coupling factor between transmitter primary coil and secondary coil
k_{23}	Coupling factor between transmitter secondary coil and receiver primary coil
$k_{23\_P\_3}$	Optimal coupling factor between primary and secondary coil for load power of three-coil configuration
$k_{23\_P\_4}$	Optimal coupling factor between primary and secondary coil for load power in four-coil configuration
$k_{23\_\eta\_4}$	Optimal coupling factor between primary and secondary coil for transfer efficiency of four-coil configuration
k_{34}	Coupling factor between receiver primary coil and secondary coil
$k_{34\_P\_3}$	Optimal coupling factor between receiver primary and secondary coil for load power of three-coil configuration
$k_{34\_\eta\_4}$	Optimal coupling factor between receiver primary and secondary coil for transfer efficiency of three-coil configuration
$k_{C\_SR\_SR}$	Critical coupling factor of SR-SR topology
$k_{critical}$	Coupling demarcation point for over coupled and under coupled regime
L	Inductance
L_1	Inductance of primary coil of transmitter
L_2	Inductance of secondary coil of transmitter
L_3	Inductance of secondary coil of receiver

L_4	Inductance of secondary coil of receiver
L_{adj}	Adjoined inductance
L_{eff}	Effective measured value of inductance
L_s	Transmitter inductance when receiver coil is short circuit
L_{self}	Self inductance
L_{sl}	Side length of the OCA
M	Mutual inductance
M_{12}	Mutual inductance between primary coil and secondary coil of transmitter
M_{23}	Mutual inductance between secondary coil of transmitter and primary coil of receiver
M_{34}	Mutual inductance between primary coil and secondary coil of receiver
m_p	Number of testing positions in CSCZ
M_{t1}	Mutual inductance between each coil of 4coil structure and primary coil of receiver
M_{tot}	Mutual inductance between 4-coil structure and primary coil of receiver
N	Number of turns
N_2	Number of turns of primary coil
N_3	Number of turns of secondary coil
N_a	Number of coaxial layers

n_c	Number of coils of the transmitter matrix
n_p	Number of testing positions in edge of SCZ
N_s	Number of strands per bunch
N_t	Number of turns per layer
P_{in}	Output power of power supply
$P_{L\_C\_SR\_SR}$	Maximal load power of SR-SR topology at critical coupling factor
$P_{L\_SR\_SR}$	Load power of SR-SR topology
P_R	Consumed power of resistor
Q_s	Quality factor of series resonance
Q_p	Quality factor of parallel resonane
Q_1	Quality factor of primary coil of transmitter
Q_{1sc}	Quality factor of series connection primary coil of transmitter circuit
Q_2	Quality factor of secondary coil of transmitter
Q_{2sc}	Quality factor of series connection secondary coil of transmitter circuit
Q_3	Quality factor of primary coil of receiver
Q_{3pc}	Quality factor of parallel connection primary coil of receiver circuit
Q_{3sc}	Quality factor of series connection primary coil of receiver circuit
Q_4	Quality factor of secondary coil of receiver
Q_{4sc}	Quality factor of series connection secondary coil of receiver circuit

R	Resistance
r	Radius of coil
R_1	Resistance of primary coil of transmitter
R_2	Resistance of secondary coil of transmitter
r_2	Radius of the primary coil
R_{23sp}	Reflected resistance of series and parallel secondary coil circuit
r_{2in}	Inner radius of the primary coil
r_{2out}	Outer radius of the primary coil
R_3	Resistance of primary coil of receiver
r_3	Radius of the secondary coil
R_{34}	Reflected resistance from secondary coil to primary coil of receiver
R_{23}	Reflected resistance from the receiver to the transmitter
r_{3in}	Inner radius of the secondary coil
r_{3out}	Outer radius of the secondary coil
R_4	Resistance of secondary coil of receiver
R_{ac}	AC resistance
R_{adj}	Adjoined resistance
R_{dc}	DC resistance
R_{eff}	Effective measured value of resistance
R_H	High resistor for parallel circuit

r_{in}	Inner radius of coil
R_{L}	Load resistance
$R_{\text{L\_}P\text{\_SR\_SR}}$	Load resistance when maximal load power achieved of SR-SR topology
$R_{\text{L\_}\eta\text{\_3}}$	Load resistance when maximal transmission efficiency achieved of three-coil configuration
$R_{\text{L\_}\eta\text{\_SR\_SR}}$	Load resistance when maximal transmission efficiency achieved of SR-SR topology
r_{opt}	Optimal radius of transmitter matrix
r_{out}	Outer radius of coil
R_{r}	Resistance reflected from secondary to primary coil circuit
R_{ref}	Resistance reflected from receiver to 4-coil structure transmitter
R_{s}	Inner resistance of power source
r_s	Radius of each single strand
R_{te}	Small test resistor for current measurement
r_ρ	Actual distance between transmitter center and the projected of receiver
$\acute{r}_\rho$	Estimated distance between transmitter center and the projected of receiver
$r_{\rho\text{avg\_center}}$	Lateral misalignment distance as projection of receiver center in CSCZ
$r_{\rho\text{avg\_edge}}$	Lateral misalignment distance as projection of receiver center in marginal area of SCZ

S	Area of receiver coil
S	Breakover switches
$S(\gamma)$	Sum of the squares of the residuals
$S11$	Ratio of power reflected
$S21$	Power transferred from port 1 to port 2
t	Time
T	One cycle
$T_{2\text{height}}$	Thickness of primary coil
$T_{3\text{height}}$	Thickness of secondary coil
T_{height}	Thickness of coil
$u_{2\text{parallel}}$	Unification of primary coil parallel connection G multiply by I
$u_{2\text{series}}$	Unification of primary coil series connection G multiply by I
U_{C}	Voltage of capacitor
U_{L}	Voltage of inductance
U_{s}	Supply voltage
U_{DC}	DC voltage
U_{L11}	Voltage generated by itself
U_{L12}	Voltage generated by other coil
$U_{\text{Lin\_phase}}$	Voltage of series connection inductance in phase
$U_{\text{Lout\_phase}}$	Voltage of series connection inductance out phase

U_R	Voltage of resistor
U_{ripple}	Superimposed ripple voltage
U_{sm}	Peak voltage
W_0	Total stored energy in the resonant loop circuit
W_C	Electric energy
W_L	Magnetic energy
W_R	Load consumed energy
X_{23sp}	Reflected reactance of series and parallel secondary coil circuit
X_r	Reactance reflected from secondary to primary coil circuit
Y	Equivalent admittance
Z	Impendence
Z_{12s}	Reflected impedance from series connection secondary coil to primary coil of transmitter
Z_2	Impedance of the primary circuit
Z_{23p}	Reflected impedance from parallel connection secondary to primary coil circuit
Z_{23s}	Reflected impedance from series connection secondary to primary coil circuit
Z_{2p}	Parallel connection impedance of primary coil
Z_{2s}	Series connection impedance of primary coil
Z_{3p}	Parallel connection impedance of secondary coil

Z_{3s}	Series connection impedance of secondary coil
Z_{load}	Load impedance
Z_r	Impedance reflected from secondary to primary coil circuit
Z_{source}	Source impedance
α, β	Weighting coefficient
γ	Non-linear regression coefficient
δ	Skin depth
ε_0	Permittivity of free space
ε_{in}	Induced electromotive force
ε_r	Relative permittivity of strand insulation
η_{12}	Efficiency of primary and secondary coil of transmitter
η_{4str}	Efficiency of 4-coil structure
η_{4str_max}	Maximal efficiency of 4-coil structure
η_a	Area efficiency of the coil
η_b	Area efficiency per bunch
$\eta_{C\_SR\_SR}$	Efficiency of SR-SR topology at critical coupling factor
η_{CE}	Gain ratio of weighted overall efficiency and the total expense
$\eta_{average}$	Efficiency average
$\eta_{average\_diff}$	Average efficiency difference CSCZ and marginal area of SCZ
η_{ratio}	Weighted overall efficiency per unit length of coil

η_{SR_SR} Efficiency of SR-SR topology

$\eta_{weighted\_ave}$ Weighted average efficiency

$\eta_{weighted\_overall}$ Weighted overall efficiency

θ Angle between d_o and the z-axis

κ Coupling coefficient

μ_0 Magnetic permeability of vacuum

μ_r Relative permeability

ρ Resistivity of the conductive material

σ Conductivity of the wire

ς Thickness of insulation layer

φ Angle of integration

ϕ Angle between d_ρ and the x-axis

χ Residual vectors

ψ Magnetic flux linkage

ω Angular frequency

ω_0 Resonant angular frequency

ω_h Angular frequency of power dissipation twice dc power dissipation

ω_{self} Self-resonant angular frequency

Γ_D Intrinsic losses rates of device

Γ_S Intrinsic losses rates of source

Abbreviations

A4WP	Alliance for Wireless Power
AC	Alternating Current
CE	Cost Efficiency
CENELEC	European Committee for Electrotechnical Standardization
CEPT	European Conference of Postal and Telecommunications Administrations
CISPR	International Special Committee on Radio Interference
CLC	CENELEC Body Responsible for the Work
CSCZ	Center of Sub-Charging Zone
DC	Direct Current
DUT	Device Under Test
ECC	Electronic Communications Committee
EMC	Electromagnetic Compatibility
EMF	Electromagnetic Field
EMI	Electromagnetic Interference
EMS	Electromagnetic Susceptibility
ERCPT	Electric Resonance Coupled Power Transfer

ERM	Radio Spectrum Matters
ERT	Error Range Tolerance
ESR	Effective Series Resistance
ESR&T	Exploration Systems Research & Technology
ETSI	European Telecommunications Standards Institute
Evs	Electric Vehicles
FCC	Federal Communications Commission
FEM	Finite Element Method
IC	Integrated Circuit
ICNIRP	International Commission on Non-lonizing Radiation Protection
ICPT	Inductively Coupled Power Transfer
IEC	International Electrotechnical Commission
IEEE	Institute of Electrical and Electronics Engineers
IEF	Induced Electromotive Force
IM	Impedance Matching
IM	Imaginary Part
IPT	Inductive Power Transfer
ISM	Industrial, Scientific and Medical
IT	Information Technology
ITE	Information Technology Equipment

JAXA	Japan Aerospace Exploration Agency
JPL	Jet Propulsion Laboratory
KAIST	Korean Advanced Institute of Science and Technology
KVL	Kirkoff Voltage Law
LPT	Laser Power Transfer
MINIX	Microwave Ionosphere Nonlinear Interaction Experiment
MOSFET	Metal-Oxide-Semiconductor Field-Effect Transistor
MPT	Microwave Power Transfer
MRCPT	Magnetic Resonance Coupled Power Transfer
MSFC	Marshall Space Flight Center
NASA	US National Aeronautics and Space Administration
NLSP	Non-linear Least Squares Problem
OCA	Overall Charging Area
OF	Operating Frequency
OLEV	On-Line Electric Vehicle
PDL	Power Delivered to the Load
PMA	Power Matters Alliance
PR	Parallel Resonance
PTE	Power Transfer Efficiency
RX	Receiver

RCC	Receiver center coordinates
RC	Receiver in the center of SCZ
RE	Receiver in the edge of SCZ
SAE	Society of Automotive Engineers
SCZ	Sub-Charging Zone
SERT	SSP Exploratory Research and Technology
SHARP	Stationary High Altitude Relay Platform
SPS	Solar Power Satellite
SR	Series Resonance
SRD	Short Range Devices
SRF	Self-Resonant Frequency
SSP	System Solar Power
TC100	Technical Committee 100
TC69	Technical Committee 69
TX	Transmitter
VLF	Very Low Frequency
WHO	World Health Organization
WiTricity	Wireless Electricity
WPC	Wireless Power Consortium
WPT	Wireless Power Transfer

WRC-19	World Radio Communication Conference
WSN	Wireless Sensor Networks
μC	Microcontroller

Publications of the Author

[Che13] Chen, Wei et al.: Optimization Spatial Multiple Coil Transmitter Structure for Wireless Power Transfer, in *Antennas and Propagation Society International Symposium (APSURSI), 2013 IEEE*, Orlando, 2013, pp. 854-855.

[Che14a] Chen, Wei ; Bai, Zijian ; Rickers, Sebastian ; Bruck, Guido H. ; Jung, Peter : Transmitter with Cooperative Coils Matrix for robust Wireless Power Transfer Systems, in *International Symposium on Electromagnetic Compatibility (EMC Europe)*, Gothenburg, 2014, pp. 48-52.

[Che14b] Chen, Wei ; Rickers, Sebastian ; Bruck, Guido H. ; Jung, Peter : Cooperative Transmitter Structure for Improving Efficiency in Wireless Power Transfer, in *International Symposium on Antennas&Propagation (ISAP)*, Taiwan, 2014, pp. 405-406.

[Che14c] Chen, Wei ; Rickers, Sebastian ; Bai, Zijian , Bruck, Guido H. ; Jung, Peter : Design of Spatial Transmitter for Freely Positioned Wireless Power Transfer, in *sixteenth Biennial IEEE Conference on Electromagnetic Field Computation*, Annecy, 2014, pp. 1.

[Che15] Chen, Wei ; Rickers, Sebastian ; Bruck, Guido H. ; Jung, Peter : Localization System Using Resonant Magnetic Coupling Factor for Improving Efficiency in Wireless Power Transfer, in *9th European Conference on Antennas and Propagation*, Portugal, 2015, pp. 1-2.

[Zha12] Zhao, Duan et al.: Magnetic Field Forming of Spatial Multiple Antennas for Wireless Power Transfer, in *International Symposium on Antennas and Propagation (ISAP)* , Nagoya, 2012, pp. 1204-1207.